國 立 交 通 大 學

電信工程研究所

博 士 論 文

高性能多用戶平行傳輸多重天線架構之研究

High Performance MIMO Architectures for Multiuser Personalized Parallel Transmissions

研 究 生： 葉倬榮

指導教授： 王蒞君

中 華 民 國 九十九 年 八 月

高性能多用戶平行傳輸多重天線架構之研究

High Performance MIMO Architectures for Multiuser Personalized Parallel Transmissions

研究生：葉偉榮　　Student: Chu-Jung Yeh

指導教授：王蒞君　博士　　Advisor: Dr. Li-Chun Wang

國立交通大學

電信工程研究所

博士論文

A Dissertation
Submitted to Institute of Communications Engineering
College of Electrical and Computer Engineering
National Chiao Tung University
in Partial Fulfillment of the Requirements
for the Degree of Doctor of Philosophy
in
Communication Engineering
Hsinchu, Taiwan

2010 年　八月

高性能多用戶平行傳輸多重天線架構之研究

研究生：葉倬榮　　指導教授：王蒞君　博士

國立交通大學

電信工程研究所

摘要

隨著對高速資料量的不斷需求，多輸入多輸出多重天線技術在現今與未來的無線通訊系統變的極為重要。而經由多重天線技術得到的巨大容量增益將能透過點對多點的傳輸模式更進一步增加。這種點對多點的傳輸能同時支援多組個人化的資料服務，並傳送給多位使用者。在本篇論文中，我們研究透過在不同維度上使用多重天線技術，進而實現個人化的平行傳輸。

在第一個部份中，我們利用多重天線技術在空間維度上，實現個人化的平行傳輸給多位使用者，此技術稱為多重天線廣播系統。首先，我們比較了使用傳送端波束為基礎以及使用接收端波束為基礎的多重天線廣播系統。我們發現利用通道回授資訊作使用者選取的強制歸零接收端波束多重天線廣播系統對於回授資訊不確定性的容忍度較強。而使用通道回授資訊來計算天線波束權重的傳送端波束多重天線廣播系統則會嚴重受到回授資訊不確定性的影響。接著，我們透過對傳送端波束多重天線廣播系統的分析，介紹使用多用戶排程來增加涵蓋範圍與連線品質。多天線系統將不需要使用額外的傳送功率就可以達到涵蓋範圍與連線品質的增益。最後，我們評估了通道資訊估測錯誤對於強制歸零接收端波束多重天線廣播系統的影響。透過分析，我們發現錯誤的估測資訊將使得系統容量會有一個上限值且不隨著訊號對雜訊比的增加而提升。此結果完全不同於回授資訊錯誤所造成的影響。此外，在連線品質效能上，錯誤的估測資訊會造成涵蓋範圍縮減及增加連線中斷的機率。

在第二個部份中，我們使用網路多重天線系統在多細胞中進行個人化平行傳輸。此系統為多重天線廣播系統在多細胞環境下的應用。結合基地台間地理位置的關係與頻帶的分割，我們使用多重天線在多個細胞內進行合作式的傳輸。在此部份提出了一個結合細胞扇區化、部分頻率重複使用之三細胞合作為

基礎的網路多重天線系統。此架構用來降低多細胞系統中嚴重的細胞間干擾問題。從系統架構與佈局的觀點，我們提供的三細胞合作為基礎之網路多重天線系統不僅可以有效對抗細胞間干擾，也能降低多個基地台合作時的複雜度。

在第三個部份中，我們結合多重天線技術於正交分頻多工系統，並透過頻帶使用之排程與分配達到多使用者的個人化平行傳輸。在此部分的設計目標為補償空間多工多重天線系統所缺乏的連線品質可靠度。首先，我們探討如何透過多用戶維度與多頻帶維度來增加多重天線正交分頻多工系統的涵蓋範圍。透過分析與模擬，我們發現要有效率的延展多重天線正交分頻多工系統涵蓋範圍的關鍵在於設計同時考慮多用戶與多頻帶兩個維度的排程。接下來，我們設計一排程機制可以動態地根據給定的容量比例做資源分配。此機制包含兩步驟，低複雜度的子通道分配與功率分配。透過模擬，即使在各使用者擁有不同的通道衰減效應下，所提出的方法可達到使用者間的預設容量比例。另外，所提供的機制也可以改善使用者的連線品質。

總結來說，在這篇論文中我們探討了三種用來實現個人化平行傳輸的多重天線系統：(1) 多重天線廣播系統；(2) 網路多重天線系統；(3) 多重天線正交分頻多工系統。透過在多用戶、多頻帶、以及基地台間地理位置關係等不同維度的多樣性，我們提升了系統連線品質、涵蓋範圍、以及系統容量之效能。

High Performance MIMO Architectures for Multiuser Personalized Parallel Transmissions

A Dissertation

Presented to

The Academic Faculty

By

Chu-Jung Yeh

In Partial Fulfillment

of the Requirements for the Degree of

Doctor of Philosophy in Communication Engineering

Institute of Communications Engineering

National Chiao-Tung University

August, 2010

High Performance MIMO Architectures for Multiuser Personalized Parallel Transmissions

Student: Chu-Jung Yeh Advisor: Dr. Li-Chun Wang

Institute of Communications Engineering
National Chiao Tung University

Abstract

With the increasing demand for high-speed data rates, multiple-input multiple-output (MIMO) antenna techniques become extremely important in current and future wireless communication systems. The huge capacity gain offered by MIMO antenna techniques can be further exploited in point-to-multiple transmissions, which can support personalized data services to multiple users concurrently. In this dissertation, we investigate MIMO antenna techniques to realize personalized parallel transmissions in different domains.

In the first part, we utilize MIMO antenna techniques in the spatial domain to carry out personalized parallel transmissions among multiple users, named as the MIMO broadcast systems. At first, we quantitatively compare the MIMO broadcast systems with transmit and receive beamforming techniques. We find that utilizing feedback channel state information (CSI) for user selection in the receive zero-forcing (ZF) MIMO broadcast systems is more robust to feedback channel variations compared with utilizing feedback CSI for calculating antenna beamforming weights in the transmit MIMO broadcast systems. Next, we provide analytic formulas for the transmit MIMO broadcast systems to illustrate how multiuser scheduling can function as a link diversity compensation and soft coverage enhancement technique to improve the deficient diversity. Finally, we evaluate the effects of channel estimation errors on the receive ZF MIMO broadcast systems. Our analysis indicates the

sum rate affected by estimated channel errors will be bounded by a value as signal-to-noise ratio (SNR) increases. This result is different from the effects of feedback errors which only causes certain sum-rate degradation. In addition, channel estimation errors will also cause shrinkage on reliable coverage and zero link diversity order on outage performance.

In the second part, an extended application of the MIMO broadcast systems, named as the network MIMO systems, transfers personalized data transmissions from single-cell scenario to multi-cell environment. In the network MIMO systems, we utilize the MIMO antenna techniques to coordinate parallel transmissions among multiple cells in geographically separated spatial domain. We propose a three-cell network MIMO architecture combined with sectorization and fractional frequency reuse (FFR) to reduce inter-cell interference in a multi-cellular system. From the aspects of architecture and deployment, the proposed FFR-based 3-cell network MIMO architecture can not only effectively overcome the inter-cell interference, but can relieve the burden of executing complex multi-base stations joint processing for a huge number of cells.

In the third part, we apply MIMO antenna techniques to broadband orthogonal frequency division multiplexing (OFDM) system and achieve parallel transmissions among users in the frequency domain by scheduling and allocating personalized resource. Our design focuses on compensating the drawback of degraded link reliability in the diversity-deficient spatial multiplexing MIMO-OFDM systems. First, we execute scheduling from the perspective of exploiting multiuser diversity and frequency diversity to extend the coverage region of the MIMO-OFDM systems. Our analysis and simulations indicate that the key of coverage enhancement is to jointly utilize multiuser and frequency diversity. Next, we design a scheduler to adaptively assign resource among users under a predetermined proportional rate constraint. Our method including two stages: a low-complexity subchannel allocation algorithm at first and a computational efficient power allocation method later. Simulation results show that the proposed algorithm can achieve the capacity to the algorithm with the maximal-rate scheduling but provides better link reliability. Additionally, the proposed two-stage method can meet the predetermined rate requirements well even if service users are under different large-scale power decay conditions.

In summary, we investigate three kinds of MIMO antenna techniques to realize personalized parallel transmissions: (1) MIMO broadcast systems; (2) network MIMO systems;

and (3) MIMO-OFDM systems. We utilize diversity in various domains including multiuser, frequency, and geographic location of base stations to enhance system performance in terms of link reliability, achievable reliable coverage, and sum-rate capacity.

Acknowledgements

Foremost, I would like to express my sincere gratitude to my advisor Dr. Li-Chun Wang, for providing me important insights on research. Importantly, Dr. Li-Chun Wang always encourages and support me when I face difficulties throughout my Ph. D. studies. Without his advice, guidance, and timely comments, this work could not have been done. Undoubtedly, I will keep in my mind the principles he taught me for research: **Think big**, **Think different**, and **Think simple**.

Special thanks to my mates of Wireless System Lab in NCTU. They gave me kindly help and suggestions in many aspects. Dr. Chiung-Jang Chen, Jane-Hwa Huang, Chih-Wen Chang, Anderson Chen, Wei-Cheng Liu, and Meng-Lin Ku constantly gave me valuable suggestions in my research. My dear mates, Chung-Wei Wang, Ang-Hsun Tsai, Wai-Chi Li, Chiao Lee, and Chien-Cheng Tien, always encouraged me when I felt frustrated.

Finally, I am deeply indebted to my family whose love and understanding have been supporting me without any hesitation through these years. They always warmly back me up from their deeply inside mind. I would also like to thank my lovely lady, Yi-Hui Lin, who gave me sincerely mental and emotional support during this long journey.

Contents

List of Tables

List of Figures

Abbreviations

- 3GPP : third Generation Partnership Project
- BD : block-diagonalization
- BER : bit-error rate
- CDF : cumulative distribution function
- CDI : channel direction information
- CDMA : code division multiple access
- CoMIMO : collaborative multiple-input multiple-output
- CoMP : coordinated multi-point
- COUS : coverage-oriented user selection
- COSA : coverage-oriented joint scheduling and subchannel allocation
- CP : cyclic prefix
- CQI : channel quality information
- CSI : channel state information
- CSI-R : CSI at receiver side
- CV : coefficient of variations
- dB : decibel
- DPC : dirty-paper coding

- FDMA : frequency division multiple access
- FFR : fractional frequency frequency
- FOSA : fairness-oriented joint scheduling and subchannel allocation
- Hz : hertz
- IGI : inter-group interference
- LTE-A : Long-Term Evolution-Advanced
- i.i.d : independent and identically distributed
- MAC : multiple access channel
- KKT : Kurush-Kuhn-Tucker
- MCS : modulation and coding schemes
- MIMO : multiple-input multiple-output
- MMSE : minimum mean square error
- OFDM : orthogonal frequency division multiplexing
- OFDMA : orthogonal frequency division multiple access
- SINR : signal-to-interference-plus noise ratio
- SISO : single input single output
- SNR : signal-to-noise ratio
- SWNSF : strongest-weakest-normalized-subchannel-first
- PDF : probability density function
- RR : round-robin
- RU : resource unit
- RZFS : receive zero-forcing scheduler (appeared in Figs. 3.7 $\sim$ 3.10)

- SVD : singular value decomposition
- TDMA : time division multiple access
- TZFS : transmit zero-forcing scheduler (appeared in Figs. 3.7 $\sim$ 3.10)
- WiMAX : Worldwide Interoperability for Microwave Access
- ZF : zero-forcing
- ZFB : (transmit) zero-forcing beamforming
- ZFR : zero-forcing receiver
- ZF-DPC : zero-forcing dirty-paper coding

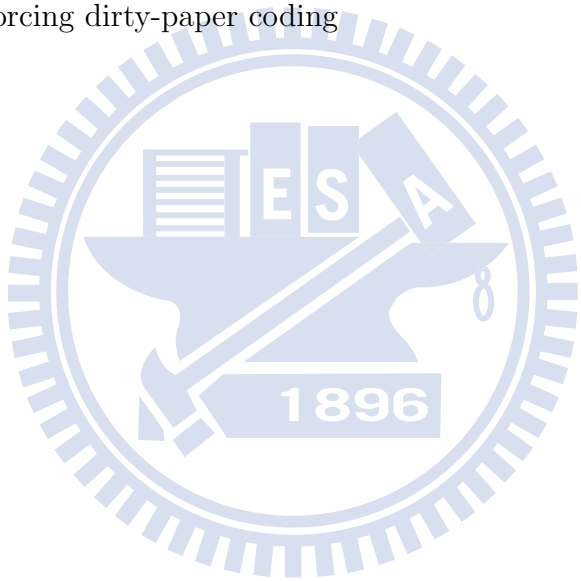

Notations

- $|\mathcal{S}|$: cardinality of a set $\mathcal{S}$, i.e., the number of members of $\mathcal{S}$
- $\mathbf{I}_n$: $n \times n$ identity matrix
- $\mathbf{A}^H$: complex conjugate transpose of the matrix $\mathbf{A}$
- $\mathbf{A}^{-1}$: inverse of $\mathbf{A}$
- $\mathbf{A}^T$: transpose of $\mathbf{A}$
- $[\mathbf{A}]_{ij}$: (i,j)-th entry of $\mathbf{A}$
- $\mathbf{A}^\dagger$: pseudo-inverse of $\mathbf{A}$
- $\mathbf{A} \in \mathbb{C}^{n \times m}$: $n \times m$ matrix $\mathbf{A}$ with complex-valued entries
- $E[\,\cdot\,]$: expectation operation
- $\mathcal{N}(0, \sigma^2)$: Gaussian random variable with zero mean and variance σ^2
- $\mathcal{CN}(0, \sigma^2)$: complex circular symmetric Gaussian random variable with zero mean and variance σ^2
- $\mathcal{X}^2_{2a}$: Chi-squared random variable with $2a$ degrees of freedom
- $E_r(x)$: exponential integer function of order r, defined as $E_r(x) = \int_1^\infty e^{-xt} t^{-r} dt$
- $\Gamma(a)$: complete gamma function, defined as $\Gamma(a) = \int_0^\infty t^{a-1} e^{-t} dt$
- $\Gamma(a, x)$: upper incomplete gamma function, defined as $\Gamma(a, x) = \int_x^\infty t^{a-1} e^{-t} dt$
- $\Upsilon(a, x)$: lower incomplete gamma function, defined as $\Upsilon(a, x) = \int_0^x t^{a-1} e^{-t} dt$

- $\Gamma_{\mathrm{R}}(a,x)$: regularized gamma function, defined as $\Gamma_{\mathrm{R}}(a,x)=\frac{\Gamma(a,x)}{\Gamma(a)}$
- $\Gamma_{\mathrm{R}}^{-1}(a,z)$: inverse function of regularized gamma function, i.e., $z=\Gamma_{\mathrm{R}}(a,x) \Rightarrow x=\Gamma_{\mathrm{R}}^{-1}(a,z)$
- $I_p(a,b)$: regularized incomplete beta function, defined as $I_p(a,b)=\frac{\int_0^p t^{a-1}(1-t)^{b-1}dt}{\int_0^1 t^{a-1}(1-t)^{b-1}dt}$ (For $a>0,\ b>0$ and $0\leq p\leq 1$)
- $I_z^{-1}(a,b)$: inverse function of regularized incomplete beta function, i.e., $z=I_p(a,b) \Rightarrow p=I_z^{-1}(a,b)$
- $f_X(x)$: PDF of the random variable X
- $F_X(x)$: CDF of the random variable X
- $[x]_+$: represents $\max\{x,0\}$
- $\lceil x \rceil$: the smallest integer greater or equal to x
- $\lfloor x \rfloor$: the largest integer smaller or equal to x
- $\min\{x_1,x_2\}$: minimum of x_1 and x_2
- $\max\{x_1,x_2\}$: maximum of x_1 and x_2

Symbols

- M_T : number of transmit antennas
- M_R : number of receive antennas
- M_R^k : number of receive antennas for user k
- M : number of antenna in the case of $M_T = M_R$
- M_c : coordinated size in network MIMO systems
- L : $L = M_T - M_R$
- K : number of users
- N : number of subchannels; number of frequency resource (used in Chapter 6)
- $\bar{N}_k$: predetermined number of subchannels will be assigned to user k
- $\bar{N}$: number of unallocated subchannels
- $\mathcal{K}$: user set
- $\mathcal{N}$: subchannel set
- $\mathcal{N}_k$: allocated subchannels index set for user k
- $\mathcal{S}$: selected user/antenna set
- $\mathcal{U}$: total receive antenna set
- $\mathcal{I}$: interfering base station set
- $\mathcal{I}_G$: the set of index for the interfering network MIMO groups

- $\mathbf{H}$: channel matrix between the base station and user terminal (fading)
- $\mathbf{G}$: channel matrix between the base station and user terminal (fading + path loss)
- $\mathbf{h}_i$: i-th row vector of $\mathbf{H}$
- $\mathbf{u}$: input signal vector at the base station
- $\mathbf{x}$: transmitted signal vector at the base station
- $\mathbf{y}$: received signal vector at user terminal
- $\mathbf{n}$: spatially white noise vector for user terminal
- $\mathbf{W}$: beamforming weight matrix
- $\mathbf{w}_i$: i-th column vector of $\mathbf{W}$
- $\mathbf{L}$: lower triangular matrix of the QR-type decomposition of $\mathbf{H}$
- $\mathbf{Q}$: unitary matrix of the QR-type decomposition of $\mathbf{H}$
- $\mathbf{T}_k$: user k's precoding matrix for BD-based transmit beamforming
- $\mathbf{R}_k$: user k's equalizer matrix for BD-based transmit beamforming
- $\lambda_{\max}$: the maximum eigenvalue of $\mathbf{H}\mathbf{H}^H$
- $\lambda_{\min}$: the minimum eigenvalue of $\mathbf{H}\mathbf{H}^H$
- $h_{i,j}$: channel gain from the j-th transmit antenna to the i-th receive antenna
- g_k : path loss between the base station and user k
- g_0 : a constant subject to certain path loss models
- μ : path loss exponent
- P_T : transmission power
- ρ : average received SNR
- σ^2 : thermal noise power

- k^* : the selected user for service from the base station after scheduling
- $\hat{k}^*$: the selected user with feedback channel variations
- γ_i^k : i-th effective output SNR at user k
- b_i : i-th effective channel gain of the transmit ZF MIMO broadcast systems
- d_i : i-th effective channel gain of the transmit ZF-DPC MIMO broadcast systems
- q_i : i-th effective channel gain of the receive ZF MIMO broadcast systems
- P_{out} : link outage probability, defined as $P_{\text{out}} \triangleq P_r\{\gamma < \gamma_{th}\}$ where γ is effective output SNR and γ_{th} is the required SNR value
- D_{order} : link diversity order, defined as $D_{\text{order}} \triangleq -\lim_{\rho \to \infty} \frac{\log P_{\text{out}}(\rho)}{\log \rho}$
- $A(\theta)_{\text{dB}}$: antenna gain at angle θ (in dB)
- $\theta_{3\text{dB}}$: 3 dB beamwidth angle
- A_m : the maximum attenuation for the sidelobe (in dB)
- $\alpha_{k,j}$: fast Rayleigh fading between mobile k and base station j
- $\beta_{k,j}$: shadowing between mobile k and base station j
- $d_{k,j}$: distance between mobile k and base station j
- d_{ref} : a reference distance between the center and the vertex of a cell
- Γ : the interference-free SNR, defined as the SNR measured at d_{ref} with only considering pass loss, and the noise power is normalized to unity
- $\gamma_{k,j}$: SINR of mobile k served by base station j
- γ_k^{IGI} : SINR of mobile k under IGI
- $\gamma_{k,\text{ZF}}^{\text{IGI}}$: SINR of mobile k with ZF-based network MIMO transmission under IGI
- $\gamma_{k,\text{ZFDPC}}^{\text{IGI}}$: SINR of mobile k with ZF-DPC network MIMO transmission under IGI

- f_A : inner frequency band in a tri-sector FFR cell
- f_{B_p} : outer frequency subband in a tri-sector FFR cell with N RUs, i.e., $f_{B_p} = \{f_{B_{p,1}}, \ldots, f_{B_{p,N}}\}$ for $p = 1, 2, 3$
- $h_{(x),y}$: channel response (including fast fading, path loss, shadowing, and antenna gain pattern) between cell y and the served user of cell x
- C_{DPC} : sum rate of DPC
- C_{TZF} : sum rate of the transmit ZF MIMO broadcast systems
- $C_{\text{RZF}|_M}$: sum rate of the receive ZF MIMO broadcast systems with equal power allocation ($M_T = M_R = M$)
- $C^{\epsilon_e^2}_{\text{ZFR}|_M}$: sum rate of the receive ZF MIMO broadcast systems with equal power allocation under estimation error ϵ_e^2 ($M_T = M_R = M$)
- $C^{\epsilon_e^2}_{\text{ZFR}}$: sum rate of the receive ZF MIMO broadcast systems with equal power allocation under estimation error ϵ_e^2 ($M_T \neq M_R$)
- $C^{\text{water}}_{\text{RZF}|_M}$: sum rate of the receive ZF MIMO broadcast systems with water-filling power allocation ($M_T = M_R = M$)
- $C^{\text{water}}_{\text{RZF}}$: sum rate of the receive ZF MIMO broadcast systems with water-filling power allocation ($M_T \neq M_R$)
- R_{B2B} : the base-station-to-base-station distance in a cellular system
- $R_{\texttt{ZFDPC}}$: reliable coverage of the transmit ZF-DPC MIMO broadcast systems
- $R_{\texttt{RZF}}$: reliable coverage of the receive ZF based MIMO broadcast systems
- $\eta^1_{\texttt{ZFDPC}}$: coverage extension ratio on the strongest link of the transmit ZF-DPC MIMO broadcast systems
- R_{RS} : reliable coverage of the spatial multiplexing-based MIMO-OFDM system with random scheduling

- R_{COUS} : reliable coverage of the spatial multiplexing-based MIMO-OFDM system with COUS
- R_{COSA} : reliable coverage of the spatial multiplexing-based MIMO-OFDM system with COSA
- R_{SISO} : reliable coverage of the SISO-OFDM system
- G_{COUS} : coverage gain of MIMO-OFDM system with COUS over random scheduling, defined as $G_{\text{COUS}} \triangleq \frac{R_{\text{COSA}} - R_{\text{RS}}}{R_{\text{RS}}}$
- G_{COSA} : coverage gain of MIMO-OFDM system with COSA over random scheduling, defined as $G_{\text{COSA}} \triangleq \frac{R_{\text{COSA}} - R_{\text{RS}}}{R_{\text{RS}}}$
- η_{RS} : coverage ratio of MIMO-OFDM system with random scheduling to SISO-OFDM system, defined as $\eta_{\text{RS}} \triangleq \frac{R_{\text{RS}}}{R_{\text{SISO}}}$
- η_{COUS} : coverage ratio of MIMO-OFDM system with COUS to SISO-OFDM system, defined as $\eta_{\text{COUS}} \triangleq \frac{R_{\text{COUS}}}{R_{\text{SISO}}}$
- η_{COSA} : coverage ratio of MIMO-OFDM system with COSA to SISO-OFDM system, defined as $\eta_{\text{COSA}} \triangleq \frac{R_{\text{COSA}}}{R_{\text{SISO}}}$
- $\{\eta_k\}_{k=1}^{K}$: predetermined rate requirement ratios among users

Chapter 1

Introduction

No one believes that we can deliver messages over the air and speak to each other through a small device before the development of wireless communications and cellular systems. However, it is true that human's desire is endless. As people are no longer satisfied with the conventional service, the old saying "Nothing is difficult to a man whom ambition fires" becomes a strong driving force for researchers to develop new techniques on wireless communication systems. In recent years, multiple-input multiple-output (MIMO) techniques [1] [2] become strong candidate for supporting high-speed data services. In this dissertation, we will present a story about utilizing MIMO techniques in different domains to realize personalized parallel transmissions.

In this dissertation, one of the domain for realizing multiuser personalized parallel transmission is the **spatial** domain. As shown in Fig. 1.1, the MIMO broadcast antenna techniques can transmit personalized data streams to multiple users concurrently in the point-to-multipoint scenario through the spatial domain [3, 4]. Unlike a TV broadcast system, the MIMO broadcast system transmits *different* **personalized** data streams to a group of selected users. In the point-to-multipoint multiuser MIMO broadcast channels, even with only one single receive antenna at the user end, the spatial multiplexing gain can be also achieved by sending precoded data across multiple transmit antennas to a group of users simultaneously [4]. For M_T transmit antennas and K users, the capacity of the MIMO broadcast system is $\min\{M_T, K\}$ times higher than that of a time division multiple access (TDMA) scheduling system which selects one user at a time [5–7]. When complete channel state information (CSI) is available at the transmitter, the dirty paper coding (DPC) scheme can maximize the sum rate of the MIMO broadcast system [8–11].

Another domain that we can exploit to realize multiuser personalized parallel transmission is the **frequency** domain. Orthogonal frequency division multiplexing (OFDM) has become a popular modulation technique for transmission of broadband signals and has been regarded as an efficient scheme to combat the adverse effects of multipath delay spread.

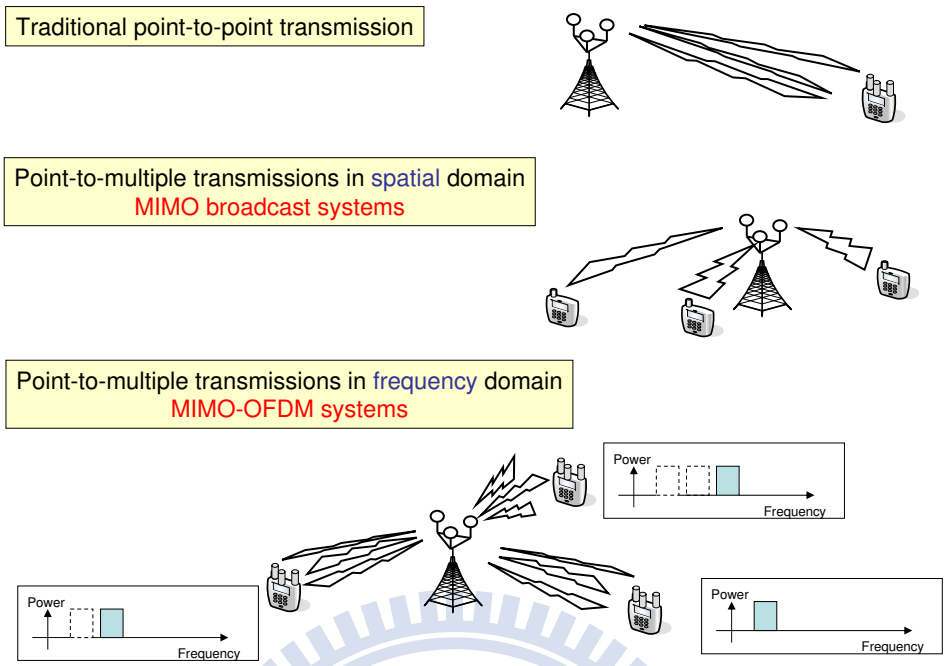

Figure 1.1: Illustration of MIMO antenna techniques for point-to-multipoint transmissions.

OFDM can convert a frequency selective fading channel into a parallel collection of frequency flat fading subchannels and thus can overcome the inter-symbol interference (ISI) [12] [13]. Meanwhile, MIMO antenna techniques can provide spatial multiplexing gain and diversity gain to increase spectrum efficiency and link reliability, respectively. Combining MIMO with OFDM (MIMO-OFDM) together, the broadband frequency selective MIMO channel can be separated into many flat fading MIMO channel. Due to the existence of parallel subchannels in the frequency and space domain, MIMO-OFDM systems can transmit **personalized** data to multiple service users across parallel subchannels through suitable scheduling and resource allocation as shown in Fig. 1.1. The promise of high system performance has led MIMO-OFDM systems to become an attractive air-interface solution for the next generation high speed wireless systems, e.g. the standards of IEEE 802.16m Worldwide Interoperability for Microwave Access (WiMAX) and the third Generation Partnership Project (3GPP) Long-Term Evolution-Advanced (LTE-A).

In the multi-celluar systems, we will also address the application of MIMO technique in a distributed manner. This application is the so called network MIMO technique. Recently, network MIMO transmission becomes a hot topic in both industry and academia [14–21]. It

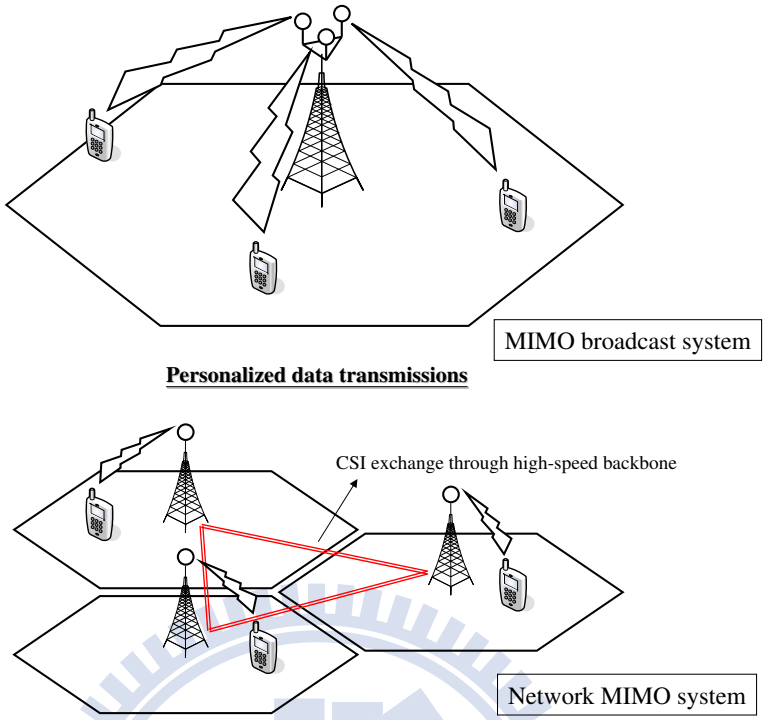

Figure 1.2: The concept of how single-cell MIMO broadcast systems transfers to multi-cell network MIMO systems.

is called the coordinated multi-point (CoMP) transmission in 3GPP LTE-A and the collaborative MIMO (Co-MIMO) transmission in the IEEE 802.16m WiMAX, respectively [15, 16]. Network MIMO transmission aims to mitigate the inter-cell interference by coordinating the transmission of a few geographically separated base stations, but requires reliable high-speed backbone connections and high computational complexity [17–20]. With synchronized base stations, the inter-cell interference in a multi-cell network MIMO system can be mitigated by applying the joint transmission techniques of the multi-user MIMO broadcast systems [4, 8, 9]. Fig. 1.2 illustrate how a single-cell MIMO broadcast system transfers to a multi-cell network MIMO system. Separated base stations execute cooperatively joint transmissions among multiple cells via a high-speed backbone connection to exchange CSI.

1.1 Problem and Solutions

In this section, we briefly describe our problem formulations and the corresponding solutions. Those issues we addressed here will be respectively presented in Chapters 3 to 6.

1.1.1 Beamforming Techniques for Multiuser MIMO Broadcast Systems

The objective of this part is to quantitatively compare the sum rate and the feedback requirements for the transmit and the receive MIMO broadcast systems with user selection, where both base stations and user terminals are equipped with multiple antennas as shown in Fig. 1.3. Our goal is not to claim that one scheme outperforms the other, but try to suggest a feasible MIMO broadcast system subject to the constraint of feedback bandwidth. It is too costly to use frequency spectrum not for transmitting user's data, but only for sending CSI. Thus, we put an emphasis on using feedback information in an effective way and its robustness to channel variations. Specifically, we discuss whether feedback CSI is suitable for selecting users or for calculating antenna beamforming[1] weights.

In this part, we define the **transmit zero-forcing (ZF) scheduler** as the channel-inverse-based transmit ZF beamforming combined with multiuser scheduling, where the beamforming weights are multiplied at the transmit antennas and scheduling is an opportunistic transmission technique to exploit multiuser diversity [22,23]. Furthermore, we investigate another type of ZF MIMO broadcast systems – the **receive ZF scheduler**, where the ZF algorithm is implemented at the multiple receive antennas of the user terminal to cancel the inter-stream interference. In the IEEE 802.11n wireless local area networks, 3GPP LTE-A and WiMAX broadband cellular radio systems, a user terminal is equipped with multiple antennas. Thus, [24–26] exploited the advantage of multiple receive antennas and showed that receive ZF scheduler can be also used in MIMO broadcast systems. In other words, the

[1]Here we use beamforming to represent the situation when antenna elements are multiplied by certain weights. It is not implied that a physical beam pattern is formed. The term "beamforming" for a MIMO broadcast systems in the transmitter side is also called as precoding usually. The term "beamforming" in the user end is actually an equalizer/receiver combined with multiuser scheduling for broadcasting multiple data.

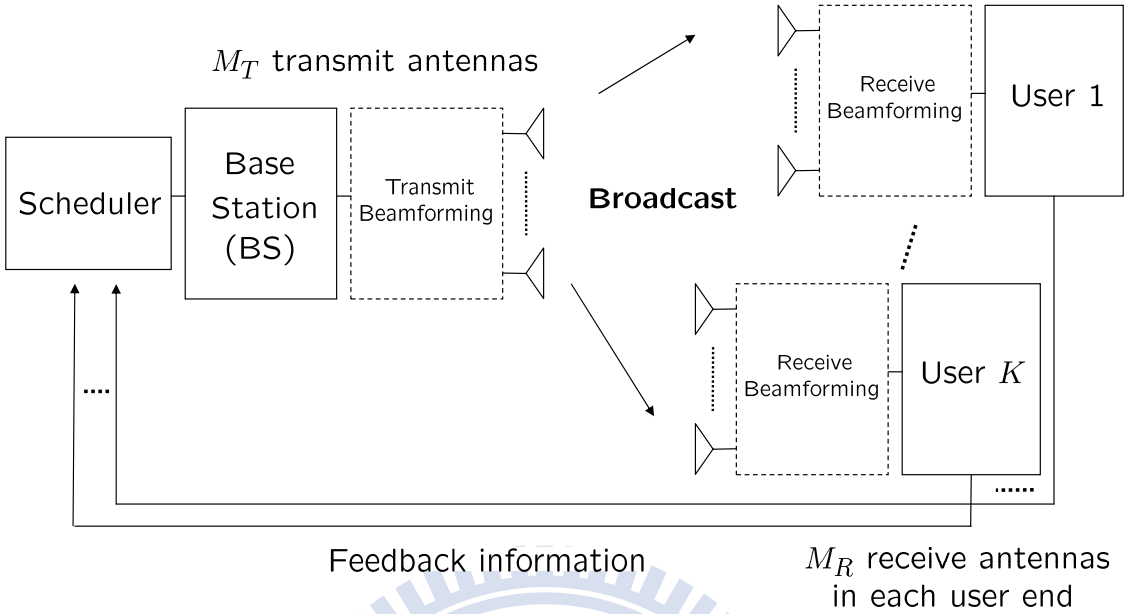

Figure 1.3: System model of multiuser MIMO broadcast systems with M_T transmit antennas and M_R receive antennas per user.

transmit ZF scheduler and receive ZF scheduler are "pre-ZF" and "post-ZF" combined with multiuser scheduling for broadcasting multiple independent data, respectively.

The contributions of this part can be summarized as follows:

- Subject to feedback channel variations and the amount of feedback information, we quantitatively compare the sum rate of the receive ZF MIMO broadcast systems and the three considered transmit MIMO broadcast systems with multiuser scheduling (including QR-based zero-forcing dirty paper coding (ZF-DPC), channel-inverse-based ZF beamforming, and the block diagonalization (BD) approach [27]). We find that utilizing feedback CSI for **user selection** in receive ZF MIMO broadcast systems is more robust to feedback channel variations compared with utilizing feedback CSI for calculating **antenna beamforming weights** in transmit MIMO broadcast systems. As a result, the receive ZF MIMO broadcast system can deliver the same or even higher sum rate than the transmit MIMO broadcast systems, especially in the presence of channel variations. If an error-free feedback channel is available, the transmit ZF MIMO broadcast system can achieve higher sum rate than the receive ZF MIMO

broadcast system.

- Different from the sum rate scalability laws for a large number of users in [6, 7, 25, 28], the derived analytical expression for the sum rate of the transmit ZF scheduler is applicable for a small number of scheduled users. Furthermore, the newly derived sum rate analysis formula of the receive ZF scheduler based on water-filling power allocation is also more general in comparison with the receive ZF scheduler based on equal power allocation [26].

1.1.2 Analysis of Multiuser MIMO Broadcast Systems with Transmit Beamforming

Although the capacity issues of MIMO broadcast systems have been extensively investigated, to our knowledge, the studies on the link quality and coverage performance of MIMO broadcast systems are rarely seen in the literature. From the perspective of tradeoff between multiplexing and diversity for a MIMO system [29], the transmit MIMO broadcast systems may be a diversity-deficient scheme due to it realizes spatial-multiplexing personalized transmissions. In this part, we derive the analytical closed-form expressions for the link outage probability, link diversity order, and the reliable coverage radius of a multiuser MIMO broadcast system with transmit based beamforming. It is found that multiuser scheduling can function as a **link diversity compensation and soft coverage extension** technique for the MIMO broadcast systems. The concept of soft coverage extension by multiuser scheduling was suggested for point-to-point MIMO systems in [30] since multiuser scheduling can improve the coverage of MIMO broadcast systems without increasing transmission power in the physical layer. However, [30] only considered the single-user MIMO system that serves one single user at any time instant, rather than the MIMO broadcast systems that serves a group of users simultaneously. Our developed analytical framework can evaluate to what extent the multiuser scheduling can improve the coverage performance of the multiuser MIMO broadcast systems.

1.1.3 Analysis of Multiuser MIMO Broadcast Systems with Receive Beamforming

Based on the results provided in [31], we know that the receive ZF MIMO broadcast system achieves similar sum rate compared to the transmit ZF MIMO broadcast system with less feedback requirement and provides robust resistance to feedback error variations. Inspired by the potential advantage, we think the receive ZF MIMO broadcast system may become a possible canadine for realizing personalized parallel transmissions. Hence, we aim to analyze performance metrics of the receive ZF MIMO broadcast system including link reliability, reliable coverage, and sum-rate capacity. For a traditional single-user ZF MIMO system, the diversity order is $M_R - M_T + 1$ [32]. However, under simultaneously serving a group of users by K-user scheduling selectivity, we show that the link diversity order of the receive ZF MIMO broadcast systems becomes $K(M_R - M_T + 1)$. In additional, we consider a more general case that the receiver end may have estimation errors on CSI. That is, each user terminal has **imperfect CSI at receiver** (CSI-R). In the presence of estimation errors, [33] had provided approximated bit-error rate (BER) analysis for point-to-point single-user MIMO system with ZF receiver. The achievable sum rate of point-to-multipoint MIMO broadcast system with receive ZF beamforming combined with multiuser diversity was analyzed in [26]. However, the provided closed-form expression is constrained to the case of $M_R = M_T$, i.e. the number of receive antennas at user end equals to the number of transmit antennas at the base station. In this dissertation, we relax our analysis to any $M_R \geq M_T$ cases and further consider the effect of estimation error on various performance metrics.

1.1.4 Architecture for Coordinated Multicell MIMO Systems

One fundamental issue for designing the network MIMO system is the following: **how many cells** shall be coordinated together to provide sufficient signal-to-interference-plus noise ratio SINR) performance. Obviously, it is impractical to coordinate too many cells in a network MIMO system because synchronization among a huge number of cells is of high complexity. In both WiMAX and LTE-A standards, the default number of the neighboring base stations for the joint MIMO processing is three [15, 16, 34, 35]. Even if the number of the coordinated cells of the network MIMO system increases, a group of coordinated cells in network MIMO

systems are still affected by the co-channel interference from the neighboring coordinated groups. This kind of the **inter-group interference (IGI)** should be taken into account when evaluating the performance of network MIMO systems [34, 35]. Hence, it becomes an important and interesting problem to design a network MIMO systems subject to the constraint of three coordinated cells per group and evaluate its performance under the IGI effects simultaneously.

The ultimate goal of this part is to investigate which kind of 3-cell fractional frequency reuse (FFR)-based network MIMO architectures are feasible and can deliver the most performance improvements in terms of SINR and capacity subject to the IGI effects. In this part, we propose a 3-cell FFR-based tri-sector network MIMO architecture with a sector-frequency rearrangement scheme. Specifically, the proposed sector-frequency rearrangement schemes can amplify the performance gain of the network MIMO even with a small number of coordinated cells, i.e. in the three-cell case. We examine various tri-sector architectures [36, 37] and determine which directional antenna scheme can effectively reduce the impact of IGI in the multi-cellular system and enable the frequency rearrangement scheme for the 3-cell network MIMO architecture. Furthermore, we discuss how to determine the uncoordinated inner region for the tri-sector network MIMO with FFR cell planning.

1.1.5 Coverage Enhancement for Multiuser MIMO-OFDM Systems

MIMO-OFDM is an important transmission technique for broadband wireless systems because both spatial and frequency domains can be exploited simultaneously for performance enhancement. Compared to MIMO flat-fading channels, MIMO frequency-selective fading channels can yield higher diversity gain as well as multiplexing gain [38]. However, the total transmit power of MIMO systems is split over multiple antennas resulting in lower transmit power per antenna and poorer coverage. That is, from a single-input single-output (SISO) system extend to a MIMO system, increasing the number of transmit antennas results in a smaller signal-to-noise ratio (SNR) per degree of freedom because the total available transmit power is divided across transmit antennas. For example, Fig. 1.4 provides an illustration of the coverage shrinkage issue from SISO system to three-antennas equipped MIMO sys-

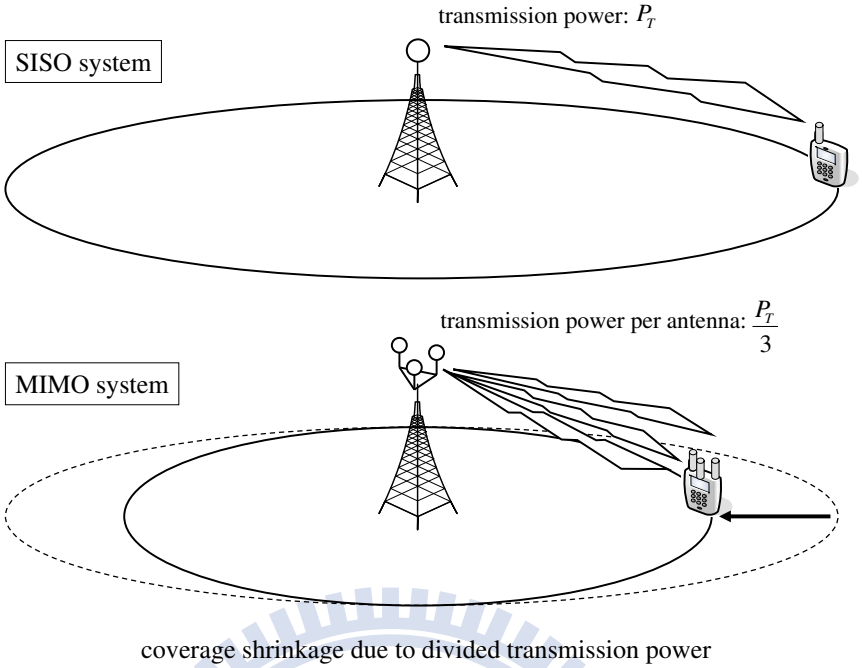

Figure 1.4: Illustration of coverage shrinkage from a SISO system to a MIMO system.

tem. This issue has been investigated originally in [39] and a multiuser scheduling solution in MIMO flat-faded channels was proposed in [30]. In addition, many techniques, such as enhanced space-time codes [40] and space-frequency codes [41–45] has been suggested in the literature to overcome the link reliability for MIMO-OFDM systems.

In this part, we investigate the subchannel assignment problem for multiuser MIMO-OFDM systems with an emphasis on **coverage enhancement**. According to the max-min criterion for selecting the largest minimum eigenmode of the MIMO channel matrix from a group of users, a low-complexity coverage-oriented joint scheduling and subchannel allocation algorithm (COSA) is proposed to improve the cell coverage of a multiuser MIMO-OFDM system. In addition to COSA, another type max-min-based subchannel assignment scheme, called the fairness-oriented joint scheduling and subchannel allocation algorithm (FOSA), is also discussed for the spatial multiplexing based multiuser MIMO-OFDM systems. To quantify the performance improvements on the coverage of MIMO-OFDM systems due to joint multiuser scheduling and subchannel assignment, another coverage-oriented user selection (COUS) algorithm which only takes advantage of multiuser diversity is presented. We derive the closed-form expressions for the reliable cell coverage of the spatial multiplexing

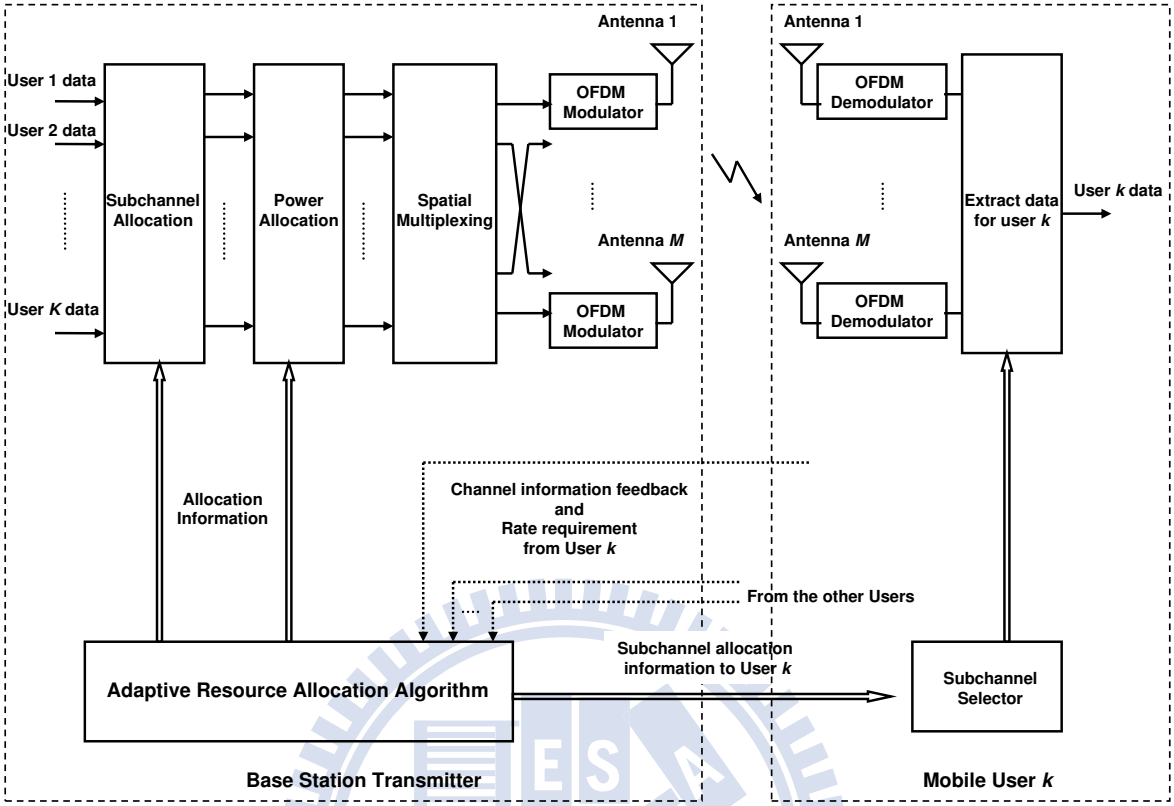

Figure 1.5: Block diagram of the spatial multiplexing based multiuser MIMO-OFDM systems with adaptive resource allocation scheduler.

based multiuser MIMO-OFDM systems using COSA, COUS and random user scheduling in the frequency-selective fading channel. Compared with FOSA and COUS, we find that COSA will provide better coverage performance and lower complexity and almost the same fairness performance as FOSA does as long as the number of subchannels is large enough.

1.1.6 Capacity Enhancement for Multiuser MIMO-OFDM Systems

In this part, we propose low-complexity subchannel allocation algorithms and power allocation scheme for spatial multiplexing based multiuser MIMO-OFDM system. Continuous with previous part, we focus on a spatial multiplexing based multiuser MIMO-OFDM system in which each user has better link quality under full multiplexing and larger coverage in all subchannel bands. As the block diagram of the spatial multiplexing based multiuser MIMO-

OFDM system shown in Fig. 1.5, we execute suitable user scheduling and resource allocation in the scheduler. We emphasize on resource assignment with flexible capacity among served users. That is, we consider different required rate constraints among users due to different levels of service. Our work is different from past works mainly focus on achieving maximal capacity but neglecting the intrinsic coverage issue of a spatial multiplexing MIMO system.

1.2 Dissertation Outline

This dissertation consists of three themes as shown in Fig. 1.6. The first part including Chapters 3, 4 and 5 considers a narrowband wireless system and realizes parallel transmission among users in spatial domain by personalized broadcasting data. In the second part, i.e. Chapter 6, we utilize geographically separated spatial antennas combined with frequency partitions to personalized transmit data among multiple cells. The third part including Chapters 7 and 8 considers a broadband wireless system and achieves parallel transmission among users in frequency domain by scheduling and allocating personalized resource.

To enhance system performance, Fig. 1.7 categorizes the degrees of freedom that we utilize in this dissertation. For Chapters 3, 4 and 5 related to the MIMO broadcast systems, we utilize multiuser diversity to enhance system performance in terms of sum-rate capacity and link reliability. For the network MIMO systems addressed in Chapter 6, we arrange frequency partition in different geographic allocations to enhance the received signal quality. As for the MIMO-OFDM systems, we execute scheduling and resource assignment by taking advantage of both multiuser diversity and frequency diversity to extend coverage region and assign resource among users in Chapters 7 and 8.

The remaining chapters of this dissertation are organized as follows. Chapter 2 introduces the background and related work about this dissertation. We also define the considered link performance metrics including link outage probability, link diversity order, and reliable coverage. In Chapter 3, we provide a quantitative comparison between the MIMO broadcast systems with transmit and receive based beamformings. In Chapter 4, we analyze the coverage performance of transmit based MIMO broadcast systems and show the soft coverage gain benefited from multiuser diversity. In the presence of estimation error at receiver end, Chapter 5 evaluates the performance of receive ZF based MIMO broadcast systems in

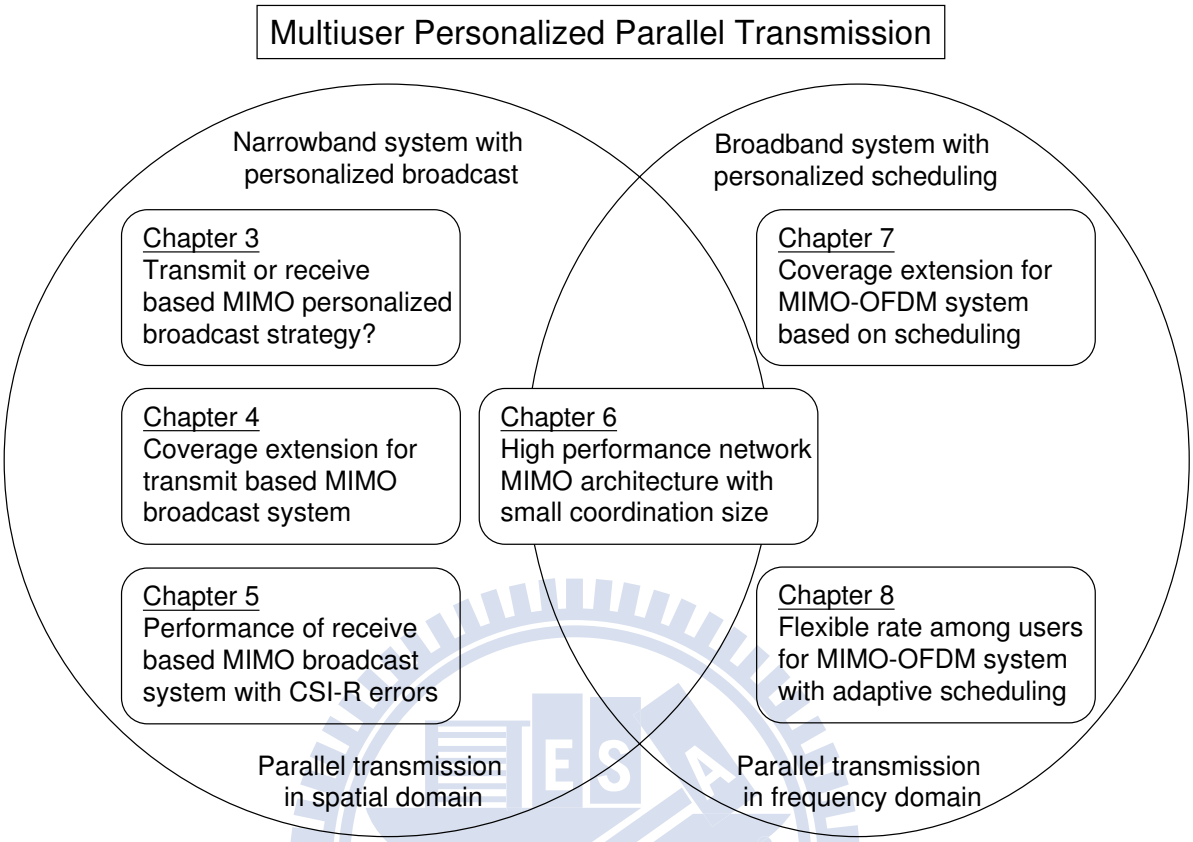

Figure 1.6: Chapter organization of the dissertation.

terms of link reliability, coverage and sum-rate capacity. Chapter 6 proposes a 3-cell FFR-based network MIMO architecture to reduce inter-cell interference in a multi-cellular system. Then, in Chapter 7, we show the potential gains on coverage enhancement for a spatial multiplexing based MIMO-OFDM system by suitable taking advantage of user diversity and frequency diversity. Continuous with Chapter 7, we propose link reliability enhanced based subchannel assignment algorithms and low-complexity power allocation method to flexible assign resource among served users of a spatial multiplexing based MIMO-OFDM system. Finally, we offer our concluding remarks and future work of this dissertation in Chapter 9.

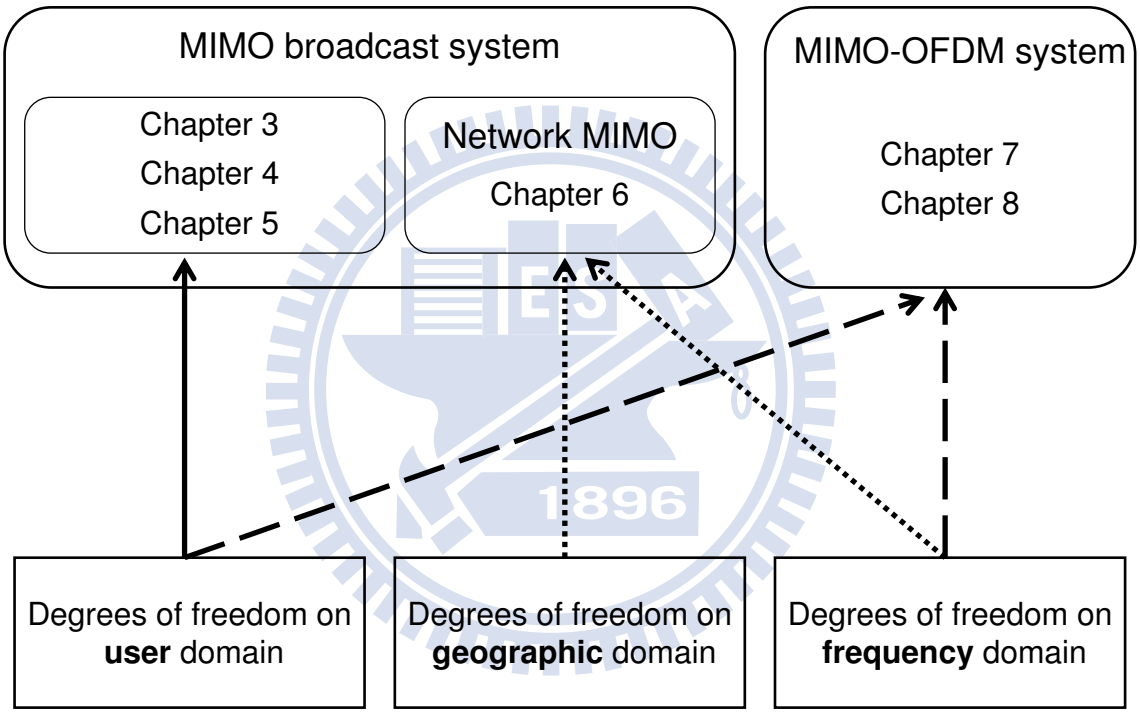

Figure 1.7: Exploited degrees of freedom in the dissertation.

Chapter 2

Background and Literature Survey

In this chapter, we briefly introduce the background of MIMO broadcast systems, multi-cell FFR and network MIMO systems, and spatial multiplexing based MIMO-OFDM system. Then we survey related works for the three considered topics in this dissertation. Finally, we define the link performance metrics, including link outage probability, link diversity order, and reliable coverage.

2.1 Background

Generally speaking, the new lines of research from multiuser MIMO broadcast systems are classified into three categories:

- First, rather than using the optimal DPC, the suboptimal but more practical MIMO broadcast schemes were proposed [4,27,46], such as the ZF-DPC, ZF beamforming, and orthogonal random beamforming. Because the DPC MIMO broadcast system faces the serious computation complexity issue, it requires huge amount of feedback information. These suboptimal schemes can asymptotically achieve the same throughput of DPC when the number of users approaches to the infinity.

- Second, another important research direction for MIMO broadcast systems is to investigate the impacts of limited CSI due to the finite-rate or erroneous CSI feedback [47–55]. In [48], it was shown that the feedback load per user must be scaled together with both the number of transmit antennas as well as the system SNR to achieve the full multiplexing gain with the near-perfect CSI.

- Third, MIMO broadcast transmission strategies were also applied to the multi-cellular scenario to cancel the inter-cell interference for improving spectral efficiency [17–21].

For the first category, two types of suboptimal MIMO broadcast systems were proposed in the literature: (1) the orthogonal random beamforming [46, 56–58] and (2) ZF based

beamforming [4].

- Firstly, recent research works regarding the orthogonal random beamforming for MIMO broadcast systems are briefly introduced as follows. In [46], it was proved that the orthogonal random beamforming strategy can asymptotically achieve the same throughput slope of DPC when the number of users increases. To solve the difficulty of calculating the random beamformer's weights for a large number of users, some low-complexity random beamformer approaches were proposed in [56–58].

- Secondly, we introduce the recent research results about the ZF-based beamforming for MIMO broadcast systems. In [4], a QR-based ZF-DPC MIMO broadcast system was proposed to maximize the sum rate of the MIMO broadcast system. Furthermore, the channel-inverse-based ZF beamforming was also proposed in [4], which is easier in calculating the beamforming weights than the ZF-DPC scheme. However, the effects of user selection and user ordering were not considered in [4], and the number of users is assumed to be smaller than that of transmit antennas. Thus, many researches aimed to relax this assumption and examine a more general MIMO broadcast system when the number of users is larger than the number of transmit antennas. The authors of [59] proposed a greedy user-selection procedure for the ZF-DPC MIMO broadcast systems. In [60], it was shown that the slope of throughput against SNR in dB for the greedy ZF-DPC MIMO broadcast system is the same as that for the capacity-achieving DPC strategy. In [28], it was proved that the channel-inverse-based transmit ZF beamforming combined with multiuser scheduling can asymptotically approach the capacity of the DPC-type MIMO broadcast system when the number of users approaches infinity. To overcome the prohibitively high complexity of exhaustively searching users, [28, 59–62] proposed low-complexity and effective user selection approaches for the MIMO broadcast systems.

Generally speaking, the objective of orthogonal random beamforming is to select a group of users to maximize their SINR according to partial CSI, whereas ZF-based beamforming is to nullify the mutual interference among users according to complete CSI.

For multi-cellular systems, the conventional widely-used inter-cell interference mitigation techniques are frequency reuse and FFR. The former scheme avoids utilizing the same fre-

quencies in the neighboring cells, while the later scheme allows universal frequency reuse for cell-center users. Conventional frequency reuse scheme yields lower spectrum utilization due to fewer available channels in each cell. To reduce the impact of frequency reuse on the throughput for each base station, the FFR scheme (or called reuse partition) assigns a larger frequency reuse factor for the cell-edge users and a smaller frequency reuse factor for the cell-center users. For example, Fig. 2.1 shows a conventional FFR planning in a cellular system with omni-cells [63]. The whole frequency band is partitioned into different zones, including the inner cell region with inner frequency band f_A and the outer cell region with outer frequency bands f_B. The outer frequency bands f_B is further partitioned into three subbands f_{B_1}, f_{B_2}, and f_{B_3}. Under this framework, signal quality at cell edge can be improved at the cost of lower spectrum usage. To maintain spectrum efficiency among each cell, FFR principle is applied to the case of a sectorized cellular system as shown in Fig. 2.2 [64]. Because the inter-cell interference problem in the orthogonal frequency division multiple access (OFDMA) multi-cellular systems is more serious than that in the code division multiple access (CDMA) systems, FFR once again becomes an important option for the next generation OFDMA broadband cellular mobile systems [63].

Clearly, combining the network MIMO and FFR techniques can have the advantages of complexity reduction and throughput enhancement. The joint FFR-based network MIMO system can execute the multi-base-station joint transmission only for the cell-edge users, and can apply the simple distance separation method for the cell-center users. Thus, the FFR-based network MIMO system can provide the sufficient SINR performance and avoid executing the joint multi-BS transmission at all time. Additionally, the universal frequency reuse for the cell-center users can improve the throughput due to higher trunking efficiency of the assigned channels. That is, the geographical locations of cells as well as mobiles now become another degree of freedom to be exploited for improving the performance of wireless systems. However, the study of network MIMO techniques on top of the FFR cellular system is rarely seen in the literature. Although both FFR and multi-base-station joint transmission are already considered for possible inter-cell interference cancelation techniques in the 3GPP LTE-A and the IEEE 802.16m WiMAX standards, to our knowledge, how to effectively integrate network MIMO with FFR is still an open issue.

In general, MIMO-OFDM systems can be classified into two types.

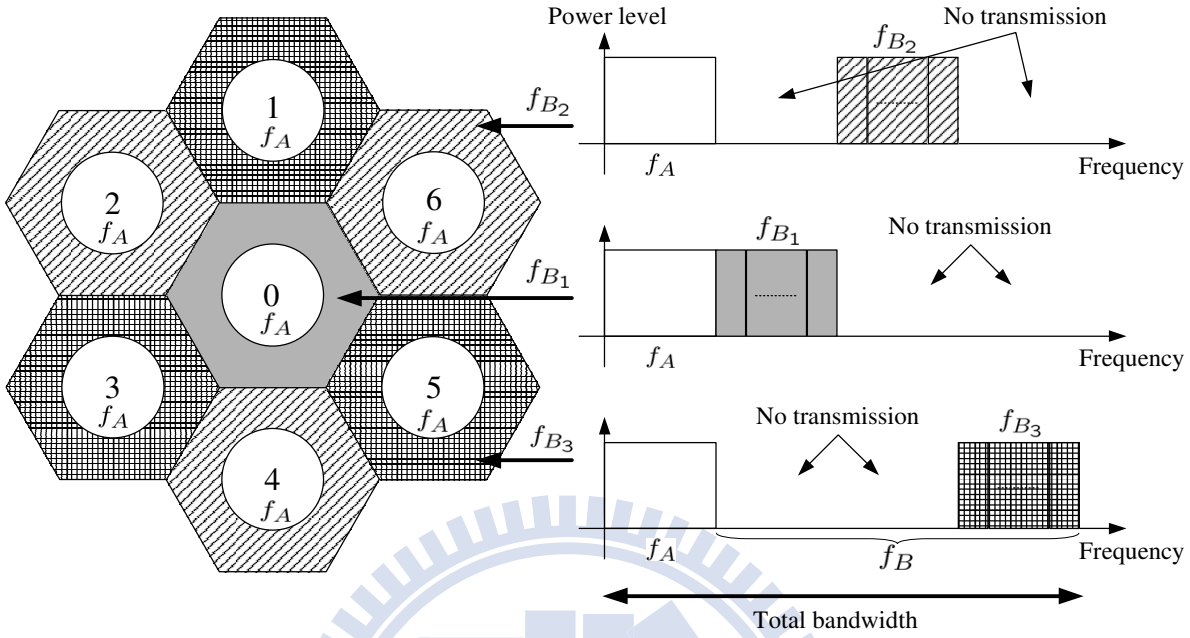

Figure 2.1: An example of FFR in a cellular system with omni-cells.

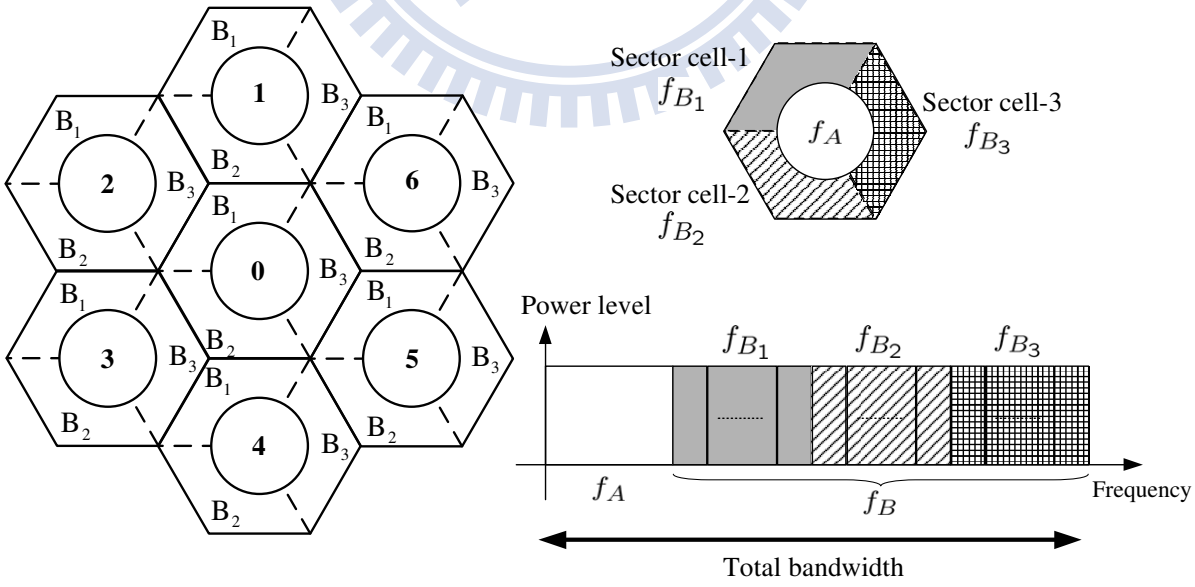

Figure 2.2: An example of FFR in a cellular system with sectorized cells.

- Diversity-based MIMO-OFDM systems: to improve link reliability by exploiting the spatial and frequency diversity gains without CSI at the transmitter [40–45].

- Multiplexing-based MIMO-OFDM systems: to increase capacity by exploiting multiplexing gain in the spatial domain [38]. The capacity of OFDM-based multiplexing-based MIMO systems was investigated in [38]. It was shown that MIMO frequency-selective fading channels can provide higher ergodic capacity and outage capacity than MIMO flat-fading channels when delay paths can increase the total angular spread. If perfect CSI is also available at both the transmitter and receiver, the singular value decomposition (SVD)-based MIMO-OFDM systems, can decouple the MIMO channel matrix and reduce the subchannel interference with the pre-processing and post-processing filters at the transmitter and receiver, respectively [65–68].

Compared with the diversity-based MIMO-OFDM systems, the spatial multiplexing based MIMO-OFDM systems have higher capacity in the inner region of a cell, but face more severe link reliability and coverage issues in the edge of cell. This is because diversity is deficient in the spatial multiplexing based MIMO system and the transmit power is split over multiple transmit antennas. In general, it is desirable to design a high-capacity wireless system with large coverage. In the literature, most MIMO-OFDM papers focus more on the capacity issue [38], [65–70] than the link quality improvement and coverage issues.

To improve coverage performance of MIMO-OFDM systems, a few approaches can be considered. The simplest way is to increase the transmit power. This approach is not desirable in general. The other approach is to design more powerful space-time codes or space-frequency codes with higher coding gain [45]. These kind of approaches are not suitable for the spatial multiplexing based MIMO-OFDM systems. Thus, we turn to exploit the user domain by developing an effective multiuser scheduling algorithm to improve the coverage performance of the spatial multiplexing based MIMO-OFDM systems.

Scheduling can enhance the performances of multiuser MIMO systems from different aspects [6, 26, 30, 59]. First, multiuser scheduling was designed to raise the sum-rate capacity of multiuser MIMO broadcast systems [6, 59]. Secondly, [30] showed that a max-min multiuser scheduling can enhance coverage as well as capacity for the spatial multiplexing based MIMO systems. Furthermore, multiuser scheduling integrated with the simple zero-

forcing MIMO receiver can approach the capacity of the optimal MIMO receiver [24–26]. Resource allocation for multiuser MIMO-OFDM systems is also an important research area because multiuser diversity, frequency diversity, and spatial diversity can be exploited simultaneously. Various scheduling algorithms for multiuser MIMO-OFDM systems were proposed for different objectives, including maximizing data rates [71–74] (for SISO-OFDM systems) [65–70] (for MIMO-OFDM systems) and minimizing transmit power [75–78]. However, to our knowledge, few radio resource management studies address the coverage issue for the spatial multiplexing based multiuser MIMO-OFDM systems.

2.2 Literature Survey

2.2.1 MIMO Broadcast Systems

In the following, we categorize the related work for the MIMO broadcast systems according to different beamforming types including transmit, receive, and joint transmit plus receive beamforming based MIMO broadcast systems.

- *MIMO broadcast systems with transmit beamforming:*

  In the literature, the sum rate analysis of the transmit MIMO broadcast systems for a large number of users has been studied extensively. It has been shown that the MIMO broadcast system using ZF beamforming [28] as well as the MIMO broadcast system using orthogonal random beamforming [46] can achieve the same asymptotic sum rate as that of DPC. For M_T transmit antennas and K users equipped with M_R receive antennas, using transmit beamforming and DPC can achieve the same $M_T \log\log(KM_R)$ scaling law for MIMO broadcast systems [6, 7]. Furthermore, [62] proposed a vector feedback mechanism using SVD and analyzed the sum rate of transmit ZF MIMO broadcast systems based on SVD vector feedback. [50] provided asymptotical sum rate analysis for transmit MIMO broadcast systems using the feedback-based scheduling architecture according to the quantized CSI, where a strong form of throughput optimality of the proposed MIMO broadcast system was demonstrated. Much of the above analysis has focused on the asymptotical sum rate of MIMO broadcast systems with user selection by the extreme value theorem, while [49] showed the asymptotic

sum rate for the finite large number of users. To our knowledge, however, the sum rate analysis for the transmit MIMO broadcast system for a small number of users has rarely seen.

Recently, the sum rate analysis of transmit MIMO broadcast system with respect to different feedback assumptions has become a hot research subject. [53] investigated the effect of imperfect received CSI on a ZF-based MIMO broadcast system with random user selection, and derive the capacity bound with analog or digital feedback information. Under the assumption of random user selection and equal power allocation the effects of delayed and quantized CSI on the sum rate of ZF-based MIMO broadcast systems were further analyzed in [54]. For the ZF-based receive beamforming implemented at the base station, [55] derived the asymptotic rate scaling with the uplink limited feedback system.

- *MIMO broadcast systems with receive beamforming:*

  Now let us discuss the receive beamforming MIMO broadcast systems. The concept of the receive ZF MIMO broadcast systems was first introduced in [24, 25] in which the term "independent stream scheduler" was used to describe a scheduler that allocates antennas in an independent manner. In [25], the authors demonstrated that the sum rate of the receive ZF MIMO broadcast systems scales with the same slope as the optimal DPC scheme when the number of users approaches infinity. For a finite number of users, a close-form sum rate expression was derived for the receive ZF MIMO broadcast systems based on equal power allocation [26]. The receive ZF MIMO broadcast systems only requires *vector* feedback for user selection [25, 79], whereas the transmit ZF MIMO broadcast systems requires channel matrix feedback or SVD-based vector feedback [62].

- *MIMO broadcast systems with joint transmit and receive beamforming:*

  Joint transmitter precoding and receiver processing is another method to broadcast personalized data in a point-to-multipoint scenario when multiple receive antennas are available. The BD joint transmitter and receiver beamforming approach consists of a precoding matrix for cancelling the inter-user interference and an equalizer matrix for cancelling the inter-antenna interference [80–84]. One key challenge for the BD-

Table 2.1: Literature survey for the MIMO broadcast systems.

	Tx	BD	Rx	Note
[3, 4]	∘	×	×	The concepts of DPC, ZF-DPC and ZF beamforming
[5–7]	∘	×	×	The gain of the broadcast systems over point-to-point transmission (scaling law)
[8–10]	∘	×	×	Theoretical capacity region of the MIMO broadcast systems
[28, 59–62]	∘	×	×	Scheduling algorithms and sum-rate performance evaluation and analysis
[47–55]	∘	×	×	The capacity and codebook/scheduling algorithms with limited feedback
[46, 56–58]	∘	×	×	The concept, scaling law, and design of orthogonal random beamforming
[27, 80–84]	×	∘	×	The concept, theoretical capacity, scheduling algorithms of BD
[24–26]	×	×	∘	The concept, scaling law, and sum-rate analysis ($M_R = M_T$ case)
Our work	∘	∘	◯	Effects of feedback channel variations (Chapter 3) Link performance analysis (Chapter 4) Effects of channel estimation errors for receive ZF beamforming (Chapter 5)

based precoder is its high complexity. Both the precoding matrix and the equalizer matrix are determined at the base station. Extra overhead is required to send the information of the equalizer matrix to serving users. The BD-based precoder also needs complete channel matrix information as the transmit ZF beamforming. In [81] an opportunistic user selection algorithm was proposed to select a group of users with the highest sum rate. Based on [81], two low-complexity user/antenna selection algorithms were proposed to select the number of data streams for each user adaptively and thus realize multi-mode transmissions [82]. Based on the search tree concept, [83] suggested an efficient search and scheduling algorithm. To reduce search space, [84] proposed a simplified user selection and receive antenna selection algorithm according to a spatial correlation threshold.

Table 2.1 shows the summary of literature survey for the MIMO broadcast systems, where "Tx", "Rx", and "BD" denote the MIMO broadcast systems with transmit beamforming (precoding), receive beamforming (equalizer), and block-diagonalization transmissions, respectively. The theoretical concept of point-to-multipoint MIMO transmissions was first appeared in [3] and the suboptimal solutions were proposed in [4]. [5–7] showed the gain of point-to-multipoint MIMO transmissions over point-to-point MIMO transmission is $\min\{M_T, K\}$ by scaling law. [8–10] derived the theoretical capacity region of the MIMO

broadcast systems by utilizing the duality of the downlink broadcast channel and uplink multiple access channel (MAC). For low-complexity suboptimal ZF-based transmit broadcast schemes, ZF-DPC and ZF beamforming, [28, 59–62] provided scheduling algorithms and performance evaluations to demonstrate the sum rate is achievable to optimal DPC as number of users is large. [46, 56–58] provided another suboptimal approach, orthogonal random beamforming, for concurrently broadcasting data. The concept of BD was proposed in [27] firstly. The authors in [80–84] provided theoretical capacity analysis and various scheduling algorithms to reduce implementation complexity. For realistic consideration, the limited feedback issue was extensively discussed in [47–55] in terms of performance evaluations and codebook/scheduling algorithms design. The concept of ZF receiver with independent scheduling across different antennas was first introduced in [24, 25]. The sum rate of the receive ZF beamforming with equal power allocation was derived in [26] in the case of $M_R = M_T$.

2.2.2 Network MIMO Systems

In the literature, the related work for the network MIMO techniques for downlink as well as uplink and the FFR techniques can be summarized as follows.

- *Coordination for downlink multicell MIMO transmission:*

  For downlink cellular networks, the concept of enhancing downlink capacity of a cellular system by the co-processing at transmitting end in a cellular system was proposed [21]. Also, [85] proposed a distributed multi-cell beamforming and analyzed its the performance based on Wyner's circular array model [86]. The coordinated strategies with grouped interior and edges users based on Wyner's circular array model were analyzed in [87]. The authors in [88] compared downlink network MIMO coordination with denser BS deployment. In [89] a BD scheme was used to form a cluster coordination in a multi-cellular system, including intra-and inter-cluster coordination, to enhance the sum rate and reduce the interference for the cluster-edge users, respectively. In [90], downlink coordination with limited distributed antenna arrays was compared to that with centralized antenna arrays. Under a fixed number of antennas per cell, [91] evaluated the impact of different number of sectors per cell, and the impact of the number

of coordinated cells.

- *Coordination for uplink multicell MIMO transmission:*

  The network MIMO technique has been also studied for the uplink case [92–96] . For the uplink network MIMO system, the coordinated base stations simultaneously receive the multiple users' signals within the area of the coordinated group of cells and suppress the mutual interference between users by means of coherent linear (received) beamforming across BS. An important issue in uplink network MIMO is which base stations shall be cooperated. The authors in [94] provided dynamic base station clustering approach for uplink base stations coordination which resulted in significant sum rate gain compared to the static base station clustering schemes proposed in [95, 96]. Additionally, the issue of how to select a subset of users for jointly coordinated detection to reduce the burden of backhaul was addressed in [92]. It proposed an isolation-based user grouping algorithm to optimize system capacity under a strongly constrained backhaul between seven-coordinated cells, which was also modified to downlink scenario for capacity improvement under a limited backhaul [93].

- *Applications of FFR in OFDMA systems:*

  The recent researches on FFR were mostly related to the OFDMA systems [64, 97–101]. The outage capacity performance of an FFR-based OFDMA cellular system with proportional fair scheduling was studied in [97]. The joint effects of the FFR system parameters, the interior region, and the bandwidth assignment on cell throughput was formulated as an optimization problem in [98]. The resource allocation problem in an FFR-based multi-cell OFDMA system was translated to a graph-coloring problem in [99]. The concept of FFR can be also applied to a tri-sector cellular system [64]. For example, [100] considered the FFR-based tri-sector cellular OFDMA system and showed that the inter-cell interference can be reduced and cell throughput is improved as well by the proposed subcarrier scheduling algorithms. Under similar FFR-based tri-sector cellular OFDMA systems, [101] proposed an interference mitigation scheme by combining partial reuse and soft handover.

In Table 2.2, we list the literature for inter-cell interference cancellation by FFR or network MIMO, where "DL" represents downlink and "UL" represents uplink. In the past,

Table 2.2: Literature survey for the network MIMO systems.

	Using FFR?	Sector or omni?	Network MIMO?	DL or UL?	Note
[97–99]	∘	omni	×	DL	Scheduling and interior region design
[100, 101]	∘	sector	×	DL	SINR improvement by FFR combined with sectoring cells
[17–21]	×	omni	∘	DL	The concept of joint multi-base stations coordination
[85, 87]	×	circular	∘	DL	Performance analysis based on Wyners circular cell array model
[89]	×	omni	∘	DL	BD-based network MIMO design and performance evaluation
[90, 91]	×	sector	∘	DL	Effects of number of sectors per cell in a network MIMO system
[92–96]	×	omni	∘	UL	Coordinated cell partners and users selection in uplink case
[15, 16]	allow	sector	allow	DL/UL	Joint multi-base stations coordinated transmissions: CoMP in LTE-A and CoMIMO in IEEE 802.16m standards
Our work	◯	sector	◯	DL	Design a 3-cell network MIMO system with FFR tri-sector cells

we utilized FFR to reduce inter-cell interference in omni- or sectoring cells [97–101]. The idea of jointly multi-base stations coordinated transmissions creates a new way to deal with the interference issue in a cellular system. Particularly, the two schemes, FFR and network MIMO, are probably feasible candidates for inter-cell interference cancellation in next generation wireless systems, e.g. LTE-A and IEEE 802.16m WiMAX. In this dissertation, we will provide a 3-cell network MIMO architecture combined with FFR in tri-sector cells to reduce the complexity of cells coordination and maintain the spectral usage in each cell.

2.2.3 MIMO-OFDM Systems

Resource allocation is an important issue for multiuser OFDM systems due to an large amount of available frequency resources. The related work for resource allocation of multiuser OFDM systems is categorized into SISO-OFDM systems and MIMO-OFDM systems.

- *Resource allocation in the multiuser OFDM systems:*

  In the past, a amount of works have concentrated on adaptive resource allocation for multiuser OFDM systems in the scenario of SISO architecture [71–76]. [71] described a fair resource allocation trough maximizing the minimum rate among users under the assumption all users achieve a similar rate. Then it proposed a low-complexity sub-optimal subchannel allocation algorithm which performs almost as well as the optimal

solution. In [73], the fairness was extended to incorporate different priorities. Instead of maximizing the minimum user's rate, the total capacity was maximized subject to proportional user's rate requirement. [74] modified the subchannel and power allocation algorithm proposed in [73] to enable a non-iterative linear power allocation instead of the nonlinear method proposed in [73].

- *Resource allocation in the multiuser MIMO-OFDM systems:*

  Recently research of resource allocation strategy for downlink multiuser OFDM environments based on spatial multiplexing becomes popular [68–70, 77, 78, 102, 103]. Spatial multiplexing based MIMO-OFDM is one of the categories of MIMO-OFDM techniques. The main goal of spatial multiplexing based MIMO-OFDM technique is to increase capacity by exploiting multiplexing gain in the spatial domain, i.e. transmitting independent data streams across antennas and tones. [69] derived the optimal subchannel allocation criterion and the optimal power loading criterion for downlink MIMO-OFDM systems. Two suboptimal subchannel allocation schemes, product-criterion and sum-criterion, were also proposed to be used in high and low SNR regions, respectively. [70] proposed a low-complexity suboptimal subchannel allocation scheme and driven a lower bound on the system capacity and an upper bound on the BER when using ZF and minimum mean square error (MMSE) receivers. For SVD-based MIMO-OFDM systems, [78] proposed adaptive power allocation algorithm based on convex optimization theory to minimize the total transmit power while satisfying users' target rates. In [68], a three-step algorithm based QR decomposition was proposed to adaptively allocate power, bandwidth, and antennas among users to maximize capacity under fairness constraint. In the presence of imperfect CSI, [102] utilized adaptive beamforming combined with proposed power allocation and subchannel allocation to improve the reduced BER performance caused by channel estimation errors. By exploiting the stationary ergodicity of subchannel amplitudes, [103] proposed an adaptive transmission algorithm to reduce the complexity of subchannel assignment.

Finally, we summarize the literature survey of resource allocation for OFDM based systems in Table 2.3.

Table 2.3: Literature survey for the MIMO-OFDM systems.

	Minimize Tx power	Maximize Capacity	Rate fairness	Enhance link quality	Note
[75–78]	∘	×	×	×	Subchannel assignment and power allocation
[69–72]	×	∘	×	×	Subchannel assignment only
[73, 74]	×	∘	∘	×	Subchannel assignment and power allocation for SISO-OFDM systems
[65–68]	×	∘	×	×	SVD and QR based MIMO-OFDM design
[41–45]	×	×	×	∘	Space-frequency coding for diversity enhancement
Our work	×	◯ Chapter 8	◯ Chapter 8	◯ Chapters 7, 8	Subchannel assignment (scheduling) and power allocation for MIMO-OFDM systems

2.3 Performance Metrics

2.3.1 Link Outage Probability

The link outage probability reflects how reliably a system can support the corresponding link quality. For a **SISO** system, a common definition of link outage is the probability that the effective out SNR γ being less than a predetermined value γ_{th}, that is, $P_{\text{out}} = P_r\{\gamma < \gamma_{th}\}$ [104]. For different MIMO transmission scenarios considered in this dissertation, the definitions of link outage can be listed as

- **Point-to-point spatial multiplexing MIMO system**: With all the eigenmodes of the spatial multiplexing MIMO system are used for parallel independent data transmissions, the link outage for the point-to-point spatial multiplexing MIMO system can be defined as the event when the receive effective output SNR of any substream is less than γ_{th}. That is, for a MIMO system with M eigenmodes in the ascending order,

$$\begin{aligned} P_{\text{out}} &= P_r\{\gamma_1 < \gamma_{th} \cup \gamma_2 < \gamma_{th} \cdots \cup \gamma_M < \gamma_{th}\} \\ &= 1 - P_r\left\{\min_{\forall i}\{\gamma_i\} = \gamma_1 \geq \gamma_{th}\right\} \\ &= P_r\{\gamma_1 < \gamma_{th}\} \ . \end{aligned} \tag{2.1}$$

  Therefore, the weakest substream with the lowest SNR in the point-to-point spatial multiplexing MIMO system dominates the outage probability performance since the

weakest substream is most likely to incur transmission errors.

- **Point-to-point spatial multiplexing MIMO-OFDM system**: For a spatial multiplexing based MIMO-OFDM system in a frequency-selective fading channel, each flat-faded subchannel executes point-to-point transmission. As a result, the system can be viewed as the sum of flat-fading MIMO channels. Therefore, we consider the average weakest eigenmode over a series of N MIMO flat-faded subchannels with the definition of link outage probability:

$$P_{\text{out}} = P_r \left(\frac{1}{N} \sum_{n=1}^{N} \gamma_{n,1} \leq \gamma_{th} \right) , \tag{2.2}$$

  where $\gamma_{n,1}$ represents the effective output SNR of the weakest substream in subchannel n corresponding for $n = 1, \ldots, N$.

- **Point-to-multipoint spatial multiplexing MIMO broadcast system**: Different from point-to-point scenario, the point-to-multipoint MIMO broadcast systems can transmit personal data to different user terminals simultaneously. Therefore, all the data links serve different separated users results in many individual SISO links. For a MIMO broadcast system with M transmission links, we define the link outage probability of the i-th link the same as in the SISO case, i.e. $P_{\text{out}}^{i} = P_r\{\gamma_i < \gamma_{th}\}$ for $i = 1, \ldots, M$.

2.3.2 Diversity Order

Let link outage probability $P_{\text{out}}(\cdot)$ be a function of SNR. Then, the link diversity order D_{order} is defined as [105]

$$D_{\text{order}} \triangleq - \lim_{\rho \to \infty} \frac{\log P_{\text{out}}(\rho)}{\log \rho} , \tag{2.3}$$

where ρ is the receive SNR. The metric can provide an intuitional observation on link performance.

2.3.3 Reliable Coverage

Referring to the link outage probability P_{out}, we further define $(1 - P_{\text{out}})$ as the link coverage reliability for its corresponding link radius associated with the required SNR as shown in Fig.

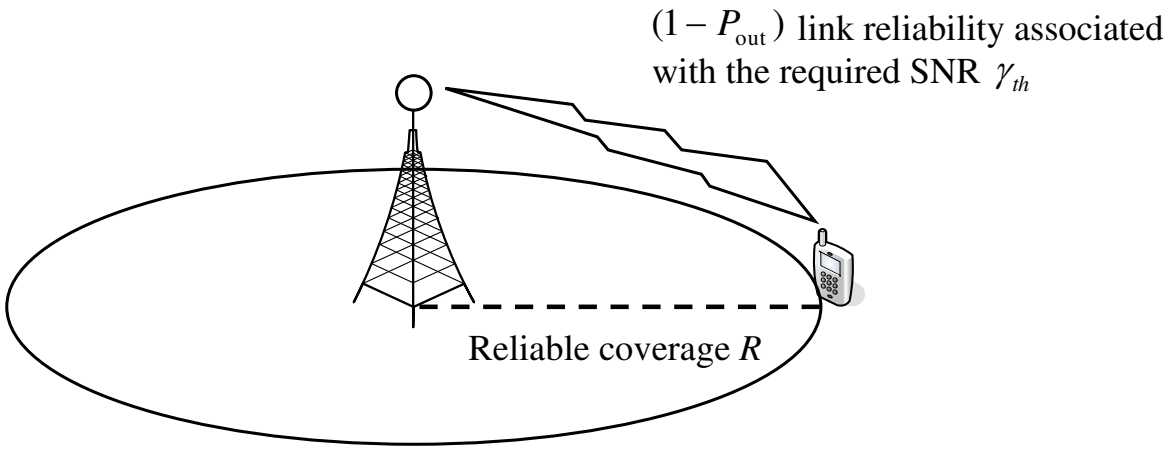

Figure 2.3: Illustration of link reliability and reliable coverage.

2.3. Specifically, for link coverage reliability $(1 - P_{\text{out}})$, it means that the probability of the effective output SNR being higher than γ_{th} is no less than $(1-P_{\text{out}})$. For example, by writing (2.1) as $P_r\{\gamma_1 \geq \gamma_{th}\} = 1 - P_{\text{out}}$, (2.1) can be also interpreted as that all the receive SNR in substreams of the MIMO system are required to be greater than γ_{th} with the probability of $(1 - P_{\text{out}})$. Therefore, the link radius associated with the required SNR and $(1 - P_{\text{out}})$ reliability is defined as the **reliable coverage**. Typically, 90% link reliability is required for most wireless systems. In Chapters 4 5 7, we will relate P_{out} to the corresponding reliable cell coverage.

Chapter 3

Beamforming Techniques for Multiuser MIMO Broadcast Systems

In this chapter, we present an approximation formula and the close-form expression for the sum rate of the transmit and the receive ZF MIMO broadcast systems with user selection, respectively. Instead of assuming a large number of users to obtain a scaling law as most current work, we derive the sum rate formulas of the ZF MIMO broadcast systems with a small number of scheduled users. By analysis and simulations, we find that when taking the variations of feedback channel into account, the receive ZF MIMO broadcast system is more robust to feedback errors and can deliver equal or even higher sum rate than the transmit ZF MIMO broadcast system. We discuss whether a feedback channel is suitable to send CSI for calculating transmit antenna beamforming weights, or suitable to send CSI for selecting users in the receive ZF MIMO broadcast system. Our results show that as the variation of feedback channel errors increases from 0.5 to 1.5, the receive ZF 3×3 MIMO broadcast system can provide 36% to 116% higher sum rate than the transmit ZF 3×3 MIMO broadcast system in the case of 20 users at SNR equal to 20 dB. Providing that more feedback bandwidth and an error-free feedback channel are available, the transmit ZF MIMO broadcast system can achieve higher sum rate than the receive ZF MIMO broadcast system.

3.1 Background

We consider a multiuser MIMO broadcast system with an M_T- transmit-antenna base station and K users each of which has M_R receive antennas as shown in Fig. 1.3. The base station is designed to transmit different data streams up to M_T users simultaneously. For handling the inter-user interference in the multiuser MIMO broadcast systems, beamforming can be implemented at either the transmitter side or the receiver side.

3.1.1 Transmit ZF Beamforming of MIMO Systems

The transmit ZF beamforming multiples the beamforming weights at the transmitter to decouple the MIMO channel matrix $\mathbf{H}$ into parallel subchannels. Based on the ZF principle, the beamforming matrix is written as $\mathbf{W} = \mathbf{H}(\mathcal{S})^H(\mathbf{H}(\mathcal{S})\mathbf{H}(\mathcal{S})^H)^{-1}$, where $\mathcal{S}$ represents the subset of the total receive antennas $\mathcal{U}$, and $(\cdot)^H$ represents the conjugate transpose operation. Note that $|\mathcal{U}| = KM_R$ and $|\mathcal{S}| = M_T$. Then, the received signal vector becomes

$$\begin{aligned} \mathbf{y} &= \mathbf{H}(\mathcal{S})\mathbf{W}\mathbf{x} + \mathbf{n} \\ &= \mathbf{H}(\mathcal{S})\mathbf{H}(\mathcal{S})^H(\mathbf{H}(\mathcal{S})\mathbf{H}(\mathcal{S})^H)^{-1}\mathbf{x} + \mathbf{n} = \mathbf{x} + \mathbf{n} \ , \end{aligned} \tag{3.1}$$

where $\mathbf{x}$ is the transmit vector, $\mathbf{n} \in \mathbb{C}^{M_T \times 1}$ is the circularly complex additive white Gaussian noise vector with covariance matrix $\mathrm{E}[\mathbf{n}\mathbf{n}^H] = \sigma^2\mathbf{I}$. According to [4], the sum rate of the transmit ZF-based MIMO broadcast system is given by

$$C_{\mathrm{TZF}}(\mathcal{S}) = \sum_{i \in \mathcal{S}} [\log(\varsigma b_i)]_+ \ , \tag{3.2}$$

where ς is the water-level satisfying the criterion $\sum_{i\in\mathcal{S}} \left[\varsigma - \frac{1}{b_i}\right]_+ = P_T$, $[z]_+$ represents $\max\{z, 0\}$, and the effective channel gain b_i of the i-th subchannel is

$$b_i = \frac{1}{\left[\left(\mathbf{H}(\mathcal{S})\mathbf{H}(\mathcal{S})^H\right)^{-1}\right]_{ii}} \ . \tag{3.3}$$

Here $[\mathbf{A}]_{ij}$ denotes the (i, j) entry of the matrix $\mathbf{A}$. Note that the transmit ZF beamforming weighting matrix $\mathbf{W} = \mathbf{H}(\mathcal{S})^H(\mathbf{H}(\mathcal{S})\mathbf{H}(\mathcal{S})^H)^{-1}$ leads to higher transmission power equivalent to the noise enhancement effect of the receive ZF beamforming.

3.1.2 Receive ZF Beamforming of MIMO Systems

With ZF algorithm implemented at the receiver end, data streams can be independently decoded to recover the spatially multiplexed signals. For a certain user terminal k, by multiplying received signal $\mathbf{y}_k$ with the pseudo-inverse $\mathbf{H}_k^\dagger = (\mathbf{H}_k^H\mathbf{H})_k^{-1}\mathbf{H}_k^H$, the decoded received signal $\hat{\mathbf{y}}_k$ becomes

$$\hat{\mathbf{y}}_k = \mathbf{H}_k^\dagger\mathbf{y}_k = \mathbf{x} + \mathbf{H}_k^\dagger\mathbf{n}_k \ . \tag{3.4}$$

The noise covariance matrix after the ZF receiver becomes $\sigma^2[(\mathbf{H}_k^H\mathbf{H}_k)^{-1}]^H$, which may have nonzero off-diagonal elements and results in correlated noise across different data streams. To lower complexity, the noise correlation is usually ignored and each stream is decoded independently [24, 106]. With the noise power per subchannel $\sigma^2[(\mathbf{H}_k^H\mathbf{H}_k)^{-1}]_{ii}$, the equal power principle results in the output SNR at the i-th subchannel for user terminal k as

$$\gamma_i^k = \frac{P_T}{M_T\sigma^2\left[(\mathbf{H}_k^H\mathbf{H}_k)^{-1}\right]_{ii}} \quad , \quad i = 1, \cdots, M_T \tag{3.5}$$

where $q_i = 1/\left[\left(\mathbf{H}_k^H\mathbf{H}_k\right)^{-1}\right]_{ii}$ is defined as the effective channel gain of the i-th subchannel [25]. Because $\{q_i\}_{i=1}^{M_T}$ are characterized as Chi-square distributed random variables with $2(M_R - M_T + 1)$ degrees of freedom [26, 106, 107], the probability distribution function (PDF) of q_i is

$$f_{q_i}(q) = \frac{q^{M_R-M_T}e^{-q}}{(M_R - M_T)!} \quad , \quad \text{for } i = 1, \ldots, M_T \ . \tag{3.6}$$

3.1.3 Sum Rate with Long-Term Power Constraint

Let ς_0 be the solution of the water-filling equation for the long-term power constraint

$$E\left[\sum_{i=1}^{M_T}[\varsigma - \frac{1}{z_i}]_+\right] = \sum_{i=1}^{M_T} E\left[\varsigma - \frac{1}{z_i}\right]_+ = P_T \ . \tag{3.7}$$

Subject to this long-term power constraint with water-level solution ς_0, the average sum rate with the water-filling power allocation is

$$\begin{aligned} C_{\text{sum rate}} &= E\left[\sum_{i=1}^{M_T}[\log(\varsigma_0 z_i)]_+\right] \\ &= \sum_{i=1}^{M_T} E\left[\log(\varsigma_0 z_i)\right]_+ \\ &= \sum_{i=1}^{M_T}\int_{1/\varsigma_0}^{\infty}\log(\varsigma_0 z) f_{z_i}(z)dz \ , \end{aligned} \tag{3.8}$$

where $f_{z_i}(z)$ represents the PDF of effective channel gain z_i for the transmit ZF beamforming or receive ZF beamforming.

3.2 Scheduling for Transmit ZF Beamforming

Because the number of users (K) is usually larger than the number of transmit antennas (M_T), scheduling is necessary for the transmit MIMO broadcast systems to select M_T receive antennas out of KM_R antennas. Scheduling can exploit the multiuser diversity gain for the transmit ZF-based MIMO broadcast system. For large K, the sum rate of the transmit ZF-based MIMO broadcast system can asymptotically achieve the sum rate of DPC (denoted by C_{DPC}) in slope [28], that is,

$$E[C_{\text{TZF}}] \sim M_T \log\left(1 + \frac{P_T}{M_T} \log \sum_{k=1}^{K} M_R^k\right) \sim E[C_{\text{DPC}}] \ , \tag{3.9}$$

where M_R^k denotes the number of receive antennas of the kth user. Note that we consider the case where all users have the same number of receive antennas. A stronger convergence result was shown in [108]

$$\lim_{K\to\infty} (C_{\text{DPC}} - C_{\text{TZF}}) = 0 \ . \tag{3.10}$$

The maximal sum rate scheduling algorithm selects the user set according to

$$C_{\text{TZF}}^{\max} = \max_{\mathcal{S}\subset\mathcal{U}:\ |\mathcal{S}|=M_T} C_{\text{TZF}}(\mathcal{S}) \ . \tag{3.11}$$

For the case $M_R = 1$, this combinatorial optimization problem is to select the best one from $\binom{K}{M_T}$ combinations. The closed-form expression for the sum rate of transmit ZF-based MIMO broadcast systems is not easy to obtain. One of the goals in this chapter is to develop an estimation approach to analyze the sum rate of the downlink transmit ZF-based MIMO broadcast systems.

3.2.1 Sum Rate Estimation with Exhaustively Searched Users

First we reformulate the transmit ZF-based MIMO broadcast system into the point-to-point MIMO scheduling system. Specifically, a transmit ZF-based MIMO broadcast system with M_T transmit antennas at the base station and K users with single antenna is translated into a receive ZF MIMO system with M_T transmit antennas at the base station and M_T receive antennas, as shown in Fig. 3.1. In (3.11), exhaustive search in a transmit ZF-based MIMO broadcast system selects the best M_T antennas from K users. Thus, each of the $\binom{K}{M_T}$

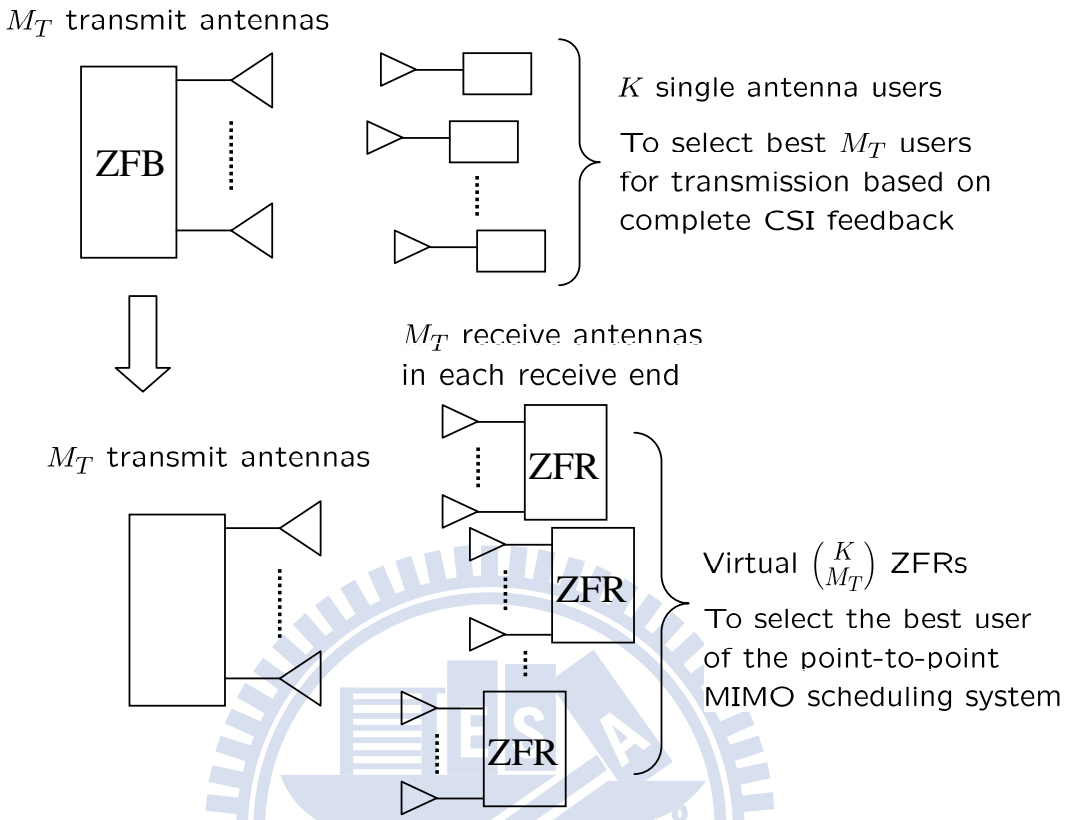

Figure 3.1: The modified problem model for the transmit ZF beamforming with the exhaustive-search based scheduling.

combinations can be viewed as a virtual receive ZF MIMO user with M_T antennas. As a result, the sum rate of the transmit ZF-based MIMO broadcast system with exhaustive user search can be approximated by the receive ZF MIMO system with one user at a time using TDMA scheduling. This approximation will be considered in two scenarios, both of which can lead to the closed-form sum rate performance and will be verified by simulations later.

- In the low SNR region, because of the property of the logarithm function $\log_2(1+x) \approx x \log_2 e$ for $x \approx 0$, the ideal policy for achieving the maximal sum rate for the point-to-point TDMA-based scheduling is to find a user having the maximal strongest subchannel and to allocate all the power only to the strongest subchannel. This principle coincides with the max-max scheduling scheme. That is, a user with the best effective channel gain will be selected most likely.

- In the high SNR region, the property of the logarithm function is $\log_2(1+x) \approx \log_2 x$ for $x \gg 1$. Therefore, improving all subchannels with suitable scheduling gains and corresponding power will yield the maximal sum rate. It is implied that no subchannel will be omitted in each scheduling run. From [30] and [109], the max-min scheduling scheme can uniformly provide the scheduling gains to all subchannels and deliver the maximal sum rate approximately. Thus, we use the max-min scheduling to approximate the sum rate of the transmit ZF-based MIMO broadcast system in the high SNR region.

In [26], the *order statistics* analysis techniques were applied to derive the closed-form expression for the sum-rate capacity of the point-to-point MIMO system with ZF receiver based on the max-max and max-min scheduling. From the above discussions, we present the approximate sum-rate estimations of the transmit ZF-based MIMO broadcast system as follows.

Low SNR Region (Max-Max Approach)

The max-max scheduling algorithm selects the target user with the maximal strongest subchannel among virtual $\binom{K}{M_T}$ users at each time slot. Denote $\{b_i^k\}_{i=1}^{M_T}$ as the set of all subchannel effective channel gains for the kth virtual user ($k = 1, \ldots, Z = \binom{K}{M_T}$) and $b_{1:M_T}^k \leq \ldots \leq b_{M_T:M_T}^k$ as the ordered effective channel gains in ascending order of magnitude. With the information of $\{b_{M_T:M_T}^k\}_{k=1}^{Z}$ from all users, the transmitter chooses the target user according to

$$k^* = \arg\max_k b_{M_T:M_T}^k \quad . \tag{3.12}$$

After determining the target user k^*, we have $\tilde{b}_{i:M_T}^{\max} = b_{i:M_T}^{k^*}$ for $i = 1, \ldots, M_T$ where the superscript *max* denotes the max-max approach. Based on the order statistics analysis proposed in [30], we can obtain the PDFs of $\{\tilde{b}_{i:M_T}^{\max}\}_{i=1}^{M_T}$ as follows:

$$f_{\tilde{b}_{M_T:M_T}^{\max}}(b_{M_T}) = Z M_T \, e^{-b_{M_T}} \left(1 - e^{-b_{M_T}}\right)^{Z M_T - 1} \quad , \tag{3.13}$$

and

$$f_{\tilde{b}^{\max}_{i:M_T}}(b_i)$$
$$= \frac{ZM_T(M_T-1)!}{(i-1)!(M_T-i-1)!}\sum_{a_1=0}^{i-1}\binom{i-1}{a_1}\sum_{a_2=0}^{M_T(Z-1)}\binom{M_T(Z-1)}{a_2}$$
$$e^{-(a_1+a_2+1+M_T-i)b_i}\sum_{a_3=0}^{M_T-i-1}\binom{M_T-i-1}{a_3}\frac{(-1)^{a_1+a_2+a_3}}{a_2+a_3+1} \quad . \tag{3.14}$$

From (3.13) and (3.14), we have all the PDFs of $\tilde{b}^{\max}_{i:M_T}$ for $i = 1, \cdots, M_T$. Applying (3.13) and (3.14) to (3.8) and (3.7), we can obtain the sum rate and long-term power constraint equation, respectively.

High SNR Region (Max-Min Approach)

Unlike the max-max scheme, the max-min scheduling selects the target user according to the maximal weakest subchannel among virtual Z users. Based on the information of $\{b^k_{1:M_T}\}_{k=1}^{Z}$, the base station arranges the transmission during each time slot according to

$$k^* = \arg\max_k b^k_{1:M_T} \quad . \tag{3.15}$$

Once the target user k^* is selected, we have $\tilde{b}^{\min}_{i:M_T} = b^{k^*}_{i:M_T}$ for $i = 1, \ldots, M_T$ where the superscript *min* indicates the max-min scheduling. Similarly, we can get the PDFs of $\{\tilde{b}^{\min}_{i:M_T}\}_{i=1}^{M_T}$ based on the analysis in [30] as follows:

$$f_{\tilde{b}^{\min}_{1:M_T}}(b_1) = ZM_T\, e^{-b_1 M_T}\left(1-e^{-b_1 M_T}\right)^{Z-1} \quad , \tag{3.16}$$

and

$$f_{\tilde{b}^{\min}_{i:M_T}}(b_i)$$
$$= \frac{ZM_T\prod_{j=2}^{i}(M_T-j+1)}{(i-2)!}\sum_{a_1=0}^{Z-1}\sum_{a_2=2}^{i}(-1)^{i+a_1+a_2}\binom{Z-1}{a_1}$$
$$\binom{i-2}{a_2-2}\frac{\left[e^{-b_i(M_T-a_2+1)}-e^{-b_i(M_T+a_1M_T)}\right]}{(M_Ta_1+a_2-1)} \quad . \tag{3.17}$$

With all the PDFs of $\{\tilde{b}^{\min}_{i:M_T}\}_{i=1}^{M_T}$, we can obtain the sum rate by substituting (3.16) and (3.17) into (3.8) and the long-term power constraint (3.7).

3.2.2 Sum Rate Analysis with Randomly Searched Users

To compare with the transmit ZF scheduler[1] with exhaustively searched users, the sum rate of the transmit ZF-based MIMO broadcast system with randomly searched user is also provided. The random user selection is also called the round robin (RR) scheduling policy, which selects users in turn and does not exploit the multiuser diversity gain. The average sum rate of the transmit ZF-based MIMO broadcast system with randomly selected user is given by

$$\begin{aligned} C_{\text{TZF}} &= \sum_{i=1}^{M_T} E\left[\log(\varsigma_0 b_i)\right]_+ \\ &= M_T \int_{1/\varsigma_0}^{\infty} \log(\varsigma_0 z) e^{-z} dz = M_T \Gamma\left(0, \frac{1}{\varsigma_0}\right) \quad , \end{aligned} \tag{3.18}$$

where $\Gamma(a,x) = \int_x^\infty t^{a-1}e^{-t}dt$ is the incomplete gamma function [110] and ς_0 is the water-level solution satisfying the following long-term water-filling equation:

$$\begin{aligned} \sum_{i=1}^{M_T} E\left[\mu - \frac{1}{b_i}\right]_+ &= M_T \int_{1/\varsigma}^{\infty} \left(\varsigma - \frac{1}{z}\right) e^{-z} dz \\ &= M_T \left(\varsigma e^{-1/\varsigma} - \Gamma\left(0, \frac{1}{\varsigma}\right)\right) = \quad P_T \ . \end{aligned} \tag{3.19}$$

With ς_0 the average sum rate in (3.18) becomes $M_T \varsigma_0 e^{-1/\varsigma_0} - P_T$.

3.2.3 Scheduling for Transmit ZF Beamforming with Multiple Receive Antennas

In Section 3.2.1 and Section 3.2.2, the sum rate formulas of the transmit ZF-based MIMO broadcast system with exhaustive and random user selection are derived for the case when a user has one single receive antenna. For $M_R > 1$, the analysis in Section 3.2.1 and Section 3.2.2 can also be extended by treating each antenna as a virtual user. That is, there are total KM_R virtual users, each of which has one single receive antenna.

Although the sum rate analysis for the transmit ZF-based MIMO broadcast system with exhaustive user selection has been discussed in Section 3.2.1, the exhaustive search algorithm

[1] As mentioned in Chapter 1, we call the transmit and receive ZF MIMO broadcast systems combined with multiuser scheduling as respectively the transmit ZF scheduler and receive ZF scheduler in this chapter.

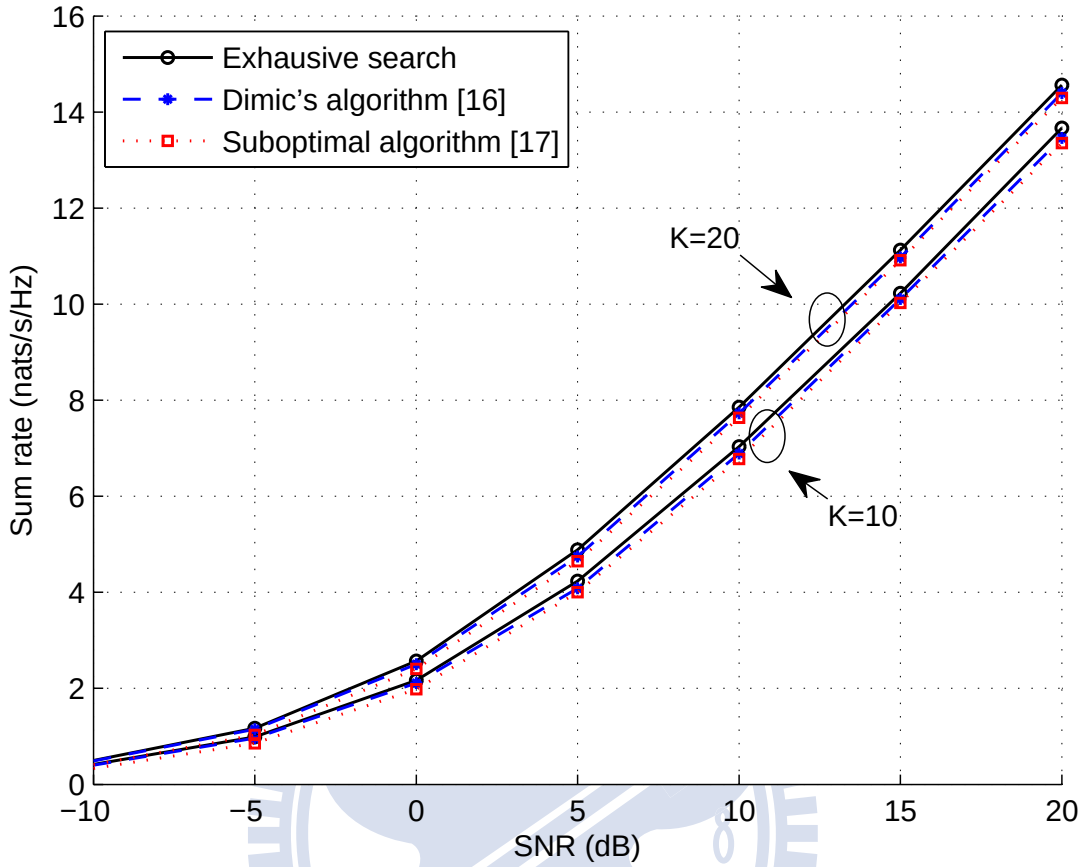

Figure 3.2: Sum rate of the transmit ZF beamforming with the exhaustive-search based scheduling and the suboptimal scheduling algorithms when $K = 10, 20$ users, $M_T = 3$ and $M_R = 1$.

with large K may not be practical because of the huge search space $\binom{KM_R}{M_T}$. Low-complexity suboptimal user selection algorithms were proposed for the transmit ZF-based MIMO broadcast system [28,60,61]. In this chapter, we extend the algorithm of [61] to the case with user terminals having multiple receive antennas. Figure 3.2 shows the sum rates of the transmit ZF-based MIMO broadcast system using various user selection algorithms, including the exhaustive search and the suboptimal algorithms proposed in [60,61]. One can see that both suboptimal algorithms approach the same sum rate as the exhaustive user search.

The user scheduling algorithm extended from [61] is briefly explained as follows. First, the scheduler selects a user with the best channel quality. Next, the second user is selected so that the signal vectors of the two user are nearly orthogonal. Repeat this procedure until

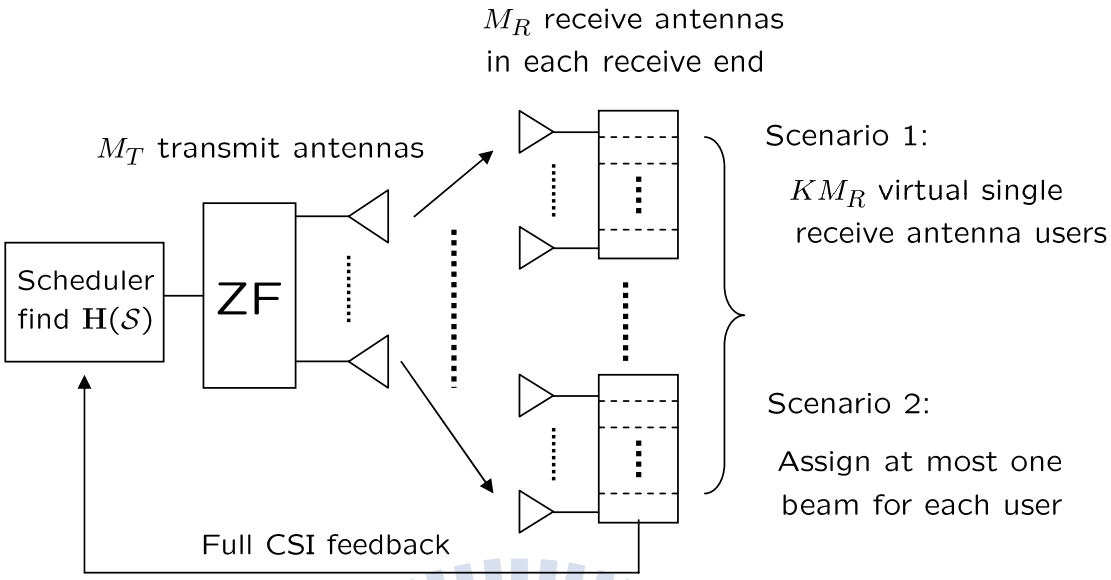

Figure 3.3: Diagram of the transmit ZF beamforming with scheduling (or the transmit ZF scheduler) when multiple receive antennas are available.

all the M_T selected signal vectors are nearly orthogonal. We consider the following two scenarios for selecting receive antenna.

1. Scenario 1 (*users have multiple data streams*): In this case, we have KM_R virtual users each of which is equipped with one single receive antenna as shown in Fig. 3.3.

2. Scenario 2 (*users have at most one data stream*): Referring to Fig. 3.3, this scenario is to prevent unfairness when some users have good channel quality in the short term.

The scheduling algorithm for the first scenario is described as:

- Step 0: Denote the individual channel vector as $\mathbf{h}_i$, where $i \in \mathcal{U} = \{1, 2, \ldots, KM_R\}$.

- Step 1: Initialize $\mathcal{U} = \{1, 2, \ldots, KM_R\}$, $\mathcal{S} = \phi$.

- Step 2: Find link j such that

$$j = \arg\max_{i \in \mathcal{U}} ||\mathbf{h}_i|| \ , \quad \mathbf{H}(\mathcal{S}) = [\mathbf{h}_j] \ . \tag{3.20}$$

  Set $\mathcal{S} = \{j\}$ and $\mathcal{U} = \mathcal{U} - \mathcal{S}$.

- Step 3: Find $Null(\mathbf{H}(\mathcal{S})) = \mathbf{V}_2$ by the SVD of $\mathbf{H}(\mathcal{S}) = \mathbf{U}\mathbf{\Sigma}\mathbf{V}^T$, where $\mathbf{V}_2 = [\mathbf{v}_{r+1}\ \mathbf{v}_{r+2}\ \ldots\ \mathbf{v}_{M_T}]$ and $r = |\mathcal{S}|$.

- Step 4: Find link j such that

$$j = \arg\max_{i \in \mathcal{U}} ||\mathbf{h}_i \cdot Null(\mathbf{H}(\mathcal{S}))|| \ , \quad \mathbf{H}(\mathcal{S}) = \begin{bmatrix} \mathbf{H}(\mathcal{S}) \\ \mathbf{h}_j \end{bmatrix}. \tag{3.21}$$

  Set $\mathcal{S} = \mathcal{S} \bigcup \{j\}$ and $\mathcal{U} = \mathcal{U} - \{j\}$.

- Step 5: Iterate Steps 3 and 4 until $|\mathcal{S}| = M_T$.

- Power Loading Principle: Water-filling.

In scenario 2, the way of updating $\mathcal{U}$ is different. If any link is selected for a user, its other antennas will not be considered.

3.3 Scheduling for Receive ZF Beamforming

3.3.1 Scheduling Algorithm

Now we consider the receive ZF scheduler. Each user feedbacks the channel vector $\{\gamma_i^k\}_{i=1}^{M_T}$ to the transmitter for scheduling the target group of users, where γ_i^k is the output SNR at the i-th receive antenna of user k defined in (3.5) under equal power allocation. Since the ZF receiver can change an $M_R \times M_T$ channel matrix into M_T parallel channels, the scheduler at the transmitter assigns a transmit antenna to serve one of the selected target users. It is unnecessary to assign all the subchannels to a single user [24–26]. The scheduler transmits data packets to the target user k^* via the i-th transmit antenna according to the criterion:

$$k^* = \arg\max_k \gamma_i^k \ . \tag{3.22}$$

Since there are K spatially-independent choices for an arbitrary transmit antenna, such broadcast scheduling algorithm is called spatially-independent scheduling in [26] and termed the receive ZF scheduler in this chapter. Figure 3.4 is an example of the receive ZF scheduler for $M_T = M_R = M = 3$ and $K = 3$. The output SNRs of users 1, 2, and 3 are [1.25, 0.49, 0.50], [0.81, 0.70, 2.25], and [0.49, 1.69, 1.21], respectively. The receive ZF scheduler allows

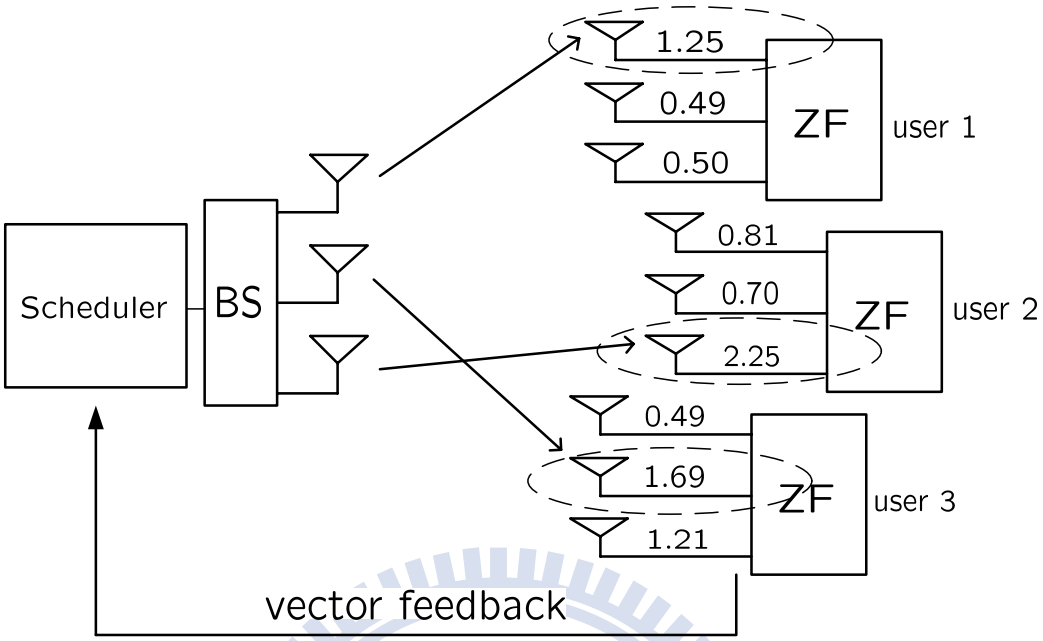

Figure 3.4: An example of the receive ZF beamforming with scheduling (or the receive ZF scheduler) for $M_T = M_R = 3$ and $K = 3$.

each transmit antenna to select its target user according to (3.22) independently. Among the first antennas, user 1 has the highest SNR (i.e. 1.25). Similarly, the highest SNR of the second antennas among three users is 1.69 belonging to user 3. Also, the third antenna's SNR of user 2 is the largest (i.e. 2.25). Thus, the data streams of the first, the second, and the third antennas at the base station correspond to the first, the second, and the third antennas of users 1, 3, and 2, respectively.

3.3.2 Sum Rate Analysis

Now the order statistics technique is applied to derive the closed-form expression for the sum-rate capacity of the receive ZF scheduler C_{RZF} for $M_T = M_R = M$ under the condition of equal power allocation. Denote $\tilde{\gamma}_i$ as the output SNR of the i-th selected subchannel, the PDF of $\tilde{\gamma}_i$ is

$$f_{\tilde{\gamma}_i}(\gamma_i) = \frac{KM}{\rho}\left(1 - e^{\frac{-M\gamma_i}{\rho}}\right)^{K-1} e^{\frac{-M\gamma_i}{\rho}}, \quad \text{for } i = 1, \ldots, M \ , \tag{3.23}$$

where $\rho = P_T/\sigma^2$. After independently scheduling across all transmit antennas in the space domain, $\{\tilde{\gamma}_i\}_{i=1}^{M}$ are i.i.d. with respect to i. The resulting sum rate is

$$C_{\mathrm{RZF}|_M} = \frac{KM^2}{\rho} \sum_{i=0}^{K-1} \binom{K-1}{i} (-1)^i h\left(\frac{(i+1)M}{\rho}\right) \ , \tag{3.24}$$

where

$$h(x) \triangleq \int_0^\infty e^{-xt} \log(1+t) dt = \frac{e^x \, E_1(x)}{x} \ , \tag{3.25}$$

and $E_1(x) = \int_1^\infty e^{-xt} t^{-1} dt$ is the exponential integer function of the first order [110].

Since $\{\tilde{\gamma}_i\}_{i=1}^{M}$ are known at the base station through the feedback channel vector, all effective channel gains $\{\tilde{q}_i\}_{i=1}^{M}$ (as defined in Section 3.1.2) of selected subchannels are available in the base station. Thus, the sum rate of the receive ZF scheduler can be further improved by using water-filling power allocation. From (3.5) and (3.23), the PDF of $\tilde{q}_i$ is $f_{\tilde{q}_i}(q_i) = K\left(1 - e^{-q_i}\right)^{K-1} e^{-q_i}$ and the long-term power constraint in (3.7) becomes

$$\begin{aligned}
&\sum_{i=1}^{M} E\left[\mu - \frac{1}{\tilde{q}_i}\right]_+ \\
&= KM \int_{1/\varsigma}^{\infty} \left(\varsigma - \frac{1}{z}\right) \left(1 - e^{-z}\right)^{K-1} e^{-z} dz \\
&\overset{(a)}{=} KM \sum_{i=0}^{K-1} \binom{K-1}{i} (-1)^i \int_{1/\varsigma}^{\infty} \left(\varsigma - \frac{1}{z}\right) e^{-z(i+1)} dz \\
&= KM \sum_{i=0}^{K-1} \binom{K-1}{i} (-1)^i \left(\frac{\varsigma}{1+i} e^{-(1+i)/\varsigma} - E_1\left(\frac{1+i}{\mu}\right)\right) \\
&= P_T \ ,
\end{aligned} \tag{3.26}$$

where (a) comes from the binomial expansion $(1-x)^n = \sum_{i=0}^{n} \binom{n}{i} (-1)^i x^i$. The resulting average sum rate of the receive ZF scheduler with water-filling power allocation is given by

$$\begin{aligned}
C_{\mathrm{RZF}|_M}^{\mathrm{water}} &= \sum_{i=1}^{M} E\left[\log(\tilde{\varsigma}_0 \tilde{q}_i)\right]_+ \\
&= KM \int_{1/\tilde{\varsigma}_0}^{\infty} \log(\tilde{\varsigma}_0 z) \left(1 - e^{-z}\right)^{K-1} e^{-z} dz \\
&= KM \sum_{i=0}^{K-1} \binom{K-1}{i} (-1)^i \int_{1/\tilde{\varsigma}_0}^{\infty} \log(\tilde{\varsigma}_0 z) e^{-z(1+i)} dz \\
&= KM \sum_{i=0}^{K-1} \binom{K-1}{i} (-1)^i \frac{\Gamma\left(0, 1 + i/\tilde{\varsigma}_0\right)}{1+i} \ ,
\end{aligned} \tag{3.27}$$

where $\tilde{\varsigma}_0$ is the water-level solution which satisfies (3.26).

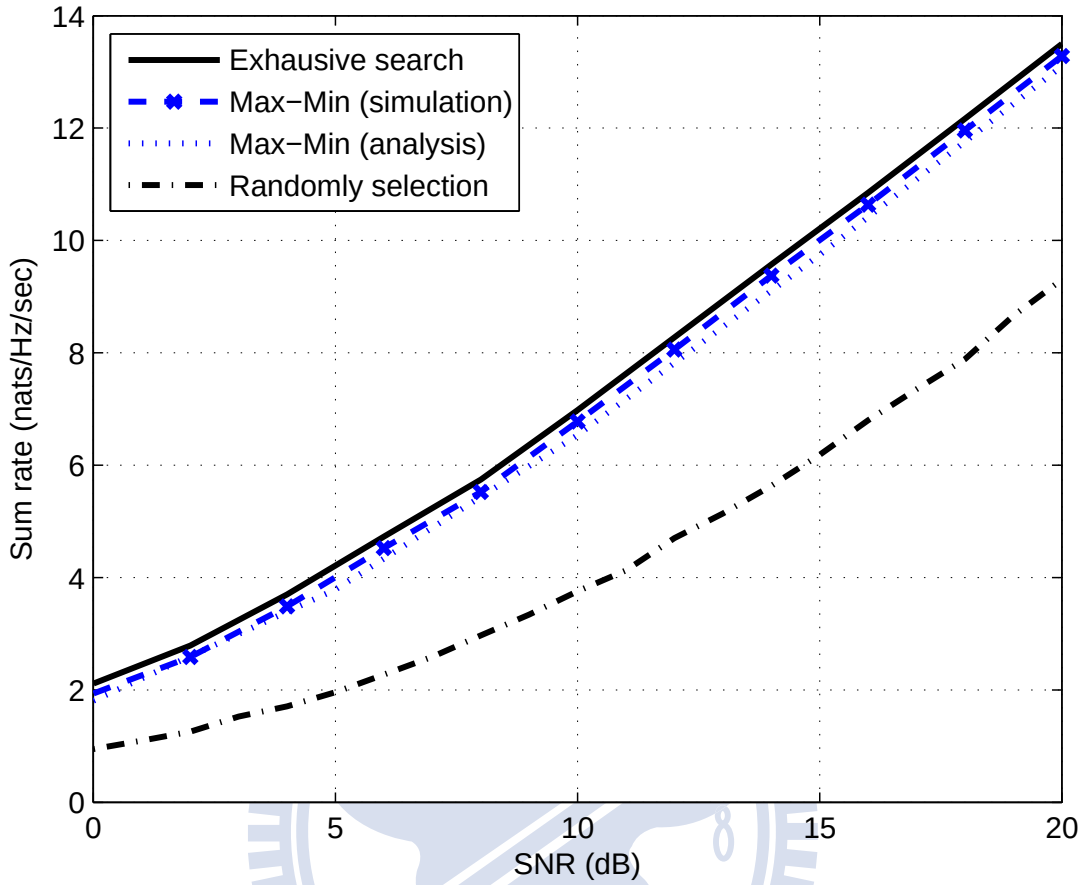

Figure 3.5: Comparison of the sum rate of the transmit ZF beamforming with various multiuser scheduling policies for $K = 10$ and $M_T = 3$ in the high SNR region.

3.4 Numerical Results

3.4.1 Sum Rate Approximation for Transmit ZF Scheduler with Exhaustive Searched Users

We first show the sum-rate capacity of the transmit ZF beamforming with random user selection and exhaustive search scheduling for various received SNRs when each user has only single antenna. For SNRs $= 0 \sim 20$ dB and $K = 10$ users, Fig. 3.5 compares the sum rate of the transmit ZF scheduler based on the exhaustive user selection with that based on the max-min analytical approach. As shown, the sum rate of the max-min analytical approach matches that of the exhaustive user selection quite well. At SNR $= 5$ dB, the sum

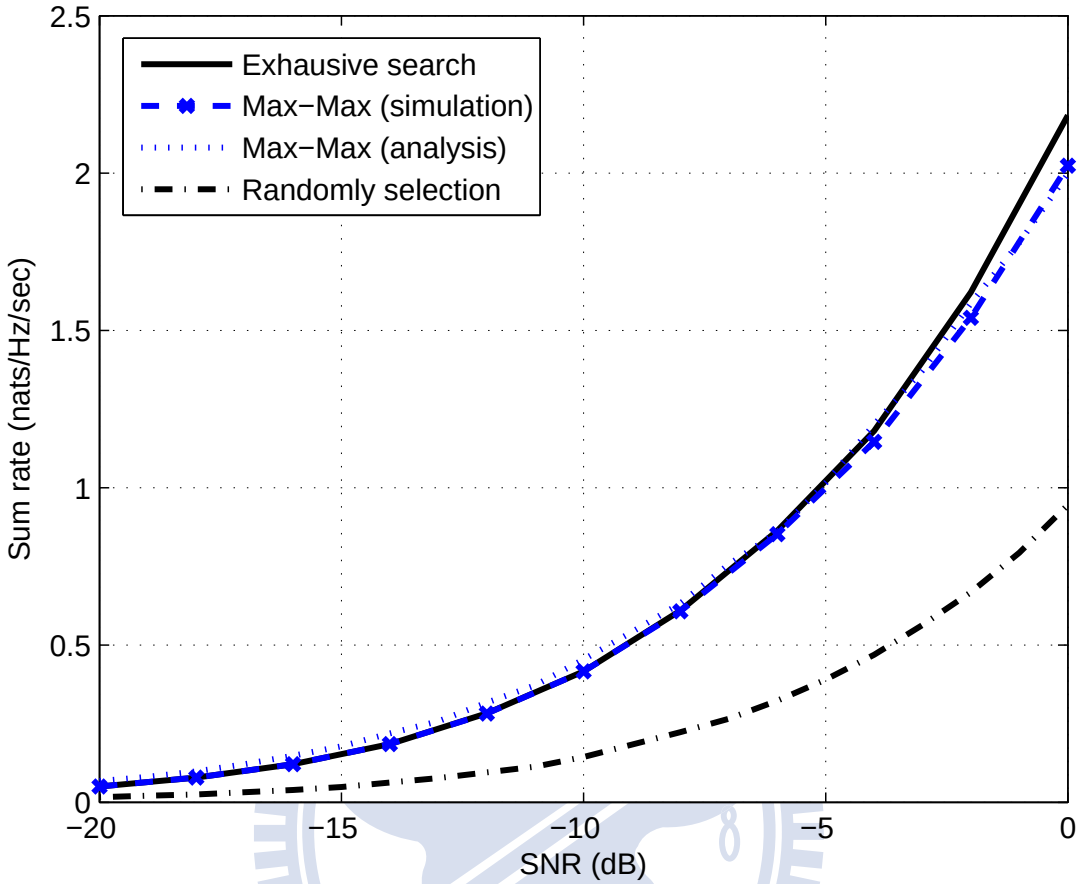

Figure 3.6: Comparison of the sum rate of the transmit ZF beamforming with various multiuser scheduling policies for $K = 10$ and $M_T = 3$ in the low SNR region.

rates of the exhaustive search and random user selection are 4 nats/s/Hz and 2 nats/s/Hz, respectively.

Figure 3.6 shows the sum rate of the transmit ZF scheduler in the low SNRs region from -20 to 0 dB and $K = 10$ users based on the exhaustive search and the max-max analytical approaches. As shown in the figure, the sum rate of the max-max can match that of the exhaustive search in the low SNR region. For comparison, the sum rate with random user selection is also shown in the figure. At SNR $= -5$ dB, the exhaustive user search can provide the sum rate of 1 nats/s/Hz, while the random user selection can provide only 0.4 nats/s/Hz. Basically, Figs. 3.5 and 3.6 show that even for $K = 10$ the impact of multiuser diversity is quite significant.

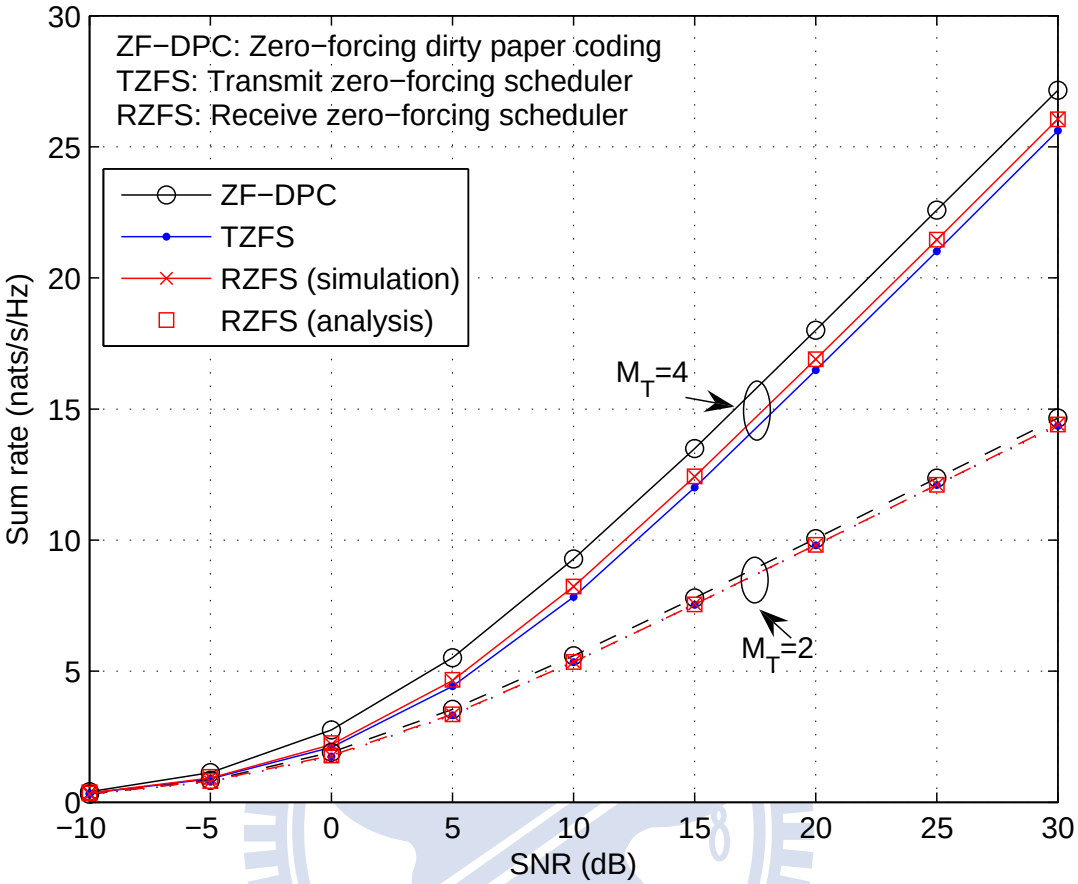

Figure 3.7: Comparison of the sum rate for the receive ZF scheduler ($M_T = M_R = 4$ and $M_T = M_R = 2$) and the transmit ZF and ZF-DPC schedulers ($M_T = 4$, $M_R = 1$ and $M_T = 2$, $M_R = 1$) with $K = 10$.

3.4.2 Sum Rate Comparison of Transmit and Receive ZF Schedulers

Next, we compare the sum-rate capacity of the receive ZF scheduler with that of the transmit ZF scheduler for various SNRs. We consider two conditions: (1) under the similar available feedback but different antenna architectures; and (2) under the same antenna architecture but different feedback requirements. For comparison, we also provide the sum rate performance of ZF-DPC transmit beamforming [60] combined with the greedy multiuser scheduling algorithm [59].

In Figure 3.7 the sum rate performance of the receive ZF scheduler is compared with

both the transmit beamforming approaches (ZF-DPC and ZF) for different values of M_T and M_R as $K = 10$. We mainly focus on the transmit beamformings with $M_R = 1$ which has similar feedback overheads (M_T complex values) compared to the receive ZF scheduler (M_T scalar values). From the figure, we have the following observations:

- For the receive ZF scheduler, the provided sum rate analysis (3.27) (with the legends of square) matches the simulated results (with the legends of cross) quite well.
- With similar amount of feedback, transmit ZF-DPC has the highest sum rate and the transmit and receive ZF schedulers result in almost the same sum rate. However, as the number of transmit antennas decreases, the sum rate of transmit and receive beamformings are very close to each other.
- With similar available feedback, the transmit and receive ZF schedulers result in almost the same sum rate. The selecting degrees of freedom per link is K for the receive ZF scheduler, and is $K - i + 1$ for determining the i-th link of the transmit ZF scheduler. Two schedulers have almost the same selecting degrees of freedom when $K \gg M_T$. With similar feedback overheads and selecting degrees of freedom, one can expect that two schedulers yield the similar sum rate.

Figure 3.8 compares the sum rate of the transmit ZF scheduler when user terminals are equipped with single and multiple receive antennas for $K = 10$ and $M_T = 3$. For multiple receive antennas $M_R = 3$, antenna selection scenarios 1 and 2 yield similar sum rates by the transmit ZF scheduler. For comparison, the sum rates of the transmit ZF-DPC, the transmit ZF beamforming based on the exhaustive user search and the receive ZF scheduler are plotted. From the figure, some observations can be made as follows:

- The suboptimal user selection methods can approach the performance of the complicated exhaustive search method for the transmit ZF scheduler.
- The transmit ZF scheduler with multiple receive antennas improves the sum rate by 20% over the transmit ZF scheduler with single antenna for SNR $= 0 \sim 5$ dB. The performance gain results from a higher multiuser diversity gain because more receive antennas imply more virtual users. From (3.9), the extra channel gain induced by larger diversity is $\log M_R$.

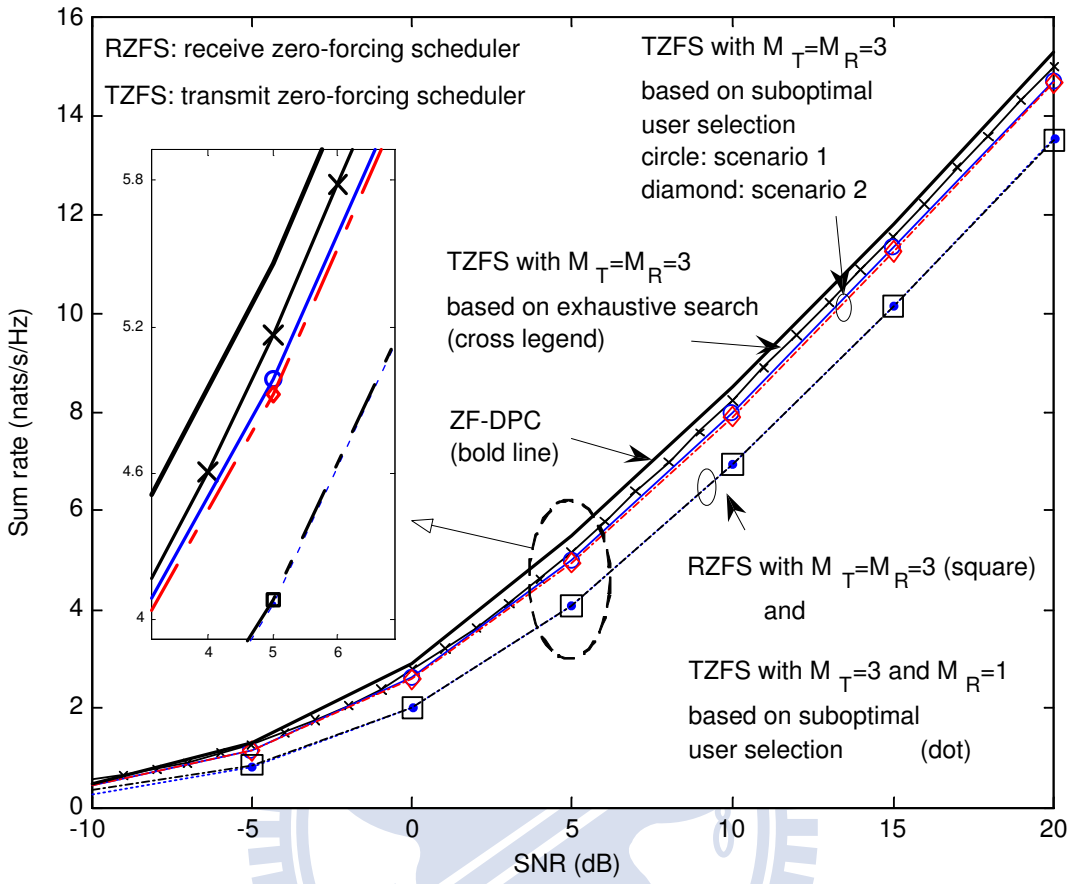

Figure 3.8: Effects of the number of receive antennas on the sum rate of the transmit ZF scheduler for $K = 10$ and $M_T = 3$.

3.5 Performance Issues

3.5.1 Feedback Requirement

The amount of required feedback information is an important parameter for designing the transmit and receive multiuser MIMO broadcast systems. The receive ZF scheduler requires M_T real scalar values, $\{\gamma_i^k\}_{i=1}^{M_T}$, in the feedback channel for each user $k \in \{1, \ldots, K\}$. For example user 1 in Fig. 3.4 feedbacks a channel state vector $[1.25, 0.49, 0.50]$. In general, complete channel matrix information is required for the transmit ZF scheduler to calculate antenna beamforming weights. For M_R receive antennas, user k needs to feedback $M_T M_R$ complex-valued entries of $\mathbf{H}_k$. Even if $M_R = 1$, the transmit ZF scheduler still needs to

feedback M_T complex-valued entries. Codebook-based feedback is another efficient channel quality feedback apparatus, where feedback information includes the channel direction information (CDI) and channel quality information (CQI) [49–52]. The transmit ZF scheduler needs both CQI and CDI, but the receive ZF scheduler requires CQI only. Nevertheless, certain indices are required to informing each antenna of its corresponding CQI in the receive ZF scheduler. Providing that each user is equipped with multiple antennas, the transmit ZF scheduler also have the same overhead for sending the indices of each antenna's corresponding CQI as the receive ZF scheduler.

3.5.2 Effects of Feedback CSI Variations

Now we evaluate the impacts of feedback CSI variations on the performance of the transmit and receive beamforming in MIMO broadcast systems. Feedback CSI variations are introduced to characterize the difference of the exact CSI and the measured CSI at a feedback channel. Feedback CSI variations may result from the noisy estimated information, the outdated information due to feedback delay, and quantization errors, etc. In this chapter, we quantify feedback CSI variations by the coefficient of variations (CV), which is defined as the ratio of the standard deviation σ_X of a random variable X to its mean $E[X]$, i.e. $\text{CV} = \sigma_X / E[X]$. The case with $\text{CV} = 0$ is equivalent to perfect feedback CSI. The larger the CV value, the more the perturbation on the feedback information. In this chapter, we model the combined effects of feedback CSI variations as a normal random variable $\Delta \sim \mathcal{N}(0, \sigma^2)$. For the perfect CSI ($x$), the perturbed CSI ($x'$) received at the base station is written as $x' = x + \Delta$, in which $\text{CV} = \sigma / x$.

Figure 3.9 compares the sum rate performance of three transmit beamforming techniques (denoted by ZF-DPC, BD, TZFS) and the ZF-based receive beamforming (denoted by RZFS), in which for $\text{CV} = 0.5$, $M_T = M_R = 3$ and $K = 20$. The three considered transmit beamforming techniques ZF-DPC, the BD-based precoder, and the transmit ZF scheduler respectively adopt the greedy scheduling algorithm [59], the norm-based user/antenna selection algorithm [82], and the scheduling algorithm in Section 3.2.3. In [111], we only considered the ZF-based receive and transmit beamforming multiuser MIMO broadcast systems. In this figure, we have the following observations:

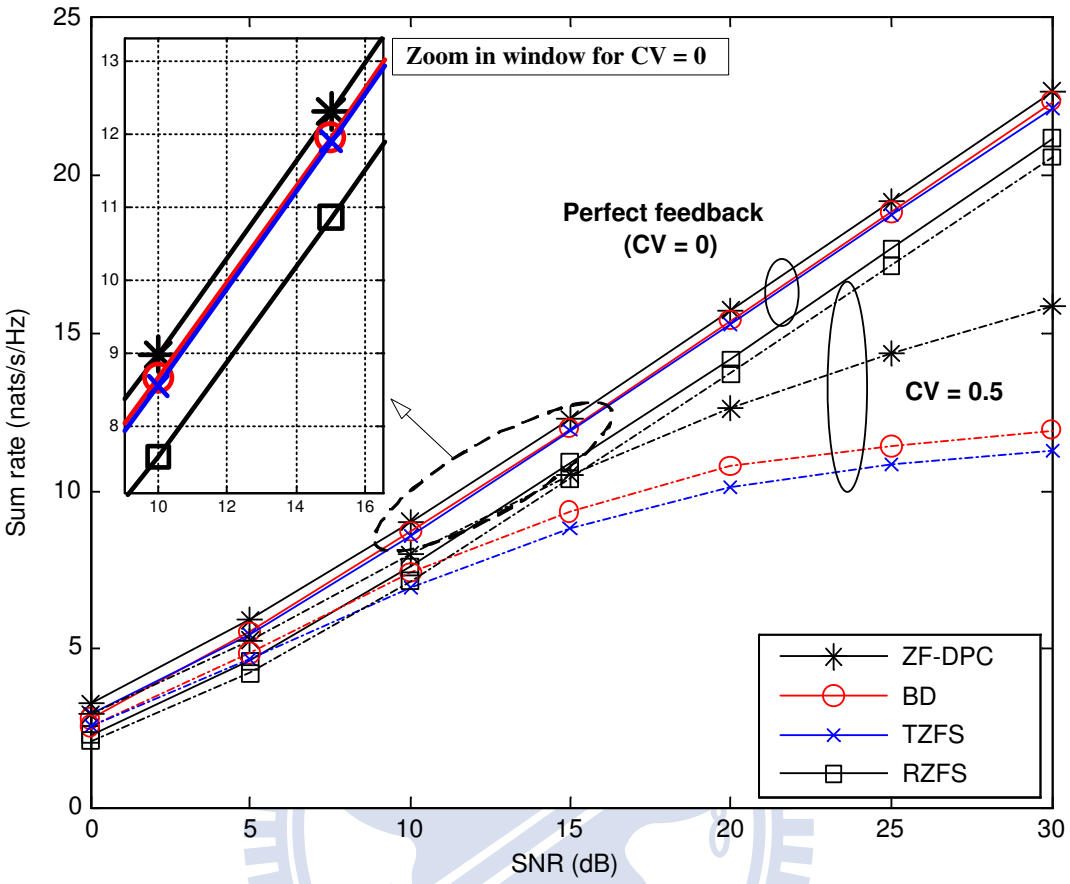

Figure 3.9: Sensitivity to feedback channel variations on the sum rate of the transmit-type MIMO broadcast schedulers and receive ZF scheduler for $K = 20$, $M_T = 3$, and low variation (CV = 0.5).

- For CV = 0, the ZF-DPC, BD, and ZF based transmit beamformings result in a similar sum rate, and their sum rates are about 10% (i.e. $1 \sim 1.5$ nats/s/Hz) higher than that of the receive ZF scheduler. For SNR = 20 dB, the sum rates for the ZF-DPC, BD, TZFS and RZFS are 15.73, 15.43, 15.28, and 14.21 nats/s/Hz, respectively. Among the three considered transmit beamforming techniques, ZF-DPC has the highest sum rate, and the BD-based transmit beamforming is only slightly better than the transmit ZF scheduler. The superiority of the BD-based transmit beamforming over the transmit ZF scheduler results from the joint processing of transmit precoding and receive equalizer.

- As the feedback CSI variation increases, the performance advantages of the transmit

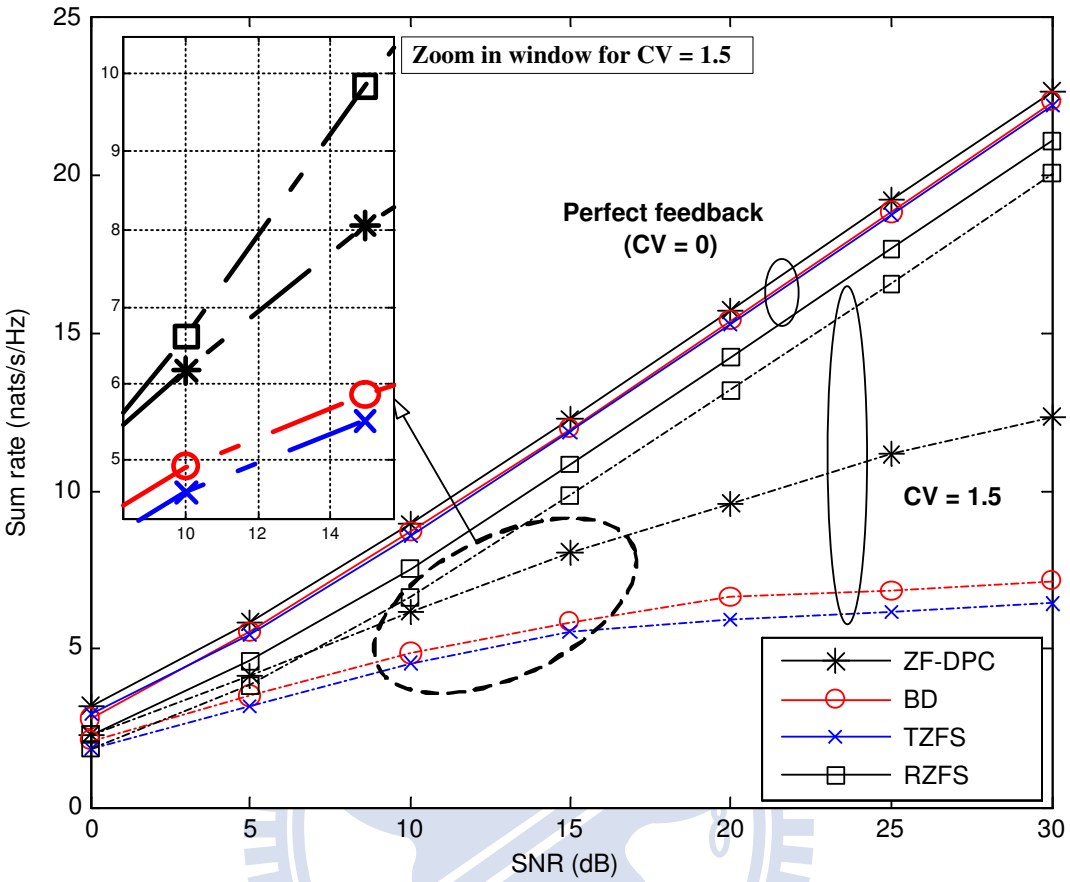

Figure 3.10: Sensitivity to feedback channel variations on the sum rate of the transmit-type MIMO broadcast schedulers and receive ZF scheduler for $K = 20$, $M_T = 3$, and high variation (CV = 1.5).

beamforming over the receive beamforming disappear. When CV increases from 0 to 0.5 at SNR = 20 dB, the sum rates of ZF-DPC, BD, transmit ZF scheduler decrease 19.7% to 12.63 nats/s/Hz, 30.4% to 10.73 nats/s/Hz, and 33.8% to 10.11 nats/s/Hz, respectively. By contrast, the sum rate of the receive ZF scheduler is only reduced 3.5% to 13.71 nats/s/Hz.

Fig. 3.10 shows that the increase of the feedback CSI variation up to CV = 1.5 will degrade the sum rates of the three considered transmit beamforming techniques seriously, i.e. 38.8%, 56.9%, 61.1% for ZF-DPC, BD, and TZFS, respectively. However, the sum rate of the receive ZF beamforming only decreases 7%. From Figs. 3.9 and 3.10, one can observe

that transmit beamforming is more sensitive to feedback CSI variations than the receive ZF beamforming.

3.5.3 Usage of Feedback Channel State Information

Noteworthily, the feedback information in transmit beamforming is applied to *calculate the beamforming weight* for **interference cancellation**, whereas the feedback information in receive beamforming is to *select the appropriate users*. In this part, we further discuss why different usage of feedback CSI affects the sensitivity of MIMO broadcast systems with respect to feedback channel variations. Consider the ZF-DPC and ZF-based transmit beamforming techniques. The i-th received signal in (3.1) can be written as

$$y_i = \mathbf{h}(\mathcal{S})_i \mathbf{w}_i x_i + \underbrace{\mathbf{h}(\mathcal{S})_i \sum_{j=1, j\neq i}^{M_T} \mathbf{w}_j x_j}_{\text{Interference}} + n_i \ , \tag{3.28}$$

where $\mathbf{h}(\mathcal{S})_i$ is the channel vector of the i-th receiver and $\mathbf{w}_i$ is the i-th column of the beamforming matrix $\mathbf{W}$, respectively. To cancel the inter-stream interference, i.e. making $\mathbf{h}(\mathcal{S})_i \mathbf{w}_j = 0 \ (\forall j \neq i)$ in (3.28), the complete channel state matrix is required. More importantly, it is implied that large feedback channel variations make it difficult to cancel inter-stream interference and thus significantly affect the performance of the ZF-DPC and ZF-based transmit beamforming techniques.

For the BD-based transmit beamforming, the received signal of user k with the BD precoder is represented as

$$\mathbf{y}_k = \mathbf{R}_k^T \mathbf{H}_k \mathbf{T}_k \mathbf{x}_k + \underbrace{\mathbf{R}_k^T \mathbf{H}_k \sum_{j=1, j\neq k}^{K} \mathbf{T}_j \mathbf{x}_j}_{\text{Interference}} + \mathbf{R}_k^T \mathbf{n}_k \ , \tag{3.29}$$

where $\mathbf{T}_k \in \mathcal{C}^{M_T \times L_k}$ and $\mathbf{R}_k \in \mathcal{C}^{M_R \times L_k}$ are the precoding matrix and the equalizer matrix, respectively, and $\mathbf{x}_k$ is the $L_k \times 1$ transmit vector for user k. The principle of the BD-based transmit beamforming is to design $\mathbf{T}_k \in \mathbf{U}^{M_T \times L_k}$ and $\mathbf{R}_k \in \mathbf{U}^{M_R \times L_k}$ so that

$$\mathbf{R}_k^T \mathbf{H}_k \mathbf{T}_j = 0 \quad \forall 1 \leq k \neq j \leq K \ , \tag{3.30}$$

where $\mathbf{U}$ represents an unitary matrix. With perfect feedback information, the interference term in (3.29) can be cancelled as long as the conditions (3.30) are satisfied. Similar to

the ZF-DPC and the ZF-based transmit beamforming techniques, the sum rate of the BD-based transmit beamforming is quite sensitive to the feedback channel errors due to the requirement of an accurate channel state matrix for inter-stream interference cancelation.

Now we consider the ZF-based receive beamforming. Assume that the received feedback information from K users at the i-th transmit antenna be $\{\hat{\gamma}_i^k\}_{k=1}^K$ in which $\hat{\gamma}_i^k = \gamma_i^k + \varepsilon_i^k$, where γ_i^k is the exact SNR value and ε_i^k is the distortion term. The scheduler at the base station selects the target user for the i-th transmit antenna according to

$$\hat{k}^* = \arg\max_k \hat{\gamma}_i^k \quad . \tag{3.31}$$

Compared to the correct decision in (3.22), the effect of feedback CSI variations may lead to $\hat{k}^* \neq k^*$, i.e. the best user may not be chosen. Unlike the transmit beamforming is affected by inter-stream interference, the ZF-based receive beamforming will not suffer from inter-stream interference. Although the best user is not chosen due to feedback CSI errors, the selected user (e.g. the second best user) can still receive reasonably good sum rate. Therefore, the sum rate scaling of the receive ZF scheduler can be maintained much better than the transmit beamforming techniques for MIMO broadcast system under the impact of feedback CSI variations.

3.5.4 Complexity

Here the complexity of the link selection procedures and the search space for the transmit ZF scheduler is compared with those of the receive ZF scheduler. For the suboptimal selection algorithm of the transmit ZF beamforming, one 2-norm vector calculation $||\mathbf{h}_i||$ per $i \in \mathcal{U}$ in Step 2 is required. Next, we search the link with the maximum norm in $\mathcal{U}$ of which the complexity is proportional to $|\mathcal{U}|$. This link selection procedure will be finished only in the first run and determine the first link. Note that $\mathcal{U}$ will be updated when finishing one link search and the following Steps 3 and 4 will be iterated $M_T - 1$ times to determine the remaining $M_T - 1$ links. In Step 3, the orthonormal basis $Null(\mathbf{H}(\mathcal{S}))$ is calculated, which requires SVD computation. In Step 4, we need to perform a vector-matrix multiplication for a $1 \times M_T$ vector and an $M_T \times (M_T - n)$ matrix and a 2-norm calculation per $i \in \mathcal{U}$ to search for the link with the maximum norm $||\mathbf{h}_i \cdot Null(\mathbf{H}(\mathcal{S}))||$, where n represents the number of iterations for $n = 1, \ldots, M_T - 1$. Therefore, the computational complexity per $i \in \mathcal{U}$ in Step

4 is a constant c_1 which is related to one vector-matrix multiplication and 2-norm calculation. Further, the size of search space for scenario 1 is equal to $\sum_{n=0}^{M_T-1}\binom{M_RK-n}{1}$. That is, the first link is chosen from $\binom{M_RK}{1}$, the second from $\binom{M_RK-1}{1}$, and so on. Similarly, the size of search space for scenario 2 is equal to $\sum_{n=0}^{M_T-1}\binom{M_RK-nM_R}{1}$. To sum up, the complexity of the link selection procedures for scenario 1 is approximately $c_1\sum_{n=1}^{M_T-1}\binom{M_RK-n}{1}+c_2(M_T-1)$, where c_2 is a proportional constant related to SVD procedures in the n-th iteration and the computation of searching the maximum norm is omitted.

The computing complexity for the receive ZF scheduler lies in selecting a certain link with a highest SNR from K users. Specifically, the size of search space for the receive ZF scheduler is $\sum_{n=1}^{M_T}\binom{K}{1}$, which is close to search size of the transmit ZF scheduler with $M_R=1$ for large K. However, the receive ZF scheduler induces the extra cost of implementing ZF algorithm at the user terminals. To sum up, since $\sum_{n=1}^{M_T}\binom{K}{1}<\sum_{n=0}^{M_T-1}\binom{M_RK-n}{1}$ for scenario 1 and $\sum_{n=1}^{M_T}\binom{K}{1}<\sum_{n=0}^{M_T-1}\binom{M_RK-nM_R}{1}$ for scenario 2, one can conclude that the size of search space of the receive ZF scheduler is much smaller than that of the transmit ZF scheduler.

3.5.5 Fairness Issue

To achieve the fairness among users, one should maintain the same probability of obtaining services at each time slot. Consider the transmit ZF scheduler in scenario 2 as an example. To assign M_T data streams, there are $(M_RK)(M_RK-M_R)\cdots(M_RK-M_R(M_T-1))$ possible outcomes. When all M_T transmit antennas are assigned to other $(K-1)$ users, user k is not served. Therefore, the probability p_k of user k to obtain services at each time slot is

$$\begin{aligned} p_k &= 1-\Pr\{\text{user } k \text{ is not selected}\} \\ &= 1-\frac{(M_RK-M_R)(M_RK-2M_R)\cdots(M_RK-M_RM_T)}{(M_RK)(M_RK-M_R)\cdots(M_RK-M_R(M_T-1))} \\ &= \frac{M_T}{K}\ . \end{aligned} \tag{3.32}$$

As for the receive ZF scheduler, total K^{M_T} possible outcomes for the M_T transmit antennas assigning to K users. The probability of user k to obtain services at each time slot is $\left[1-(1-\frac{1}{K})^{M_T}\right]\approx\frac{M_T}{K}$ for $K\gg M_T$. Therefore, both the transmit and receive ZF scheduler can achieve the same fairness performance in terms of the probability of users to obtain services during a scheduling time slot.

Table 3.1: Performance comparison and tradeoff between the transmit and receive ZF schedulers.

	Transmit ZF scheduler (TZFS)	Receive ZF scheduler (RZFS)
Sum Rate	Achieve the same scaling law with DPC [28]. Better sum rate performance than RZFS.	Achieve the same scaling law with DPC [25]. Slight poorer sum rate performance than TZFS.
Feedback Requirement	$M_R \times M_T$ complex-valued entries. Use for interference cancellation. (matrix feedback; need CQI and CDI feedback)	M_T real-valued scalar values. Use for user selection. (vector feedback; CQI feedback)
Effect of Feedback Error on sum rate	Sensitive to feedback channel variation. Degradation largely especially in high SNR region. Interference domination.	Robust to feedback channel variation. Degradation slightly compared to TZFS. Maintain sum rate scaling.
Search Space	$\sum_{n=0}^{M_T-1} \binom{M_R K-n}{1}$ More computational complexity at base station.	$\sum_{n=0}^{M_T-1} \binom{K-n}{1}$ Extra ZF implementation at each user side.
Note	Suitable for huge feedback to support higher sum rate.	As a candidate for scarce feedback environment.

In summary, simultaneously "broadcast" data to multiple users can be implemented by the transmit beamforming and receive beamforming. While there are enough feedback bandwidth and the accuracy of the feedback channel state can be ensured, transmit beamforming is a good multi-user MIMO broadcast strategy and have better sum rate performance than the ZF-based receive beamforming. However, because imperfect feedback may cause significant inter-stream interference, the ZF-DPC, BD, and ZF-based transmit beamformings may not be feasible in the presence of large feedback CSI variations, which will cause the loss of opportunity to exploit the potential of having multiple receive antennas at the user terminal. By contrast, in the case that feedback channel bandwidth is constrained and feedback channel states have certain uncertainty, then the ZF-based receive beamforming can be a good candidate for multi-user MIMO broadcast strategy at the cost of ZF implementation at the user side. As shown in Table 3.1, both the transmit and receiver ZF schedulers can have the same scaling law as DPC for an extremely large number of users. However, the transmit ZF scheduler needs perfect CSI and is sensitive to imperfect CSI feedback. The receive ZF scheduler can relax the feedback requirement and is robust to feedback channel variations.

Chapter 4

Analysis of Multiuser MIMO Broadcast Systems with Transmit Beamforming

In this chapter, we present the closed-form expressions for the link outage and coverage of the transmit ZF and ZF-DPC MIMO broadcast systems. We find that the ZF-PDC MIMO broadcast system has a larger diversity order and better coverage compared with the transmit ZF MIMO broadcast system. Furthermore, it is observed that the transmit ZF MIMO broadcast system with RR scheduling has only the diversity order of one and its reliable coverage can only approach to that of the weakest link of the ZF-DPC MIMO broadcast system. By selecting the best group of users, multiuser scheduling can function as a link quality compensation and soft coverage enhancement technique to improve the deficient diversity of the spatial multiplexing based MIMO broadcast systems without increasing the extra transmission power. Our analytical formula can estimate to what extent the coverage performance of the ZF-DPC MIMO broadcast system can be improved as the number of users increases. Hence, the effect of increasing the number of antennas on the coverage performance of the ZF-DPC MIMO broadcast system can be quantitatively analyzed subject to the same transmission power from base station.

4.1 Background

4.1.1 System Model

Consider a single-cell multiuser MIMO broadcast system with a base station and K users. The base station is equipped with M_T transmit antennas, but each of K user terminals has only one receive antenna. Thus, M_T users are selected from K users for simultaneous transmission with different data streams. The subset of users' indices to which a base station intends to transmit different information is denoted by $\mathcal{S} \subset \{1, \ldots, K\}$, $|\mathcal{S}| = M_T$.

The beamforming weight matrix at the transmitter is denoted by $\mathbf{W} = [\mathbf{w}_1 \ \ldots \mathbf{w}_{M_T}]$,

where $\mathbf{w}_i \in \mathbb{C}^{M_T \times 1}$ and the input signal vector is denoted by $\mathbf{u} = [\sqrt{p_1}u_1, \ldots, \sqrt{p_{M_T}}u_{M_T}]^T$. Here u_i and p_i represent the uncorrelated unit-power signal symbol and the power of the symbol associated with user i, respectively. Then, the transmitted signal vector $\mathbf{x}$ is written as $\mathbf{x} = \mathbf{W}\mathbf{u} = \sum_{i=1}^{M_T} \sqrt{p_i}\mathbf{w}_i u_i \in \mathbb{C}^{M_T \times 1}$. Let $\mathbf{y} \in \mathbb{C}^{M_T \times 1}$ be the received signal vector, and $\mathbf{G}(\mathcal{S})$ be the $M_T \times M_T$ channel matrix corresponding to $\mathcal{S}$. Denote $\mathbf{n} \in \mathbb{C}^{M_T \times 1}$ as the complex Gaussian noise vector with $\mathrm{E}[\mathbf{n}\mathbf{n}^H] = \sigma^2 \mathbf{I}_{M_T}$, where $(\cdot)^H$ denotes conjugate transpose. Then, the received signal can be expressed as

$$\mathbf{y} = \mathbf{G}(\mathcal{S})\mathbf{x} + \mathbf{n} = \mathbf{g}\mathbf{H}(\mathcal{S})\mathbf{x} + \mathbf{n} \ , \tag{4.1}$$

where $\mathbf{g}$ is an $M_T \times M_T$ diagonal matrix with $\mathbf{g} = \mathrm{diag}\{\sqrt{g_1}, \sqrt{g_2}, \ldots, \sqrt{g_{M_T}}\}$ and g_i depicts the path loss between the base station and user i. For a user at a distance of R from the base station, g_i can be written as [112]

$$10 \log_{10} g_i = -10\mu \log_{10} R + g_0 \quad [\mathrm{dB}] \ , \tag{4.2}$$

where μ is the path loss exponent and g_0 is a constant subject to certain path loss models. Assume that all users experience independent flat Rayleigh fading and the transmission power is constrained by $\mathrm{E}[\mathbf{x}^H\mathbf{x}] = P_T$.

4.1.2 Transmit ZF-DPC Beamforming

Based on QR-type decomposition, a suboptimal solution of $\mathbf{W}$ was found in [4]. Let $\mathbf{H}(\mathcal{S}) = \mathbf{L}\mathbf{Q}$ be the QR-type decomposition of $\mathbf{H}(\mathcal{S})$, where $\mathbf{L}$ is a lower triangular matrix and $\mathbf{Q}$ is a unitary matrix. With $\mathbf{W} = \mathbf{Q}^H$, the corresponding system model in (4.1) can be written as

$$y_i = l_{i,i}\sqrt{g_i p_i}u_i + \sum_{j<i} l_{i,j}\sqrt{g_j p_j}u_j + n_i \ , \quad i = 1, \ldots, M_T. \tag{4.3}$$

Note that $\mathbf{W} = \mathbf{Q}^H$ can cancel the interference from users with indices $j > i$. The remaining interference terms with indices $j < i$ are taken care of by applying DPC successively. For simplicity, we consider the equal power allocation, that is, $p_i = P_T/M_T$, where $i = 1, \ldots, M_T$. The rate of the i-th link for ZF-DPC is $\log_2(1 + |l_{i,i}|^2\rho_i/M_T) = \log_2(1 + \gamma_i)$, where ρ_i is the average received SNR, γ_i is the effective output SNR, and the term $|l_{i,i}|^2$ can be viewed as

the effective channel gain at the i-th link. Specifically, ρ_i can be represented as

$$\rho_i = \frac{P_T g_i}{\sigma^2} = \frac{P_T 10^{g_0/10}}{\sigma^2 R_i^{\mu}} \quad . \tag{4.4}$$

4.1.3 Transmit ZF Beamforming

As introduced in Chapter 3.1.1. the transmit ZF beamforming scheme [4] aims at inverting the channel matrix to create orthogonal channels between the transmitter and the receiver. By choosing the weight matrix $\mathbf{W} = \mathbf{H}(\mathcal{S})^H(\mathbf{H}(\mathcal{S})\mathbf{H}(\mathcal{S})^H)^{-1}$, the corresponding system model in (4.1) can be written as

$$\mathbf{y} = \mathbf{gH}(\mathcal{S})\mathbf{H}(\mathcal{S})^H(\mathbf{H}(\mathcal{S})\mathbf{H}(\mathcal{S})^H)^{-1}\mathbf{u} + \mathbf{n} = \mathbf{gu} + \mathbf{n} \ , \tag{4.5}$$

and the i-th received signal is given by $y_i = \sqrt{g_i p_i} u_i + n_i$. Due to the transmit power constraint $E[\mathbf{x}^H\mathbf{x}] \leq P_T$, we have the following relation:

$$\|\mathbf{w}_1\|^2 p_1 + \ldots + \|\mathbf{w}_{M_T}\|^2 p_{M_T} \leq P_T \ , \tag{4.6}$$

where $\|\mathbf{w}_i\|^2 = [(\mathbf{H}(\mathcal{S})\mathbf{H}(\mathcal{S})^H)^{-1}]_{i,i}$. In (4.6), it implies that transmit ZF beamforming incurs an excess transmission power penalty due to the required interference cancellation power on $\mathbf{W}$. According to (4.6), power loading is $\|\mathbf{w}_i\|^2 p_i = P_T/M_T$, where $i = 1, \ldots, M_T$. As a result, the data rate at the i-th link of transmit ZF beamforming is

$$\log_2\left(1 + \frac{g_i P_i}{\sigma^2}\right) = \log_2\left(1 + \frac{b_i \rho_i}{M_T}\right) = \log_2(1 + \gamma_i) \ , \tag{4.7}$$

where $b_i = 1/\|\mathbf{w}_i\|^2$ is the effective channel gain.

4.2 Performance Metrics

4.2.1 Link Outage Probability

As defined in Chapter 2.3.1, the link outage of a SISO system is usually defined as the probability of the effective output SNR is less than a predetermined value γ_{th}, i.e. $P_{\text{out}} = P_r\{\gamma < \gamma_{th}\}$ [104]. As for the MIMO broadcast systems, all the data links serve different individual users. Thus, we define the link outage probability of the i-th link the same as a SISO link, i.e. $P_{\text{out}}^i = P_r\{\gamma_i < \gamma_{th}\}$.

4.2.2 Diversity Order

Let link outage probability $P_{\text{out}}(\cdot)$ be a function of SNR. Then, the link diversity order D_{order} is defined as [105]

$$D_{\text{order}} \triangleq -\lim_{\rho \to \infty} \frac{\log P_{\text{out}}(\rho)}{\log \rho} \quad , \tag{4.8}$$

where ρ is the receive SNR.

4.2.3 Link Reliable Coverage

With the requirement of link outage probability P_{out}, the link coverage reliability for its corresponding link radius associated with the required SNR γ_{th} is $(1 - P_{\text{out}})$. In this chapter, we focus on the reliable coverage with 90% link reliability.

4.3 Analysis of Transmit MIMO Broadcast Systems without Scheduling

4.3.1 Transmit ZF-DPC without Scheduling

At first we analyze the coverage performance of ZF-DPC MIMO broadcast systems without user selection, i.e. based on RR scheduling. Clearly, selecting users randomly cannot result in multiuser diversity gain. By Lemma 2 in [4], $d_i = |l_{i,i}|^2$ is independent central Chi-squared random variable $\mathcal{X}^2_{2(M_T - i + 1)}$ with $2(M_T - i + 1)$ degrees of freedom. The PDF of a Chi-squared random variable $\mathcal{X}^2_{2a}$ is $f(z) = z^{a-1}e^{-z}/(a-1)!$ for $z > 0$. Thus, the PDF of the effective channel gain d_i can be written as

$$f_{d_i}(z) = \frac{z^{M_T - i} e^{-z}}{(M_T - i)!} \quad \text{for} \quad i = 1, \ldots, M_T \quad , \tag{4.9}$$

where $i = 1$ and $i = M_T$ represent the strongest and the weakest links in the statistics, respectively. The corresponding cumulative distribution function (CDF) of d_i can be written as

$$F_{d_i}(z) = \quad 1 - \frac{\Gamma(M_T - i + 1, z)}{\Gamma(M_T - i + 1)} = 1 - \Gamma_{\text{R}}\left(M_T - i + 1, z\right) \quad , \tag{4.10}$$

where $\Gamma(a) = \int_0^\infty t^{a-1}e^{-t}dt$ is the complete gamma function, $\Gamma(a,x) = \int_x^\infty t^{a-1}e^{-t}dt$ is the upper incomplete gamma function, and $\Gamma_{\mathrm{R}}(a,x) = \frac{\Gamma(a,x)}{\Gamma(a)}$ is the regularized gamma function. The CDF of the effective output SNR $\gamma_i = d_i\rho_i/M_T$ for the i-th link is

$$F_{\gamma_i}(\gamma) = F_{d_i}\left(\frac{M_T\gamma}{\rho_i}\right) = 1 - \Gamma_{\mathrm{R}}\left(M_T - i + 1, \frac{M_T\gamma}{\rho_i}\right) \ . \tag{4.11}$$

Thus, for a given threshold $\gamma_{th} > 0$, the link outage probability for the i-th link of the ZF-DPC MIMO broadcast system is

$$P_{\mathrm{out}}^i = F_{\gamma_i}(\gamma_{th}) = \quad 1 - \Gamma_{\mathrm{R}}\left(M_T - i + 1, \frac{M_T\gamma_{th}}{\rho_i}\right) \ . \tag{4.12}$$

The following shows the analysis of the link diversity order.

Theorem 1. *The diversity order of the i-th link for an M_T-link ZF-DPC MIMO broadcast system without scheduling and ordering is $M_T - i + 1$.*

Proof. See Appendix A. □

This theorem provides a surprising result that the ZF-DPC MIMO broadcast systems can support extra diversity gains for $M_T - 1$ links instead of traditional diversity order of one in the spatial multiplexing based MIMO systems. For example, the link diversity orders are respectively three for $i = 1$, two for $i = 2$, and three for $i = 3$ as $M_T = 3$. The first two links obtain extra diversity gains under the ZF-DPC MIMO broadcast transmissions.

To derive cell coverage $R_{\texttt{ZFDPC}}^i$ from (4.12), we first introduce the inverse of the regularized incomplete gamma function as follows:

$$z = \Gamma_{\mathrm{R}}(a,x) \ \Rightarrow \ x = \Gamma_{\mathrm{R}}^{-1}(a,z) \ . \tag{4.13}$$

That is, with the regularized incomplete gamma function $\Gamma_{\mathrm{R}}(a,x)$, the term $\Gamma_{\mathrm{R}}^{-1}(a,z)$ is the solution for x in $z = \Gamma_{\mathrm{R}}(a,x)$. By substituting (4.4) and (4.13) into (4.12), the link coverage can be written as

$$R_{\texttt{ZFDPC}}^i = \left[\frac{P_T 10^{g_0/10}}{M_T\gamma_{th}\sigma^2} \ \Gamma_{\mathrm{R}}^{-1}\left(M_T - i + 1, 1 - P_{\mathrm{out}}^i\right)\right]^{\frac{1}{\mu}} \quad , \quad i = 1, \ldots, M_T \ . \tag{4.14}$$

4.3.2 Transmit ZF Beamforming without Scheduling

Alternately, we analyze the coverage performance of the transmit ZF MIMO broadcast system without user selection. In this case, all the elements in each channel vector are Rayleigh faded. Due to the same statistics, we can view the system as an point-to-point $M_T \times M_T$ (single user) MIMO system with a ZF receiver. The PDFs of the effective channel gain $\{b_i\}_{i=1}^{M_T}$ can be obtained through the PDFs of the ZF receiver's substream SNRs. According to [107], the distribution of the substream SNRs $\{\gamma_i\}_{i=1}^{M_T}$ for an $M_T \times M_R$ MIMO system with ZF receiver under equal power allocation are identically distributed $\mathcal{X}^2_{2(M_R-M_T+1)}$. In the case of $M_T = M_R$, the PDF of unordered $\{b_i\}_{i=1}^{M_T}$ can be obtained from (4.9) by letting $i = M_T$, which result in exponentially distributed random variable with parameter one.

Therefore, the link outage probability and the coverage performance of the transmit ZF MIMO broadcast system can be obtained from (4.12) and (4.14) with $i = M_T$. Clearly, under the same link outage requirement, all transmit ZF beamforming's substream links equal the ZF-DPC's weakest link and has the diversity order of one.

Corollary 1. *The link diversity order of the transmit ZF MIMO broadcast system without scheduling is one.*

4.4 Analysis of Transmit MIMO Broadcast Systems with Scheduling

4.4.1 Transmit ZF-DPC with Greedy Scheduling

Now we consider the effects of multiuser scheduling in the MIMO broadcast systems. We focus on the strongest stream link which has the largest radius to determine the cell range. In [59], the authors proposed a greedy scheduling algorithm to *select* M_T users out of K users to form $\mathbf{H}(\mathcal{S})$ and *ordering* those selected channel row vectors in the Gram-Schmidt orthogonalization to maximize the system throughput.

The strongest link can be determined by the first selected user's channel row vector $\mathbf{h}_k \in \mathcal{C}^{1\times M_T}$ for $k = 1, \ldots, K$. According to the greedy selection algorithm, the selected user

k^* is

$$k^* = \arg \max_{k \in \{1,\ldots,K\}} d_{1,k} \ , \tag{4.15}$$

where $d_{1,k} = \mathbf{h}_k \mathbf{h}_k^*$. Note that $d_{1,k}$ is the sum of M_T squared magnitudes of circularly symmetric, zero-mean, unit-variance complex Gaussian random variables. Therefore, $d_{1,k} \sim \mathcal{X}^2_{2M_T}$ with PDF $f_{d_{1,k}}(z) = z^{M_T-1}e^{-z}/(M_T-1)!$. The effective channel gain of the strongest link for the greedy scheduling algorithm is $\tilde{d}_1 = d_{1,k^*}$ of which PDF can be obtained by the order statistics analysis as follows:

$$f_{\tilde{d}_1}(z) = K f_{d_{1,k}}(z)[F_{d_{1,k}}(z)]^{K-1} \ . \tag{4.16}$$

Hence the link outage probability is

$$P^1_{\text{out}} = F_{\tilde{\gamma}_1}(\gamma_{th}) = F_{\tilde{d}_1}\left(\frac{M_T\gamma_{th}}{\rho_1}\right) = \left(1 - \Gamma_{\text{R}}\left(M_T, \frac{M_T\gamma_{th}}{\rho_1}\right)\right)^K \ . \tag{4.17}$$

The following theorem gives the diversity order of the strongest link in the ZF-DPC MIMO broadcast system.

Theorem 2. *The diversity order of the strongest link for the M_T-link ZF-DPC broadcast system with K-user greedy scheduling is KM_T.*

Proof. See Appendix B. □

To derive the link coverage $\tilde{R}^1_{\texttt{ZFDPC}}$ of the strongest link from (4.17), we use the inverse of the regularized incomplete gamma function to obtain

$$\tilde{R}^1_{\texttt{ZFDPC}} = \left[\frac{P_T 10^{g_0/10}}{M_T\gamma_{th}\sigma^2} \ \Gamma^{-1}_{\text{R}}\left(M_T, 1 - \sqrt[K]{P^1_{\text{out}}}\right)\right]^{\frac{1}{\mu}} \ . \tag{4.18}$$

Effect of User Ordering

Even with random user selection, the ZF-DPC MIMO broadcast system can still take advantage of user ordering. This case is similar to the multiuser MIMO broadcast system with $K = M_T$ users. The benefit of pure user ordering (not combined with users selection) will be shown in the section of numerical results.

Soft Coverage Extension by Scheduling

To examine the benefits of multiuser scheduling, we define the *coverage extension ratio* $\eta^1_{\texttt{ZFDPC}}$ as

$$\eta^1_{\texttt{ZFDPC}} = \frac{\tilde{R}^1_{\texttt{ZFDPC}}}{R^1_{\texttt{ZFDPC}}} = \left[\frac{\Gamma_{\mathrm{R}}^{-1}\left(M_T, 1-\sqrt[K]{P^1_{\mathrm{out}}}\right)}{\Gamma_{\mathrm{R}}^{-1}(M_T, 1-P^1_{\mathrm{out}})}\right]^{\frac{1}{\mu}}, \tag{4.19}$$

where $\eta^1_{\texttt{ZFDPC}}$ is a function of $\{M_T, K, P^1_{\mathrm{out}}, \mu\}$ and can be used to examine how M_T and K affect the reliable coverage range of the MIMO broadcast system.

4.4.2 Transmit ZF Beamforming with Scheduling

For the transmit ZF MIMO broadcast system with scheduling, some suboptimal user selection algorithms [28, 60] were proposed to reduce the complexity of the exhaustive search. However, it is difficult to find the exact per link closed-form expression for the transmit ZF MIMO broadcast system with scheduling. To compare with the ZF-DPC MIMO broadcast system, we will show the simulation results of the transmit ZF MIMO broadcast system based on exhaustive search in Section 4.5.

4.5 Numerical Results

In this section, we illustrate the achievable link outage and link coverage performances of both the ZF-DPC and transmit ZF MIMO broadcast systems. Assume that the predetermined value $\gamma_{th} = 2$ dB, $\sigma^2 = -103$ dBm, $g_0 = -32$ dB, $\mu = 4$ and $M_T = 3$.

Figure 4.1 shows the simulative and analytical link outage performances of both the ZF-DPC and transmit ZF MIMO broadcast systems without scheduling when user terminals are at the distance of $R = 1$ km from base station and path loss exponents $\mu = 3.9$ or 4. Clearly, the link outage probability becomes higher for a larger path loss exponent. The diversity orders of different links match our analytical results in Theorem 1. For example, the strongest link $i = 1$ has the diversity order of three, the link $i = 2$ has the diversity order of two, but the weakest link $i = 3$ has only the diversity order of one.

Figure 4.2 shows the link outage for the strongest links of both the ZF-DPC and transmit ZF MIMO broadcast systems with and without scheduling for five users ($K = 5$) at the

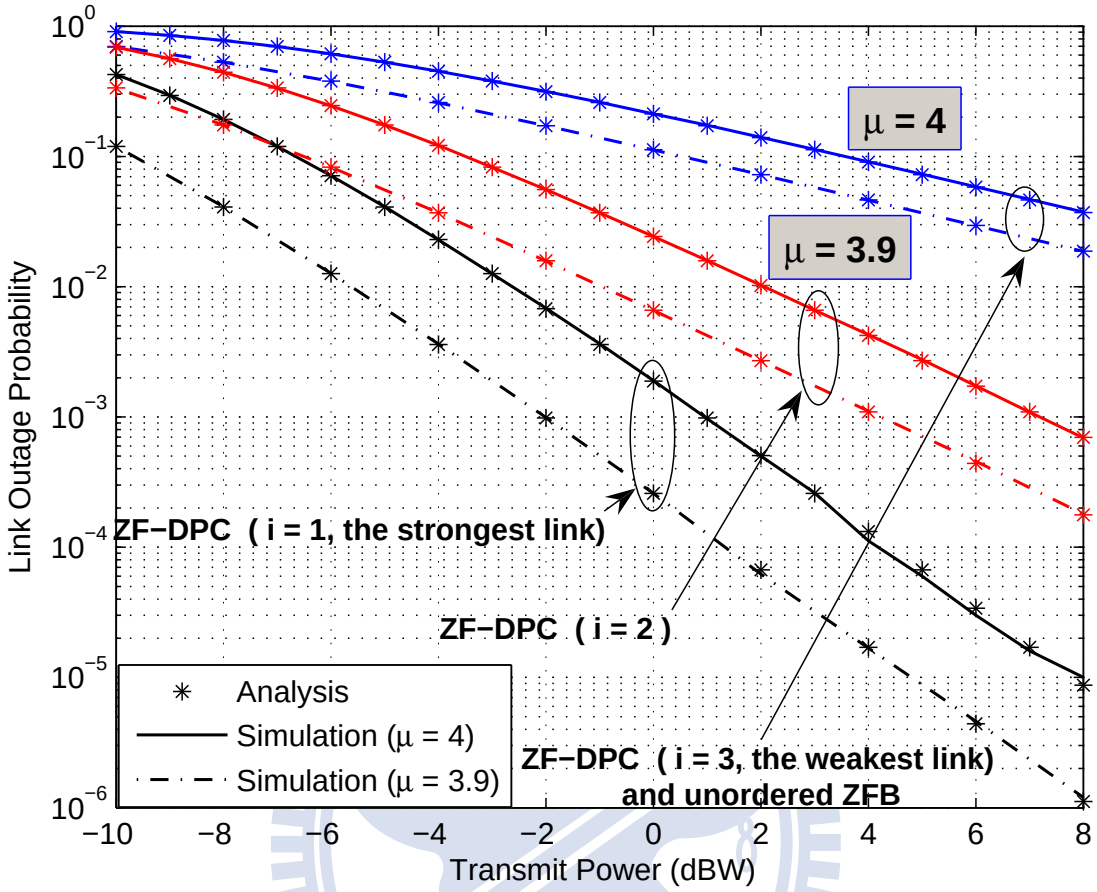

Figure 4.1: Link outage probability performance against the transmit power P_T when path loss exponent $\mu = 3.9$ and 4 for both the transmit ZF-DPC and ZF MIMO broadcast systems, where $M_T = 3$, $\sigma^2 = -103$ dBm, $R = 1$ km and $\gamma_{th} = 2$ dB.

distance of $R = 2$ km from base station. In the figure, it is shown that the multiuser diversity gain is still significant even if the degree of freedom is merely $K = 5$. From this figure, the curve of ZF-DPC with greedy scheduling tends to have the diversity of order $KM_T = 15$.

Figure 4.3 shows the corresponding link coverage performance of Fig. 4.2 in which we set the link reliability as 0.9 under $\gamma_{th} = 2$ dB. Clearly, coverage is extended in both the ZF-DPC and transmit ZF MIMO broadcast systems with scheduling even with $K = 5$. For example, it can only maintain 90% link reliability as far as about 1.6 km radius without scheduling, but can extend to 2.1 km with scheduling for the ZF-DPC MIMO broadcast systems when $P_T = 0$ dBW, i.e. the achievable coverage increases 31.25% by the help of

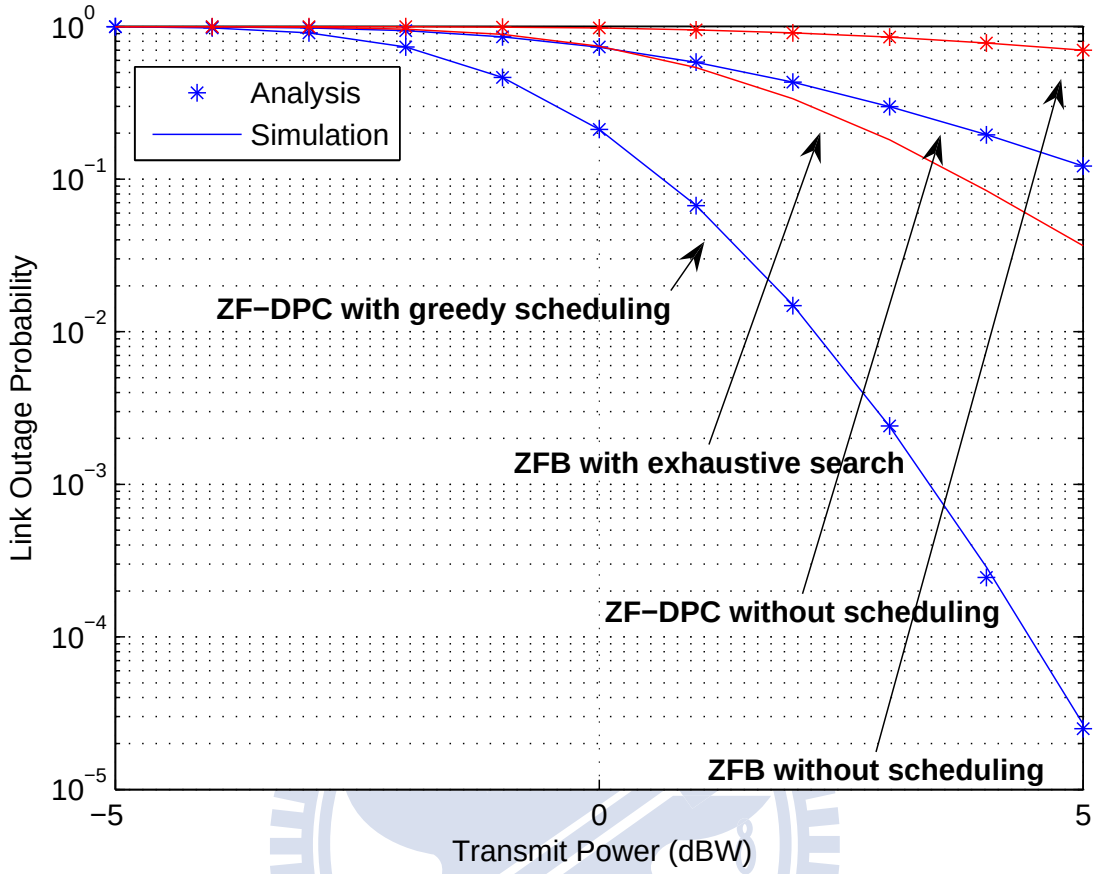

Figure 4.2: Link outage probability performance against the transmit power P_T for the strongest links of both the transmit ZF-DPC and ZF MIMO broadcast systems with and without scheduling when $M_T = 3$, $\sigma^2 = -103$ dBm, $\mu = 4$, $R = 2$ km, $K = 5$ and $\gamma_{th} = 2$ dB.

multiuser scheduling.

Figure 4.4 shows the coverage improvement for a different numbers of users in the ZF-DPC and transmit ZF MIMO broadcast systems when $P_T = 0$ dBW. The benefit of user ordering can be clearly observed from the coverage enhancement of ZF-DPC's strongest link at $K = M_T = 3$. Specifically, the cell radius is improved from 1.46 km to 1.8 km.

Figure 4.5 shows the coverage extension gain with different M_T and K according to (4.19). One can see that the benefit of multiuser scheduling is significant as K increases. However, the multiuser scheduling gain will reduce as more antennas are employed at the base station, i.e. for a larger M_T. From the above numerical results, we know that **soft**

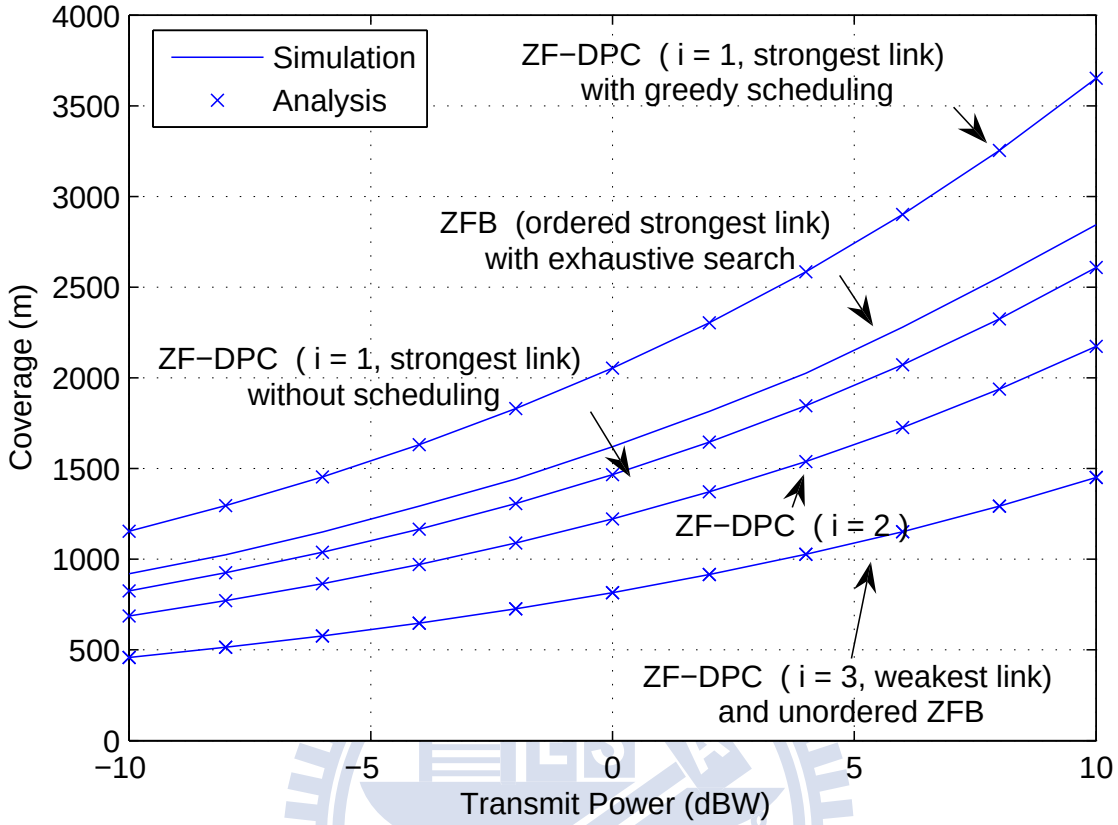

Figure 4.3: Link coverage performance against the transmit power P_T for different stream links of both the transmit ZF-DPC and ZF MIMO broadcast systems when $M_T = 3$, $\sigma^2 = -103$ dBm, $\mu = 4$, $P_{\text{out}} = 0.1$, $K = 5$ and $\gamma_{th} = 2$ dB.

coverage enhancement can be achieved by applying multiuser scheduling techniques without increasing transmission power.

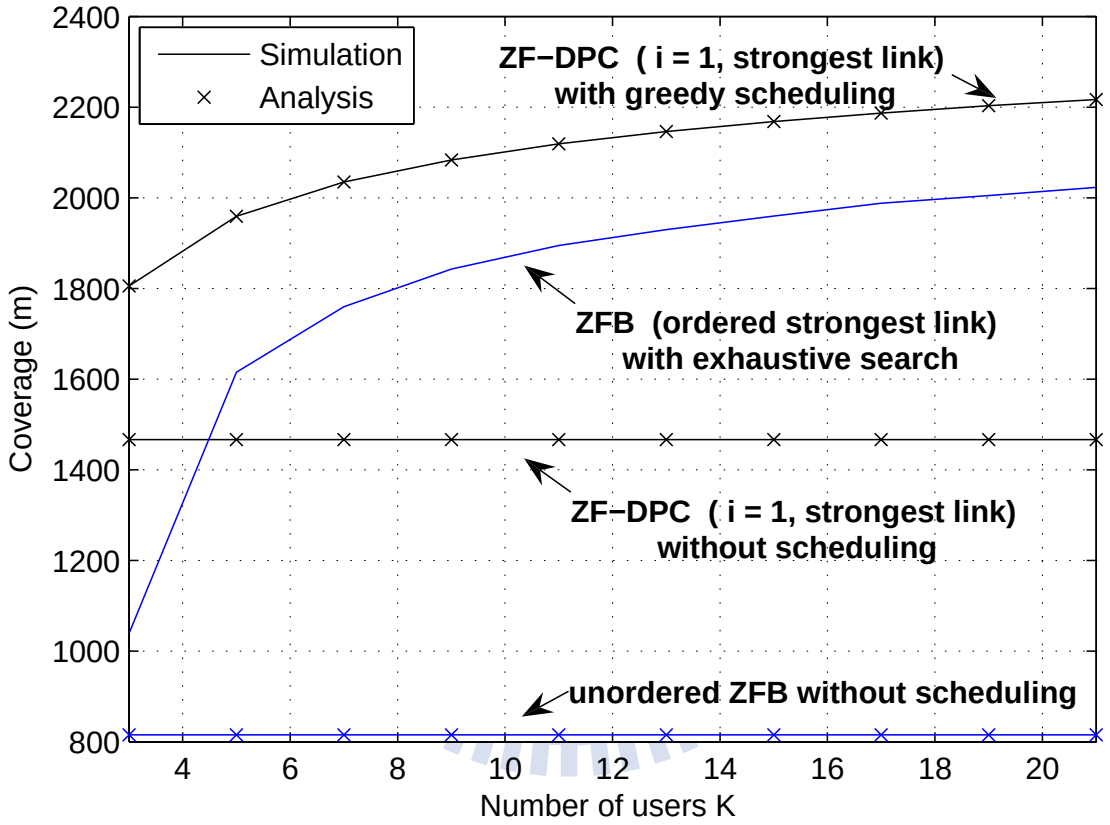

Figure 4.4: Link coverage performance against the number of users K for different stream links of both the transmit ZF-DPC and ZF MIMO broadcast systems when $M_T = 3$, $\sigma^2 = -103$ dBm, $\mu = 4$, $P_{\text{out}} = 0.1$, $P_T = 0$ dBW and $\gamma_{th} = 2$ dB.

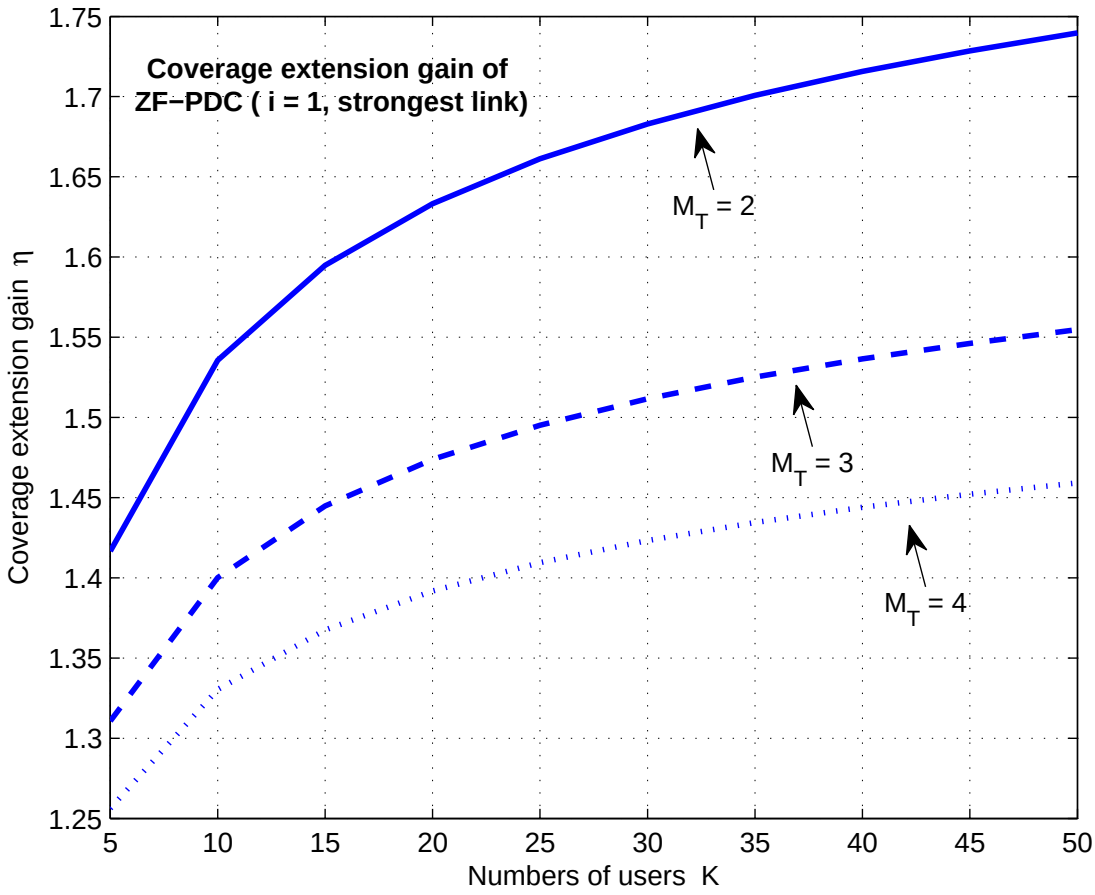

Figure 4.5: Coverage extension gain against the number of users K for the strongest link of the transmit ZF-DPC MIMO broadcast systems with $M_T = 2, 3$, and 4.

Chapter 5

Analysis of Multiuser MIMO Broadcast Systems with Receive Beamforming

Based on the study in Chapter 3, we know that the receive ZF based beamforming can be an attractive candidate to support tolerance toward *feedback errors* for realizing MIMO broadcast transmissions. One interesting issue is what performance the receive ZF MIMO broadcast systems can achieve in the presence of *estimation errors*. In this chapter, we provide performance analysis of the receive ZF MIMO broadcast systems in terms of link outage, link diversity order, reliable coverage, and sum-rate capacity for arbitrary $M_R \geq M_T$ cases. From simulation and analysis we find that the sum rate of the receive ZF MIMO broadcast systems will be bounded by a value in the presence of estimation errors. This result is different from the effect of feedback errors which only causes slightly sum-rate degradation. In addition, channel estimation errors will also cause shrinkage on reliable coverage and zero link diversity order on outage performance.

5.1 Background

5.1.1 System Model

Consider a downlink MIMO system with one base station and K user terminals. The number of transmit antennas and receive antennas is M_T and $M_R \geq M_T$, respectively. Denote $\mathbf{x} \in \mathbb{C}^{M_T \times 1}$ be the transmitted signal vector with power $E[\mathbf{x}\mathbf{x}^H] = \frac{P_T}{M_T}\mathbf{I}_{M_T}$ and $\mathbf{y} \in \mathbb{C}^{M_R \times 1}$ be the received signal vector. Let $\mathbf{n} \in \mathbb{C}^{M_T \times 1}$ as the complex Gaussian noise vector with $E[\mathbf{n}\mathbf{n}^H] = \sigma^2\mathbf{I}_{M_R}$. Then, the input-output system model for arbitrary base station and user pair with flat fading MIMO channel is

$$\mathbf{y} = \sqrt{g}\,\mathbf{H}\mathbf{x} + \mathbf{n} \ , \tag{5.1}$$

where $\mathbf{H}$ is the $M_R \times M_T$ channel matrix with independent Rayleigh faded entries and $0 < g \leq 1$ depicts the large-scale slowly-varying behavior of the local average channel gain as defined in (4.2):

$$10 \log_{10} g = -10\mu \log_{10} R + g_0 \quad [\text{dB}] \ .$$

Assume that imperfect CSI is obtained at the receiver with the following model [33]

$$\hat{\mathbf{H}} = \mathbf{H} + \mathbf{E} \ , \tag{5.2}$$

where $\hat{\mathbf{H}} \in \mathbb{C}^{M_R \times M_T}$ is the available CSI at the receiver with an uncorrelated error matrix $\mathbf{E} \in \mathbb{C}^{M_R \times M_T}$. Each entry of $\mathbf{E}$ is distributed by $\sim \mathcal{CN}(0, \epsilon_e^2)$ The uncertainty ϵ_e^2 is caused by estimation error at the receiver with $E[\mathbf{E}\mathbf{E}^H] = M_T \epsilon_e^2 \, \mathbf{I}_{M_R}$ [113].

5.1.2 MIMO Systems with ZF Receiver under Imperfect CSI-R

In Chapter 3, we have introduced MIMO systems with ideal receive ZF beamforming, i.e. ZF receiver at each user terminal. In this chapter, we consider MIMO systems with ZF receiver under imperfect CSI-R. With ZF receiver to recover the spatially multiplexed signals, the received signal $\mathbf{y}_k$ is multiplied the pseudo-inverse of estimated channel matrix as $\hat{\mathbf{H}}^\dagger = (\hat{\mathbf{H}}^H \hat{\mathbf{H}})^{-1} \hat{\mathbf{H}}^H$. The post-processed received signal $\hat{\mathbf{y}}$ becomes

$$\begin{aligned} \hat{\mathbf{y}} &= \hat{\mathbf{H}}^\dagger \mathbf{y} \\ &= (\hat{\mathbf{H}}^H \hat{\mathbf{H}})^{-1} \hat{\mathbf{H}}^H \left[\sqrt{g}(\hat{\mathbf{H}} - \mathbf{E})\mathbf{x} + \mathbf{n} \right] \\ &= \sqrt{g}\mathbf{x} + \underbrace{(\hat{\mathbf{H}}^H \hat{\mathbf{H}})^{-1} \hat{\mathbf{H}}^H \mathbf{n} - \sqrt{g}(\hat{\mathbf{H}}^H \hat{\mathbf{H}})^{-1} \hat{\mathbf{H}}^H \mathbf{E}\mathbf{x}}_{\triangleq \hat{\mathbf{n}}} \ . \end{aligned} \tag{5.3}$$

The noise covariance matrix $E[\hat{\mathbf{n}}\hat{\mathbf{n}}^H]$ of the ZF receiver is

$$\begin{aligned} E[\hat{\mathbf{n}}\hat{\mathbf{n}}^H] &= E\left\{ (\hat{\mathbf{H}}^\dagger \mathbf{n} - \sqrt{g}\hat{\mathbf{H}}^\dagger \mathbf{E}\mathbf{x})(\hat{\mathbf{H}}^\dagger \mathbf{n} - \sqrt{g}\hat{\mathbf{H}}^\dagger \mathbf{E}\mathbf{x})^H \right\} \\ &= \sigma^2 \hat{\mathbf{H}}^\dagger (\hat{\mathbf{H}}^\dagger)^H + \frac{P_T g}{M_T} \hat{\mathbf{H}}^\dagger E[\mathbf{E}\mathbf{E}^H] (\hat{\mathbf{H}}^\dagger)^H \\ &\overset{(a)}{=} (\sigma^2 + P_T g \epsilon_e^2)(\hat{\mathbf{H}}^H \hat{\mathbf{H}})^{-1} \ , \end{aligned} \tag{5.4}$$

where (a) comes from the fact $\hat{\mathbf{H}}^\dagger (\hat{\mathbf{H}}^\dagger)^H = (\hat{\mathbf{H}}^H \hat{\mathbf{H}})^{-1}$. Based on (5.4), it may have nonzero off-diagonal elements which results in correlated noise across different data streams. To lower complexity, the noise correlation is usually ignored and each stream is decoded independently

[24] [106]. Under equal power across transmit antennas, the output post processing SNR at the i-th stream is

$$\begin{aligned}\gamma_i &= \frac{P_T g/M_T}{\left[E\left\{\hat{\mathbf{n}}\hat{\mathbf{n}}^H\right\}\right]_{i,i}} \\ &= \frac{\rho}{M_T(1+\rho\epsilon_e^2)\left[(\hat{\mathbf{H}}^H\hat{\mathbf{H}})^{-1}\right]_{i,i}} \quad , \quad i = 1, \cdots, M_T \,, \end{aligned} \tag{5.5}$$

where $\rho = P_T g/\sigma^2$ is the mean received SNR and $[\mathbf{A}]_{i,i}$ represents the i-th diagonal element of a squared matrix $\mathbf{A}$. The term $z = 1/\left[(\hat{\mathbf{H}}^H\hat{\mathbf{H}})^{-1}\right]_{i,i}$ is Chi-square distributed with $l = 2(M_R - M_T + 1)$ degrees of freedom [24] [106] with PDF be [114]

$$f_Z(z) = \frac{z^{\frac{l}{2}-1}\, e^{-z/2\Sigma^2}}{\Sigma^l\, 2^{l/2}\, \Gamma(l/2)} \quad , \quad z \geq 0 \ , \tag{5.6}$$

where $\Sigma^2 = (1+\epsilon_e^2)/2$ and $\Gamma(a) = \int_0^\infty t^{a-1}e^{-t}dt$ is the complete gamma function. As a result, the ZF receiver has identical post processing SNR γ_i with PDF for all i

$$f_{\gamma_i}(\gamma) = \frac{M_T}{\hat{\rho}} \frac{e^{-M_T\gamma/\hat{\rho}}}{(M_R - M_T)!} \left(\frac{M_T}{\hat{\rho}}\gamma\right)^{M_R - M_T} \quad , \quad \gamma \geq 0 \ , \tag{5.7}$$

where $\hat{\rho} \triangleq \rho(1+\epsilon_e^2)/(1+\rho\epsilon_e^2)$. The corresponding CDF of γ_i is expressed by

$$\begin{aligned} F_{\gamma_i}(\gamma) &= 1 - \frac{\Gamma\left(M_R - M_T + 1, \frac{M_T\gamma}{\hat{\rho}}\right)}{\Gamma\left(M_R - M_T + 1\right)} \\ &= 1 - \Gamma_{\mathrm{R}}\left(M_R - M_T + 1, \frac{M_T\gamma}{\hat{\rho}}\right) \quad , \end{aligned} \tag{5.8}$$

where $\Gamma(a,x) = \int_x^\infty t^{a-1}e^{-t}dt$ is the upper incomplete gamma function and $\Gamma_{\mathrm{R}}(a,x) = \frac{\Gamma(a,x)}{\Gamma(a)}$ is the regularized gamma function.

5.1.3 MIMO Broadcast Systems with Receive ZF Beamforming

As we discussed in Chapter 3.2.3, for receive ZF MIMO broadcast systems, each user feedbacks the channel SNR vector $\{\gamma_i^k\}_{i=1}^{M_T}$ to the transmitter for scheduling the target group of users, where γ_i^k is the output SNR at the i-th receive antenna of user k defined in (5.7). Since the ZF receiver can change an $M_R \times M_T$ channel matrix into M_T parallel subchannels, the scheduler at the transmitter can assign each transmit antenna to serve one of the selected target users. It is unnecessary to assign all the subchannels to a single user in a point-to-point way [24–26]. Under homogeneous environment, i.e. all users have the same ρ value,

the scheduler transmits data to the target user k^* via the ith transmit antenna according to the criterion:

$$k^* = \arg\max_k \gamma_i^k \ . \tag{5.9}$$

Since there are K spatially-independent choices for an arbitrary transmit antenna, such **broadcast** scheduling algorithm is called independent stream scheduler in [24,25] and called spatially-independent scheduling in [26].

5.2 Link Performance Analysis for Arbitrary $M_R \geq M_T$ Case

In this section, we provide various link performance metric analysis including link outage, link diversity order, and reliable coverage for the receive ZF MIMO broadcast systems. In this chapter, we have the following definition for ZF MIMO broadcast systems

Definition 1: We denote (M_T, M_R, K) receive ZF MIMO broadcast systems as the MIMO broadcast systems with receive ZF beamforming and equips with M_T transmit antennas at base station and M_R receive antennas at each of K users.

5.2.1 Link Outage and Link Diversity Order

As first, we focus on link outage and link diversity order performance for a (M_T, M_R, K) receive ZF MIMO broadcast systems. Note that each stream can be linked with different individual users for the receive ZF MIMO broadcast systems. As defined in Chapter 2.3.1, for a point-to-multipoint spatial multiplexing MIMO broadcast systems, each link's outage probability is individually defined as $P_{\text{out}}^i = P_r\{\gamma_i < \gamma_{th}\}$ for all multipoint transmission links. In addition, since the SNR distribution of each stream is the same, the provided link performance analysis can be applied to all transmission links to drop the subscript i.

Based on (5.8) and the scheduling rule in (5.9), we have the link outage probability of receive ZF MIMO broadcast systems by

$$\begin{aligned} P_{\text{out}}(\gamma_{th}) &= P_r\{\gamma_n < \gamma_{th}\} \\ &= \left(1 - \Gamma_{\text{R}}\left(M_R - M_T + 1, \frac{M_T \gamma_{th}(1+\epsilon_e^2\rho)}{\rho(1+\epsilon_e^2)}\right)\right)^K \ . \end{aligned} \tag{5.10}$$

Let link outage probability $P_{\text{out}}(\cdot)$ be a function of SNR. As defined in Chapter 2.3.2, the link diversity order D_{order} is

$$D_{\text{order}} \triangleq -\lim_{\rho \to \infty} \frac{\log P_{\text{out}}(\rho)}{\log \rho} \ , \tag{5.11}$$

where ρ is the receive SNR. The analysis of the link diversity order is given by as follows.

Theorem 3. *The link diversity order of a (M_T, M_R, K) receive ZF MIMO broadcast systems with perfect CSI-R is $K(M_R - M_T + 1)$.*

Proof. See Appendix C. □

Theorem 4. *The link diversity order of a (M_T, M_R, K) receive ZF MIMO broadcast systems will be zero if there exists channel estimation errors ϵ_e^2.*

Proof. See Appendix D. □

Clearly, there will exist a minimal achievable outage value under different configurations (M_T, M_R, K) and required γ_{th} when user ends have imperfect CSI-R ϵ_e^2. As ρ increases, the value $P_{\text{out}}(\rho)$ can not be smaller any more results in an *outage probability floor*. We define the link outage floor $F_{\text{out}}(\gamma_{th})$ under a requirement γ_{th} as

$$F_{\text{out}}(\gamma_{th}) \triangleq \lim_{\rho \to \infty} P_{\text{out}}(\gamma_{th}) = \left(1 - \Gamma_{\text{R}}\left(M_R - M_T + 1, \frac{M_T \gamma_{th} \epsilon_e^2}{(1+\epsilon_e^2)}\right)\right)^K \ . \tag{5.12}$$

5.2.2 Reliable Coverage

Another important link performance metric is the achievable link coverage we have defined in Chapter 2.3.3. Identical to Chapter 4, we focus on the achievable reliable coverage with 90% link reliability, i.e. a corresponding link radius associated with the required SNR γ_{th} under $P_{\text{out}} = 0.1$.

To derive the reliable link coverage $R_{\texttt{RZF}}$ based on (5.10), we utilize the inverse function skill similar to that we used in Chapter 4, i.e.

$$z = \Gamma_{\text{R}}(a, x) \ \Rightarrow \ x = \Gamma_{\text{R}}^{-1}(a, z) \ . \tag{5.13}$$

By substituting $\rho = \frac{P_T g}{\sigma^2} = \frac{P_T 10^{g_0/10}}{\sigma^2 R^\mu}$ and (5.13) into (5.10), the link coverage can be written as

$$\begin{aligned} R_{\texttt{RZF}} &= \left[\frac{P_T 10^{g_0/10}(1+\epsilon_e^2)}{M_T \gamma_{th} \sigma^2} \ \Gamma_{\mathrm{R}}^{-1}\left(M_R - M_T + 1, 1 - \sqrt[K]{P_{\mathrm{out}}}\right) - \frac{P_T 10^{g_0/10}\epsilon_e^2}{\sigma^2} \right]^{\frac{1}{\mu}} \\ &= \left[r_{\texttt{Perfect}} - r_{\texttt{Error}} \right]^{\frac{1}{\mu}} \ , \end{aligned} \tag{5.14}$$

in which

$$r_{\texttt{Perfect}} = \left[\frac{P_T 10^{g_0/10}}{M_T \gamma_{th} \sigma^2} \ \Gamma_{\mathrm{R}}^{-1}\left(M_R - M_T + 1, 1 - \sqrt[K]{P_{\mathrm{out}}}\right) \right] \ , \tag{5.15}$$

and

$$r_{\texttt{Error}} = \left[\frac{\epsilon_e^2 P_T 10^{g_0/10}}{M_T \gamma_{th} \sigma^2} \ \left(M_T \gamma_{th} - \Gamma_{\mathrm{R}}^{-1}\left(M_R - M_T + 1, 1 - \sqrt[K]{P_{\mathrm{out}}}\right)\right) \right] \ . \tag{5.16}$$

Based on (5.14), the coverage $R_{\texttt{RZF}}$ with $(1-P_{\mathrm{out}})$ link reliability will shrink as the estimation error ϵ_e^2 increases. Specifically, under perfect CSI-R, i.e. $\epsilon_e^2 = 0$, the reliable coverage of the receive ZF MIMO broadcast systems is $r_{\texttt{Perfect}}^{1/\mu}$. However, the corresponding coverage will be shrunk due to the term $r_{\texttt{Error}}$ caused by imperfect CSI-R. The link coverage shrinkage ratio due to estimation error ϵ_e^2 is defined as

$$\eta_{\epsilon_e^2} = \left[1 - \frac{r_{\texttt{Error}}}{r_{\texttt{Perfect}}} \right]^{\frac{1}{\mu}} \ . \tag{5.17}$$

In fact, the receive ZF MIMO broadcast systems can only support serving coverage with γ_{th} requirement and $(1 - P_{\mathrm{out}})$ link reliability under the condition achieves

$$\epsilon_{th}^2 = \frac{\Gamma_{\mathrm{R}}^{-1}\left(M_R - M_T + 1, 1 - \sqrt[K]{P_{\mathrm{out}}}\right)}{M_T \gamma_{th} - \Gamma_{\mathrm{R}}^{-1}\left(M_R - M_T + 1, 1 - \sqrt[K]{P_{\mathrm{out}}}\right)} \geq \epsilon_e^2 \ . \tag{5.18}$$

As number of scheduling users K increase, the term ϵ_{th}^2 will increase results in a larger resistance on estimation error by taking advantage of multiuser diversity.

5.3 Sum Rate Analysis for Arbitrary $M_R \geq M_T$ Case

Besides link performance metrics discussed above, the sum rate performance of a (M_T, M_R, K) receive ZF MIMO broadcast systems with imperfect CSI-R is addressed here. According to the order statistics analysis, the PDF of post processing SNR for a (M_T, M_R, K) receive ZF

MIMO broadcast systems is

$$f_{\gamma_i^*}(\gamma) = K f_{\gamma_i}(\gamma) \left[F_{\gamma_i}(\gamma)\right]^{K-1} = \frac{KA}{L\,!}\, e^{-A\gamma}(A\gamma)^L \left[1 - \Gamma_{\mathrm{R}}\left(L+1, A\gamma\right)\right]^{K-1} \quad . \tag{5.19}$$

with

$$A \triangleq \frac{M_T}{\hat{\rho}} = \frac{M_T(1+\rho\epsilon_e^2)}{\rho(1+\epsilon_e^2)} \quad \text{and} \quad L \triangleq M_R - M_T \ . \tag{5.20}$$

With the aid of the following property of $\Gamma(n,x)$ [115, p.900] to help the analysis

$$\Gamma(a,x) = (a-1)!\, e^{-x} \sum_{m=0}^{a-1} \frac{x^m}{m!} \qquad a = 1, 2, \cdots \ , \tag{5.21}$$

then we have

$$\begin{aligned}
\left[1 - \Gamma_{\mathrm{R}}\left(L+1, A\gamma\right)\right]^{K-1} &= \left(1 - \frac{L!\, e^{-A\gamma} \sum_{m=0}^{L} \frac{(A\gamma)^m}{m!}}{\Gamma(L+1)}\right)^{K-1} \\
&\overset{(a)}{=} \left(1 - e^{-A\gamma} \sum_{m=0}^{L} \frac{(A\gamma)^m}{m!}\right)^{K-1} \\
&\overset{(b)}{=} \sum_{i=0}^{K-1} \binom{K-1}{i} (-1)^i e^{-iA\gamma} \left(\sum_{m=0}^{L} \frac{(A\gamma)^m}{m!}\right)^i \\
&= \sum_{i=0}^{K-1} \binom{K-1}{i} (-1)^i e^{-iA\gamma} \left(\sum_{m_1=0}^{L} \frac{(A\gamma)^{m_1}}{m_1!}\right) \cdots \left(\sum_{m_i=0}^{L} \frac{(A\gamma)^{m_i}}{m_i!}\right) \\
&= \sum_{i=0}^{K-1} \binom{K-1}{i} (-1)^i e^{-iA\gamma} \left(\sum_{m_1=0}^{L} \cdots \sum_{m_i=0}^{L} \frac{(A\gamma)^{m_1+\ldots+m_i}}{m_1! \cdots m_i!}\right)
\end{aligned} \tag{5.22}$$

where (a) follows by $\Gamma(a) = (a-1)!$ for a is positive integer and (b) comes from the binomial expansion $(1-x)^n = \sum_{i=0}^{n} \binom{n}{i} (-1)^i x^i$. The average sum rate of the (M_T, M_R, K) receive ZF

MIMO broadcast systems can thus be written as the exactly capacity closed-form expression

$$
\begin{aligned}
&C_{\mathrm{ZFR}}^{\epsilon_e^2} \\
&= \sum_{n=1}^{M_T} E\left\{\log(1+\gamma_n)\right\} \\
&= M_T \int_0^{\infty} \log(1+\gamma) f_{\gamma^*}(\gamma) d\gamma \\
&= \frac{M_T K A}{L\,!} \int_0^{\infty} \log(1+\gamma) \sum_{i=0}^{K-1} \binom{K-1}{i} (-1)^i e^{-(i+1)A\gamma} \left(\sum_{m_1=0}^{L} \cdots \sum_{m_i=0}^{L} \frac{(A\gamma)^{m_1+\ldots+m_i+L}}{m_1! \cdots m_i!} \right) d\gamma \\
&\overset{(a)}{=} \frac{M_T K A}{L\,!} \sum_{i=0}^{K-1} \binom{K-1}{i} (-1)^i \sum_{m_1=0}^{L} \cdots \sum_{m_i=0}^{L} \left(\frac{(m_1+\ldots+m_i+L)! A^{m_1+\ldots+m_i+L}}{m_1! \cdots m_i!} e^{(i+1)A} \times \right. \\
&\qquad \left. \sum_{j=1}^{m_1+\ldots+m_i+L+1} \frac{\Gamma\left(j-(m_1+\ldots+m_i+L+1),(i+1)A\right)}{(i+1)^j A^j} \right) ,
\end{aligned}
\tag{5.23}
$$

where the parameters A and L are defined in (5.20) and equality (a) is based on the following integral identity [116]

$$
\int_0^{\infty} \log(1+t)\, e^{-\alpha t} t^{\beta-1} dt = (\beta-1)!\, e^{\alpha} \sum_{i=1}^{\beta} \frac{\Gamma(i-\beta,\alpha)}{\alpha^i}, \;\; \alpha > 0; \;\; \beta = 1, 2, \cdots \;\; . \tag{5.24}
$$

Note that as SNR approaches to infinite, i.e. $\rho \to \infty$, the sum rate of the (M_T, M_R, K) receive ZF MIMO broadcast systems with channel estimation error $\epsilon_e^2 \neq 0$ will be bounded by a value $\overline{C_{\mathrm{ZFR}}^{\epsilon_e^2}}$ we called that as the *sum rate floor*

$$
\overline{C_{\mathrm{ZFR}}^{\epsilon_e^2}} = \lim_{\rho \to \infty} C_{\mathrm{ZFR}}^{\epsilon_e^2} = C_{\mathrm{ZFR}}^{\epsilon_e^2}\big|_{A=\frac{M_T \epsilon_e^2}{(1+\epsilon_e^2)}} \;\; . \tag{5.25}
$$

5.3.1 Special Case: $M_T = M_R$

In the special case $M_R = M_T = M$, i.e. $L = 0$, the corresponding average sum rate of the (M_T, M_T, K) receive ZF MIMO broadcast systems becomes

$$
\begin{aligned}
C_{\mathrm{ZFR}|_M}^{\epsilon_e^2} &= M_T K A \sum_{i=0}^{K-1} \binom{K-1}{i} (-1)^i e^{(i+1)A} \frac{\Gamma\left(0,(i+1)A\right)}{(i+1)A} \\
&\overset{(a)}{=} M_T K A \sum_{i=0}^{K-1} \binom{K-1}{i} (-1)^i h\left((i+1)A\right) \;\; ,
\end{aligned}
\tag{5.26}
$$

where (a) is obtained by the property $\Gamma(0,x) = E_1(x)$ and $E_r(x) = \int_1^\infty e^{-xt}t^{-r}dt$ is the exponential integer function of order r. Note that the function $h(\cdot)$ in (5.26) is defined in [26] as

$$h(x) \triangleq \int_0^\infty e^{-xt}\log(1+t)\,dt = \frac{e^x E_1(x)}{x} \quad . \tag{5.27}$$

Furthermore, if there is no estimation errors in receiver sides, says $\epsilon_e^2 = 0$, the term A in (5.20) becomes M_T/ρ and the ergodic capacity is now

$$C_{\text{RZF}|_M} = \frac{KM_T^2}{\rho}\sum_{i=0}^{K-1}\binom{K-1}{i}(-1)^i h\left(\frac{(i+1)M_T}{\rho}\right) \quad , \tag{5.28}$$

which is identical to the closed-form expression provided in [26].

5.3.2 Sum Rate under Water-Filling Power Allocation

When receiver end has perfectly estimated channel knowledge to feed back the base station, the scheduler can further improve sum rate using water-filling power allocation instead of equally allocated power among the transmit antennas. With the help of the long-term power constraint method provided in [60], we had provided the sum-rate closed form under water-filling power allocation for the case $M_R = M_T$ in Chapter 3.3 and [31]. In the section, we release our analytical expressions to general case $M_R \geq M_T$.

Based on (5.5), we define the term $d_i = 1/\left[(\mathbf{H}^H\mathbf{H})^{-1}\right]_{i,i}$ as the effective channel gain of the i-th substream due to $\epsilon_e^2 = 0$ and $\hat{\mathbf{H}} = \mathbf{H}$. Similar to the approach in (5.19), we have the PDF of scheduled d_n^* from (5.7)

$$f_{d_i^*}(d) = \frac{K}{L!}\,e^{-d}d^L\left[1-\Gamma_{\text{R}}\left(L+1,d\right)\right]^{K-1} \quad . \tag{5.29}$$

Subject to the long-term power constraint (5.32) with water-level solution ς_0, the average sum rate of the (M_T, M_R, K) receive ZF MIMO broadcast systems with water-filling power

allocation is given by

$$
\begin{aligned}
C_{\mathrm{RZF}}^{\mathrm{water}} &= \sum_{n=1}^{M_T} E\left[\log(\varsigma_0 d_n)\right]_+ \\
&= M_T \int_{1/\varsigma_0}^{\infty} \log(\varsigma_0 z) f_{d_n^*}(z) dz \\
&\overset{(a)}{=} \frac{M_T K}{\varsigma_0 L\,!} \int_1^{\infty} \log(z) \sum_{i=0}^{K-1} \binom{K-1}{i} (-1)^i e^{-\frac{i+1}{\varsigma_0} z} \left(\sum_{m_1=0}^{L} \cdots \sum_{m_i=0}^{L} \frac{\left(\frac{d}{\varsigma_0}\right)^{m_1+\ldots+m_i+L}}{m_1! \cdots m_i!} \right) dz \\
&\overset{(b)}{=} \frac{M_T K}{L\,!} \sum_{i=0}^{K-1} \binom{K-1}{i} (-1)^i \sum_{m_1=0}^{L} \cdots \sum_{m_i=0}^{L} \left(\frac{(m_1+\ldots+m_i+L)!}{m_1! \cdots m_i! \, (i+1)^{m_1+\ldots+m_i+L+1}} \times \right. \\
&\qquad \left. \sum_{j=0}^{m_1+\ldots+m_i+L} \frac{\Gamma\left(j, \frac{(i+1)}{\varsigma_0}\right)}{j!} \right) ,
\end{aligned}
\tag{5.30}
$$

where (a) is based on modifying (5.22) and changing integral variable, and (b) is derived from the integral identity provided in [116]

$$
\int_1^{\infty} \log(t)\, e^{-\alpha t} t^{\beta-1} dt = \frac{(\beta-1)!}{\alpha^{\beta}} \sum_{i=0}^{\beta-1} \frac{\Gamma(i,\alpha)}{i!}, \;\; \alpha > 0; \; \beta = 1, 2, \cdots \; . \tag{5.31}
$$

The details of long-term power constraint is

$$
\begin{aligned}
\sum_{n=1}^{M_T} E\left[\varsigma - \frac{1}{d_n}\right]_+ &= \frac{M_T K}{L\,!} \sum_{i=0}^{K-1} \binom{K-1}{i} (-1)^i \sum_{m_1=0}^{L} \cdots \sum_{m_i=0}^{L} \left(\frac{1}{m_1! \cdots m_i!} \times \right. \\
&\qquad \left[\varsigma^{-(m_1+\ldots+m_i+L)} E_{-(m_1+\ldots+m_i+L)}\left(\frac{i+1}{\varsigma}\right) \right. \\
&\qquad \left. \left. -(i+1)^{-(m_1+\ldots+m_i+L)} \Gamma\left(m_1+\ldots+m_i+L, \frac{i+1}{\varsigma}\right) \right] \right) \\
&= P_T \;\; ,
\end{aligned}
\tag{5.32}
$$

where the water-level solution ς_0 can be found by mathematical tools. Note that the general forms (5.30) and (5.32) will be identical to the analytical results provided in Chapter 3.3 and [31] as $M_T = M_R$.

5.4 Numerical Results

In this section, we illustrate the achievable link and sum rate performances of the receive ZF MIMO broadcast systems with imperfect CSI-R effect. For link performance evaluation, the

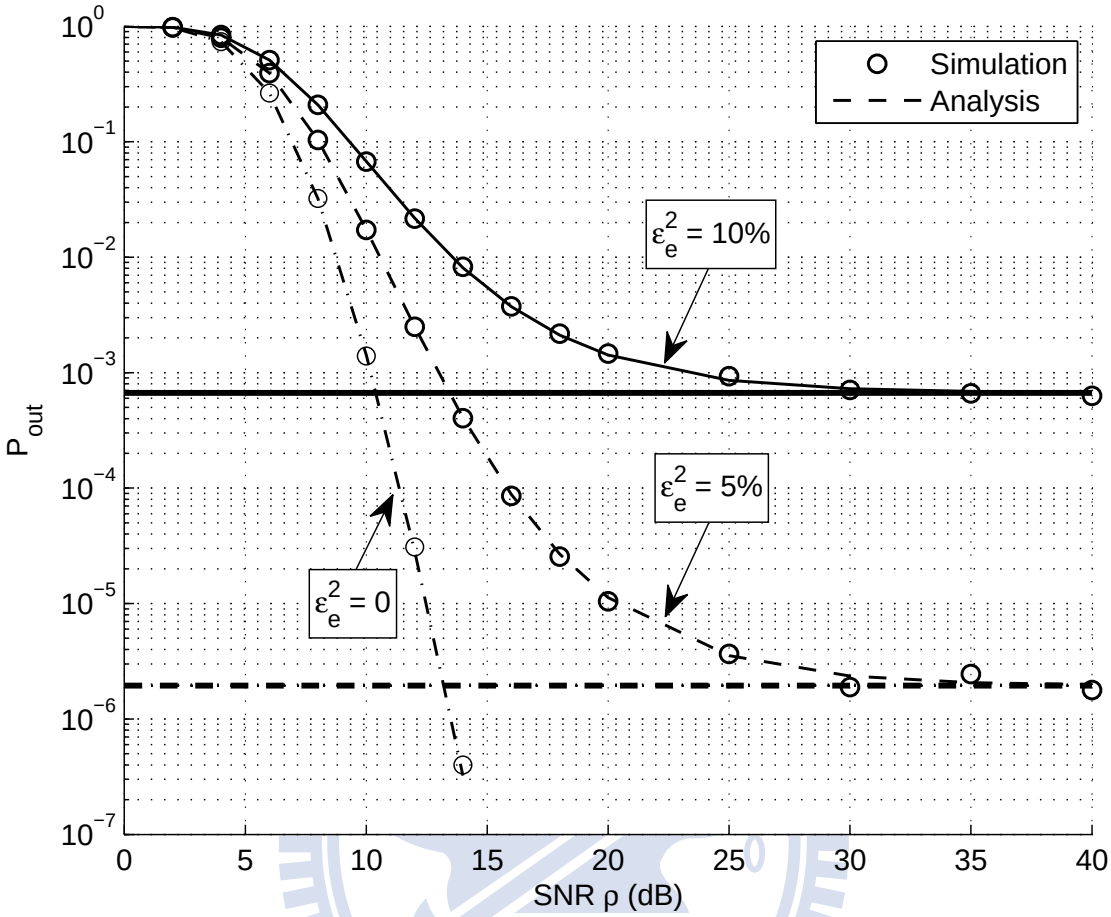

Figure 5.1: Link outage performance of the $(M_T = 3, M_R = 4, K = 6)$ receive ZF MIMO broadcast systems with $\epsilon_e^2 = 0, 5\%$, and 10%. The predetermined required SNR is $\gamma_{th} = 6$ dB.

required γ_{th} is according to the predetermined SNR values supported for various modulation and coding schemes (MCS) in the IEEE 802.16e standard [117]. That is, {QPSK$\frac{1}{2}$, QPSK$\frac{3}{4}$, 16-QAM$\frac{1}{2}$, 16-QAM$\frac{3}{4}$, 64-QAM$\frac{2}{3}$, 64-QAM$\frac{3}{4}$} with the corresponding SNR requirements {6, 8.5, 11.5, 15, 19, 21} dB.

5.4.1 Effects of Imperfect CSI-R on Link Performance

Figure 5.1 shows the simulative and analytical link outage performances of the $(M_T = 3, M_R = 4, K = 6)$ receive ZF MIMO broadcast systems under different degrees of channel estimation errors $\epsilon_e^2 = 0, 5\%$, and 10%. The desired link quality is $\gamma_{th} = 6$ dB. In this

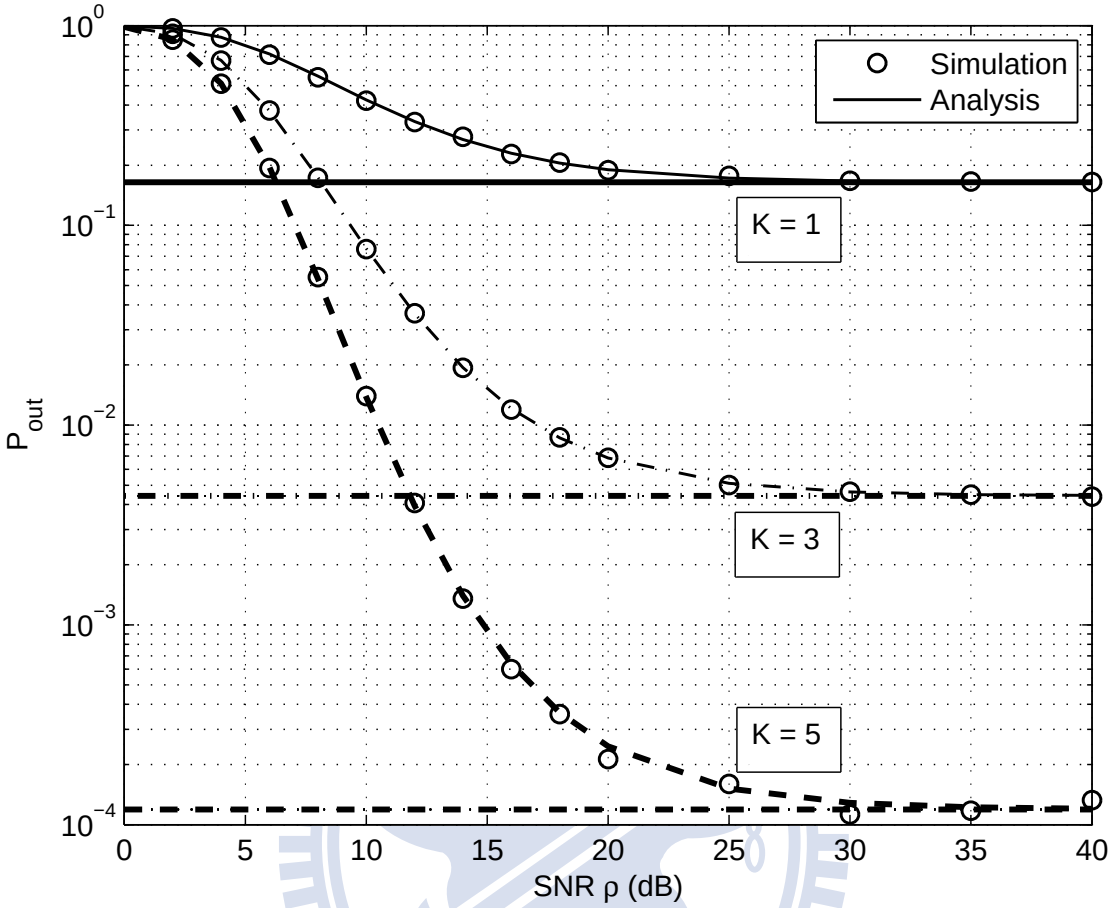

Figure 5.2: Link outage performance of the $(M_T = 2, M_R = 3, K)$ receive ZF MIMO broadcast systems with different number of users K under $\epsilon_e^2 = 10\%$. The predetermined required SNR is $\gamma_{th} = 6$ dB.

figure, the receive ZF MIMO broadcast systems can provide rapidly decreased link outage performance with diversity order $K(M_R - M_T + 1) = 12$ in perfect estimated condition. However, the link diversity order will become zero in the presence of estimation error ϵ_e^2. For example, as $\rho > 30$ dB, P_{out} is bounded for both cases $\epsilon_e^2 = 5\%$ and 10% with corresponding outage floors $F_{\text{out}}(\gamma_{th}) = 1.944 \times 10^{-6}$ and 6.692×10^{-4}. It also makes sense that more serious estimation error will cause poorer link outage performance for the receive ZF MIMO broadcast systems.

The benefit of **multiuser diversity** on link reliability enhancement is shown in Fig. 5.2 for the receive ZF MIMO broadcast systems with $M_T = 2, M_R = 3, \epsilon_e^2 = 10\%, \gamma_{th} = 6$ dB and

Table 5.1: Coverage performance (meters) of $(M_T = 2, M_R = 4, K = 5)$ receive ZF MIMO broadcast systems for various SNR requirements and $P_{\text{out}} = 0.1$ under different ϵ_e^2.

MCS	QPSK $\frac{1}{2}$	QPSK $\frac{3}{4}$	16-QAM $\frac{1}{2}$	16-QAM $\frac{3}{4}$	64-QAM $\frac{2}{3}$	64-QAM $\frac{3}{4}$
SNR (dB)	6	8.5	11.5	15.0	19.0	21.0
$\epsilon_e^2 = 0$	3005	2602	2189	1790	1422	1267
$\epsilon_e^2 = 1\%$	2994	2580	2146	1701	1208	883
$\epsilon_e^2 = 5\%$	2949	2485	1939	945	N/A	N/A
$\epsilon_e^2 = 10\%$	2890	2349	1519	N/A	N/A	N/A
$\epsilon_e^2 = 15\%$	2826	2185	N/A	N/A	N/A	N/A

Table 5.2: Coverage enhancement (meters) by multiuser scheduling for 16-QAM 3/4 link requirement and $P_{\text{out}} = 0.1$ with $M_T = 2$ and $M_R = 4$.

	$\epsilon_e^2 = 0$	$\epsilon_e^2 = 1\%$	$\epsilon_e^2 = 5\%$	$\epsilon_e^2 = 10\%$	$\epsilon_e^2 = 15\%$	ϵ_{th}^2 in (5.18)
$K = 5$	1790	1701	945	N/A	N/A	0.054
$K = 30$	2064	2011	1736	355	N/A	0.100
$K = 210$	2263	2223	2046	1724	642	0.151

various K values. In the point-to-point single-user MIMO system with ZF receiver, it has only at most 83.6% link reliability (i.e. $F_{\text{out}}(\gamma_{th}) = 0.164$) as SNR ρ approaches to infinity. The link reliability can be significantly improved by taking advantage of multiuser diversity. For example, the link outage probabilities are respectively reduced to $F_{\text{out}}(\gamma_{th}) = 4.421 \times 10^{-3}$ and 1.191×10^{-4} for merely $K = 3$ and $K = 5$. However, we can find that multiuser diversity can not cure the effect of zero link diversity order caused by estimation error.

To evaluate how channel estimation error could affect the reliable coverage of a receive ZF MIMO broadcast system, Table 5.1 lists the achievable coverage for different SNR requirements with $P_{\text{out}} = 0.1$. The evaluated parameters are $M_T = 2, M_R = 4, K = 5$, path loss exponent $\mu = 4$, transmit power $P_T = 10$ dBW, and various ϵ_e^2 values. Clearly, it is hard for a system to support high MCS level under the same transmit power due to strict link requirement, e.g. $R_{\texttt{RZF}}$ is 3005 m for supporting QPSK$\frac{1}{2}$ transmission but $R_{\texttt{RZF}}$ becomes 1267 m for supporting 64-QAM$\frac{3}{4}$ transmission as $\epsilon_e^2 = 0$. When estimation error appears in receiver end, the achievable reliable coverage will be shrunk or even become unsupported. For

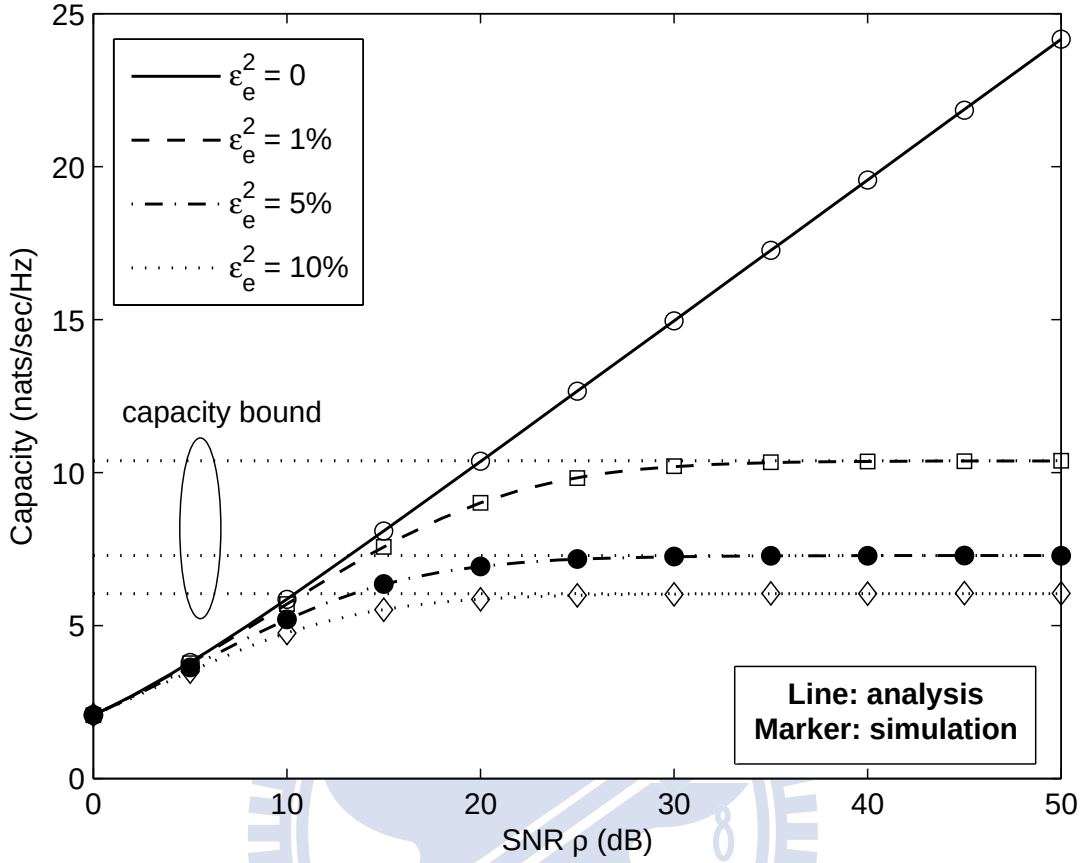

Figure 5.3: Capacity of the $(M_T = 2, M_R = 3, K = 5)$ receive ZF MIMO broadcast systems with $\epsilon_e^2 = 0, 1\%, 5\%$, and 10%.

example, the receive ZF MIMO broadcast systems can originally support 16-QAM$\frac{3}{4}$ transmission under 1790 m for $\epsilon_e^2 = 0$. The region is reduced to 1701 m and 945 m for $\epsilon_e^2 = 1\%$ and $\epsilon_e^2 = 5\%$, respectively. The system even can not support 16-QAM$\frac{3}{4}$ transmission as ϵ_e^2 becomes 10%.

Similar to the transmit based MIMO broadcast systems discussed in Chapter 4, the concept of **soft coverage** extension can be also applied to the receive ZF MIMO broadcast systems to oppose the shrinkage caused by imperfect CSI-R. Table 5.2 shows an example for coverage enhancement by multiuser scheduling. Continue with the previous example of 16-QAM$\frac{3}{4}$ transmission, the $(M_T = 2, M_R = 4, K = 5)$ receive ZF MIMO broadcast systems can at most resist $\epsilon_e^2 = 5.4\%$ error according to (5.18) and become unsupported as $\epsilon_e^2 = 10\%$. With the help of multiuser diversity, the system can work again under $\epsilon_e^2 = 10\%$

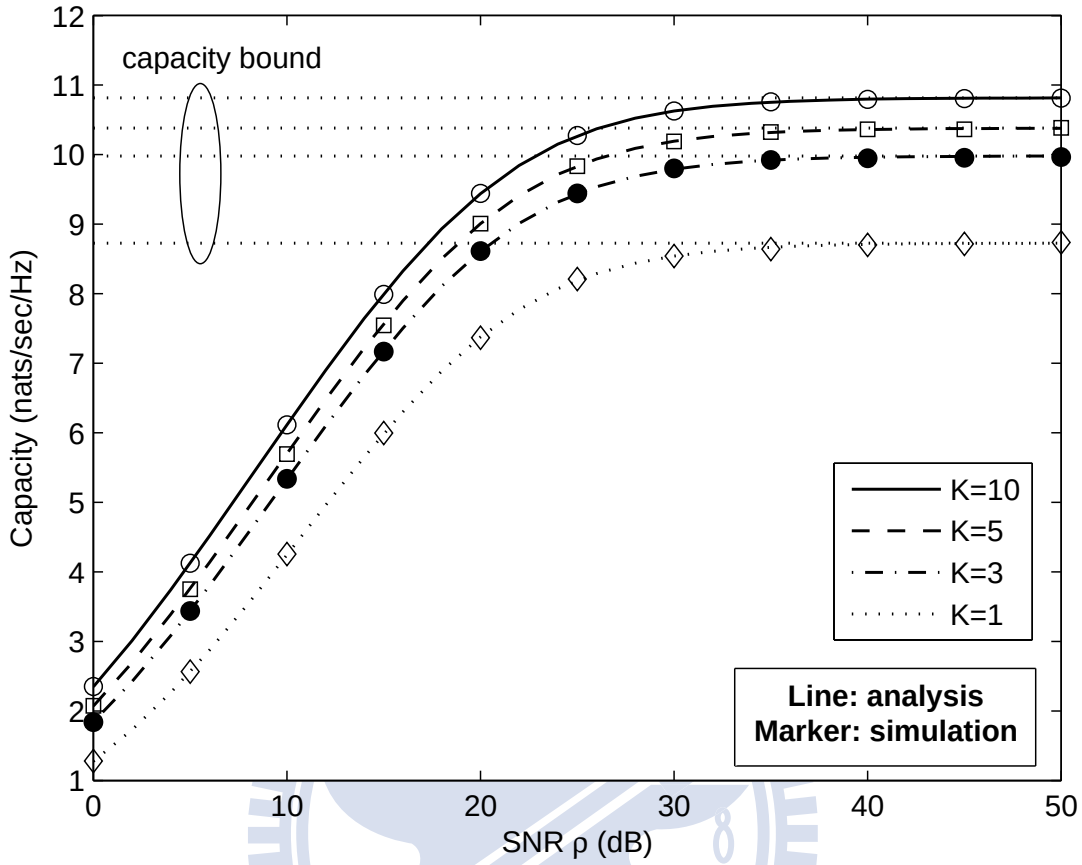

Figure 5.4: Capacity of the $(M_T = 2, M_R = 3, K)$ receive ZF MIMO broadcast systems with different number of users K under $\epsilon_e^2 = 1\%$.

and $\epsilon_e^2 = 15\%$ as K increases to 30 and 210, respectively. Although, it may be difficult for a system with enough user population (e.g. $K = 210$) to recover the reduced coverage. This numerical example provides the potential gain of multiuser diversity on soft coverage extension.

5.4.2 Effects of Imperfect CSI-R on Sum Rate

Figure 5.3 presents the sum-rate capacity of a $(M_T = 2, M_R = 3, K = 5)$ receive ZF MIMO broadcast systems with $\epsilon_e^2 = 0, 1\%, 5\%$, and 10% by simulative and analytical ways. Clearly, the sum rate will increase linearly as SNR ρ increases in dB under no estimated error condition. Different from the effect of feedback error on sum rate discussed in Chapter 3, the imperfect CSI-R will largely drop down the sum rate of the receive ZF MIMO broadcast

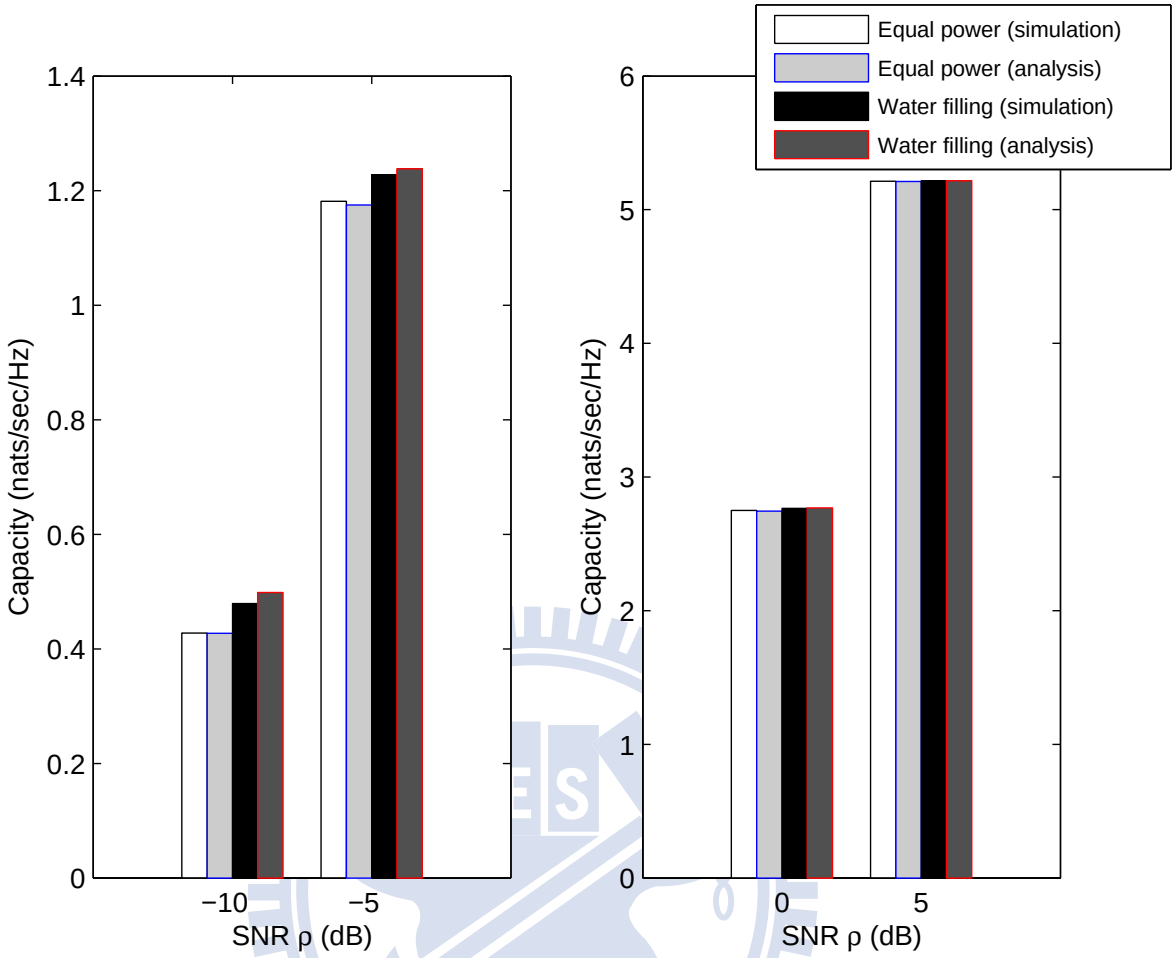

Figure 5.5: Capacity comparison of the $(M_T = 3, M_R = 4, K = 10)$ receive ZF MIMO broadcast systems under equal power and water-filling power allocations.

systems. More serious estimation error leads to more depressed sum rate performance. The resulting sum rate will no longer increase as SNR ρ increases and tend towards the value $\overline{C_{\text{ZFR}}^{\epsilon_e^2}}$ provided in (5.25). For example, the sum rate of the $(2, 3, 5)$ receive ZF MIMO broadcast systems with $\epsilon_e^2 = 0$ is 15 nats/s/Hz at SNR $\rho = 30$ dB. However, the corresponding sum rates reduce to 10.38, 7.28, and 6.04 nats/s/Hz for $\epsilon_e^2 = 1\%, 5\%$, and 10%, respectively.

Next, we want to answer what advantage can multiuser diversity reflect on sum rate for a receive ZF MIMO broadcast system with imperfect CSI-R. Fig. 5.4 shows the sum rate of the receive ZF MIMO broadcast systems with $M_T = 2, M_R = 3, \epsilon_e^2 = 1\%$ and different number of users K. In this figure, the sum-rate performance can be improved as available user population K increases, but it can not be raised any more as SNR ρ approaches to about 35

dB. In fact, multiuser diversity can not resolve the sum rate floor caused by imperfect CSI-R. The corresponding $\overline{C_{\mathrm{ZFR}}^{\epsilon_e^2}}$ values are 8.73, 9.98, 10.38, and 10.82 nats/s/Hz for $K = 1, 3, 5,$ and 10, respectively.

Finally, we illustrate the benefit of utilizing water-filling power allocation on sum-rate performance via Fig. 5.5 which evaluates a $(M_T = 3, M_R = 4, K = 10)$ receive ZF MIMO broadcast system. This figure confirms the well-known information that the advantage of water-filling power allocation over equal power allocation is significant only in the low SNR region. As shown, our provided closed-form expressions can well evaluate the sum-rate performance of the receive ZF MIMO broadcast systems under both equal and water-filling power allocations.

Chapter 6

Architecture for Coordinated Multicell MIMO Systems

In this chapter, we present a 3-cell network MIMO architecture with FFR and a novel tri-sector frequency partition scheme. One fundamental question to apply the network MIMO technique in such a high interference environment is: how many base stations should be coordinated together to provide sufficient performance? We will demonstrate that the FFR-based 3-cell network MIMO architecture with the proposed tri-sector frequency partition can not only effectively overcome the inter-group interference, but can avoid executing the complex multi-base-station joint processing for a huge number of cluster of cells at all locations. It will be shown that the proposed 3-cell network MIMO with the rearranged tri-sector frequency partition strategy can outperform the seven-cell network MIMO with omni-directional antennas. Various sector antenna architectures and the method for determining the inner region of the FFR cell planning are also discussed and analyzed on top of the network MIMO system. We hope that this study can provide important insights into the design of the network MIMO systems from the perspectives of architecture and deployment.

6.1 System Model

We consider a cellular system with $N_{\text{cell}} = 19$ cells, where the center cell has two-tier neighboring cells. In the baseline case, each base station and each user has one single transmit/receive antenna. When the cellular system with three sectors is considered, we assume that each sector is equipped with one sector antenna. The gain pattern used for each sector antenna is specified as

$$A(\theta)_{\text{dB}} = -\min\left[12\left(\frac{\theta}{\theta_{3\text{dB}}}\right)^2, A_m\right] \quad , \tag{6.1}$$

where $A(\theta)_{\text{dB}}$ is the antenna gain at angle θ in decibels and $\theta \in [-180°, 180°]$ is the angle between a mobile user with respect to the main-beam direction of the considered sector

antenna. The 3 dB beamwidth $\theta_{3\text{dB}}$ is the angle of which the antenna gain is 3 dB lower than the antenna gain at the main-beam direction, and the parameter $A_m = 20$ dB is the maximum attenuation for the sidelobe.

For the transmitted signal x_j from base station j, the received signal of mobile user k is written as

$$y_k = h_{k,j}x_j + \sum_{i \neq j,\, i \in \mathcal{I}} h_{k,i}x_i + n_k \ , \tag{6.2}$$

where $h_{k,j}$ and n_k are the channel response between mobile k and base station j and the additive noise at the k-th mobile, respectively; and $\mathcal{I}$ is the set of interfering BSs for mobile k. The radio channel models considered in this chapter include the effects of Rayleigh fading, shadowing, and path loss. Specifically, we represent the channel response $h_{k,j}$ as

$$h_{k,j} = \alpha_{k,j} \sqrt{\beta_{k,j}\, A(\theta_{k,j}) \left(\frac{d_{k,j}}{d_{\text{ref}}}\right)^{-\mu}} \ , \tag{6.3}$$

where $\alpha_{k,j}$ and $\beta_{k,j}$ are the fast Rayleigh fading and shadowing between mobile k and base station j, respectively; $d_{k,j}$ and d_{ref} are the distance between mobile k and base station j and a reference distance between the center and the vertex of a cell, respectively; and μ is the path loss exponent. $A(\theta_{k,j})$ is the antenna gain for mobile k with respect to BS j whose value is a function of $\theta_{k,j}$ based on (6.1) for the sectorized antenna and $A(\theta_{k,j}) = 1$ for the omni-directional antenna.

Considering the above signal and radio channel models, we can represent the received SNR of mobile k from base station j as

$$\text{SNR}_{k,j} = |\alpha_{k,j}|^2\, \beta_{k,j}\, A(\theta_{k,j}) \left(\frac{d_{k,j}}{d_{\text{ref}}}\right)^{-\mu} \Gamma \ , \tag{6.4}$$

where Γ represents the interference-free SNR defined as the SNR measured at the reference distance d_{ref} with only considering pass loss, and the noise power is normalized to unity. The parameter Γ captures the effect of various channel and antenna parameters including transmit power, cable loss, transmit and receive antenna heights, thermal noise power, and other link budget parameters. For $d_{\text{ref}} \cong 1.1547$ km, the reference SNR $\Gamma = 18$ dB for a base station-to-BS distance $R_{\text{B2B}} = 2$ km macrocellular system with 30 Watts transmit power [118]. For mobile k of BS j, we can express its corresponding SINR as

$$\gamma_{k,j} = \frac{\text{SNR}_{k,j}}{1 + \sum_{i \neq j,\, i \in \mathcal{I}} \text{SNR}_{k,i}} \ . \tag{6.5}$$

The corresponding channel capacity for each SINR value $\gamma_{k,j}$ can be given by $\log_2(1+\gamma_{k,j})$ bit/s/Hz. In this chapter, we consider the achievable capacity for various MCS considered in the standard [117]. For the considered MCSs {QPSK$\frac{1}{2}$, QPSK$\frac{3}{4}$, 16-QAM$\frac{1}{2}$, 16-QAM$\frac{3}{4}$, 64-QAM$\frac{2}{3}$, 64-QAM$\frac{3}{4}$}, the corresponding SINR requirements and the spectrum efficiencies are {6, 8.5, 11.5, 15, 19, 21} dB and {1.0, 1.5, 2.0, 3.0, 4.0, 4.5} bit/s/Hz, respectively.

6.2 Network MIMO

Network coordination can improve spectral efficiency by eliminating the inter-cell interference in multi-cellular systems [17,18]. With a high-speed backbone, the base stations can be synchronized, and all the base stations can exchange the CSI of each coordinated sites via the central coordinator. With full base station cooperation, the downlink network MIMO transmission can be modelled as the downlink transmission in the multi-user MIMO broadcast system. Consider a network MIMO system with M_c coordinated base stations, each of which transmits data streams to its own target mobile station. Define the transmitted signal vector with M_c elements as $\mathbf{x} = \mathbf{W}\mathbf{s} = [\mathbf{w}_1 \dots \mathbf{w}_{M_c}][s_1 \dots s_{M_c}]^T$, where s_k is the data symbol of the k-th user, $\mathbf{w}_k$ is the corresponding precoding weight column vector, and $(\cdot)^T$ is the transpose operation. Then, the received signals from M_c base stations are given by

$$\mathbf{Y} = \mathbf{H}\mathbf{x} + \mathbf{n} \ , \tag{6.6}$$

where $\mathbf{n}$ denotes the noise vector and $\mathbf{H} = [h_{k,j}]_{M_c \times M_c}$ denotes the channel matrix with the channel response $h_{k,j}$ between mobile k and base station j defined in (6.3). Note that the j-th antenna output in a network MIMO system is a linear combination of M_c data symbols, i.e. $x_j = \sum_{k=1}^{M_c} w_{j,k} s_k$. Thus, we can represent the received signals of mobile k as

$$y_k = s_k ||\mathbf{h}_k \mathbf{w}_k|| + \sum_{i=1, i\neq k}^{M_c} s_i ||\mathbf{h}_k \mathbf{w}_i|| + n_k \ . \tag{6.7}$$

Denote p_k as the power of the data symbol s_k. According to the network MIMO principle, the following constraint $E[|x_j|^2] \leq P_T$ should be satisfied for every base station $j = 1, \dots, M_c$. Then, it follows that

$$\begin{bmatrix} |w_{1,1}|^2 & \cdots & |w_{1,M_c}|^2 \\ \vdots & \ddots & \vdots \\ |w_{M_c,1}|^2 & \cdots & |w_{M_c,M_c}|^2 \end{bmatrix} \begin{bmatrix} p_1 \\ \vdots \\ p_{M_c} \end{bmatrix} \leq P_T \mathbf{1} \ , \tag{6.8}$$

where P_T is the maximum transmit power of each base station, and $\mathbf{1}$ is an $M_c \times 1$ vector with all elements equals one. It is well known that DPC can achieve the capacity of the multiuser MIMO broadcast system. Due to high complexity, suboptimal ZF and ZF-DPC multi-user MIMO algorithms were proposed. Similarly, there exist the optimal DPC network MIMO algorithm and the suboptimal ZF and ZF-DPC network MIMO algorithms. We will consider ZF and ZF-DPC network MIMO algorithms in this chapter.

6.2.1 ZF Network MIMO Transmission

The goal of ZF network MIMO transmission is to invert the channel to obtain $\mathbf{HW} = \mathbf{I}$. The weight matrix $\mathbf{W}$ can be obtained by using the pseudo-inverse of the channel matrix. The received signal vector is hence given by

$$\mathbf{Y} = \mathbf{Hx} + \mathbf{n} = \mathbf{HWs} = \mathbf{s} + \mathbf{n} \ . \tag{6.9}$$

With per-base power constraint (6.8), the objective of the network MIMO system is to maximize the minimum rate among the coordinated cells, and the corresponding maximum common rate solutions are [18]

$$p_k = \frac{P_T}{\max_j [\mathbf{WW}^H]_{(j,j)}} = \frac{P_T}{\max_j \sum_k |w_{j,k}|^2} \ , \quad \text{for all} \quad k \ , \tag{6.10}$$

where $(\cdot)^H$ is the conjugate transpose operation. Therefore, the corresponding mobile's rate is given by $\log_2(1 + p_k/\sigma^2)$ bit/s/Hz among all the coordinated cells, where σ^2 represents the noise power. From (6.10), we can observe that the actual symbol power p_k will be lower than the original available transmission power P_T due to beamforming weights.

6.2.2 ZF-DPC Network MIMO Transmission

The ZF-DPC network MIMO transmission constructs the linear weight matrix $\mathbf{W} = \mathbf{Q}^H$ through the QR decomposition of the channel matrix $\mathbf{H} = \mathbf{LQ}$, where $\mathbf{L}$ is a lower triangular matrix and $\mathbf{Q}$ is a unitary matrix with $\mathbf{QQ}^H = \mathbf{Q}^H\mathbf{Q} = \mathbf{I}_M$. The received signal is written as

$$\mathbf{Y} = \mathbf{Hx} + \mathbf{n} = \mathbf{LQQ}^H\mathbf{s} = \mathbf{Ls} + \mathbf{n} \ , \tag{6.11}$$

and the corresponding k-th mobile's received signal is $y_k = L_{k,k}s_k + \sum_{i<k} L_{k,i}s_i + n_k$. Note that the weight matrix $\mathbf{W} = \mathbf{Q}^H$ ensures no interference from data symbols with indices $i > k$. The remaining interference from data symbols $i < k$ are taken care of by the successive interference cancellation of DPC. Based on the result of ZF network MIMO transmission, if we set $p_k = p$ for all k, the per-site power constraint (6.8) becomes $E[|x_j|^2] = [\mathbf{W}\mathbf{W}^H]_{(j,j)}p = \sum_k |w_{j,k}|^2 p \leq P_T$ for all transmitted signal x_j. Recall that the weight matrix $\mathbf{W} = \mathbf{Q}^H$. We have $[\mathbf{W}\mathbf{W}^H]_{(j,j)} = [\mathbf{Q}^H\mathbf{Q}]_{(j,j)} = [\mathbf{I}]_{(j,j)} = 1$. Thus, we can set $p_k = P_T$ for each coordinated base station. Given the received signal in (6.11), mobile k can achieve the capacity $\log_2(1 + |L_{k,k}|^2 p_k/\sigma^2)$ bit/s/Hz. Note that the channel vectors of channel matrix $\mathbf{H}$ need to reorder similar to the case in traditional multi-user MIMO broadcast systems [60].

6.3 Effects of Inter-Group Interference on Network MIMO Systems

6.3.1 SINR Performance Model

When applying network MIMO in a multi-cellular environment, it is important to include the effects of IGI among the coordinated network MIMO groups. Clearly, a group of coordinated cells will cause interference to the neighboring coordinated group of cells even if the intra-group interference has been canceled by the joint multi-base station processing. Consider a cell with two-tier surrounding cells layout under M_c-cell network MIMO coordination. Denote $\mathcal{I}_G$ as the set of index for the interfering network MIMO groups and G_i as the cluster of cells for group i, $i \in \mathcal{I}_G$. Let $[w_{a,b}^{(G_i)}]_{M_c \times M_c}$ be the precoding weights for cell $a \in G_i$ with respect to mobile $b = 1, \cdots, M_c$. With data symbol $s_b^{(G_i)}$ of mobile b, the output signal transmitted from cell a can be represented as

$$x_a^{(G_i)} = \sum_{b=1}^{M_c} w_{a,b}^{(G_i)} s_b^{(G_i)} \quad . \tag{6.12}$$

From (6.7) and (6.12), we can obtain the SINR of mobile k as follows:

$$\gamma_k^{\text{IGI}} = \frac{p_k ||\mathbf{h}_k \mathbf{w}_k||^2}{1 + \sum_{i \in \mathcal{I}_G} \sum_{a \in G_i} \sum_{b=1}^{M_c} p_b^{(G_i)} |h_{k,a}^{(G_i)} w_{a,b}^{(G_i)}|^2} \quad , \tag{6.13}$$

where $p_k = s_k^2$ and $p_b^{(G_i)}$ are the data symbol power of s_k and $s_b^{(G_i)}$, respectively; and $h_{k,a}^{(G_i)}$ is the channel response between the considered mobile k and the interfering base station $a \in G_i$. According to (6.10) $p_b^{(G_i)} = p^{(G_i)}$, from (6.13), we can obtain the SINR with ZF-based network MIMO transmission as

$$\gamma_{k,\mathrm{ZF}}^{\mathrm{IGI}} = \frac{p_k}{1 + \sum_{i \in \mathcal{I}_G} \sum_{a \in G_i} \sum_{b=1}^{M_c} p^{(G_i)} |h_{k,a}^{(G_i)} w_{a,b}^{(G_i)}|^2} \ . \tag{6.14}$$

If ZF-DPC network MIMO transmission is adopted, the corresponding SINR is represented as

$$\gamma_{k,\mathrm{ZFDPC}}^{\mathrm{IGI}} = \frac{P_T |L_{k,k}|^2}{1 + \sum_{i \in \mathcal{I}_G} \sum_{a \in G_i} \sum_{b=1}^{M_c} P_T |h_{k,a}^{(G_i)} w_{a,b}^{(G_i)}|^2} \ , \tag{6.15}$$

where $L_{k,k}$ is defined in (6.11).

6.3.2 SINR Performance Degradation

In this section, we explain why IGI affects the performance of network MIMO systems by examples. Fig. 6.1 shows the three-cell and seven-cell network MIMO systems. In the case of three-cell network MIMO, cells 0, 4 and 5 forms a three-cell network MIMO group G_0. Although for cell 0 network MIMO transmission cancels the intra-group interferences from cells 4 and 5, many two-tier cells still cause interference to cell 0. In this case, $\mathcal{I}_G = \{1, 2, \ldots, 8\}$ and the corresponding cells in each group are $G_1 = \{1, 2, 8\}$, $G_2 = \{3, 10, 11\}$, $G_3 = \{12, 13\}$, $G_4 = \{14\}$, $G_5 = \{15, 16\}$, $G_6 = \{6, 17, 18\}$, $G_7 = \{7\}$, and $G_8 = \{9\}$. After the network MIMO canceling the inter-cell interference for cell 0, there still exists four and 12 first-tier and second-tier interferers, respectively. Note that all the interferers also transmit M_c-cell coordinated signals. In a seven-cell network MIMO system, the coordinated partners of cell 0 are cells {1, 2, 3, 4, 5, 6}. In this case, the IGI from the second-tier cells 7 to 18 cannot be reduced by the multi-base station joint processing.

Figure 6.2 shows the effects of IGI on the ZF-DPC network MIMO. At the 10 % outage probability, the IGI effects degrade the SINR by 14 dB and 23 dB for the seven-cell and three-cell network MIMO systems, respectively. For comparison, the performances of network MIMO without the IGI effects are also shown in the figure, i.e. 19-cell (solid line), seven-cell

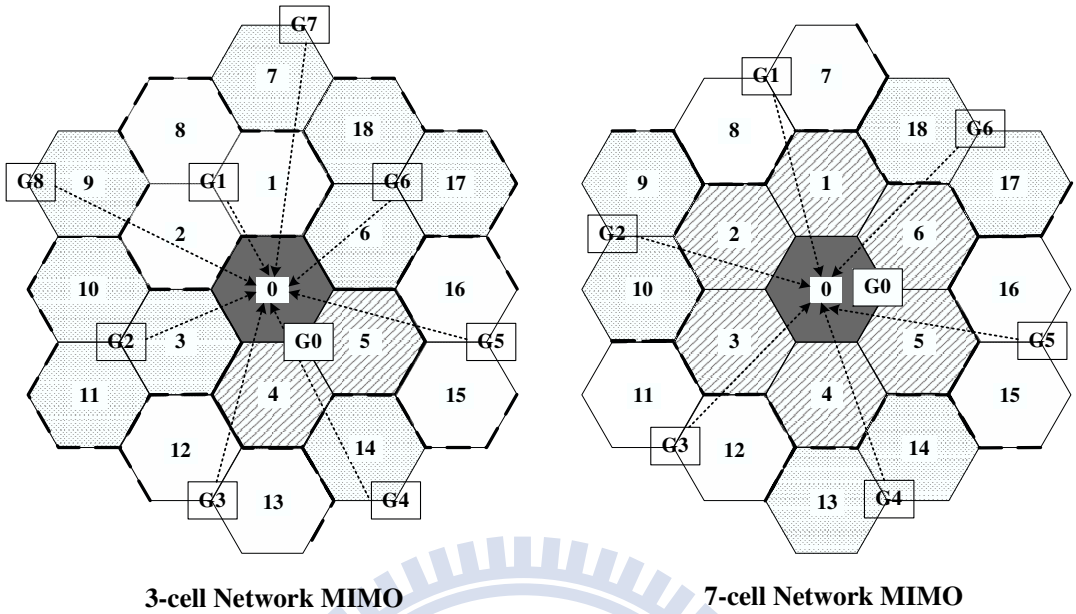

Figure 6.1: An example of inter-group interference for the three-cell and seven-cell network MIMO systems.

(diamond legend), and three-cell (circle legend). We find that without IGI effects the SINR performance of seven-cell network MIMO system approaches that of the 19-cell network MIMO system. This result implies that the coordination size $M_c = 7$ is enough for designing network MIMO systems in the case without IGI effects. However, the received signal quality of the network MIMO systems will be deeply affected when interferences from the other groups are considered.

6.3.3 Unbalanced Signal Quality Effects

Based on the observation from the seven-cell network MIMO system, the IGI incurs an unbalanced signal quality issue when a large coordination size is used. That is, the central cells among a coordinated group have better signal quality than the edged cells. Take the seven-cell network MIMO as the example. The IGI for cell 0 is from the second-tier interferers as mentioned before. However, the edged cells {1, 2, 3, 4, 5, 6} have three first-tier interferers and 15 second-tier interferers. As a result, the edge cells will suffer more serious IGI than the

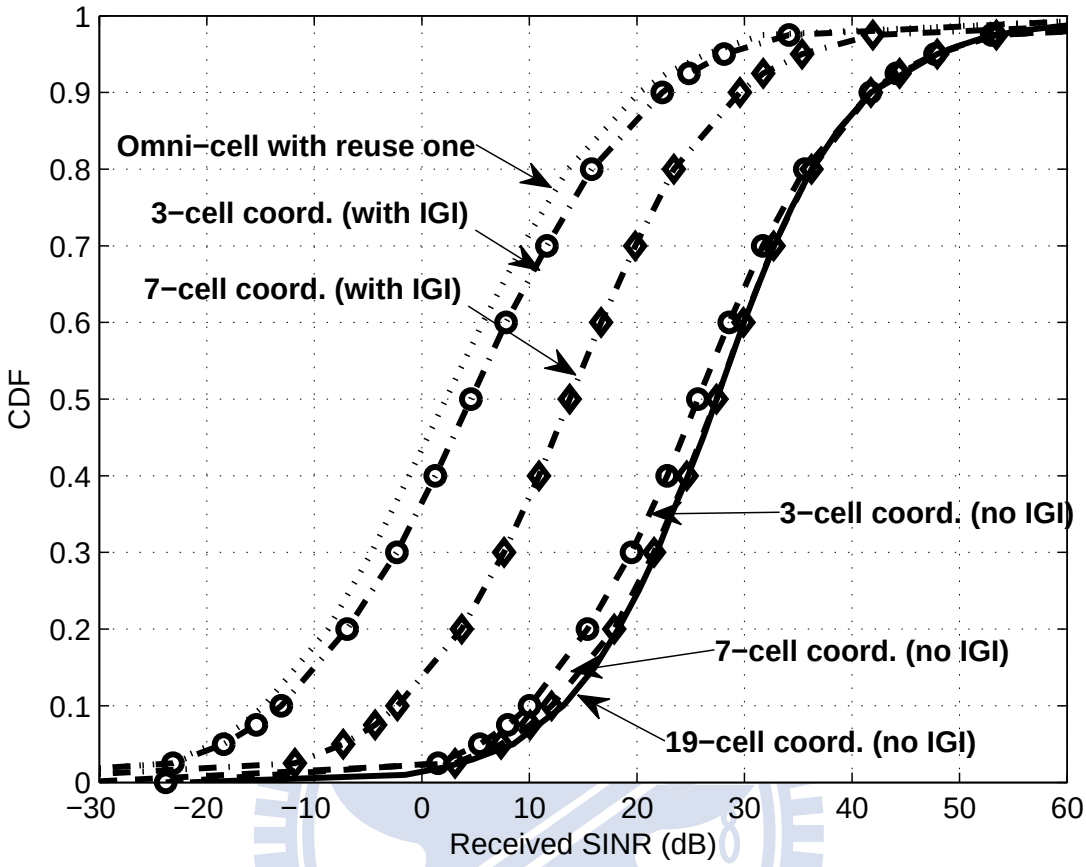

Figure 6.2: Effect of inter-group interference for the three-cell and seven-cell network MIMO systems.

central cells especially when the coordination size M_c increases. Hence, the signal quality among M_c coordinated cells is unbalanced in the conventional network MIMO architecture. To sum up, the IGI causes severe performance degradation and the unfairness issue among a group for multi-cellular network MIMO systems.

Note that the three-cell network MIMO does not suffer from this unbalanced issue because each member in a coordinated group has the same geographic condition. In other words, each cell is an "edged cell" in the three-cell group and has the same interferers distribution. However, the performance improvement resulted from such a small-size coordination is not significant from Fig. 6.2. In the following section, we propose a novel network MIMO architecture to improve the signal quality and achieve the fairness among a group of cells simultaneously.

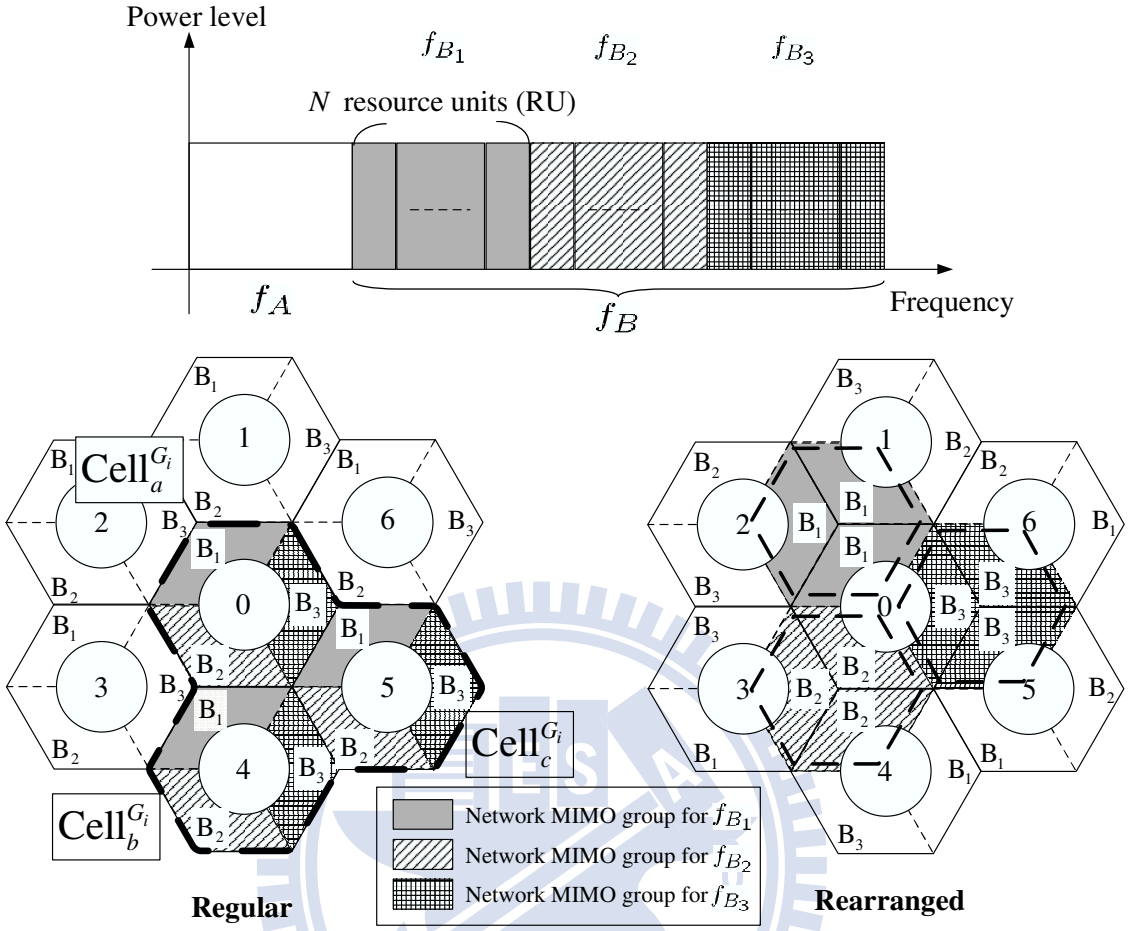

Figure 6.3: Fractional frequency reuse sectorization for proposed three-cell network MIMO coordinations.

6.4 Frequency Partition-based Three-cell Network MIMO

6.4.1 FFR with Sectorization

Figure 6.3 shows the FFR planning for a tri-sector cellular system. In this figure, frequency bands are partitioned into the inner frequency bands f_A and the outer frequency bands f_B, where f_B is further partitioned into three subbands f_{B_1}, f_{B_2}, and f_{B_3} (the gray, slash, and grid area, respectively). In general, the inner frequency bands f_A adopts universal reuse factor one with omni-directional antenna for the interior cell users; the outer frequency

bands f_B adopts reuse factor 1/3 for the users in each sector. By means of FFR, the intra-cell interference can be avoided due to four orthogonal subbands. Assume f_{B_1}, f_{B_2}, and f_{B_3} have the same bandwidth with N frequency resource units (RU) in each outer subband, i.e., $f_{B_p} = \{f_{B_{p,1}}, \ldots, f_{B_{p,N}}\}$ for $p = 1, 2, 3$.

In this chapter, we consider two kinds of tri-sector frequency planning methods: regular and rearranged frequency partitions. In the traditional regular tri-sector frequency partition, the sectors with the same main-beam direction at each cell are with the same frequency band (e.g. the left cellular system in Fig. 6.3), which can be found in [64, 100, 101]. As for the rearranged tri-sector frequency partition, the sectors with the same main-beam direction at the neighboring cells can have different frequency bands as shown in the right part of Fig. 6.3. We will design the network MIMO systems based on the above two tri-sector frequency partitions. Although the rearranged tri-sector frequency partition may yield severer co-channel interference than the regular tri-sector frequency partition, we will show that combining the three-cell network MIMO with the rearranged tri-sector frequency partition can outperform the three-cell network MIMO with regular tri-sector frequency partition.

6.4.2 FFR-based Network MIMO with Regular Tri-Sector Frequency Partition

In this section, we combine network MIMO with FFR and the regular tri-sector frequency partition. As mentioned before, the FFR method partitions the whole frequency band into different zones. Compared to the conventional omni-cell with universal frequency reuse factor of one, the tri-sector cellular system combined with FFR can significantly reduce the interference, while fully utilizing the frequency band at each cell. As an example in Fig. 6.4, when a user of cell 0 utilize one of RU $f_{B_{1,n}}$ $(n = 1, \ldots, N)$ in frequency band f_{B_1}, the interference comes from 7 cells {4, 5, 12, 13, 14, 15, 16} under the assumption of perfect 120° sector antenna rather than being interfered by all 18 cells in the omni-directional case. Here, the question is how we can further improve the SINR on top of FFR? The solution proposed in this chapter is to further incorporate the network MIMO technique with FFR.

From Fig. 6.4, we find that the seven interfering sources consists of two critical interferers coming from first-tier neighboring cells 4 and 5 and five weaker second-tier interferers due

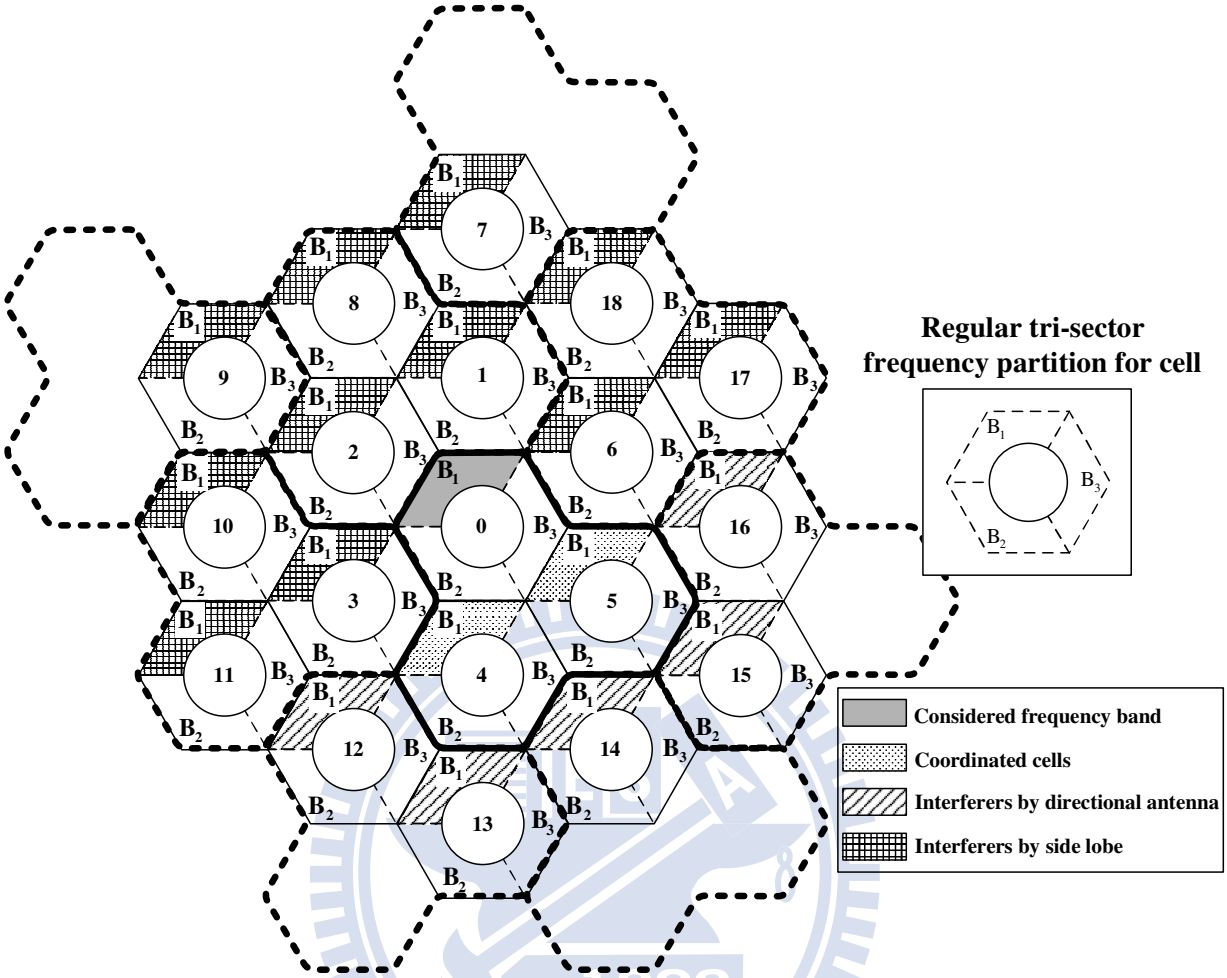

Figure 6.4: Interference example for three-cell FFR-based network MIMO with regular tri-sector frequency partition (consider cell 0).

to higher path loss. Therefore, we use the network MIMO technique to cancel the two most severe interference. Instead of coordinating huge number of cells, we propose a coordination scheme with only three cells. We define those coordinated cells as a group shown in Fig. 6.3. For the arbitrary group G_i, we label the three cells as $\text{Cell}_a^{G_i}$, $\text{Cell}_b^{G_i}$, and $\text{Cell}_c^{G_i}$, respectively. For the three-cell coordination, we can apply network MIMO transmission to each subband $f_{B_{p,n}}$ for $p = 1, 2, 3$ and $n = 1, \ldots, N$. Under the assumption of perfect sector directional antenna, the channel matrix of $f_{B_{1,n}}$ for cell 0 in the group $\{0, 4, 5\}$ is

$$\mathbf{H}(f_{B_{1,n}}) = \begin{bmatrix} h_{(0),0} & h_{(0),4} & h_{(0),5} \\ 0 & h_{(4),4} & 0 \\ 0 & 0 & h_{(5),5} \end{bmatrix}, \tag{6.16}$$

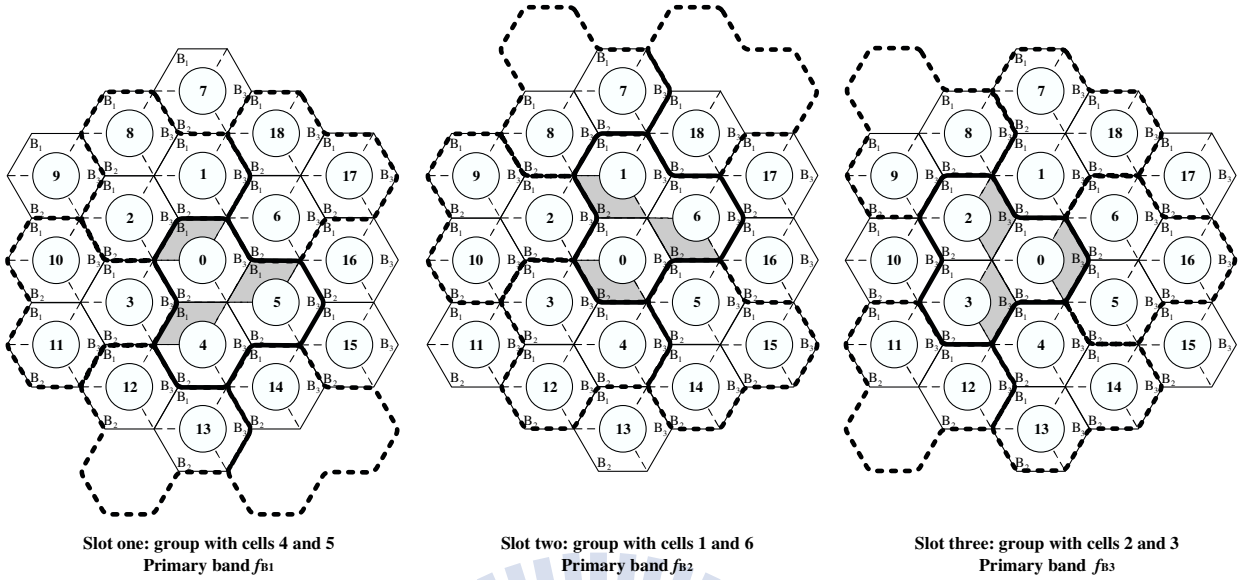

Figure 6.5: Example of cells regrouping and partner selection for cell 0.

where (x) denotes the corresponding served user in cell x. We eliminate the interference caused by $h_{(0),4}$ and $h_{(0),5}$ (from cells 4 and 5) by network MIMO. As a result, the two most severe interference is canceled through a small-sized (3×3) matrix computation. Importantly, this small-sized cooperation scheme can be applied to all the cells within the entire service area. For example in Fig. 6.4, at certain time slot we have many cooperated groups among the 19-cell layout: cells $\{0, 4, 5\}$, $\{8, 2, 1\}$, $\{10, 11, 3\}$, and $\{18, 6, 17\}$. Not only the middle cell (cell 0) is coordinated with its neighboring cells, but the cells in the outer layer are also coordinated simultaneously.

Cells Regrouping and Partner Selection

In this section, we propose a cell regrouping and partner selection scheme to address the service fairness issue caused by the network MIMO systems with the regular tri-sector frequency partition. From Fig. 6.4, among arbitrary group G_i, the cell labelled as "$\text{Cell}_a^{G_i}$" can achieve free intra-group interference within the whole subband $f_{B_1} = \{f_{B_{1,1}}, \ldots, f_{B_{1,N}}\}$ under network MIMO systems. However, subbands f_{B_2} and f_{B_3} are still affected by two first-tier cells and five second-tier cells. We therefore define f_{B_1} as the primary band of $\text{Cell}_a^{G_i}$ for group G_i. Similarly, we define f_{B_2} and f_{B_3} as the primary band of $\text{Cell}_b^{G_i}$ and

$\text{Cell}_c^{G_i}$, respectively. Therefore, the cell users served by different subbands among a group can have different signal quality. Note that this service fairness issue is different from the unbalanced signal quality issue mentioned in Section 6.3.3.

The service fairness issue can be resolved by the proposed regrouping and partner selection scheme. Assume that cell 0 is grouped with cells 4 and 5 with primary band f_{B_1} at certain time slot one, as shown in Fig. 6.5. Cell 0 will regroup with cells 1 and 6 at the next time slot two by counterclockwise rotating way to reselect coordinated partner. After this regroup, the primary band of cell 0 becomes f_{B_2}. Similarly, cell 0 regroups with cells 2 and 3 at time slot three by counterclockwise reselecting coordinated partner again and the corresponding primary band becomes f_{B_3}. In this way, all cells will simultaneously "rotate" and regroup with two new neighboring cells at a new time slot, where "rotate" means the coordinated partner reselection procedure. Take the three cells $\{0, 4, 5\}$ an example. Those cells form a group at time slot one. At time slot two, cell 0's regroup set is now $\{1, 0, 6\}$, cell 4's regroup set is $\{3, 12, 4\}$, and cell 5's regroup set is $\{5, 14, 15\}$. Similarly, cell 0's regroup becomes $\{2, 3, 0\}$, cell 4's regroup set is $\{4, 13, 14\}$, and cell 5's regroup set is $\{6, 5, 16\}$ at time slot three. Each cell has the chance to cooperate with neighboring six cells in order and each sector has the opportunity to become the primary band under this kind of TDMA-based regrouping and partner selection scheme. Similar concept can be also applied to frequency division multiple access (FDMA) manner by further partitioning each outer subband f_{B_p} into three disjoint subsets. Then each subset of f_{B_p} regroups with different neighboring cells.

6.4.3 FFR-based Network MIMO with Rearranged Tri-Sector Frequency Partition

Cell Planning for 120-degree Tri-Sector Architecture

In this section, we propose another multi-cellular architecture with rearranged tri-sector frequency partitions among cells. As shown in Fig. 6.6, there are totally three kinds of frequency partitions. After this rearranged tri-sector frequency partition among a multi-cellular system, a cell coordinates with six neighboring cells to form three individually network MIMO groups for each subband. For example, cell 0 coordinates with cells 1 and 2 for subband f_{B_1}, with cells 3 and 4 for subband f_{B_2}, and with cells 5 and 6 for subband f_{B_3}. In other words,

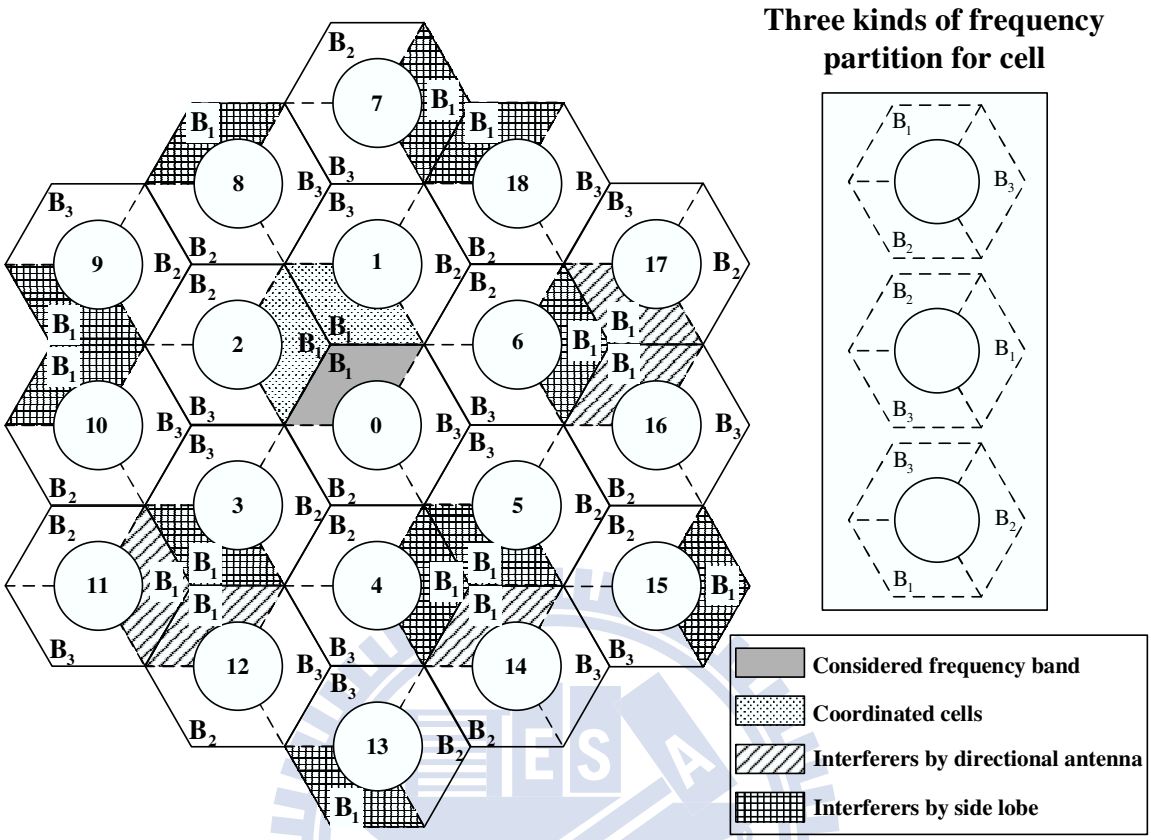

Figure 6.6: Interference example for three-cell FFR-based network MIMO with rearranged tri-sector frequency partition (consider cell 0).

we perform three-cell network MIMO transmission in each subband.

From Fig. 6.6, when a user of cell 0 unitize one of RU $f_{B_{1,n}}$ $(n = 1, \ldots, N)$ in frequency band f_{B_1}, the interference sources are cells {1, 2, 11, 12, 14, 16, 17} under the assumption of perfect 120° sector antenna. Similarly we use the network MIMO technique to cancel the two most severe interfering sources. That is, the two first-tier interference from cells 1 and 2 (the dotted area in Fig. 6.6). The channel matrix for the group $\{0, 1, 2\}$ in $f_{B_{1,n}}$ is

$$\mathbf{H}(f_{B_{1,n}}) = \begin{bmatrix} h_{(0),0} & h_{(0),1} & h_{(0),2} \\ h_{(1),0} & h_{(1),1} & h_{(1),2} \\ h_{(2),0} & h_{(2),1} & h_{(2),2} \end{bmatrix} . \tag{6.17}$$

For the users in cell 0, we now eliminate the interference caused by $h_{(0),1}$ and $h_{(0),2}$ (from cells 1 and 2) by network MIMO through a small-sized (3×3) matrix computation. Ideally,

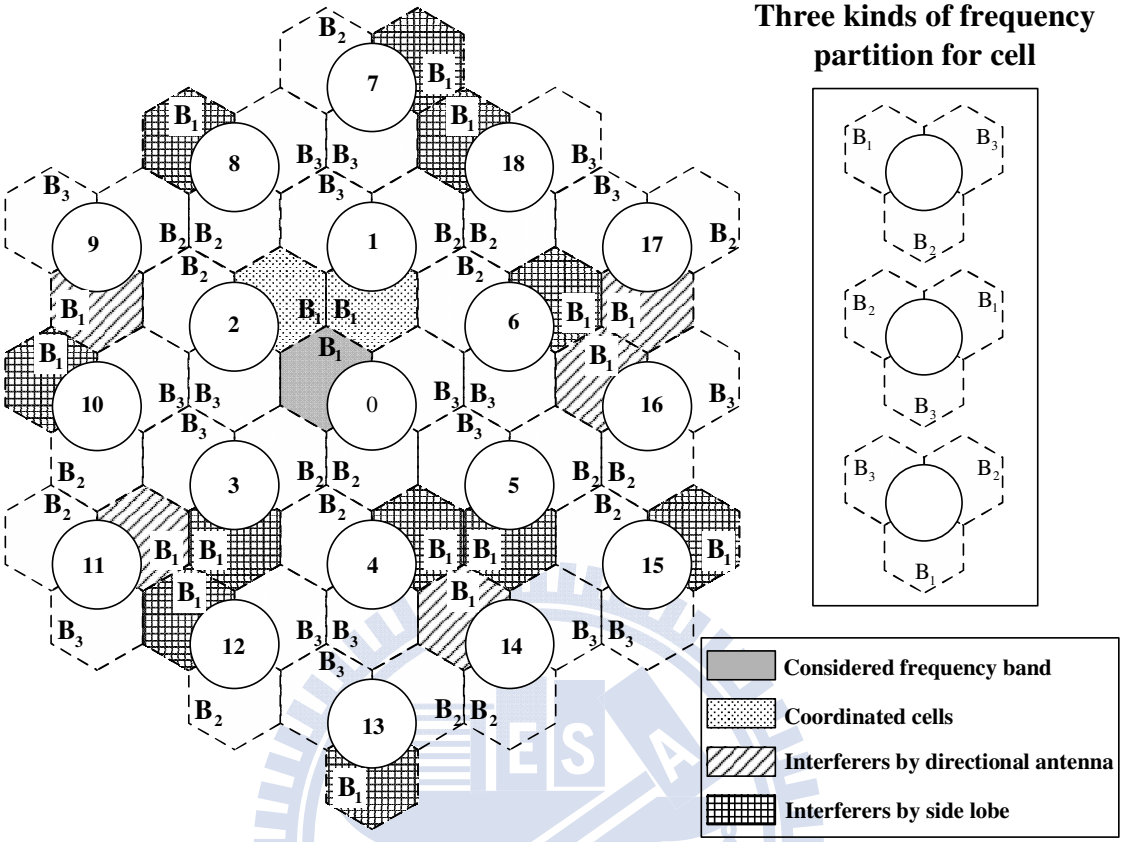

Figure 6.7: Interference example for three-cell FFR-based network MIMO with rearranged tri-sector frequency partition and 60° cell sectoring (consider cell 0)

there are only five second-tier interferers for each subband. Similar the network MIMO with regular tri-sector frequency partition, this cooperation can also be applied to all cells not only for a particular cooperated group. However, there is no service fairness issue for network MIMO systems with rearranged tri-sector frequency partition. As a result, we avoid cells regrouping to ease the complexity in deploying the network MIMO.

Cell Planning for 60-degree Tri-Sector Architecture

To address the effects of cell planning with different sectorization technique, we further design the three-cell network MIMO systems with three 60° cell sectoring. Here we consider rearranged tri-sector frequency partition to avoid the cells regrouping procedures. Figure 6.7 shows the example of the proposed rearranged 60° tri-sector network MIMO systems.

In this design, each cell has three hexagon-shaped sectors with different frequency assignment. The cells with 60° and 120° sectors are also called as the clover-leaf-shaped cells and diamond-shaped cells, respectively [36, 37]. Generally, this clover-leaf-shaped cells can match sector contour better than the cells with diamond-shaped sectors [36]. Additionally, the cells with 60° sectoring can use spectrum more efficiently [37]. Similar to the case of 120° sectoring, each cell under 60° sectoring performs three individually three-cell network MIMO coordinations with its six neighboring cells for each frequency partition. The two first-tier interferers (the dotted area in Fig. 6.7) are cancelled through network MIMO transmissions. The three-cell coordination structure can also be implemented for all the cells.

Note that actual cell sectorization cannot be perfect by using directional antenna pattern (6.1). The other cells will also affect the received signal quality of cell 0. However, by taking advantage of sectoring and FFR, the impact caused by the side-lobe and back-lobe transmissions (the grid areas in Fig. 6.4, Fig. 6.6 and Fig. 6.7) is not significant compared to the omni-cell with universal frequency reuse factor of one. Finally, we summarize the features of the proposed FFR-based three-cell network MIMO systems: (i) using a small coordination size $M_c = 3$ to perform low complexity network MIMO systems, (ii) reducing the effects of IGI via the combination of FFR and directional antennas, (iii) avoiding the unbalanced signal quality issue caused by larger coordination size M_c.

6.5 Numerical Results

In this section, we show the SINR performances of the proposed FFR-based three-cell network MIMO systems. Consider a multi-cellular system with base station-to-base station distance $R_{\text{B2B}} = 2$ km. The interference-free SNR at cell edge is $\Gamma = 18$ dB for 120° sectorized cells. The same values of base station-to-base station distance and Γ (for same transmission power comparison) are used for the clover-leaf-shaped cells. The standard deviation of shadowing is 8 dB and the path loss exponent $\mu = 4$. Mobile users are uniformly distributed within each sector/cell. The channel response between any user-and-cell pair is represented by (6.3), where the angle-depend antenna pattern is considered. We don't consider the effect of inner region here and set the inner distance be zero. In the next section,

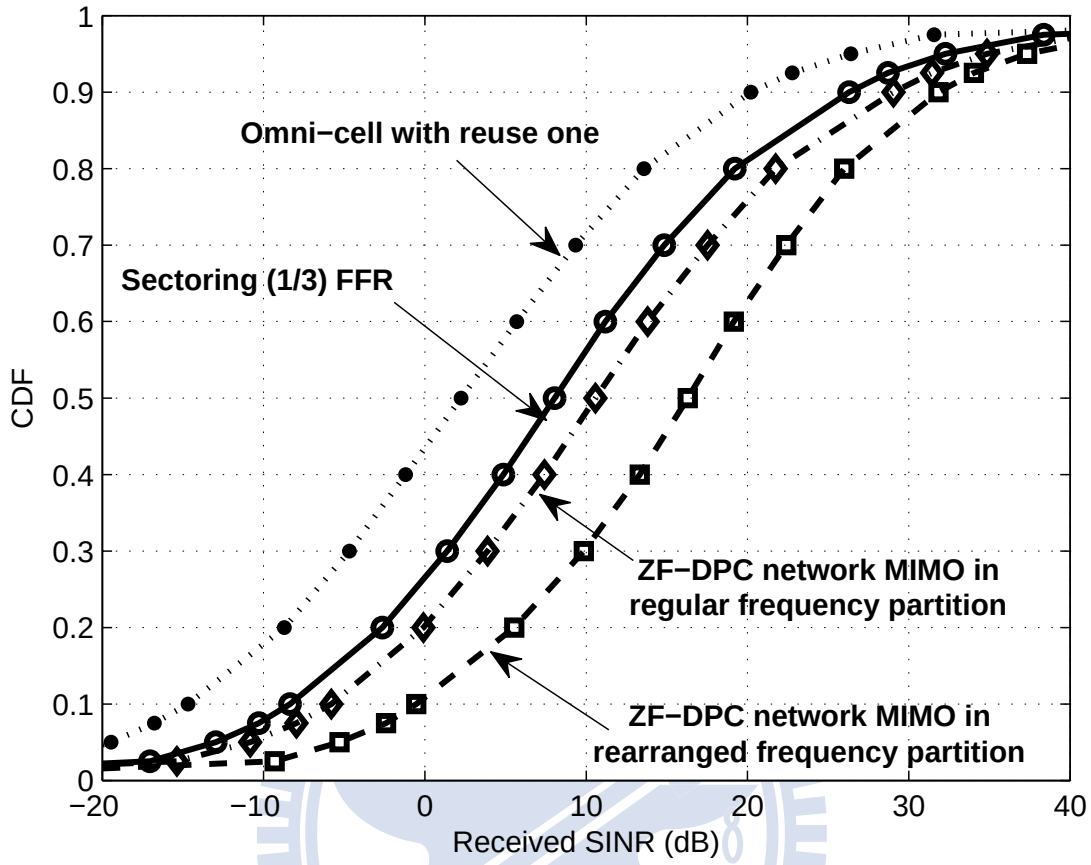

Figure 6.8: Comparison of received SINR for conventional 120° tri-sector (1/3) FFR cellular systems and three-cell ZF-DPC network MIMO systems with regular and rearranged tri-sector frequency partitions.

we will discuss how to design the uncoordinated inner region for FFR-based multi-cellular broadband system.

6.5.1 Effects of Frequency Planning among Coordinated Cells

At first, we present the received SINR performance for three-cell coordination with both regular and rearranged tri-sector frequency partitions. The performance of network MIMO with ZF-DPC and ZF are shown in Figs. 6.8 and 6.9, respectively. The cell planning is 120° sectoring. The results of the omni-cells with universal frequency reuse factor of one (black point legend) and sectoring 1/3 FFR layout (circle legend) are also presented for comparisons, where 1/3 means reuse factor = 1, but three sector per cell and each sector

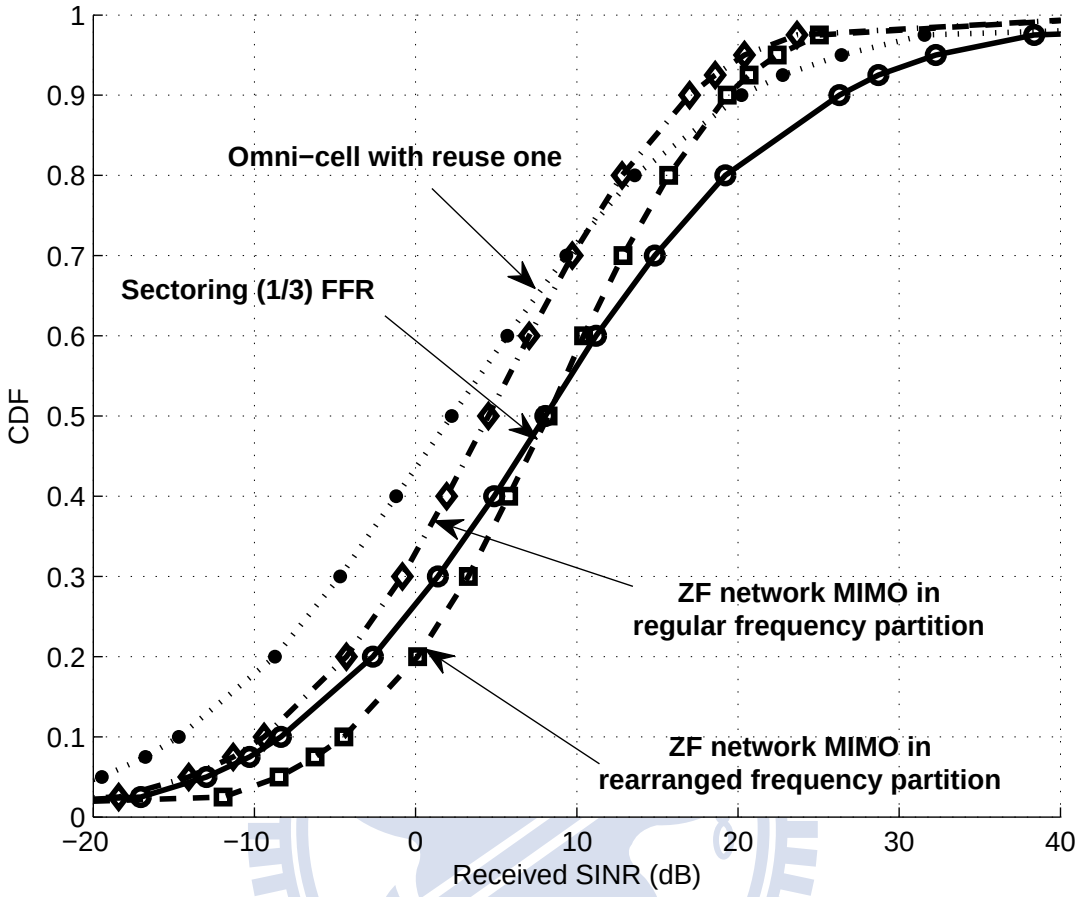

Figure 6.9: Comparison of received SINR for conventional 120° tri-sector (1/3) FFR cellular systems and three-cell ZF network MIMO systems with regular and rearranged tri-sector frequency partitions.

has different band under the regular tri-sector frequency partition.

From Fig. 6.8, we find that the gain of interfering sources reduction (from 18 reduce to 7) by sectoring 1/3 FFR is quite significant which is about 10 dB improvement at the 90-th percentile of the received SINR. With the help of three-cell ZF-DPC network MIMO, the SINR can be further improved especially for the proposed rearranged tri-sector frequency partition scenario. For example, at the 90-th percentile of the received SINR, there are 2.7 dB and 8.5 dB improvements for the regular and rearranged scenario, respectively.

Fig. 6.9 shows the jointly effects of FFR and three-cell ZF-based network MIMO. The gain of the ZF-based network MIMO is actually lower than that of the traditional 1/3 FFR-

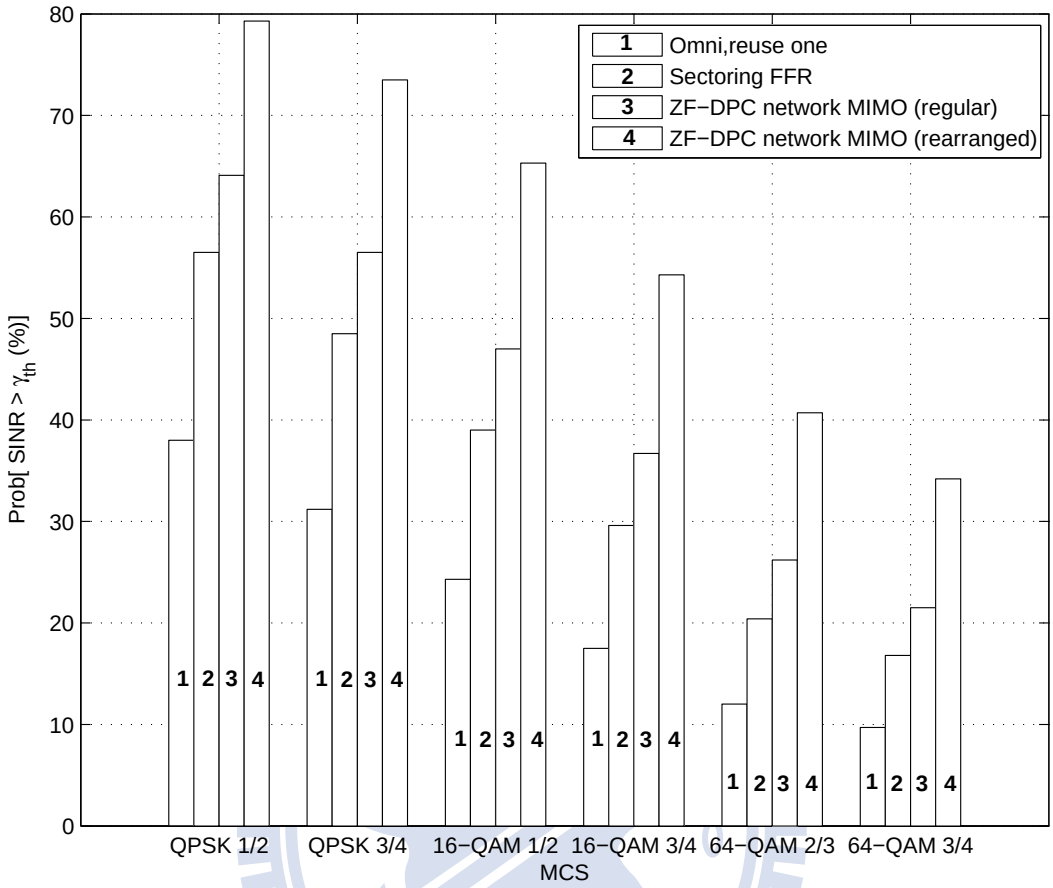

Figure 6.10: The percentage of mobile's SINR above the requirements of different MCSs under FFR-based three-cell ZF-DPC network MIMO.

based cellyar system with the regular tri-sector frequency partition. After applying the rearranged scenario, the performance gain is also not significant. It is because the actual data symbol power becomes smaller according to (6.10). Even if no first-tier interference existed through coordination, the signal quality of the ZF-based network MIMO system is lower than that of the ZF-DPC network MIMO system.

One important issue for system operators is how many users can be supported for a specific data rate. This performance metric can be quantified by the help of the coverage probability or the reliability function defined as

$$P(\gamma_{th}) \triangleq P_r\{\text{SINR} > \gamma_{th}\} \ . \tag{6.18}$$

Figures 6.10 and 6.11 shows the values $P(\gamma_{th})$ in percentage for different MCS levels. From

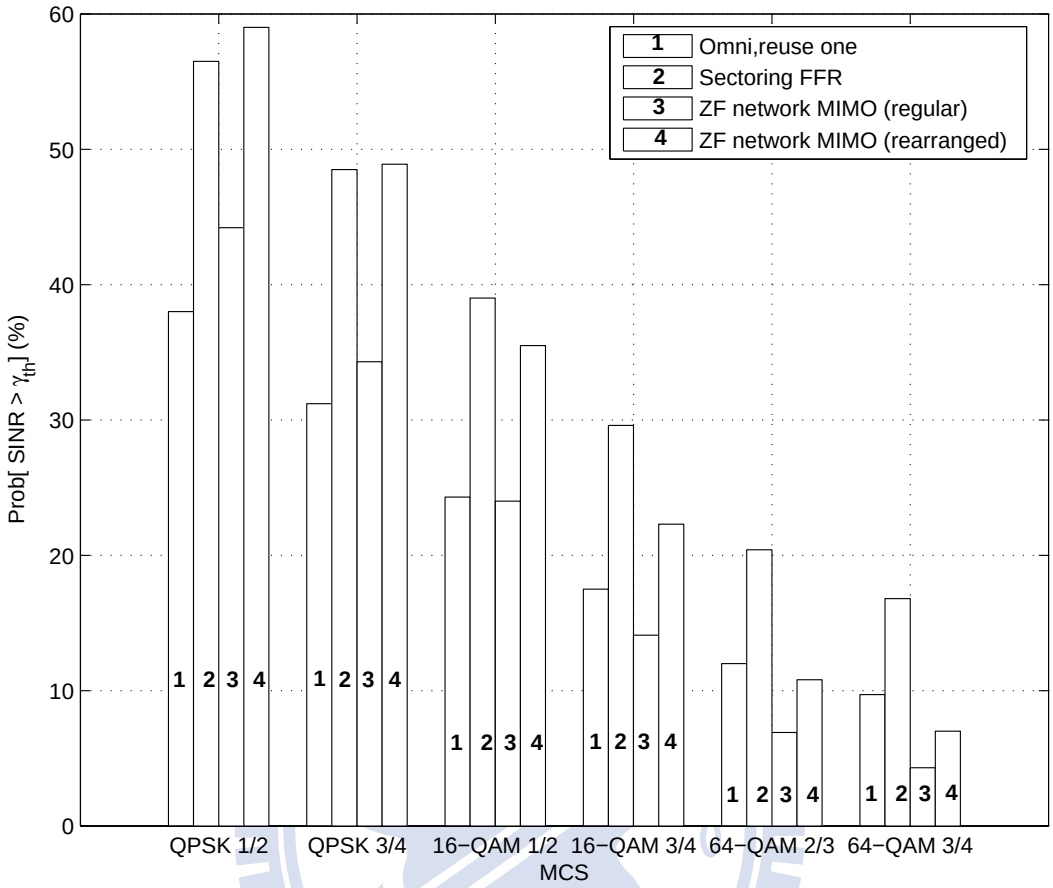

Figure 6.11: The percentage of mobile's SINR above the requirements of different MCSs under FFR-based three-cell ZF network MIMO.

Fig. 6.10, the system can support higher percentage of users with different MCSs transmission under the proposed joint FFR and ZF-DPC network MIMO scheme, especially for the rearranged tri-sector frequency partition methodsc. For example, there are about $5.5 \sim 8$ % and $15 \sim 26$ % gains over the case for the FFR system with sectoring. However, from Fig. 6.11, the benefits of joint FFR and network MIMO disappear as applying ZF scheme due to smaller data symbol power.

6.5.2 Effects of Cell Planning with Various Sectorizations

Secondly, we consider the effect of cell planning with different sector directional antenna setups. Figure 6.12 shows the received SINR performance with 60° sectorized cell planning.

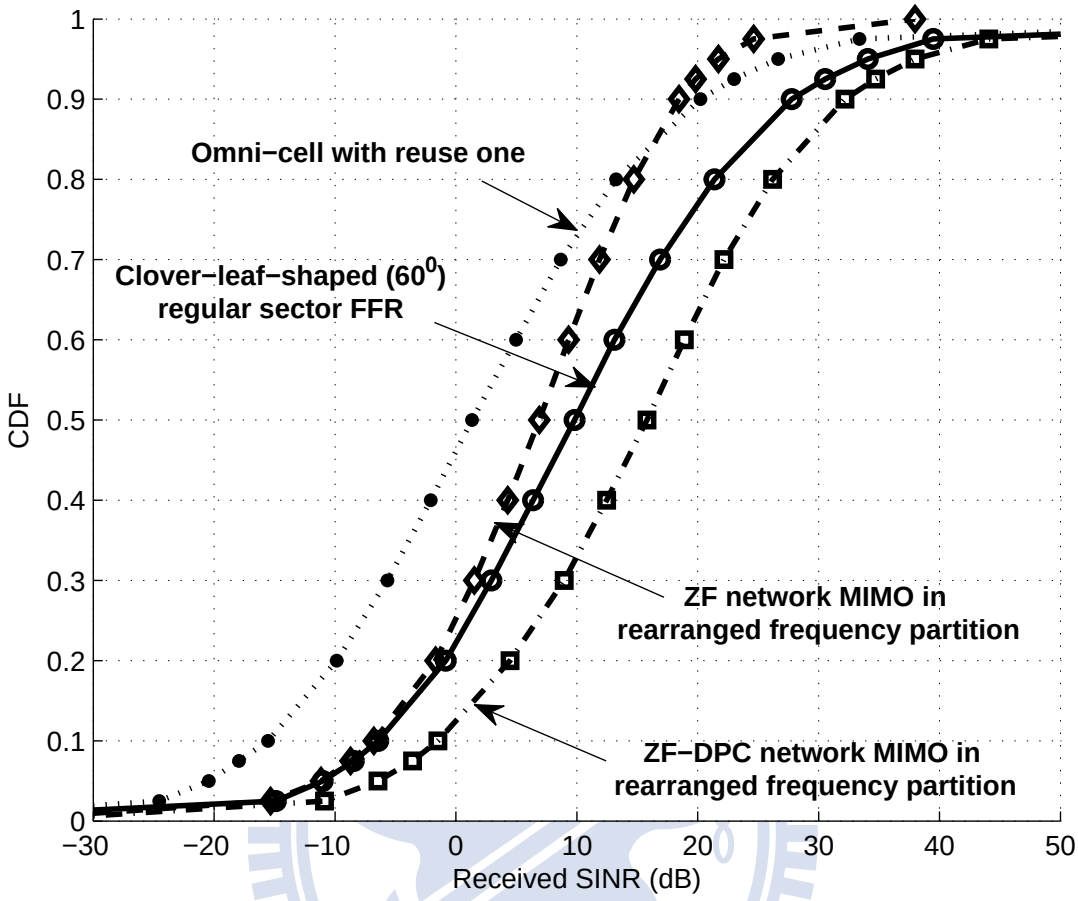

Figure 6.12: The CDFs of received SINR for omni-cell with reuse factor of one, 60° regular tri-sector (1/3) FFR cellular systems and proposed rearranged partition-based three-cell network MIMO systems in 60° cell sectoring.

We find that the advantage of pure using regular sectorization is obvious under 60° cell sectoring. It is because cell with 60° sectoring can perform better than 120° sectoring [36] [37]. When further applying three-cell network MIMO, the ZF-DPC can obtain similar SINR performance compared with 120° sectorized cells. However, the gain of ZF-based network MIMO scheme is not very significant at the 90-th percentile of the received SINR, and is actually lower than that by using tri-sector FFR scheme. In other words, under the rearranged tri-sector frequency partition, the proposed three-cell network MIMO enhances the signal quality more effectively on cell planning with 120° tri-sector architecture than with 60° tri-sector architecture. Note that the performance of the omni-cells with universal

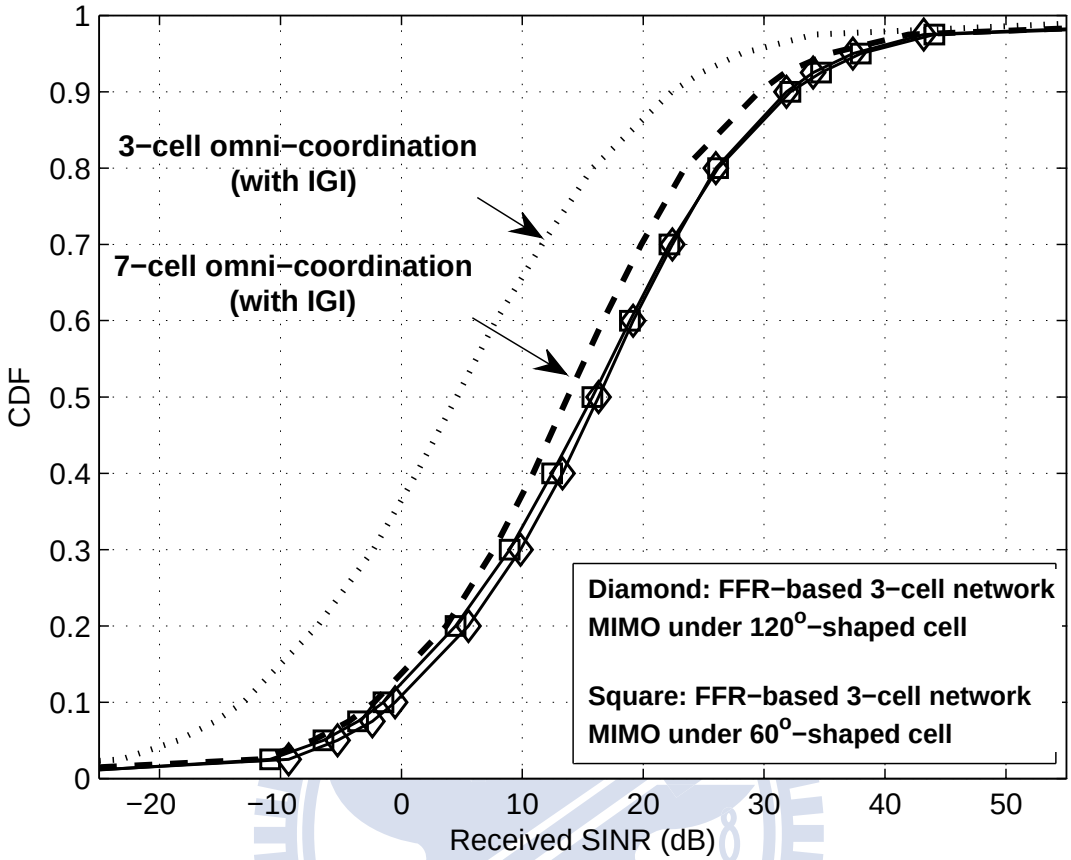

Figure 6.13: Performance comparison of proposed FFR-based three-cell network MIMO with general omni-directional three-cell and seven-cell network MIMO systems.

frequency reuse factor of one is different in Fig. 6.8 and Fig. 6.9 due to different cell planning although the difference is not much.

6.5.3 Benefit of Joint Frequency Partition and Network MIMO

Finally, we show the potential gains of combining tri-sector FFR and network MIMO in Fig. 6.13. Take ZF-DPC as the example. The performance degradations caused by IGI for the three-cell and seven-cell network MIMO systems are significant. However, taking advantage of joint tri-sector FFR and network MIMO, the proposed FFR-based three-cell network MIMO architecture (for both cell sectorizations) with rearranged tri-sector frequency partition can even outperform conventional seven-cell network MIMO system. The improvement is about 2 dB for 60° sectoring and 3 dB for 120° sectoring at 90-th percentile of the received

SINR. It shows the potential benefit of using a small number of coordinated cells.

6.6 Uncoordinated Inner Region Design

In this section, we design the uncoordinated inner region for tri-sector cell planning based on the SINR analysis in the worst case. The benefit of creating an inner region is that the allocated RUs can be more dynamically (uncoordinated) unitized for mobiles within the (usually circle) region than the sectorized outer regions with fixed RUs. In addition, although the considered coordination size $M_c = 3$ is a small value, the complexity of employing network MIMO schemes over all frequency RUs will become a burden for the system operator. To find an uncoordinated region on top of the tri-sector cell planning with reasonable signal quality is hence an important task for broadband network MIMO systems.

We focus on the 120° sectoring cell with regular and rearranged tri-sector frequency partitions. We analyze the worst-case SINR by ignoring the effects of shadowing and fast fading. By (6.4) and (6.5) (omitted index k and j), we have

$$\gamma = \frac{A(\theta)\left(\frac{d}{d_{\text{ref}}}\right)^{-\mu}\Gamma}{1+\sum_{i\in\mathcal{I}} A(\theta_i)\left(\frac{d_i}{d_{\text{ref}}}\right)^{-\mu}\Gamma} = \left[\frac{1}{A(\theta)\Gamma}\left(\frac{d_{\text{ref}}}{d}\right)^{-\mu} + \sum_{i\in\mathcal{I}}\left(\frac{A(\theta_i)}{A(\theta)}\right)\left(\frac{d_i}{d}\right)^{-\mu}\right]^{-1}$$
$$\overset{(a)}{\approx} \left[\sum_{i\in\mathcal{I}}\left(\frac{A(\theta_i)}{A(\theta)}\right)\left(\frac{d_i}{d}\right)^{-\mu}\right]^{-1}, \tag{6.19}$$

where (a) is approximated by the signal-to-interference ratio (S/I). With deterministic parameters d_i and θ_i, we can obtain the distance value d by the mathematical software tool. Because the received signal powers from the serving base station and interference power from surrounding cells vary with user locations, we consider the performance at the two extreme locations, i.e. the location **A** and the location **B** as shown in Fig. 6.14. The former represents the user locating at the main-bean direction of the tri-sector cell which has the maximal antenna gain; the latter represents the user locating at the boundary of the tri-sector cell where the antenna gain is 3 dB lower than the main-beam direction.

Here, we consider two-tier interference so that $\mathcal{I} = \{1, 2, \ldots, 18\}$ in which the number element represents cell index. Denote the cell radius as R $(= d_{\text{ref}})$ and the considered mobile at position **A** with distance d away from the serving base station. The corresponding

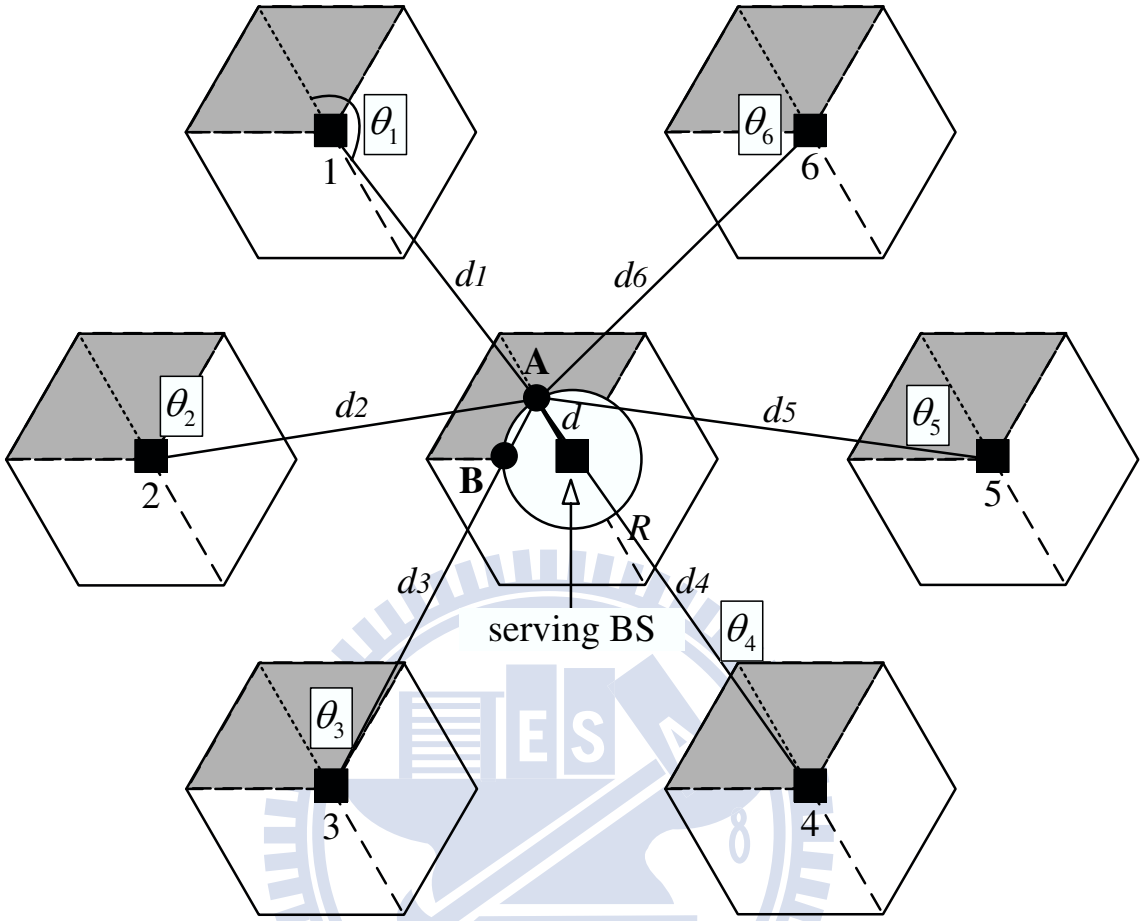

Figure 6.14: The considered interference scenario for examining the uncoordinated inner distance (region).

distances between mobile and interferers are

$$
\begin{cases}
\text{1st-tier cells} \begin{cases} d_1^A = d_2^A = \sqrt{(\sqrt{3}R/2)^2 + (3R/2 - d)^2} \\ d_3^A = d_6^A = \sqrt{(\sqrt{3}R)^2 + d^2} \\ d_4^A = d_5^A = \sqrt{(\sqrt{3}R/2)^2 + (3R/2 + d)^2} \end{cases} \\
\text{2nd-tier cells} \begin{cases} d_7^A = d_9^A = \sqrt{(\sqrt{3}R)^2 + (3R - d)^2} \\ d_{10}^A = d_{18}^A = \sqrt{(3\sqrt{3}R/2)^2 + (3R/2 - d)^2} \\ d_{11}^A = d_{17}^A = \sqrt{(2\sqrt{3}R)^2 + d^2} \\ d_{12}^A = d_{16}^A = \sqrt{(3\sqrt{3}R/2)^2 + (3R/2 + d)^2} \\ d_{13}^A = d_{15}^A = \sqrt{(\sqrt{3}R)^2 + (3R + d)^2} \\ d_8^A = 3R - d \\ d_{14}^A = 3R + d \end{cases}
\end{cases}
\quad . \tag{6.20}
$$

When mobile user locates at the position **A**, the angle between user and serving base station is $\theta^A = 0$, i.e. in the main-beam direction of the sector antenna. Due to different frequency assignments among cells, the co-channel interferers may point to different directions for regular and rearranged tri-sector frequency partitions, resulting in unequal antenna gains (angles). To be distinguishable, we use $\hat{\theta}_i^A$ and $\tilde{\theta}_i^A$ to represent the relative angles with interferer i for regular and rearranged tri-sector frequency partitions, respectively. The details of angles between the mobile and the main-beam direction of interfering base stations are listed in Appendix E.

Similarly, as a mobile locates at position **B** with distance d to the serving base station, the corresponding distances between the mobile and interferers are

$$\begin{cases} \text{1st-tier cells} \begin{cases} d_1^B = d_4^B = \sqrt{(\sqrt{3}R)^2 + d^2} \\ d_2^B = d_3^B = \sqrt{(\sqrt{3}R/2)^2 + (3R/2 - d)^2} \\ d_5^B = d_6^B = \sqrt{(\sqrt{3}R/2)^2 + (3R/2 + d)^2} \end{cases} \\ \text{2nd-tier cells} \begin{cases} d_7^B = d_{13}^B = \sqrt{(2\sqrt{3}R)^2 + d^2} \\ d_8^B = d_{12}^B = \sqrt{(3\sqrt{3}R/2)^2 + (3R/2 - d)^2} \\ d_9^B = d_{11}^B = \sqrt{(\sqrt{3}R)^2 + (3R - d)^2} \\ d_{14}^B = d_{18}^B = \sqrt{(3\sqrt{3}R/2)^2 + (3R/2 + d)^2} \\ d_{15}^B = d_{17}^B = \sqrt{(\sqrt{3}R)^2 + (3R + d)^2} \\ d_{10}^B = 3R - d \\ d_{16}^B = 3R + d \end{cases} \end{cases} . \tag{6.21}$$

The corresponding angles between the mobile and the interfering base stations are also listed in Appendix E.

For examining the inner region (distance) with omni-directional antenna, we can use above analysis by setting $A(\theta_i) = 1$. In this case, a mobile has the same SINR quality at both position **A** and **B**. In other words, the omni-directional antenna produces a circle region with radius d.

Table 6.1 shows the inner and uncoordinated distances corresponding to different SINR requirements with both regular and rearranged tri-sector frequency partitions. We find that the cells with regular frequency partitions can extend a larger distance as mobile located close to the main-beam direction of a sector antenna (**A**) than to the sector edge (**B**). The

Table 6.1: The inner and uncoordinated distances d (meters) for various required SINR values.

SINR (dB)	Inner region	Regular (at **A**)	Regular (at **B**)	Rearranged (at **A**)	Rearranged (at **B**)
6	761 m	1139 m	867 m	797 m	816 m
8.5	678 m	1021 m	774 m	716 m	721 m
11.5	584 m	879 m	669 m	626 m	620 m
15	489 m	723 m	557 m	532 m	517 m
19	395 m	571 m	447 m	437 m	418 m
21	355 m	507 m	400 m	395 m	376 m

SINR guaranteed distances are also larger than that of a tri-sector FFR cell planning which further partitions an inner region. Oppositely, the cells with rearranged tri-sector frequency partitions has similar distance extension as mobile located close to the main-beam direction or to the sector edge. This is because there are two face-to-face interferers in the rearranged scenario. When a mobile locates in the main-beam direction of a sector antenna, the interference also come from the main-beam directions. Additionally, the extended distances in both **A** and **B** are close to the value of the omni-inner region. That is, the contour of uncoordinated region will be close to that of designing a inner region. As a result, we have the following comments:

- If cell planning combined with rearranged tri-sector frequency partition, we can construct the inner region with assigning suitable spectrum for uncoordinated transmissions. In the outer region, we can use network MIMO scheme to further improve the SINR.

- If cell planning combined with regular frequency partition, it may not be easy to establish the inner region for tri-sector FFR cellular system. Mobiles out of the uncoordinated distance can use network MIMO. However, the improvements are not significant according to the discussion in Section 6.5

Acknowledgement

The authors wish to thank Dr. Jack Winters for his insightful discussion and valuable suggestions on the study of joint network MIMO and frequency reuse techniques.

Chapter 7

Coverage Enhancement for Multiuser MIMO-OFDM Systems

MIMO antennas technique combining with OFDM is an attractive technique for high-capacity wireless systems. However, because the total transmit power is split among multiple antennas, the MIMO-OFDM systems face the coverage issue especially for the spatial multiplexing based MIMO systems. In this chapter, we propose COSA scheme to improve the coverage of spatial multiplexing based MIMO-OFDM systems by simultaneously exploiting multiuser diversity and frequency diversity gains. Applying the order statistics analysis technique and *Glivenko-Cantelli theorem*, we derive the analytical expressions for the link outage probability as well as cell coverage reliability of the spatial multiplexing based MIMO-OFDM systems. Our analytical and simulation results show that the COSA scheme can significantly improve the reliability, coverage, and the fairness performance for the spatial multiplexing based MIMO-OFDM systems.

7.1 System Model

7.1.1 Modeling and Assumption

Figure 7.1 shows a point-to-point spatial multiplexing based multiuser MIMO-OFDM system with M transmit antennas at the base station serving K users each of which has M receive antennas. Meanwhile, the considered OFDM modulation has N_T subcarriers in total and form N subchannels from adjacent N_T/N subcarriers. Assume that the total bandwidth of each subchannel is smaller than the channel coherent bandwidth. As seen in Fig. 7.1, MN independent data streams are multiplexed in M transmit antennas and N subchannels. The resource scheduling algorithms are carried out at the base station. The transmit power is uniformly split into M transmit antennas. With $\mathbf{x}_{k,n}$ and $\mathbf{y}_{k,n}$ respectively denoting the

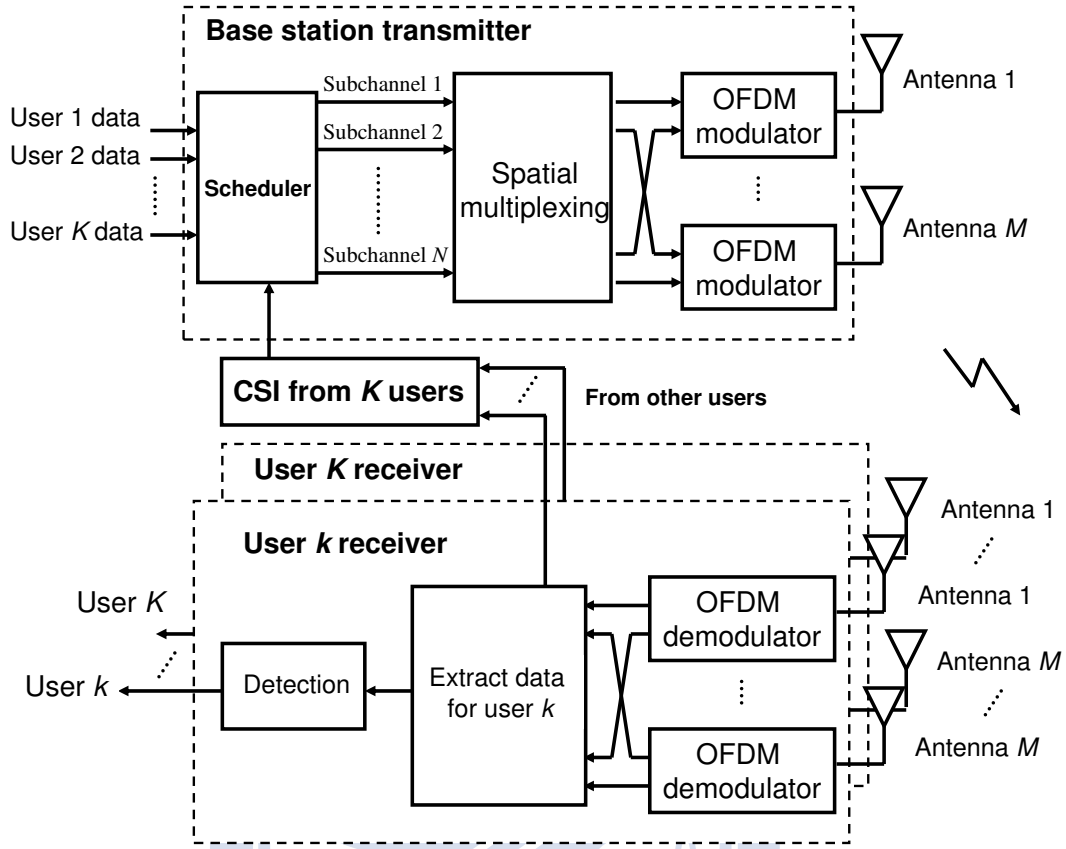

Figure 7.1: The spatial multiplexing based multi-user MIMO-OFDM systems.

$M \times 1$ transmit and receive signal vectors for the user k, we can write

$$\mathbf{y}_{k,n} = \sqrt{g_k}\,\mathbf{H}_{k,n}\mathbf{x}_{k,n} + \mathbf{n}_{k,n}, \tag{7.1}$$

where n is the subchannel index, index k represents a specific user, and $\mathbf{H}_{k,n}$ represents the flat- and independent-fading $M \times M$ channel matrix corresponding to the k-th user of the n-th subchannel. We represent $\mathbf{n}_{k,n}$ the $M \times 1$ spatially white noise vector with $E[\mathbf{n}_{k,n}\mathbf{n}_{k,n}^H] = \sigma^2\mathbf{I}_M$, σ^2 is the noise power of subchannel, and $\mathbf{I}_M$ is an $M \times M$ identical matrix. The same noise power level is assumed across subchannels and users. While $\mathbf{H}_{k,n}$ captures the channel fading characteristics, g_k characterizes the large-scale local average channel gain in terms of path loss. Under the same path loss model defined in Chapters 4 and 5, we have

$$10\log_{10}(g_k) = -10\mu\log_{10}(R_k) + g_0, \quad [\text{dB}] \tag{7.2}$$

For the sake of performance analysis, we will consider user population under homogeneous case in the following sections, i.e. $g_k = g$ for all k.

7.1.2 Performance Metric

Link Outage Probability

As defined in Chapter 2.3, when all the degrees of freedom in the spatial domain of a MIMO system are used for transmitting parallel and independent data streams to exploit the spatial multiplexing gain, the data stream with the lowest SNR in the MIMO system will dominate the link reliability performance. The spatial multiplexing based MIMO-OFDM systems in a frequency-selective fading channel can be decoupled as the sum of flat-faded MIMO subchannels. Consider the average weakest eigenmode over a series of N MIMO flat-faded subchannels, the link outage probability of the spatial multiplexing based MIMO-OFDM system is defined as:

$$P_{\text{out}} = P_r \left(\frac{1}{N} \sum_{n=1}^{N} \gamma_{k,n,1} \leq \gamma_{th} \right), \tag{7.3}$$

where $\gamma_{k,n,1}$ represents the effective output SNR of the weakest substream in subchannel n corresponding to the specific assigned user k, for $n = 1, \ldots, N$.

Reliable Coverage

With link outage probability P_{out}, the link radius associated with the required SNR and $(1-P_{\text{out}})$ reliability is called the **reliable coverage** as defined in Chapter 2.3. In this chapter, we will present various achievable reliable coverage regions for the spatial multiplexing based MIMO-OFDM system with different scheduling algorithms.

7.2 Subchannel Assignment and User Scheduling Algorithms

Subject to coverage enhancement, we present three suboptimal subchannel assignment and user selection algorithms for the spatial multiplexing based MIMO-OFDM systems as shown in Fig. 7.2. First, the COUS scheme aims to take advantage of multiuser diversity to

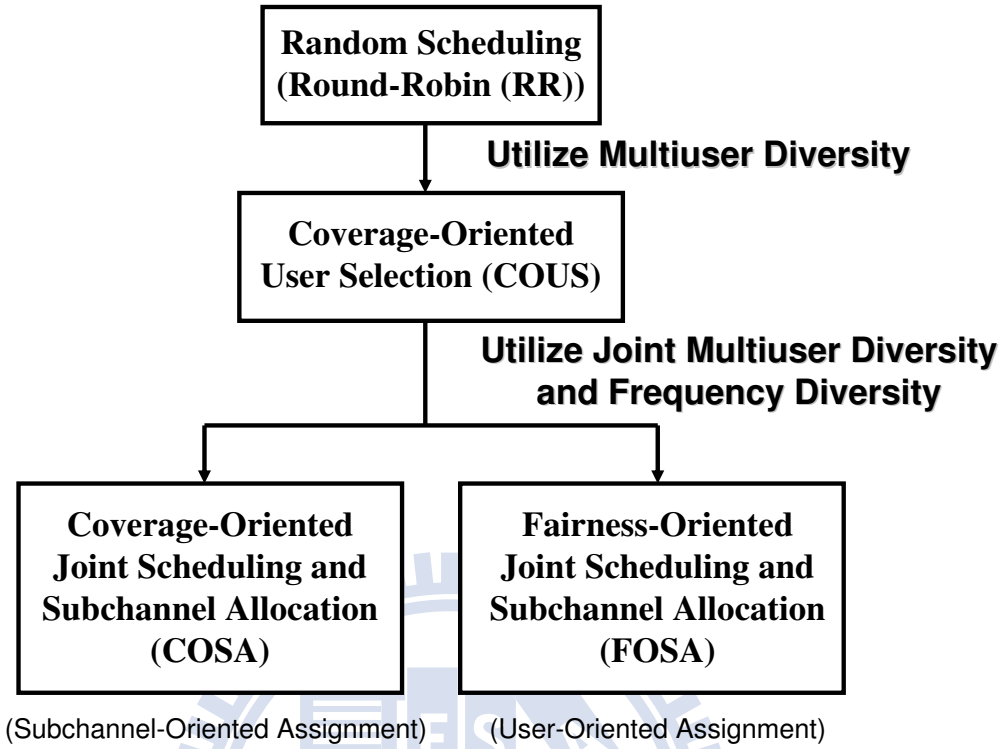

Figure 7.2: The scope of subchannel assignment and user selection algorithms in our consideration.

enhance coverage performance. To simultaneously exploit multiuser diversity and frequency diversity, we propose a low-complexity COSA algorithm for coverage extension. Then we show an extended suboptimal subchannel assignment algorithm, FOSA, developed from the work in [71] for comparison. To examine the benefit of multiuser diversity and frequency diversity, we set random user scheduling or the so called RR scheme as the benchmark for comparison.

For this chapter, our focus is the coverage issue so that the weakest eigenmode will be the metric for assignment determination. Specifically, the allocation principle of maximizing the worst substream is called as the **max-min** principle. We try to maximize the receive SNR of the worst substream in all subchannels. In the following subchannel assignment and user selection algorithms, equal amount of power is allocated to each subchannel for simplicity. Define $\mathcal{N} = \{1, 2, \ldots, N\}$, $\mathcal{K} = \{1, 2, \ldots, K\}$ and m_k as the subchannel index set, the user index set and the allocated weakest subchannel metric for the k-th user, respectively. The

notation $\lambda_{k,n,1} = \lambda_{\min}(\mathbf{H}_{k,n}\mathbf{H}_{k,n}^H)$ represents the weakest eigenmode in $\mathbf{H}_{k,n}$.

7.2.1 Coverage-Oriented User Selection (COUS)

With only taking advantage of multiuser diversity, because the link reliability of each MIMO flat-faded channel is dominated by the weakest substream, the scheduler select the target user according to

$$k^* = \arg\max_{k\in\mathcal{K}} \lambda_{k,1}^{\text{ave}} \ , \tag{7.4}$$

where the average weakest eigenmode of user k, $\lambda_{k,1}^{\text{ave}}$, is defined as

$$\lambda_{k,1}^{\text{ave}} = \frac{1}{N}\sum_{n=1}^{N} \lambda_{k,n,1} \ . \tag{7.5}$$

According to the user selection criterion (7.4), the spatial multiplexing based MIMO-OFDM system will assign **all** frequency resources to the scheduled user to enhance both the link reliability and coverage performance.

7.2.2 Coverage-Oriented Joint Scheduling and Subchannel Allocation (COSA)

With the information $\{\lambda_{k,n,1}\}_{k=1}^{K}$ from all users, the scheduler at the base station can assign the n-th subchannel to the target user according to

$$k^* = \arg\max_{k\in\mathcal{K}} \lambda_{k,n,1} \ , \quad \text{for} \ \ n \in \mathcal{N} \ . \tag{7.6}$$

Different from COUS, this assignment can take advantage of multiuser diversity and frequency diversity simultaneously by assigning frequency resource adaptively. Each subchannel n takes turns to select the target user satisfying the max-min principle compared with the other $K-1$ users. Therefore, COSA is a subchannel-oriented type resource assignment. The overall complexity of COSA is in the order of $\mathcal{O}(NK)$. Because there are K i.i.d. selectivity orders in each assignment, we have maximal scheduling gain on the worst substream for all subchannels so that we term this low-complexity assignment scheme as *coverage-oriented*. Note that when $N = 1$ the system becomes an spatial multiplexing based MIMO system as considered in [30]. The two proposed coverage-enhanced algorithms, COUS and COSA, will be the same as the strongest-weakest-normalized-subchannel-first (SWNSF) algorithm presented in [30].

7.2.3 Fairness-Oriented Joint Scheduling and Subchannel Allocation (FOSA)

The authors in [71] proposed a suboptimal subcarrier assignment for the SISO-OFDM systems. The resource allocation principle is to maximize the minimum rate among users under the assumption that all users achieve a similar rate. Different from a SISO system in which the only one channel condition can sufficiently determine the link quality, coverage and capacity, a MIMO system must consider all eigenmodes for different performance tradeoff. According to the max-min design principle, we extend the algorithm proposed in [71] to a MIMO-OFDM system and denote it as FOSA in the chapter. The assignment algorithm is shown as follows:

1. Initialization

   Set $\mathcal{N} = \{1, \ldots, N\}$ and $\mathcal{K} = \{1, \ldots, K\}$

   $m_k = 0, \quad \forall k \in \mathcal{K}$

2. for $k = 1$ to K

   (a) $n^* = \arg\max_{n \in \mathcal{N}} \lambda_{k,n,1}$

   (b) $\mathcal{N} = \mathcal{N} - \{n^*\}$

   (c) $m_k = \lambda_{k,n^*,1}$

3. while $\mathcal{N} \neq \emptyset$

   (a) $k^* = \arg\min_{k \in \mathcal{K}} m_k$

   (b) $n^* = \arg\max_{n \in \mathcal{N}} \lambda_{k^*,n,1}$

   (c) $\mathcal{N} = \mathcal{N} - \{n^*\}$

   (d) $m_{k^*} = m_{k^*} + \lambda_{k^*,n^*,1}$

The main advantage of FOSA is the negligible complexity compared with the optimal joint user and subcarrier allocation. Its complexity is in the order of $\mathcal{O}((N-K)^2)$. Each user will be assigned one subchannel in the first loop of this algorithm. Then remaining subchannels will be assigned according to the assignment metric m_k. As a result, FOSA

can ensure all mobile users to share almost the same number of subchannels to achieve good fairness performance. Note that FOSA is a user-oriented type resource assignment, which determines each subchannel assignment by each user selecting the most suitable subchannel.

7.3 Link Outage and Coverage Performance Analysis

7.3.1 The Spatial Multiplexing based MIMO-OFDM System with Random Scheduling

In this subsection, we analyze the link outage and coverage performance of the spatial multiplexing based MIMO-OFDM systems without subchannel assignment, i.e. allocate all resources to a certain user or to users randomly. This approach is also called the RR scheduling which assigns each time slot to a target user in the circular sequential manner among K users. Therefore, the RR scheduling cannot exploit multiuser diversity as well as frequency diversity because it ignores the channel conditions among users. Hence, we omit the user index term k in the notations among this subsection.

To begin with, we first analyze the effective output SNR of the weakest substream (denoted by $\gamma_{n,1}$) at the n-th MIMO flat-faded subchannel. With $\{\lambda_{n,i}\}_{i=1}^{M}$ the eigenvalues of the Wishart matrix $\mathbf{H}_n\mathbf{H}_n^H$, we can express $\gamma_{n,i}$ as

$$\gamma_{n,i} = \rho_n \lambda_{n,i}/M \ , \quad \text{for } i = 1, \ldots, M \ , \tag{7.7}$$

where ρ_n is the average received SNR of the n-th subchannel under certain distance R with the value

$$\rho_n = \rho = \frac{P_T g}{\sigma^2} = \frac{P_T 10^{g_0/10}}{\sigma^2 R^{\mu}} \quad \forall n \in \mathcal{N} \tag{7.8}$$

In (7.8), the transmission power of each subchannel is assumed as P_T and is split over multiple M transmit antennas. Arrange $\{\lambda_{n,i}\}_{i=1}^{M}$ in the ascending order $0 \leq \lambda_{n,1} \leq \lambda_{n,2} \leq ... \leq \lambda_{n,M}$. According to [30] [119], the PDF of the minimum eigenvalue $\lambda_{n,1}$ is exponentially distributed with parameter M as follows

$$f_{\lambda_{n,1}}(\lambda) = Me^{-M\lambda} \ , \ \lambda \geq 0 \ , \tag{7.9}$$

and its CDF can be written as

$$\begin{aligned} F_{\lambda_{n,1}}(\lambda) &= \int_0^{\lambda} f_{\lambda_{n,1}}(x)dx \\ &= 1 - e^{-M\lambda},\ \lambda \geq 0\ . \end{aligned} \tag{7.10}$$

The CDF of the effective output SNR $\gamma_{n,M}$ is

$$F_{\gamma_{n,1}}(\gamma) = 1 - e^{-\frac{M^2\gamma}{\rho}}\ ,\ \gamma \geq 0\ . \tag{7.11}$$

For the i.i.d. exponentially distributed random variables $\{\gamma_{n,1}\}_{n=1}^{N}$, the term $\Omega = \frac{1}{N}\sum_{n=1}^{N}\gamma_{n,1}$ becomes an Erlang distributed random variable with PDF

$$f_{\Omega}(x) = \frac{N(\frac{M^2}{\rho})^N (Nx)^{N-1} e^{-\frac{M^2 N}{\rho}x}}{\Gamma(N)}\ ,\quad x > 0 \tag{7.12}$$

and CDF

$$\begin{aligned} F_{\Omega}(x) &= \int_0^{x} f_{\Omega}(y)dy \\ &= 1 - e^{-\frac{M^2 N}{\rho}x}\sum_{j=0}^{N-1}\frac{(\frac{M^2 N}{\rho}x)^j}{j!} \\ &= 1 - \Gamma_{\mathrm{R}}\left(N, \frac{M^2 N}{\rho}x\right)\ ,\quad x > 0\ , \end{aligned} \tag{7.13}$$

where $\Gamma_{\mathrm{R}}(a,x) = \frac{\Gamma(a,x)}{\Gamma(a)}$ is the regularized gamma function with $\Gamma(a,x) = \int_x^{\infty} t^{a-1}e^{-t}dt$ and $\Gamma(a) = \int_0^{\infty} t^{a-1}e^{-t}dt$. Thus, for a given threshold $\gamma_{th} > 0$, the link outage probability of the spatial multiplexing based MIMO-OFDM system can be expressed as

$$\begin{aligned} P_{\mathrm{out}} &= P_r\left(\frac{1}{N}\sum_{n=1}^{N}\gamma_{n,1} \leq \gamma_{th}\right) \\ &= P_r\left(\Omega \leq \gamma_{th}\right) \ = \ F_{\Omega}(\gamma_{th}) \\ &= 1 - \Gamma_{\mathrm{R}}\left(N, \frac{M^2 N}{\rho}\gamma_{th}\right) \\ &= 1 - \Gamma_{\mathrm{R}}\left(N, \frac{NM^2\sigma^2 R^{\mu}}{P_T 10^{g_0/10}}\gamma_{th}\right)\ , \end{aligned} \tag{7.14}$$

which is a function of the given parameters $\{M, N, P_t, \sigma^2, \mu, \gamma_{th}, R\}$.

Based on (7.14), we derive the closed-form expression of the reliable coverage associated with link outage probability for the spatial multiplexing based MIMO-OFDM system as

$$R_{\mathrm{RS}} = \left[\left(\frac{P_T}{\sigma^2}\right)\left(\frac{10^{\frac{g_0}{10}}}{NM^2\gamma_{th}}\right)\Gamma_{\mathrm{R}}^{-1}\left(N, 1 - P_{\mathrm{out}}\right)\right]^{\frac{1}{\mu}}\ , \tag{7.15}$$

where the subscript "RS" denote "random scheduling" and we utilize the inverse function of $\Gamma_{\mathrm{R}}(a,x)$ (defined in Chapter 4.13) to derive (7.15). The closed form (7.15) is a function composed of some given parameters $\{M, N, P_t, \sigma^2, \mu, \gamma_{th}\}$ and the required P_{out}.

In the Special Case $N = 1$

For the special case $N = 1$, the term $\Gamma_{\mathrm{R}}(1,x) = e^{-x}$. Hence the closed-form expressions (7.14) and (7.15) will reduce to the results provided in [30, Section IV. B] for RR scheduling.

7.3.2 The Spatial Multiplexing based MIMO-OFDM System with COUS

With taking multiuser scheduling into consideration, COUS selects the target user according to (7.4). Denote the average effective output SNR of user k as $\Omega_k = \frac{\rho}{M}\lambda_{k,1}^{\mathrm{ave}}$, the CDF of Ω_k will be equal to (7.13) for each user k. The corresponding CDF of COUS is hence given by

$$\begin{aligned} F_{\Omega_{k^*}}(\gamma) &= P_r\left\{\max_{k\in\mathcal{K}}\{\Omega_k\} \le \gamma\right\} \\ &= \left[F_{\Omega_k}(\gamma)\right]^K , \end{aligned} \tag{7.16}$$

where k^* represents the scheduled user. The link outage of COUS can be expressed as

$$\begin{aligned} P_{\mathrm{out}} &= P_r(\Omega_{k^*} \le \gamma_{th}) = F_{\Omega_{k^*}}(\gamma) \\ &= \left[1 - \Gamma_{\mathrm{R}}\left(N, \frac{M^2 N}{\rho}\gamma_{th}\right)\right]^K \\ &= \left[1 - \Gamma_{\mathrm{R}}\left(N, \frac{NM^2\sigma^2 R^{\mu}}{P_T 10^{g_0/10}}\gamma_{th}\right)\right]^K , \end{aligned} \tag{7.17}$$

The corresponding closed-form expression of the reliable coverage is given by

$$R_{\mathrm{COUS}} = \left[\left(\frac{P_T}{\sigma^2}\right)\left(\frac{10^{\frac{g_0}{10}}}{NM^2\gamma_{th}}\right)\Gamma_{\mathrm{R}}^{-1}\left(N, 1 - \sqrt[K]{P_{\mathrm{out}}}\right)\right]^{\frac{1}{\mu}} . \tag{7.18}$$

In the Special Case $N = 1$

Similarly, by substituting $N = 1$ into (7.17) and (7.18), the equivalent results can be found in [30, Section IV. C] for the SWNSF scheduling.

In the Special Case $K = 1$

As the degrees of freedom on user domain is merely one, the performance metrics of COUS (7.17) and (7.18) are straightforwardly same to that of random scheduling in Section 7.3.1.

7.3.3 The Spatial Multiplexing based MIMO-OFDM System with COSA

With COSA scheduling algorithm, each user k competes with the other $(K-1)$ users for winning the service on each subchannel n according to (7.6). We label the selected user with a superscript k^*. Then the effective output SNR of the selected user's weakest substream in subchannel n is now denoted as $\gamma_{k^*,n}$ and its corresponding CDF is given by

$$\begin{aligned} F_{\gamma_{k^*,n}}(\gamma) &= Pr\left\{\max_{k\in\mathcal{K}}\{\gamma_{k,n}\} < \gamma\right\} = [F_{\gamma_{k,n}}(\gamma)]^K \\ &= [1 - e^{-\frac{M^2\gamma}{\rho}}]^K, \end{aligned} \tag{7.19}$$

where we omit the suffix index "1" which indicates the minimal eigenmode to ease the notations. For brevity, we use the symbol $F_{k^*,n}$ instead of $F_{\gamma_{k^*,n}}$ for the CDF of $\gamma_{k^*,n}$ in the following. With the help of **order statistics** method [120], we reorder a given sample of the N variables $\{\gamma_{k^*,1}, ...\gamma_{k^*,N}\}$ as $\gamma_{k^*,(1)} \leq \gamma_{k^*,(2)} \leq ... \leq \gamma_{k^*,(N)}$. Then $\gamma_{k^*,(i)}$ is called the i-th order statistic and $F_{k^*,(i)}(\cdot)$ is the corresponding CDF. The link outage probability of the spatial multiplexing based MIMO-OFDM systems with COSA can be written as

$$\begin{aligned} P_{\text{out}} &= Pr\left(\frac{1}{N}\sum_{n=1}^{N}\gamma_{k^*,n} \leq \gamma_{th}\right) \\ &\overset{(a)}{\simeq} Pr(\gamma_{k^*,(\tilde{\omega})} \leq \gamma_{th}) \ , \end{aligned} \tag{7.20}$$

with

$$\tilde{\omega} \simeq N\left(1 - \exp\left(K\sum_{i=0}^{K-1}\binom{K-1}{i}(-1)^{K-i}\frac{1}{(K-i)^2}\right)\right)^K , \tag{7.21}$$

where we use **Glivenko-Cantelli Theorem** to get the approximation (a) with the assumption that $\gamma_{k^*,(\tilde{\omega})}$ is the value closest to $\frac{1}{N}\sum_{n=1}^{N}\gamma_{k^*,n}$. This approximation can help us to facilitate deriving an approximated analytical closed form for reliable coverage.

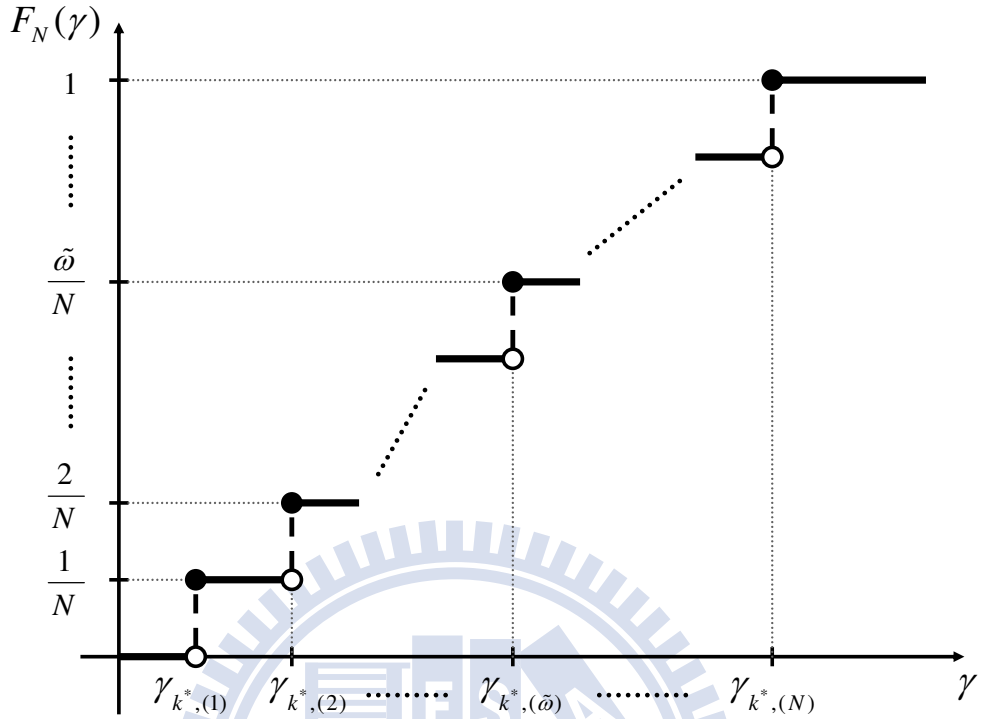

Figure 7.3: Illustration of the empirical distribution for an i.i.d. sequence.

Find the Approximate Value $\tilde{\omega}$

To find $\tilde{\omega}$, we introduce a function called the *empirical distribution* [121]. Assume that $X_1, X_2, \ldots$ are i.i.d. random variables in $\mathbb{R}$ with common CDF $F(x)$. The empirical distribution for $\{X_1, X_2, \ldots\}$ is a random variable defined as

$$F_m(x) = \frac{1}{m} \sum_{i=1}^{m} I_{(-\infty,x]}(X_i) \ , \tag{7.22}$$

where $I_{(-\infty,x]}(\cdot)$ is the indicator function, i.e.

$$I_{(-\infty,x]}(y) = \begin{cases} 1, & \text{if } \ y \leq x \\ 0, & \text{if } \ y > x \ . \end{cases} \tag{7.23}$$

The *Glivenko-Cantelli Theorem* [121] says that

$$\sup_{x \in \mathbb{R}} |F_m(x) - F(x)| \tag{7.24}$$

converges to 0 with probability 1, where "sup" means the supremum. In other words, the theorem implies the strong statement

$$P_r\left[\lim_{m\to\infty}\sup_{x\in\mathbb{R}}|F_m(x)-F(x)|=0\right]=1\ . \tag{7.25}$$

With $\{\gamma_{k^*,(1)}\le\gamma_{k^*,(2)}\le...\le\gamma_{k^*,(N)}\}$, we have the empirical distribution

$$F_N(\gamma_{k^*,(\tilde{\omega})})=\frac{1}{N}\sum_{n=1}^{N}I_{(-\infty,\gamma_{k^*,(\tilde{\omega})}]}(\gamma_{k^*,n})=\frac{\tilde{\omega}}{N}\ , \tag{7.26}$$

and Fig. 7.3 shows the diagram of $F_N(\gamma_{k^*,(\tilde{\omega})})$. To obtain the $\tilde{\omega}$ value, we have

$$\tilde{\omega}=NF_N(\gamma_{k^*,(\tilde{\omega})})\overset{(a)}{\simeq}NF_{k^*,n}(\gamma_{k^*,(\tilde{\omega})})\overset{(b)}{\simeq}NF_{k^*,n}(E[\gamma_{k^*,n}])\ , \tag{7.27}$$

where (a) comes from the Glivenko-Cantelli Theorem and (b) satisfies the assumption $\gamma_{k^*,(\tilde{\omega})}$ is the value closest to $\frac{1}{N}\sum_{n=1}^{N}\gamma_{k^*,n}$. The notation $E[\gamma_{k^*,n}]$ is the expectation value of $\gamma_{k^*,n}$. With the help of the order statistics, we have the PDF of $f_{k^*,n}(\gamma)$ as follows

$$\begin{aligned}
f_{k^*,n}(\gamma) &= \frac{KM^2}{\rho}\ e^{-\frac{M^2}{\rho}\gamma}\left(1-e^{-\frac{M^2}{\rho}\gamma}\right)^{K-1}\\
&\overset{(a)}{=} \frac{KM^2}{\rho}\ e^{-\frac{M^2}{\rho}\gamma}\sum_{i=0}^{K-1}\binom{K-1}{i}(-1)^{K-1-i}\left(e^{-\frac{M^2}{\rho}\gamma}\right)^{K-1-i}\\
&= \frac{KM^2}{\rho}\ \sum_{i=0}^{K-1}\binom{K-1}{i}(-1)^{K-1-i}e^{-\frac{M^2}{\rho}\gamma(K-i)}\ ,
\end{aligned} \tag{7.28}$$

where (a) comes from the binomial expansion $(1-x)^n=\sum_{i=0}^{n}\binom{n}{i}(-1)^i x^i$. As a result, we have

$$\begin{aligned}
E[\gamma_{k^*,n}] &= \int_0^\infty \gamma f_{k^*,n}(\gamma)d\gamma\\
&= \frac{KM^2}{\rho}\ \sum_{i=0}^{K-1}\binom{K-1}{i}(-1)^{K-1-i}\int_0^\infty \gamma\, e^{-\frac{M^2}{\rho}\gamma(K-i)}d\gamma\\
&= \frac{KM^2}{\rho}\ \sum_{i=0}^{K-1}\binom{K-1}{i}(-1)^{K-1-i}\frac{1}{(\frac{M^2}{\rho})^2(K-i)^2}\\
&= \frac{K\rho}{M^2}\ \sum_{i=0}^{K-1}\binom{K-1}{i}(-1)^{K-1-i}\frac{1}{(K-i)^2}\ .
\end{aligned} \tag{7.29}$$

By substituting (7.29) into (7.27), we obtain

$$\begin{aligned}
\tilde{w} &\simeq NF_{k^*,n}(E[\gamma_{k^*,n}])=N\left[F_{k,n}(E[\gamma_{k^*,n}])\right]^K\\
&\overset{(a)}{=} N\left(1-\exp\left(K\sum_{i=0}^{K-1}\binom{K-1}{i}(-1)^{K-i}\frac{1}{(K-i)^2}\right)\right)^K\\
&\triangleq N_{\tilde{\omega}}\ ,
\end{aligned} \tag{7.30}$$

where (a) comes from (7.19) and $N_{\tilde{\omega}}$ is an approximation integer value of $\tilde{\omega}$ by rounding $\tilde{\omega}$ to the nearest integer number and is a function of N and K.

Approximated Analytical Formula by Order Statistics

In (7.20), the link outage is transformed into another form of probability, which means at least $N_{\tilde{\omega}}$ of the $\{\gamma_{k^*,n}\}_{n=1}^{N}$ are less than or equal to γ_{th}. By applying the theories of order statistics, we obtain

$$\begin{aligned} P_{\text{out}} &\simeq P_r(\gamma_{k^*,(N_{\tilde{\omega}})} \leq \gamma_{th}) = F_{k^*,(N_{\tilde{\omega}})}(\gamma_{th}) \\ &= \sum_{i=N_{\tilde{\omega}}}^{N} \binom{N}{i} \left[F_{k^*,n}(\gamma_{th})\right]^i \left[1 - F_{k^*,n}(\gamma_{th})\right]^{N-i} \\ &\overset{(a)}{=} I_{F_{k^*,n}(\gamma_{th})}\left(N_{\tilde{\omega}}, N - N_{\tilde{\omega}} + 1\right) \\ &\overset{(b)}{=} I_{(F_{k,n}(\gamma_{th}))^K}\left(N_{\tilde{\omega}}, N - N_{\tilde{\omega}} + 1\right) \\ &\overset{(c)}{=} I_{\left[1-\exp(\frac{-M^2}{\rho}\gamma_{th})\right]^K}\left(N_{\tilde{\omega}}, N - N_{\tilde{\omega}} + 1\right) \ , \end{aligned} \tag{7.31}$$

where

$$I_p(a,b) = \frac{\int_0^p t^{a-1}(1-t)^{b-1}dt}{\int_0^1 t^{a-1}(1-t)^{b-1}dt} \quad \text{For } a > 0,\ b > 0 \text{ and } 0 \leq p \leq 1 \tag{7.32}$$

is the regularized incomplete beta function. The result (a) comes from a well-known result for the regularized incomplete beta function $I_p(l, L-l+1) = \sum_{i=l}^{L} \binom{L}{i} p^i (1-p)^{L-i}$ [122]. The equalities in (b) and (c) are based on (7.19). Now we have the analytical closed-form approximation for the link outage.

The reliable coverage R_{COSA} can be derived from this approximate formula (7.31). We first introduce the *inverse regularized incomplete beta function* which is shown as follows

$$z = I_p(a,b) \ \Rightarrow \ p = I_z^{-1}(a,b) \ . \tag{7.33}$$

By substituting (7.30) and (7.33) into (7.31), we can obtain the reliable coverage as

$$R_{\text{COSA}} \simeq \left[\left(\frac{P_T}{\sigma^2}\right)\left(\frac{10^{\frac{g_0}{10}}}{M^2\gamma_{th}}\right)\log\left(\frac{1}{1-\left(I^{-1}_{P_{\text{out}}}\left(N_{\tilde{\omega}}, N - N_{\tilde{\omega}} + 1\right)\right)^{\frac{1}{K}}}\right)\right]^{\frac{1}{\mu}} \tag{7.34}$$

where the value $N_{\tilde{\omega}}$ is shown in (7.30). Now we have an analytical closed-form approximation of the reliable coverage for the spatial multiplexing based MIMO-OFDM systems with COSA, and it is a function composed of the given parameters $\{M, N, K, P_t, \sigma^2, \mu, \gamma_{th}\}$ and required P_{out}.

Annotation of the Approximated Formula

For the spatial multiplexing based MIMO-OFDM systems with COSA, the provided approximated form will be more accurate as the number of subchannels N is large according to the Glivenko-Cantelli Theorem. In the special case $N = 1$ and $K = 1$, the integer $N_{\tilde{\omega}} = 1$ due to $\tilde{\omega} \cong 0.63$. In this case of no degrees of freedom on both user and frequency domains, the approximation (7.34) of COSA have the same value as (7.15) of random scheduling. As for the special case $N = 1$ and user population K which lacks degrees of freedom on frequency domain, the approximation (7.34) of COSA have the same value as (7.18) of COUS. It is because COUS only taking advantage of multiuser diversity.

7.4 Discussion

7.4.1 Fairness Issue

Compared with the spatial multiplexing based MIMO-OFDM systems using FOSA, the average subchannels for each user assigned using COSA is N/K. As for COUS, each user has $1/K$ probability selected in each time slot and then assigned N subchannels so that also N/K assigned subchannels on average. Thus, COSA and COUS are fair in the sense of equally resource allocation. To examine long-term fairness performance, we define the fairness index F in the multiuser spatial multiplexing based MIMO-OFDM systems according to Jain's fairness index [123]

$$F = \frac{\left(\frac{1}{K}\sum_{i=1}^{K} T_i\right)^2}{\frac{1}{K}\sum_{i=1}^{K} {T_i}^2} = \frac{\left(\sum_{i=1}^{K} T_i\right)^2}{K\sum_{i=1}^{K} {T_i}^2} \ , \tag{7.35}$$

where T_i is the cumulated number of subchannels allocated to the i-th user. For $F = 1$, it is the fairest condition between users, and it is not fair as $F \ll 1$. Figure 7.4 shows the fairness performance comparison for FOSA, COSA and COUS with system scheduling time slots when $K = 10$ and $M = 3$. We find that COSA achieves almost the same fairness performance as FOSA when the number of subchannels is larger and the scheduling time index is increasing. However, the fairness performance of COUS is poorer than FOSA

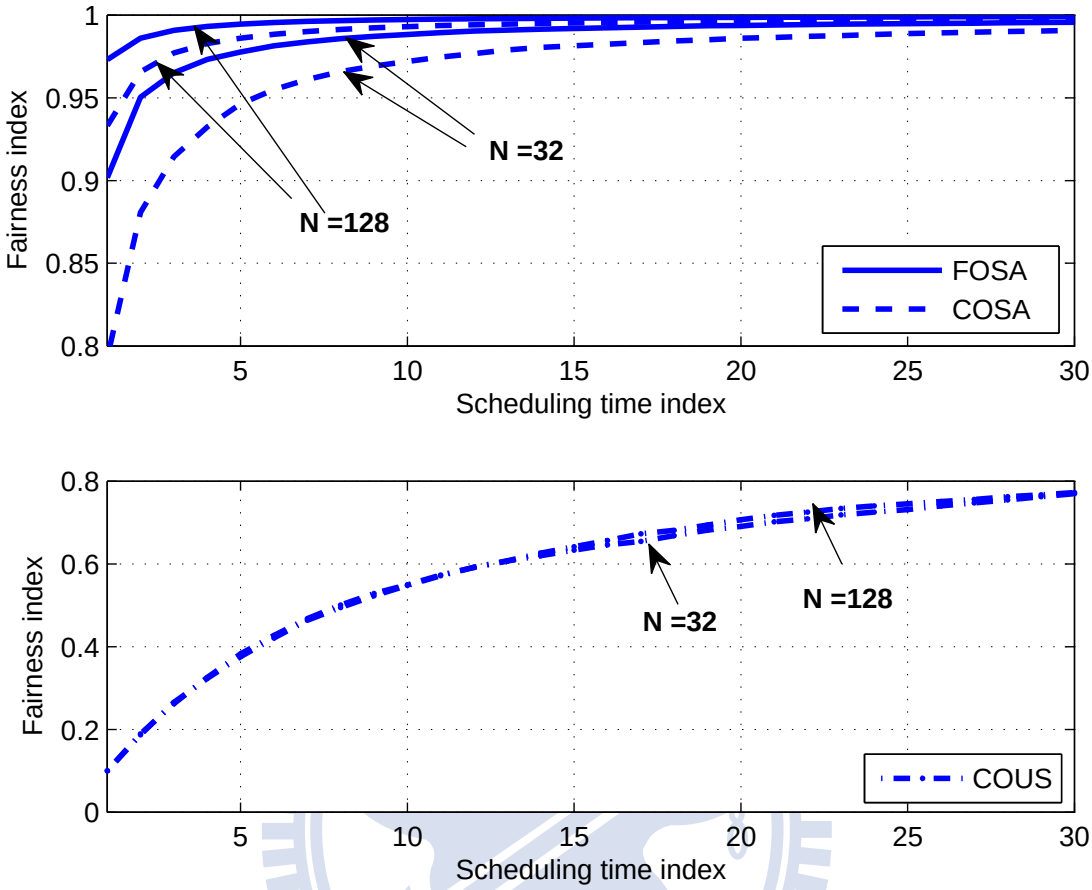

Figure 7.4: Fairness performance comparison for $K = 10$ and $M = 3$.

and COSA even if each user of COUS can get the same number of subchannels as COSA theoretically. In fact, the fairness performance of COUS can also approach that of FOSA and COSA as scheduling time slots are extremely large.

7.4.2 Coverage Gain from Multiuser and Frequency Diversity

To quantify the benefit of suitably using the degrees of freedom in term of user and frequency domains, we define the coverage gain G_{scheme} as

$$G_{\text{scheme}} \triangleq \frac{R_{\text{scheme}} - R_{\text{RS}}}{R_{\text{RS}}} \ , \tag{7.36}$$

where "scheme" denote different subchannel scheduling and assignment methods including COUS and COSA. The term (7.36) identifies the achievable gain on coverage extension

over random scheduling and assignment. Based on (7.15), (7.18) and (7.34), we obtain the respective gain values G_{COUS} and G_{COSA} for the spatial multiplexing based MIMO-OFDM systems with COUS and COSA as follows:

$$G_{\text{COUS}} = \left[\frac{\Gamma_{\text{R}}^{-1}\left(N, 1 - \sqrt[K]{P_{\text{out}}}\right)}{\Gamma_{\text{R}}^{-1}\left(N, 1 - P_{\text{out}}\right)} \right]^{\frac{1}{\mu}} - 1 \ , \tag{7.37}$$

and

$$G_{\text{COSA}} \simeq \left[\frac{N \log\left([1 - (I_{P_{\text{out}}}^{-1}\left(N_{\tilde{\omega}}, N - N_{\tilde{\omega}} + 1\right))^{\frac{1}{K}}]^{-1} \right)}{\Gamma_{\text{R}}^{-1}\left(N, 1 - P_{\text{out}}\right)} \right]^{\frac{1}{\mu}} - 1 \ . \tag{7.38}$$

Note that (7.37) and (7.38) are function of $\{N, K, P_{\text{out}}, \mu\}$ and are independent of the parameter M (number of antennas). In other word, both COUS and COSA achieve constant coverage gain over random scheduling under any antenna setup.

7.4.3 Coverage Shrinkage Issue

In this section, we address the coverage shrinkage problem for the spatial multiplexing based MIMO-OFDM systems due to the transmit power is split over multiple transmission antennas when multiple antennas is available. From the formula (7.15) for the spatial multiplexing based MIMO-OFDM systems with random assignment, we can obtain the coverage closed-form expression of the SISO-OFDM systems with random scheduling and assignment as:

$$R_{\text{SISO}} \ = \ \left[\left(\frac{P_T}{\sigma^2} \right) \left(\frac{10^{\frac{g_0}{10}}}{N\gamma_{th}} \right) \Gamma_{\text{R}}^{-1}\left(N, 1 - P_{\text{out}}\right) \right]^{\frac{1}{\mu}} \ . \tag{7.39}$$

To show the coverage shrinkage problem, we compare (7.15) and (7.39) under the same transmission power P_T, number of subchannels N, and the same link reliability requirements P_{out} and γ_{th}, and we obtain

$$\eta_{\text{RS}} \triangleq \frac{R_{\text{RS}}}{R_{\text{SISO}}} = \left(\frac{1}{M^2} \right)^{\frac{1}{\mu}} \leq 1 \ . \tag{7.40}$$

Note that the equality will hold if and only if $M = 1$. With solely taking advantage of multiuser diversity by using COUS, the coverage ratio of R_{COUS} in (7.18) to R_{SISO} is

$$\eta_{\text{COUS}} \triangleq \frac{R_{\text{COUS}}}{R_{\text{SISO}}} = \left[\frac{1}{M^2} \frac{\Gamma_{\text{R}}^{-1}\left(N, 1 - \sqrt[K]{P_{\text{out}}}\right)}{\Gamma_{\text{R}}^{-1}\left(N, 1 - P_{\text{out}}\right)} \right]^{\frac{1}{\mu}} \ . \tag{7.41}$$

With joint multiuser scheduling and subchannel allocation, the coverage ratio of R_{COSA} in (7.34) to R_{SISO} is

$$\eta_{\text{COSA}} \triangleq \frac{R_{\text{COSA}}}{R_{\text{SISO}}} \simeq \left[\frac{N}{M^2} \frac{\log\left([1 - (I^{-1}_{P_{\text{out}}}(N_{\tilde{\omega}}, N - N_{\tilde{\omega}} + 1))^{\frac{1}{K}}]^{-1} \right)}{\Gamma^{-1}_{\text{R}}(N, 1 - P_{\text{out}})} \right]^{\frac{1}{\mu}} . \tag{7.42}$$

Different from (7.40) the ratio is always smaller than one, R_{COUS} and R_{COSA} in (7.41) and (7.42) can possibly be greater than R_{SISO} as the number of users is large enough. According to (7.41), the coverage shrinkage caused by multiple antennas can be compensated by COUS as the number of users K satisfies the condition:

$$K \geq \left\lceil \frac{\log P_{\text{out}}}{\log\left[1 - \Gamma_{\text{R}}\left(N, M^2 \Gamma^{-1}_{\text{R}}(N, 1 - P_{\text{out}})\right)\right]} \right\rceil , \tag{7.43}$$

where $\lceil x \rceil$ denotes the smallest integer greater or equal to x. For the spatial multiplexing based MIMO-OFDM systems with COSA, because the parameter $N_{\tilde{\omega}}$ is also a function of K, it is not easy to directly display the condition of how large K can satisfy the ratio $\eta_{\text{COSA}} \geq 1$. However, we will show that the proposed joint multiuser scheduling and subchannel allocation algorithm can indeed improve coverage shrinkage problem in the numerical results later. From (7.41) and (7.42), we know that the coverage shrinkage performance can be reformed by taking advantage of joint multiuser scheduling and subchannel allocation for the spatial multiplexing based MIMO-OFDM systems.

7.5 Numerical Results

In this section, we present numerical results to show the benefit of multiuser scheduling and frequency diversity on coverage enhancement. We also illustrate how the number of antennas, number of subchannels (the order of frequency selectivity), and the number of users could affect the reliable coverage in the spatial multiplexing based MIMO-OFDM systems. We first assume some predetermined parameters including transmission and noise power of a subchannel $P_T = 0$ dBW and $\sigma^2 = -103$ dBm, $g_0 = -32$ dB, path loss exponent $\mu = 4$, and the required link outage $P_{\text{out}} = 0.1$ and SNR $\gamma_{th} = 6$ dB.

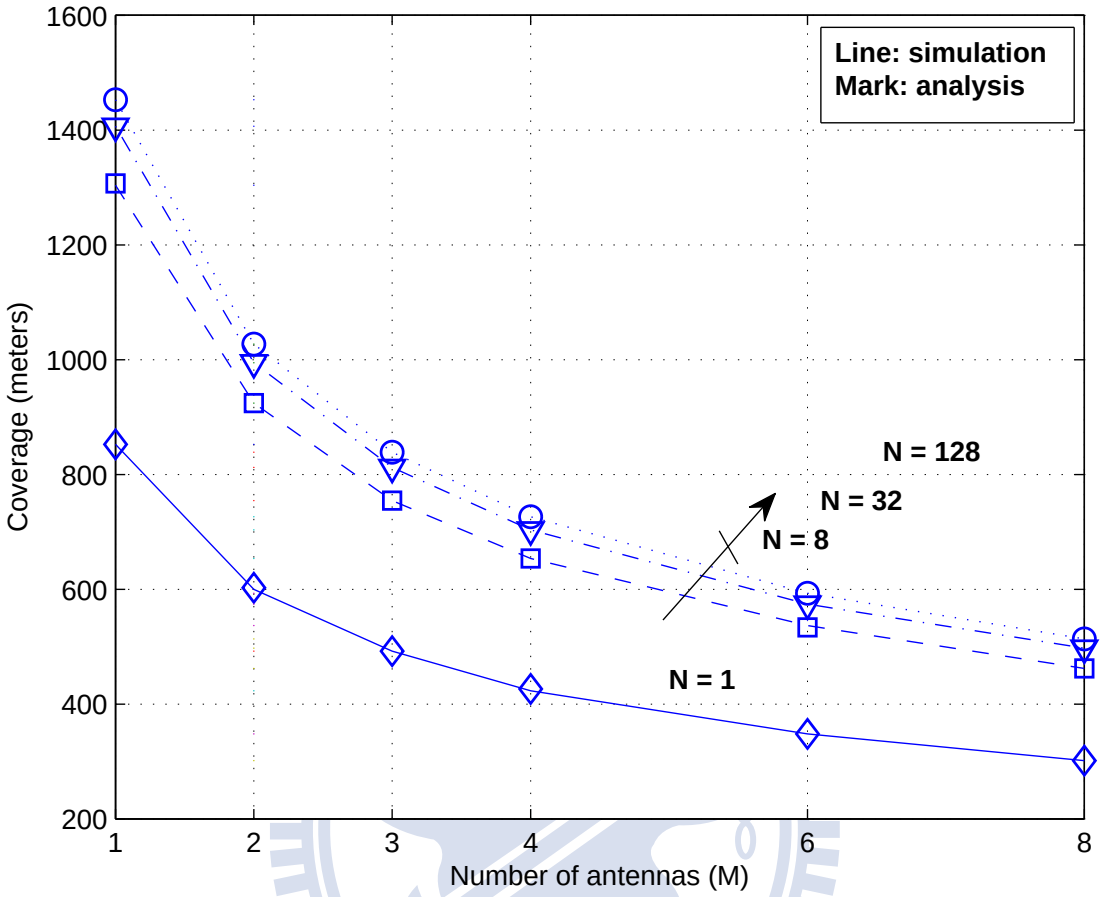

Figure 7.5: Reliable coverage of the spatial multiplexing based MIMO-OFDM without scheduling under various number of antennas $M = \{1, 2, 3, 4, 6, 8\}$ and number of subchannels $N = \{1, 8, 32, 128\}$. Parameters: $P_T = 0$ dBW, noise power $\sigma^2 = -103$ dBm, $g_0 = -32$ dB, $\mu = 4$, $P_{\text{out}} = 0.1$ and $\gamma_{th} = 6$ dB.

7.5.1 Accuracy of Provided Analytical Forms

In this part, we validate the accuracy of provided analytical formulas for reliable coverage. Figure 7.5 shows the reliable coverage of the spatial multiplexing based MIMO-OFDM with random scheduling under various number of antennas $M = \{1, 2, 3, 4, 6, 8\}$ and number of subchannels $N = \{1, 8, 32, 128\}$. Clearly, the provided analysis can match simulation very well. Based on this figure, the spatial multiplexing based MIMO-OFDM systems have larger reliable coverage in a high-frequency selectivity environment than that in a low frequency-selectivity condition. However, the coverage performance will significantly reduce if more

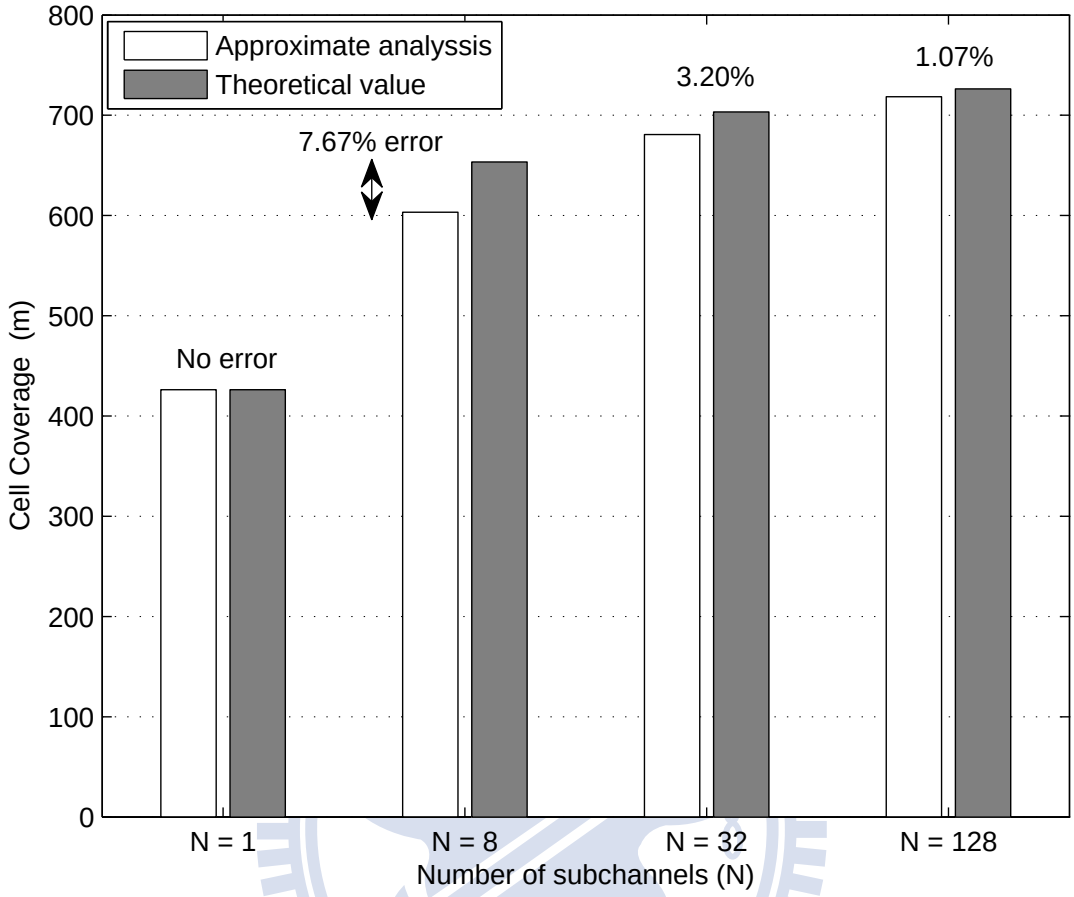

Figure 7.6: The validation of analytic formula (7.34) for COSA under $K = 1$ and different N values. Parameters: $M = 4$, $P_T = 0$ dBW, noise power $\sigma^2 = -103$ dBm, $g_0 = -32$ dB, $\mu = 4$, $P_{\text{out}} = 0.1$ and $\gamma_{th} = 6$ dB.

antennas is available. This result points out it is hard to maintain the same reliable coverage area with equally amount of power when M times of capacity is available.

For the spatial multiplexing based MIMO-OFDM systems with COSA, Fig. 7.6 shows the provided approximate analysis (7.34) compared with the theoretical performance (7.15) as $K = 1$. As mentioned before, (7.34) is equal to (7.15) under $N = 1$. In the case of $N > 1$, the error between approximate analysis and theoretical value will decrease as N increases. For example, the error is 7.67% for $N = 8$ but it becomes 1.07% for $N = 128$. In the case of $K > 1$, we validate the accuracy of approximate analysis by simulations. For the case $K = 30$, Fig. 7.7 shows the provided approximate analysis compared with simulated

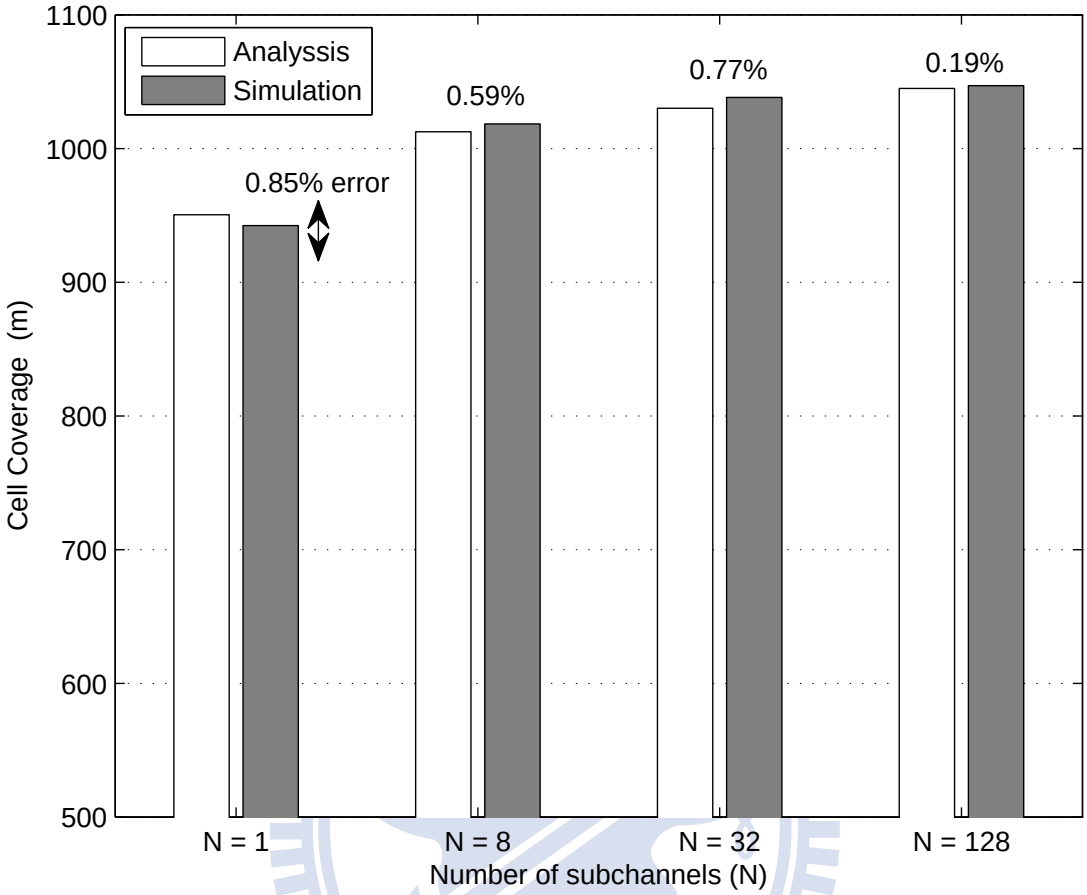

Figure 7.7: The validation of analytic formula (7.34) for COSA under $K = 30$ and different N values. Parameters: $M = 4$, $P_T = 0$ dBW, noise power $\sigma^2 = -103$ dBm, $g_0 = -32$ dB, $\mu = 4$, $P_{\text{out}} = 0.1$ and $\gamma_{th} = 6$ dB.

results which achieve the coverage with $P_{\text{out}} \pm 0.008$ reliability. We can find the approximate analysis can capture the simulated results well. For example, the maximal error between analysis and simulation in Fig. 7.7 is 0.85%.

7.5.2 Effects of Transmission Power and Number of Antennas on Coverage

Figures 7.8 and 7.9 show the coverage performance versus the number of users K for various scheduling schemes in the case of $N = 32$ under different P_T and M values, respectively. For comparison with COSA, we also show the coverage performance of FOSA by simulations.

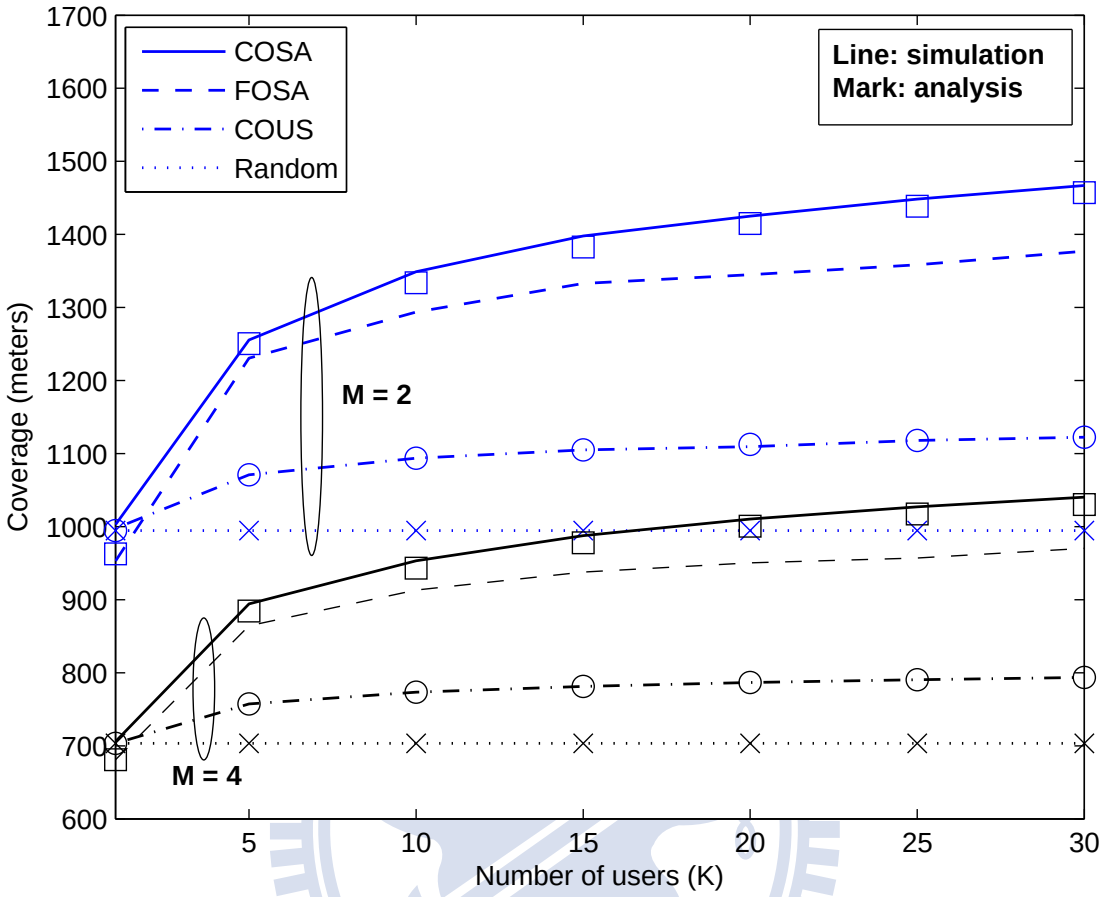

Figure 7.8: Reliable coverage versus number of users for different scheduling algorithms under $M = 2$ and $M = 4$. Parameters: $N = 32$, $P_T = 0$ dBW, noise power $\sigma^2 = -103$ dBm, $g_0 = -32$ dB, $\mu = 4$, $P_{\text{out}} = 0.1$ and $\gamma_{th} = 6$ dB.

From both figures, the random scheduling algorithm does not take advantage of multiuser diversity even though it achieves fairness among users. The results of COUS show that the coverage performance can be improved by utilizing multiuser scheduling. However, the improvement is not significant compared to the schemes, COSA and FOSA, which simultaneously exploit multiuser selection and subchannel assignment. Additionally, the reliable coverage increases as K increases and the proposed COSA can provide the best coverage performance than FOSA, COUS and random scheduling. Note that the gain of COSA over FOSA indicates the subchannel-oriented assignment is better than user-oriented assignment

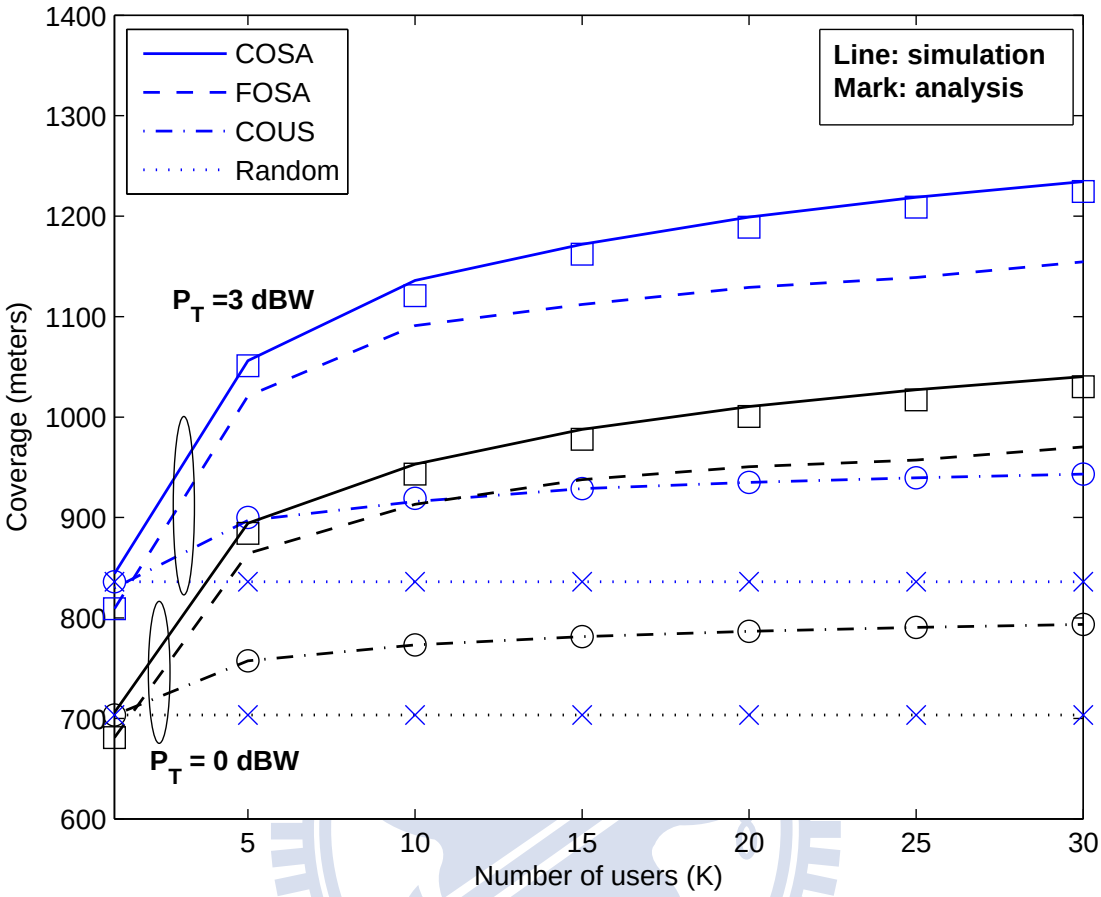

Figure 7.9: Reliable coverage versus number of users for different scheduling algorithms under $P_T = 0$ dBW and $P_T = 3$ dBW. Parameters: $N = 32$, $M = 4$, noise power $\sigma^2 = -103$ dBm, $g_0 = -32$ dB, $\mu = 4$, $P_{\text{out}} = 0.1$ and $\gamma_{th} = 6$ dB.

in terms of maximizing reliable coverage.[1]

Based on Fig. 7.8, a MIMO-OFDM system with a smaller number of antennas M can be easier to hold the desired link quality under a larger serving area. As the number of antennas increases (or decreases) from M_1 to M_2, the resulting coverage have constantly (independent

[1]For different objective and constraints, the two assignments may result in different performance results. For example, in the spatial multiplexing based MIMO-OFDM systems, the user-oriented assignment can outperform subchannel-oriented assignment subject to maximizing capacity and per user priority constraint [124]. The details will be presented in Chapter 8.

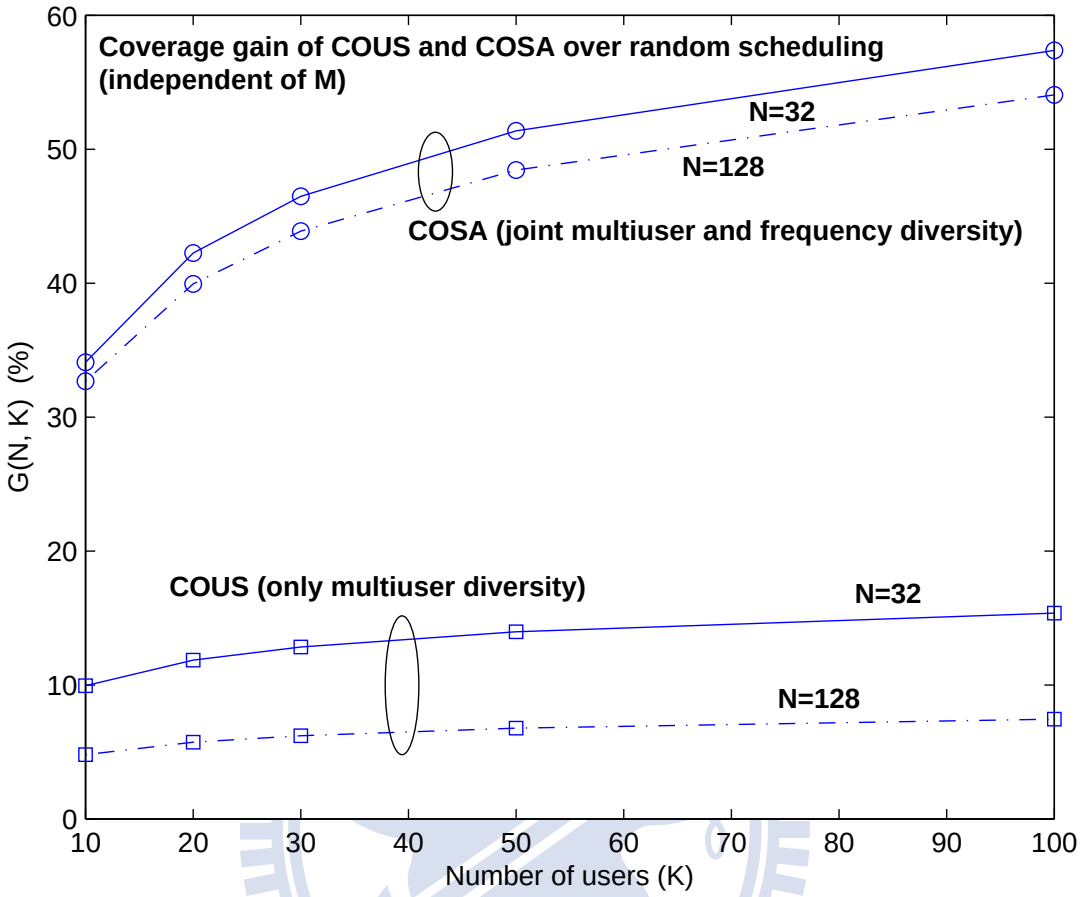

Figure 7.10: Coverage gain G in percentage of COUS and COSA over random scheduling under $\mu = 4$, $P_{\text{out}} = 0.1$ and various K values. According to (7.37) and (7.38), the gains are independent of number of antennas M.

of K) reduced (or enlarged) ratio for both COUS and COSA as follows:

$$\left(\left[\frac{M_1}{M_2} \right]^{2/\mu} - 1 \right) \times 100\% \quad \text{in percentage} \ . \tag{7.44}$$

For example in Fig. 7.8, under arbitrary K value, the reliable coverage of both COUS and COSA reduce 29.29% as $M = 2$ increases to $M = 4$.

Similarly, based on Fig. 7.9, when the available transmission power is α-fold of P_T, the reliable coverage of COUS and COSA increase $(\alpha^{1/\mu} - 1) \times 100\%$ in percentage. For example in Fig. 7.9, the coverage increases 18.92% for both COUS and COSA when the transmission power is doubled from $P_T = 0$ dBW to $P_T = 3$ dBW.

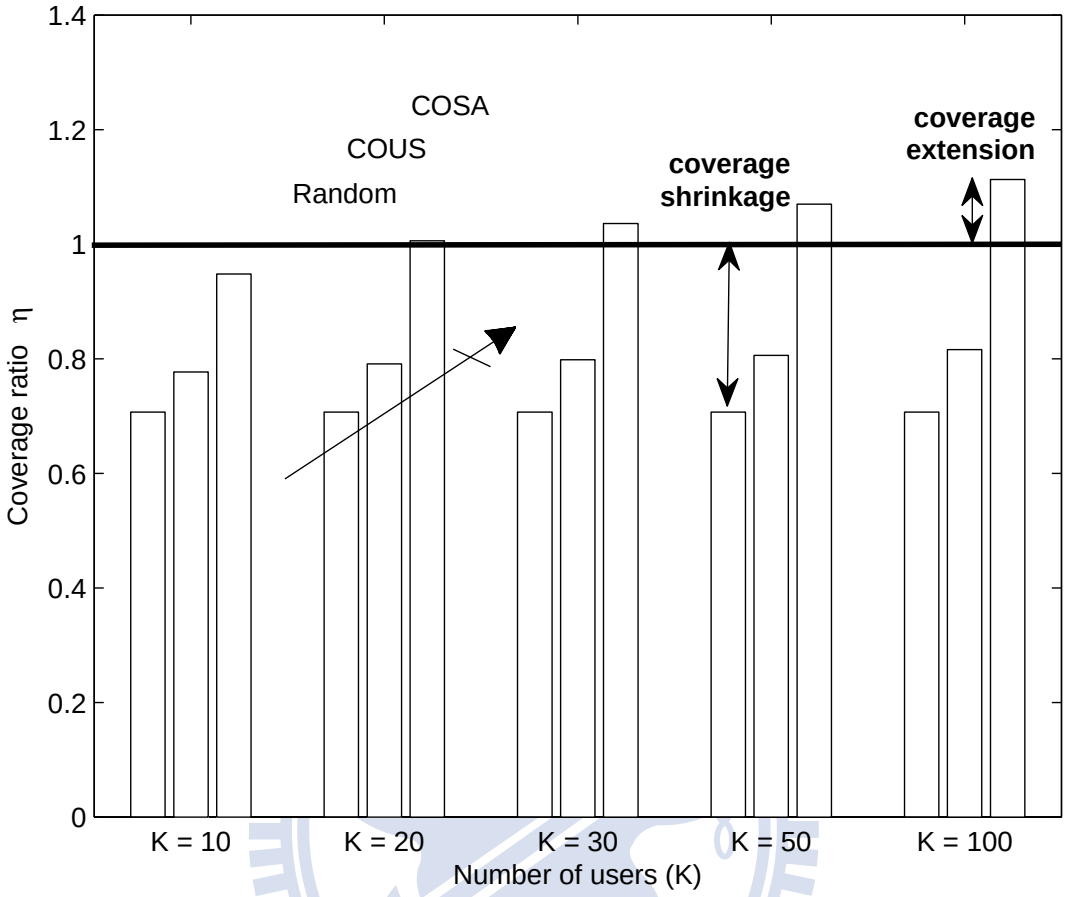

Figure 7.11: Coverage ratio η of various scheduling schemes to SISO under $N = 32$, $M = 2$, $\mu = 4$, $P_{\text{out}} = 0.1$ and various K values.

7.5.3 Coverage Gain and Extension from Multiuser and Frequency Diversity

In this section, we illustrate numerical results to quantify the benefit of jointly multiuser scheduling and subchannel assignment on coverage performance in term of the coverage gain and coverage extension discussed in Section 7.4.2 and 7.4.3, respectively. Based on (7.37) and (7.38), Fig. 7.10 shows the gains G_{COUS} and G_{COSA} under various K values with $N = 32$ and 128. Take $N = 32$ as an example, the gain of COUS over random scheduling is merely up to 15% with multiuser diversity only. However, the gain of COSA over random scheduling can significantly raise to 57% under taking advantage of joint multiuser and frequency diversities. In addition, there are smaller coverage gains G_{COUS} and G_{COSA} under

Table 7.1: Coverage performances with different scheduling schemes normalized to SISO system.

			$N=1$		$N=32$	
The spatial multiplexing based OFDM systems			$K=20$	$K=50$	$K=20$	$K=50$
$M=1$	SISO		1	1	1	1
$M=2$	Random scheduling		0.707	0.707	0.707	0.707
$M=2$	SWNSF	COUS	1.515	1.647	0.791	0.806
$M=2$	in [30]	COSA	(in [30])	(in [30])	1.006	1.070
$M=3$	Random scheduling		0.577	0.577	0.577	0.577
$M=3$	SWNSF	COUS	1.237	1.345	0.646	0.658
$M=3$	in [30]	COSA	(in [30])	(in [30])	0.821	0.874

higher frequency selectivity condition, i.e. the results of $N = 128$ in Fig. 7.10.

Figure 7.11 shows the coverage ratios η of random scheduling, COUS, and COSA to the SISO system according to (7.40), (7.41), and (7.42) under $N = 32$ and $M = 2$. Clearly, with multiple antennas $M = 2$, the coverage performance is reduced compared to a SISO system, i.e. only 0.707-fold achievable coverage of a SISO system. With multiuser and subchannel assignment, the reduced coverage can be compensated. Although we can find the K value satisfies (7.43) such that COUS can fully compensate the coverage shrinkage due to multiple antennas, the value of K is usually extremely large. For example in Fig. 7.11, the theoretical K satisfies (7.43) is 3.45664×10^{15}. However, COSA can fully compensate the coverage shrinkage issue and further achieve extra coverage extension as $K \geq 20$. This example shows again the value of joint exploiting multiuser and frequency diversities on the spatial multiplexing based MIMO-OFDM systems.

Finally, we present Table 7.1 to illustrate the improvement on reduced coverage by scheduling under $K = 20, 50$ and $M = 2, 3$. This table is an extended result for [30] which shows the coverage shrinkage ratio of the spatial multiplexing based MIMO system to SISO system, i.e. $N = 1$. In Table 7.1, we further show the coverage performance under the MIMO-OFDM systems, i.e. $N = 32$. The reliable coverage of the SISO system is normalized to unity. We find that the shrinking coverage due to split transmission power can be easier compensated (or even achieving extra coverage extension) for a low-frequency selectivity system.

Chapter 8

Capacity Enhancement for Multiuser MIMO-OFDM Systems

In this chapter, we investigate the resource allocation issue in a spatial multiplexing based multiuser MIMO-OFDM system. Different from Chapter 7, we focus on designing a scheduler to adaptively assign resource among users under different requirements and channel conditions. The key issue is the allocation of subchannels and power among users to share the system. Previous literature mainly focus on maximizing capacity but ignore the intrinsic coverage shrinkage and link reliability degradation problems in a MIMO system. Particularly, we formulate a system with better link reliability under a proportional rate requirement among users. To alleviate the complexity of jointly optimal subchannel and power allocation, we at first propose two suboptimal subchannel allocation algorithms, namely, user-oriented and subchannel-oriented allocations. We next propose a low-complexity power allocation method.

8.1 System Model and Problem Formulation

8.1.1 Modeling and Assumption

Identical to Chapter 7, we consider a spatial multiplexing-based MIMO-OFDM downlink system as shown in Fig. 1.5. There are M_T transmit antennas at the base station and M_R receive antennas at each of all K users. For simplicity, we consider the case $M_T = M_R = M$ for achieving full multiplexing gain. The total bandwidth of each subchannel is assumed to be smaller than the channel coherent bandwidth. Assume that the length of the cyclic prefix (CP) in the OFDM system is greater than the length of the discrete-time baseband channel impulse response so that the frequency-selective fading channel indeed decouples into a set of parallel frequency-flat fading channels. With channel information feedback from users, the scheduler at the base station performs adaptive resource allocation scheduling including

subchannel and power allocations based on available information and rate requirements among users.

The same with (7.1), the equivalent MIMO transmission model between the base station and user k at n-th subchannel is

$$\mathbf{y}_{k,n} = \sqrt{g_k}\,\mathbf{H}_{k,n}\mathbf{x}_{k,n} + \mathbf{n}_{k,n},$$

where $\mathbf{x}_{k,n}$ and $\mathbf{y}_{k,n}$ denote the $M \times 1$ transmit and receive signal vectors for user k, respectively. The matrix $\mathbf{H}_{k,n}$ represents the corresponding flat and independent faded $M \times M$ channel matrix, and the vector $\mathbf{n}_{k,n}$ be $M \times 1$ spatially white noise vector with $E[\mathbf{n}_{k,n}\mathbf{n}_{k,n}^H] = \sigma^2\mathbf{I}_M$. The large-scale channel gain g_k captures the path loss effect as modelled in (7.2).

8.1.2 Problem Formulation

Different from a SISO system which's channel condition can sufficiently determine the link quality, coverage and capacity, a MIMO system must consider all eigenmodes lead to some design trade off. As mentioned in Chapter 2.3, the weakest eigenmode will intuitively dominate the link outage probability since which is most likely to incur transmission errors. Besides, for a single band system, one can select a user with best channel to extend coverage. As for a multi-bands system, we hope to allocate all subchannels to suitable users to enable reliable connections at further regions as possible as we can. Therefore, instead of allocating resource to achieve maximal rate, we design a system that each user has better link quality under full multiplexing and the base station can serve users at further distance over different subchannel bands. Additionally, different rate requirement among users is practical in system design due to different service fees or priorities. We will also involve this issue in our consideration.

A general optimization problem of maximizing system capacity with a total transmit

power constraint can be shown as

$$\begin{aligned}
\max_{P_{k,n},\, I_{k,n}} \quad & \frac{1}{N}\sum_{k=1}^{K}\sum_{n=1}^{N} I_{k,n} \sum_{i=1}^{M} \log\left(1+\frac{g_k P_{k,n}\lambda_{k,n,i}}{M\,\sigma^2}\right) \qquad (8.1)\\
\text{subject to} \quad & \text{C1: } \sum_{k=1}^{K}\sum_{n=1}^{N} P_{k,n} \le P_{\max}\\
& \text{C2: } P_{k,n} \ge 0 \ \text{ for all } k,n\\
& \text{C3: } I_{k,n} = \{0,1\} \ \text{ for all } k,n\\
& \text{C4: } \sum_{k=1}^{K} I_{k,n} = 1 \ \text{ for all } n\\
& \text{C5: } C_1 : C_2 : \ldots : C_K = \eta_1 : \eta_2 : \ldots : \eta_K \ ,
\end{aligned}$$

where $P_{k,n}$ and $I_{k,n}$ are the allocated power and the subchannel assignment index function for user k in subchannel n, respectively; $\lambda_{k,n,1}$ is the weakest eigenvalue for user k in subchannel n; $P_{\max}$ is the total available power over all subchannels; σ^2 is the average noise power of a subchannel; g_k is user k's power decay due to path loss; C_k is the total data rate for user k defined as

$$C_k = \sum_{n=1}^{N} I_{k,n} \sum_{i=1}^{M} \log\left(1+\frac{g_k P_{k,n}\lambda_{k,n,i}}{M\,\sigma^2}\right), \qquad (8.2)$$

and $\{\eta_k\}_{k=1}^{K}$ are the predetermined rate requirement ratios among users. Note that we use equal power assignment among substreams instead of water-filling method in a specific subchannel in order to avoid the weakest link outage more easily.

Ideally, to achieve optimal solution should allocate power and subchannels jointly. However, solving the optimization problem could be very complex to implementation. Separating subchannel and power allocation is a generally suboptimal way to reduce complexity while maintaining reasonable performance. Generally, there are two viewpoints for subchannel assignment due to the available selection dimensions across user and subchannel. Let a user actively select a subchannel over all available subchannels – *user-oriented* type, e.g. algorithms in [71, 73, 74] and the FOSA algorithm discussed in Chapter 7; or let a subchannel choose the particular user to be assigned – *subchannel-oriented* type, e.g. [69, 70] and the COSA algorithm discussed in Chapter 7. In the chapter, we at first perform subchannel allocations individually from the two viewpoints, and then provide a complexity-reduced power allocation method. Figure 8.1 shows the flow chart of our considered two-stage suboptimal

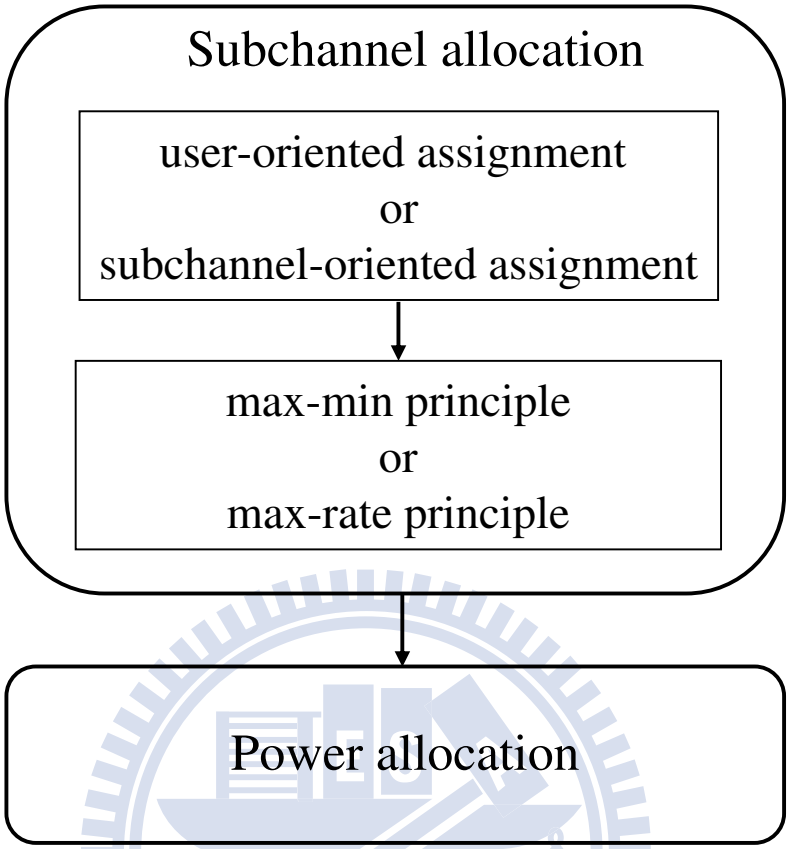

Figure 8.1: The flow chart of considered two-stage suboptimal resource allocation algorithm in this chapter.

resource allocation algorithm in this chapter. Note that equal power allocation is performed acorss each subchannel during the procedure of subchannel allocation.

8.2 Subchannel Allocation

In this chapter, we consider two kinds of principles for subchannel allocation, including **max-min** and **max-rate** designing principles. Be consistent with Chapter 7, the max-min principle is to maximize the weakest eigenmode among all candidates to enhance coverage and link reliability. By contrary, the max-rate principle is to select the one with maximal achievable capacity among all candidates. Specifically, define $\mathcal{N}$ and $\mathcal{K}$ are the subchannel index set and the user index set, respectively. In the user-oriented assignment, user k will select its favor subchannel according to (8.3) under max-min principle and according to (8.4)

under max-rate principle.

$$n^* = \arg\max_{n\in\mathcal{N}} \lambda_{k,n,1} \qquad \text{(under max-min principle)} \tag{8.3}$$

$$n^* = \arg\max_{n\in\mathcal{N}} R_{k,n} \qquad \text{(under max-rate principle)} \ , \tag{8.4}$$

where $R_{k,n}$ is the achievable capacity as user k utilizes subchannel n, defined as

$$R_{k,n} = \sum_{i=1}^{M} \log\left(1 + \frac{P_{\max}\lambda_{k,n,i}}{MN\,\sigma^2}\right) \ . \tag{8.5}$$

Note that we have no consider the effect of large-scale path loss in (8.5) because the purpose of scheduling is to take advantage of instantaneous (small-scale) channel gains over all possible candidates. Similar results applied to the subchannel-oriented assignment, subchannel n will be assigned to the suitable user k based on (8.6) under max-min principle and (8.7) under max-rate principle.

$$k^* = \arg\max_{k\in\mathcal{K}} \lambda_{k,n,1} \qquad \text{(under max-min principle)} \tag{8.6}$$

$$k^* = \arg\max_{k\in\mathcal{K}} R_{k,n} \qquad \text{(under max-rate principle)} \ . \tag{8.7}$$

8.2.1 Adaptive User-Oriented Subchannel Allocation Algorithm

The user-oriented principle is from user side to select the suitable subchannels. The allocation algorithm with max-min principle is shown as follows:

1. Initialization

   Set $\mathcal{N} = \{1, \ldots, N\}$ and $\mathcal{K} = \{1, \ldots, K\}$

   $C_k = 0$, $\mathcal{N}_k = \phi \quad \forall k \in \mathcal{K}$

   Define $\bar{N}_k = \lfloor \frac{N\eta_k}{\sum_{k=1}^{K}\eta_k} \rfloor \quad \forall k \in \mathcal{K}$

   $\bar{N} = N - \sum_{k=1}^{K} \bar{N}_k$

2. for $k = 1$ to K

   (a) Sort $\lambda_{k,n,1}$ in descending order

   (b) $n^* = \arg\max_{n\in\mathcal{N}} \lambda_{k,n,1}$

   (c) $\mathcal{N} = \mathcal{N} - \{n^*\}$, and $\mathcal{N}_k = \mathcal{N}_k \cup \{n^*\}$

(d) $C_k = R_k$

3. for $n = 1$ to $N - \bar{N}$

   (a) $k^* = \arg\min_{k \in \mathcal{K}} C_k/\eta_k$

   (b) $n^* = \arg\max_{n \in \mathcal{N}} \lambda_{k^*,n,1}$

   (c) $\mathcal{N} = \mathcal{N} - \{n^*\}$, and $\mathcal{N}_{k^*} = \mathcal{N}_{k^*} \cup \{n^*\}$

   (d) $C_{k^*} = C_{k^*} + R_{k^*}$

   (e) if $|\mathcal{N}_{k^*}| = \bar{N}_{k^*}$
   $\mathcal{K} = \mathcal{K} - \{k^*\}$

4. $\mathcal{K} = \{1, \ldots, K\}$

5. for count $= 1$ to $\bar{N}$

   (a) $k^* = \arg\min_{k \in \mathcal{K}} C_k/\eta_k$

   (b) $n^* = \arg\max_{n \in \mathcal{N}} \lambda_{k^*,n,1}$

   (c) $\mathcal{N} = \mathcal{N} - \{n^*\}$, and $\mathcal{N}_{k^*} = \mathcal{N}_{k^*} \cup \{n^*\}$

   (d) $C_{k^*} = C_{k^*} + R_{k^*}$

The first step defines the following notation: $\mathcal{N}$ and $\mathcal{K}$ as the subchannel index set, and the user index set as defined before; C_k and $\mathcal{N}_k$ as the allocated rate and the allocated subchannel index set for user k, respectively. To help later power allocation, we predetermine the number of subchannels $\bar{N}_k$ will be assigned to each user k to roughly satisfy the proportional rate constraints. The determination is based on the assumption in [74,76]: the proportion of subchannels allocated to users is approximately the same as their required rate ratios after power allocation. Denote $\bar{N}$ as the number of remaining unallocated subchannels.

The second step makes each user k take turns to select a unallocated subchannel which has maximal weakest eigenvalue compared to all unallocated subchannels. Specifically, the allocation principle of maximizing the worst substream is a max-min principle. Optimizing the quantity is try to maximize the receive SNR of the worst substream in all subchannels. Then update some variables. Note that the case of two or more users having the same subchannel as their best is possible. In general $N \gg K$, the probability of above case

occurring will be very low so that it can be negligible. In fact, the selecting order of users can depend on different billing mechanisms to guarantee users' priorities.

In the third step, a user has the least ratio of capacity to rate requirement be assigned to an extra unallocated subchannel. It realizes the proportional rate constriant among users. If user k already obtains $\bar{N}_k$ subchannels, he will leave out the competition and no longer get any more subchannels. Note that $|\mathcal{N}_k|$ represents the number of allocated subchannels for user k.

The residual subchannels will be assigned during the fourth step with the procedures similar to the step three. Particularity, the sorting procedure in the second step reduces the complexity of subchannel finding in (b) during the second, third and fourth steps and the scheduler just needs to record the selected subchannel index.

For the algorithm with max-rate principle, similar procedure can be done by modifying Steps 2(b), 3(b), and 5(b) according to (8.4).

8.2.2 Adaptive Subchannel-Oriented Subchannel Allocation Algorithm

Different from user-oriented allocation, the subchannel-oriented principle is from subchannel's viewpoint to allocate the suitable user. The allocation algorithm with max-min principle is detailed shown below:

1. Initialization

   Set $\mathcal{N} = \{1, \ldots, N\}$ and $\mathcal{K} = \{1, \ldots, K\}$

   $C_k = 0$, $\mathcal{N}_k = \phi \quad \forall k \in \mathcal{K}$

   Define $\bar{N}_k = \lfloor \frac{N\eta_k}{\sum_{k=1}^{K} \eta_k} \rfloor \quad \forall k \in \mathcal{K}$

   $\bar{N} = N - \sum_{k=1}^{K} \bar{N}_k$

2. for $n = 1$ to $N - \bar{N}$

   (a) $k^* = \arg\max_{k \in \mathcal{K}} \lambda_{k,n,1}$

   (b) $\mathcal{N} = \mathcal{N} - \{n\}$, and $\mathcal{N}_{k^*} = \mathcal{N}_{k^*} \cup \{n\}$

   (c) $C_{k^*} = C_{k^*} + R_{k^*}$

(d) if $|\mathcal{N}_{k^*}| = \bar{N}_{k^*}$

$\mathcal{K} = \mathcal{K} - \{k^*\}$

3. $\mathcal{K} = \{1, \ldots, K\}$

4. for count $= 1$ to $\bar{N}$

(a) $k^* = \arg\max_{k \in \mathcal{K}} \lambda_{k,n,1}$

(b) $\mathcal{K} = \mathcal{K} - \{k^*\}$

(c) $\mathcal{N} = \mathcal{N} - \{n\}$, and $\mathcal{N}_{k^*} = \mathcal{N}_{k^*} \cup \{n\}$

(d) $C_{k^*} = C_{k^*} + R_{k^*}$

Particularly, subchannel-oriented allocation can not adaptively determine required rate ratio in each assignment stage. Therefore, the predetermined numbers $\{\bar{N}_k\}_{k=1}^K$ are essential for this allocation viewpoint to meet the rate constraints among users. In the final step, each user can be at most assigned one unallocated subchannel in order to hold the rate ratios. Similarly, we can modify Steps 2(a) and 4(a) based on (8.7) to obtain the subchannel allocation algorithm with max-rate principle.

8.3 Power Allocation

After subchannel allocation, the optimization problem considered in (8.1) can be modified as

$$\max_{P_{k,n}} \quad \frac{1}{N} \sum_{k=1}^{K} \sum_{n \in \mathcal{N}_k} \sum_{i=1}^{M} \log\left(1 + \frac{g_k P_{k,n} \lambda_{k,n,i}}{M\,\sigma^2}\right) \tag{8.8}$$

$$\text{subject to} \quad \text{C1: } \sum_{k=1}^{K} \sum_{n \in \mathcal{N}_k} P_{k,n} \le P_{\max}$$

$$\text{C2: } P_{k,n} \ge 0 \quad \text{for all } k, n$$

$$\text{C3: } \mathcal{N}_k \quad \text{disjoint for all } k$$

$$\text{C4: } \bigcup_{k=1}^{K} \mathcal{N}_k \subseteq \{1, \ldots, N\}$$

$$\text{C5: } C_1 : C_2 : \ldots : C_K = \eta_1 : \eta_2 : \ldots : \eta_K \quad .$$

Comparing (8.1) and (8.8), we have reduce $2N$ variables $\{I_{k,n}\}$ jointly with $\{P_{k,n}\}$ in (8.1) to only N variables $\{P_{k,n}\}$ in (8.8), where $\mathcal{N}_k$ clearly indicates $\{I_{k,n}\}$ for user k. Now our work is to find out N power allocations $P_{k,n}$ which are assigned to the corresponding users. By Lagrangian multiplier optimization technique, the Lagrangian function can be expressed as

$$\begin{aligned} L_f = & -\frac{1}{N}\sum_{k=1}^{K}\sum_{n\in\mathcal{N}_k}\sum_{i=1}^{M}\log\left(1+\frac{g_k P_{k,n}\lambda_{k,n,i}}{M\,\sigma^2}\right) + \mu_1\left(\sum_{k=1}^{K}\sum_{n\in\mathcal{N}_k}P_{k,n}-P_{\max}\right) \\ & + \sum_{k=2}^{K}\theta_k\left(\sum_{n\in\mathcal{N}_1}\sum_{i=1}^{M}\log\left(1+\frac{g_1 P_{1,n}\lambda_{1,n,i}}{M\,\sigma^2}\right) - \frac{\eta_1}{\eta_k}\sum_{n\in\mathcal{N}_k}\sum_{i=1}^{M}\log\left(1+\frac{g_k P_{k,n}\lambda_{k,n,i}}{M\,\sigma^2}\right)\right) \\ & + \sum_{k=1}^{K}\sum_{n\in\mathcal{N}_k}\zeta_{k,n}\,P_{k,n}\ , \end{aligned} \tag{8.9}$$

where μ_1, , $\theta_k\,(k=2,\ldots,K)$, and $\zeta_{k,n}\,(k=1,\ldots,K;\,n\in\mathcal{N}_k)$ are all Lagrangian multipliers. The optimal solution must satisfy the following Kurush-Kuhn-Tucker (KKT) conditions [125]:

$$\frac{\partial L_f}{\partial P_{k,n}} = 0 \tag{8.10}$$

$$\mu_1,\ \zeta_{k,n} \geq 0 \tag{8.11}$$

$$\mu_1\left(\sum_{k=1}^{K}\sum_{n\in\mathcal{N}_k}P_{k,n}-P_{\max}\right) = 0 \tag{8.12}$$

$$\zeta_{k,n}P_{k,n} = 0\ . \tag{8.13}$$

Although we have above optimization equations, it is still difficult to find out the power distributions $P_{k,n}$ directly. Because scheduling can help the system to operate at high SNR condition so that we use the following assumption to ease analysis complexity. At high SNR condition, the property of the logarithm function is $\log(1+x)\approx\log(x)$ for $x\gg 1$. Under this assumption, we simplify the Lagrangian function in (8.9). We also assume all subchannels will be used and poured power, i.e. $P_{k,n}>0$. Then through KKT conditions (8.10), (8.11), and (8.13), we can obtain the following relationships:

$$\frac{\partial L_f}{\partial P_{1,n}} = \mu_1 - \frac{M}{P_{1,n}}\left(\frac{1}{N}-\sum_{k=2}^{K}\theta_k\right) = 0 \quad \text{for } n\in\mathcal{N}_1\ , \tag{8.14}$$

and

$$\frac{\partial L_f}{\partial P_{k,n}} = \mu_1 - \frac{M}{P_{k,n}}\left(\frac{1}{N}+\theta_k\frac{\eta_1}{\eta_k}\right) = 0 \quad \text{for } k=2,3,\ldots,K \text{ and } n\in\mathcal{N}_k\ . \tag{8.15}$$

For the user $k = 1$, form (8.14) we find that any two subchannels n and m belong to $\mathcal{N}_1$ have equal power relation $P_{1,n} = P_{1,m}$. As for the other users $k = 2, \ldots, K$, similarly results can be found from (8.15). It is any two subchannels n and m belong to $\mathcal{N}_k$ will have equal power relation $P_{k,n} = P_{k,m}$. Therefore, for each user k the power distribution among his allocated subchannels is equal so that the total power allocation of user k, P_k, can be written as

$$P_k = |\mathcal{N}_k| P_{k,n} \quad \text{for } k = 1, 2, \ldots, K \text{ and } n \in \mathcal{N}_k \ . \tag{8.16}$$

The original problem of solving N power allocations $P_{k,n}$ now becomes to solve K total allocated powers $\{P_k\}_{k=1}^{K}$ for each user .

Base on above results, the capacity ratio constraints C5 in (8.1) can be expressed as

$$\sum_{n\in\mathcal{N}_1}\sum_{i=1}^{M} \log\left(1 + \frac{g_1 P_1 \lambda_{1,n,i}}{M|\mathcal{N}_1|\,\sigma^2}\right) = \frac{\eta_1}{\eta_k}\sum_{n\in\mathcal{N}_k}\sum_{i=1}^{M} \log\left(1 + \frac{g_k P_k \lambda_{k,n,i}}{M|\mathcal{N}_k|\,\sigma^2}\right) \tag{8.17}$$

for $k = 2, \ldots, K$. In the same way, under high SNR condition we can obtain

$$P_k = \frac{M|\mathcal{N}_k|\sigma^2 g_k^{-1}}{\left(M|\mathcal{N}_1|\sigma^2 g_1^{-1}\right)^{\frac{|\mathcal{N}_1|\eta_k}{|\mathcal{N}_k|\eta_1}}} \left(\frac{E_1^{\frac{\eta_k}{\eta_1}}}{E_k}\right)^{\frac{1}{M|\mathcal{N}_k|}} P_1^{\frac{|\mathcal{N}_1|\eta_k}{|\mathcal{N}_k|\eta_1}} \quad \text{for } k = 2, 3, \ldots, K \tag{8.18}$$

where E_k is defined as

$$E_k = \prod_{n\in\mathcal{N}_k}\prod_{i=1}^{M} \lambda_{k,n,i} \quad \forall k \ . \tag{8.19}$$

Finally, the total system power constraint can be expressed as

$$\sum_{k=1}^{K} P_k = P_{\max} \ . \tag{8.20}$$

From (8.18) and (8.20), we can realize power allocation by solving K nonlinear equations with K variables $\{P_k\}_{k=1}^{K}$. We could need iterative methods such as Newton-Raphson method or Quasi-Newton method to obtain the solutions.

If we use the approximation $|\mathcal{N}_1| : |\mathcal{N}_2| : \ldots : |\mathcal{N}_K| \approx \eta_1 : \eta_2 : \ldots : \eta_K$ additionally, we can further simplify the power allocation solution. As a result, (8.18) can be simplified as

$$P_k = \frac{g_1|\mathcal{N}_k|}{g_k|\mathcal{N}_1|}\left(\frac{E_1^{\frac{\eta_k}{\eta_1}}}{E_k}\right)^{\frac{1}{M|\mathcal{N}_k|}} P_1 \ . \tag{8.21}$$

Substituting (8.21) into (8.20), we obtain

$$P_1 = P_{\max} / \left(1 + \sum_{j=2}^{K} \frac{g_1 |\mathcal{N}_j|}{g_j |\mathcal{N}_1|} \left(\frac{E_1^{\frac{\eta_j}{\eta_1}}}{E_j} \right)^{\frac{1}{M|\mathcal{N}_j|}} \right) \quad , \tag{8.22}$$

and

$$P_k = P_{\max} \frac{g_1 |\mathcal{N}_k|}{g_k |\mathcal{N}_1|} \left(\frac{E_1^{\frac{\eta_k}{\eta_1}}}{E_k} \right)^{\frac{1}{M|\mathcal{N}_k|}} / \left(1 + \sum_{j=2}^{K} \frac{g_1 |\mathcal{N}_j|}{g_j |\mathcal{N}_1|} \left(\frac{E_1^{\frac{\eta_j}{\eta_1}}}{E_j} \right)^{\frac{1}{M|\mathcal{N}_j|}} \right)$$

$$\text{for } k = 2, 3, \ldots, K \ . \tag{8.23}$$

Note that all parameters including $\{E_k\}, \{|\mathcal{N}_k|\}$, and $\{\eta_k\}$ for all user k are already known by ways of feedback information and subchannel allocation results. Hence, we can obtain the linear solutions of $\{P_k\}_{k=1}^{K}$ conveniently by (8.22) and (8.23).

8.4 Complexity Analysis

For finding the optimal solutions in (8.1), the optimal subchannel allocation and the optimal power distribution can not be performed separately. The optimal subchannel allocation method is an exhaustive search over all N subchannels and K users. It has K^N possibilities of subchannel allocation with complexity of order $\mathcal{O}(K^N)$. For each allocation possibility, a power allocation procedure is required.

The complexity of the proposed two algorithms will be analyzed in the following. For the user-oriented subchannel allocation, Step 1 needs constant time for initialization. Step 2(a) requires a sorting procedure for the weakest eigenmode gains $\{\lambda_{k,n,1}\}$ across all subchannels and loops for all users. This results in a complexity of $\mathcal{O}(K \times N \log_2 N)$. Note that the search operation in Step 2(b) is omitted because of the previous sorting procedure. In Step 3(a), requiring a search operation for finding the user with the least C_k/η_k ratio and performing for the remaining $N - K$ unallocated subchannels. Therefore, complexity is $\mathcal{O}((N-K) \times K)$. In the same way, the search operation in Step 3(b) is omitted by the sorting in Step 2(a). Hence the asymptotic complexity of user-oriented allocation is $\mathcal{O}(KN \log_2 N)$. As for the subchannel-oriented algorithm, requiring a complexity of $\mathcal{O}(K)$ for determining $\{\bar{N}_k\}$ additionally during initialization. Step 2(a) requires $N - \bar{N}$ times search operations through at most K choices. It results in an asymptotic complexity of $\mathcal{O}((N - \bar{N}) \times K)$.

Step 4 requires two search operations for finding the least R_k/η_k user and the corresponding subchannel during a loop and total loops $\bar{N}$ times. The resulting complexity is asymptotic $\mathcal{O}(\bar{N} \times 2K)$ due to $\bar{N}$ is at most equal to K. Therefore, the complexity of the subchannel-oriented algorithm is approximated to $\mathcal{O}(KN)$.

Different from K^N times power allocation procedures for exhaustive search, the benefit of suboptimal method is only requiring one power allocation procedure. This is to find out N power variables for N subchannels. The proposed power allocation method can reduce the number of variables from N to K.

8.5 Numerical Results

In this section, we present simulation results to justify the proposed algorithms can meet predetermined proportional rate constraints among users. Furthermore, we will show subchannel allocation algorithm combined with max-min principle can additional enhance link quality with achievable rate compared to algorithm combined with max-rate principle. In all simulation, we assume the uncorrelated Rayleigh fading for each channel realization. The total transmit power available at the base station is $P_{\max} = 46$ dBm. The total bandwidth is 10 MHz, which is divided into $N = 128$ subchannels. The noise power density is -174 dBm/Hz. The number of antennas is $M = 4$. Total $K = 8$ users are waiting for services and the proportional rate requirement among users are $\eta_1 : \eta_2 : \ldots : \eta_8 = 6 : 6 : 3 : 3 : 2 : 2 : 1 : 1$.

8.5.1 Performance Evaluation under the Same g_k among Users

At first, we consider the case of all users' power decay g_k being the same to compare various assignment methods, including user-oriented max-min, user-oriented max-rate, subchannel-oriented max-min, and subchannel-oriented max-rate. Assume cell radius $R = 1$ km and all users locates around the base station with $R/2$ distance. As a result, the power decay caused by path loss is $\{g_k\}_{k=1}^{8} = -107.96$ dB under path loss exponent $\mu = 4$. Fig. 8.2 shows the capacity distribution among users under the required rate constraints. We can find that the capacity is distributed very will among users according to the rate constraints under the four considered subchannel allocation algorithms. The corresponding normalized

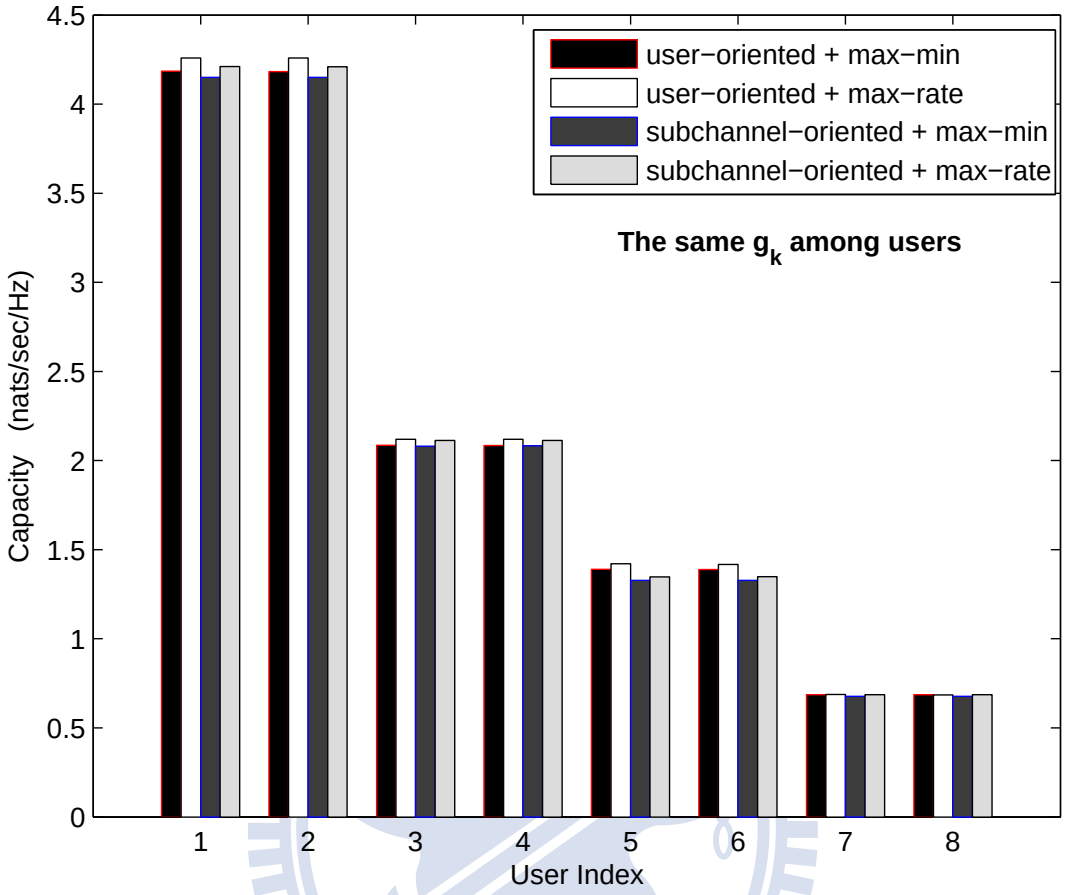

Figure 8.2: Capacity distribution among users with proposed power allocation method. Simulation parameters: $P_{\max} = 46$ dBm, $N = 128$ subchannels, and $M = 4$ antennas. Eight users with rate constraints $\eta_1 : \eta_2 : \ldots : \eta_8 = 6 : 6 : 3 : 3 : 2 : 2 : 1 : 1$. The path loss among users are the same $g_k = -107.96$ dB.

capacity distribution is shown in Fig. 8.3 according to

$$C_{\text{normalized}} = \frac{C_k}{\sum_{k=1}^{K} C_k} \quad . \tag{8.24}$$

Importantly, the performance degradation of the max-min principle to the max-rate principle is not very significant. In fact, not only enhance the weakest eignmode, [30] had shown that max-min scheduling can parallel enhance all eigenmodes with the same increment Δ_λ

$$\Delta_\lambda \triangleq E[\tilde{\lambda}_i - \lambda_i] = \frac{1}{M}[\psi(K+1) + \beta - 1] \quad \text{for} \quad i = 1, \ldots, M \ , \tag{8.25}$$

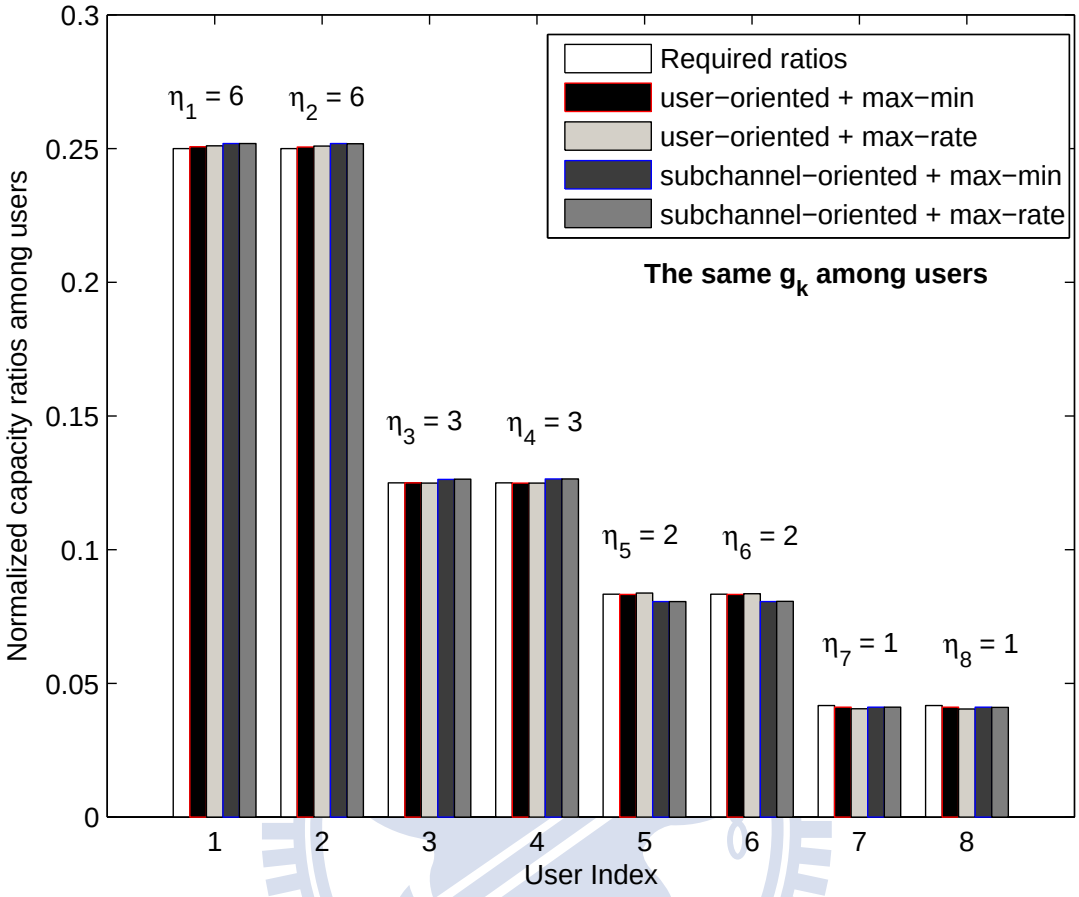

Figure 8.3: Normalized capacity distribution among users (corresponding to Fig. 8.2). The simulation parameters are the same as in Fig. 8.2. The rate constraints among users are $\eta_1 : \eta_2 : \ldots : \eta_8 = 6 : 6 : 3 : 3 : 2 : 2 : 1 : 1$. The path loss among users are the same $g_k = -107.96$ dB.

where $\tilde{\lambda}_i$ is the i-th eigenvalue after max-min scheduling, $\psi(K+1) = -\beta + \sum_{k=1}^{K} k^{-1}$ is the psi function for integer K and $\beta \simeq 0.5772$ is the Eular's constant. Hence, the algorithms with max-min principle can also provide large capacity with the help of the increment Δ_λ on all eigenmodes.

Besides the comparable capacity to the algorithm with max-rate principle, the main benefit of utilizing max-min scheduling is to enhance the link quality. Fig. 8.4 shows the average weakest link SNR per user. Obviously, max-min scheduling provides link SNR improvement over max-rate scheduling especially under user-oriented assignment. For example,

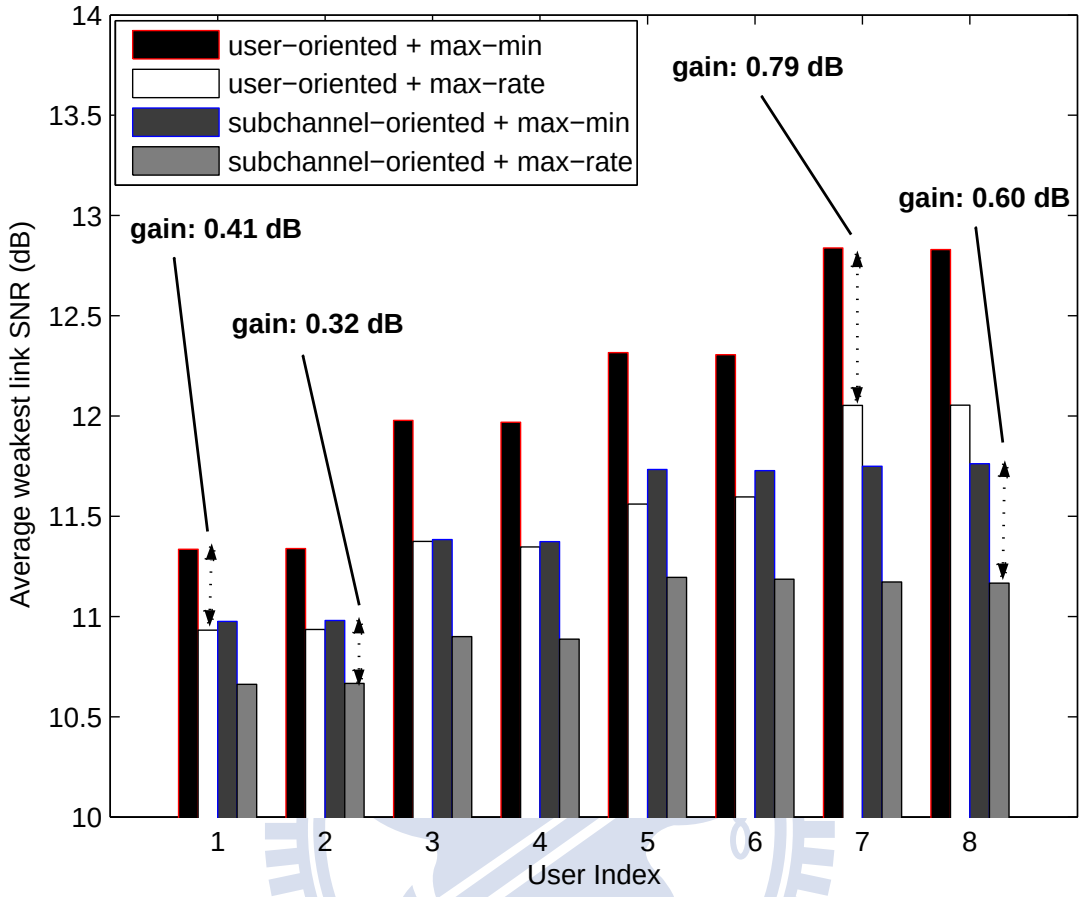

Figure 8.4: Average weakest link SNR per user (corresponding to the simulation assumptions and available capacity provided in Fig. 8.3, $g_k = -107.96$ dB for all k).

the improvement is $0.41 \sim 0.79$ dB for user-oriented assignment and is $0.32 \sim 0.60$ dB for subchannel-oriented assignment, respectively. Combined with the results provided in Fig. 8.2, allocation algorithm with max-min principle has better link SNR to feasible more reliable transmission (reduce outage probability) and provide achievable capacity compared to max-rate principle.

8.5.2 Performance Evaluation under Different g_k among Users

Now we consider different g_k among users with the scenario shown in Fig. 8.5. User near to the base station requests large rate ratio due to less power decay caused by path loss. Based on Fig. 8.5, the power decay for users 1 to 8 is $g_1 = g_2 = -107.96$ dB, $g_3 = g_4 = -112.96$

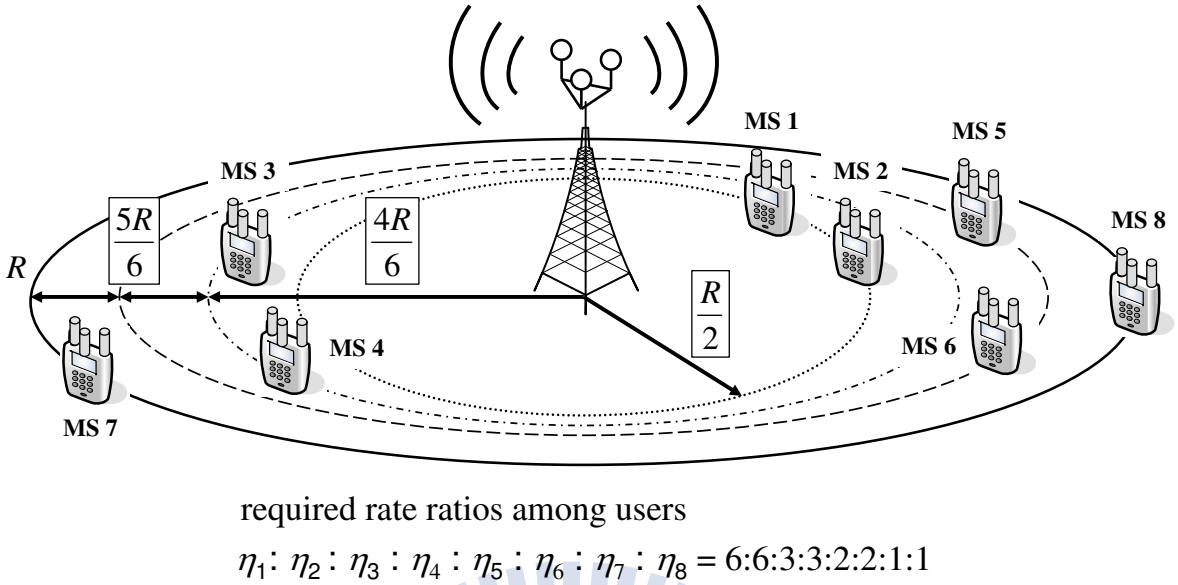

Figure 8.5: Diagram of considered various power decay g_k (path loss) and required rate ratios among users.

dB, $g_5 = g_6 = -116.83$ dB, and $g_7 = g_8 = -120.00$ dB with corresponding rate ratios $\eta_1 : \eta_2 : \ldots : \eta_8 = 6 : 6 : 3 : 3 : 2 : 2 : 1 : 1$.

The normalized capacity among users is presented in Fig. 8.6. We find that the provided subchannel allocation algorithms combined with proposed power allocation method can also match the required rate constraints well even if there are different $\{g_k\}_{k=1}^{8}$ between users. Different from the discussion in previous session, the adaptable power allocation here becomes very important as users have different large-scale channel gains. Fig. 8.7 shown the normalized capacity distribution under pure equal power allocation, i.e. ignore the second stage of Fig. 8.1. We can find that the required rate constraints are no longer satisfied. The users with less power decay g_k obtain larger rate than that with serious power decay, e.g. users 1 and 2 versus users 7 and 8. It is because the effect of different g_k is not compensated. In fact, the purpose of first stage in Fig. 8.1, subchannel allocation, is to assign most suitable subchannels to users with good *instantaneous* channel qualities. Then the second stage, power allocation, can make the final assignment to be consistent with the requirements for proportional rates due to (8.22) and (8.23) have considered the parameter g_k.

In addition to fit the rate constraints, Fig. 8.8 shows the link SNR improvement. Simi-

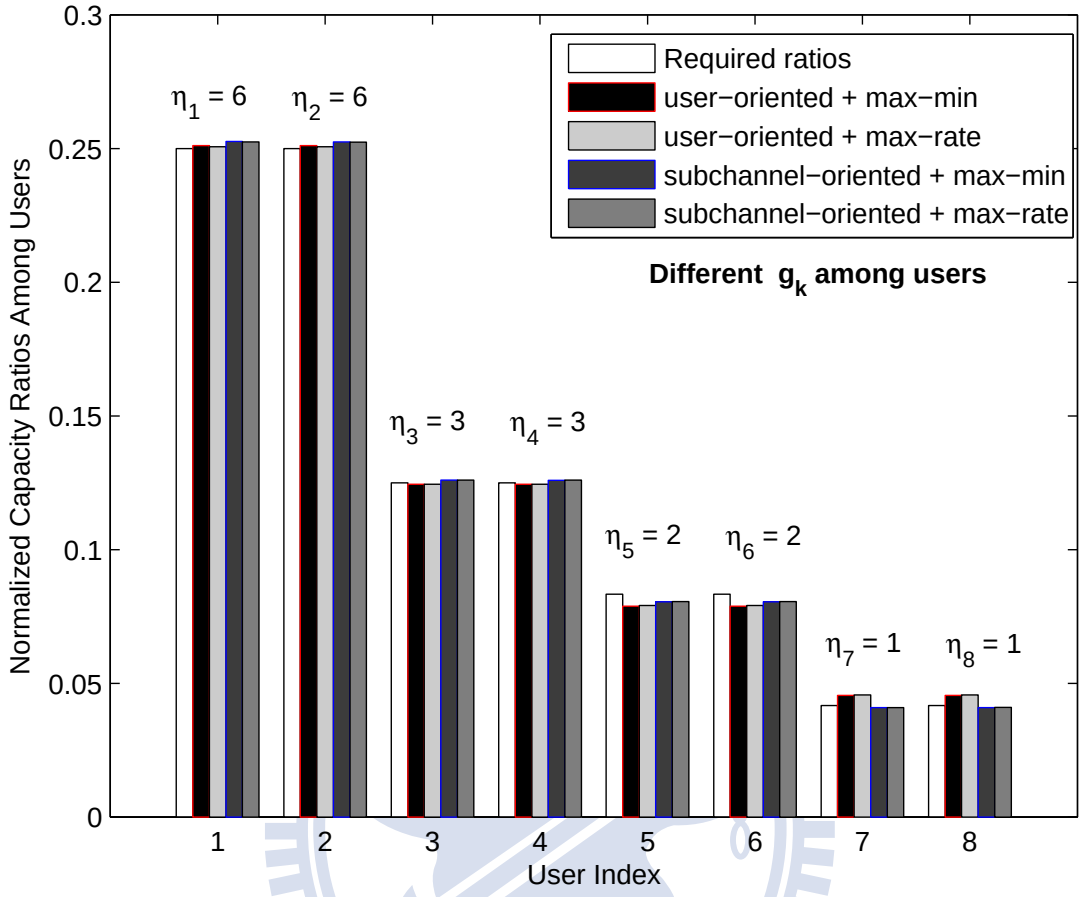

Figure 8.6: Normalized capacity distribution among users with proposed power allocation method. The same parameters as Fig. 8.2. The path loss g_k among users are based on the assumption of Fig. 8.5, i.e. $g_1 = g_2 = -107.96$ dB, $g_3 = g_4 = -112.96$ dB, $g_5 = g_6 = -116.83$ dB, and $g_7 = g_8 = -120.00$ dB.

larly, max-min scheduling can provide better link SNR performance than max-rate scheduling especially under user-oriented assignment. The enhancement is $0.35 \sim 1.44$ dB for user-oriented assignment and $0.27 \sim 0.55$ dB for subchannel-oriented assignment, respectively. Table 8.1 displays the system capacity over all users under proposed power allocation and pure equal power allocation. It is expected that pure equal power allocation produces higher capacity due to it does not compensate the effect of different g_k. However, pure equal power allocation can not meet our predetermined requirement.

Finally, we provide an extreme example that edge users request larger rate ratios than

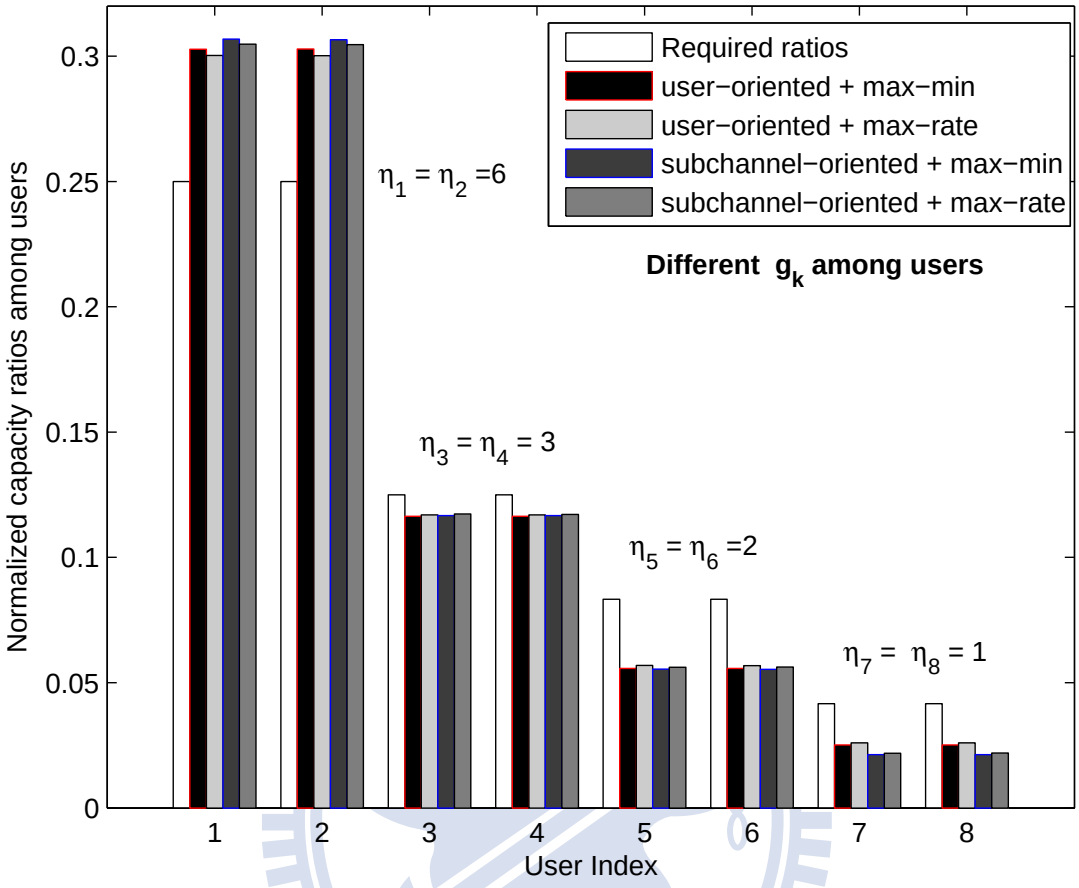

Figure 8.7: Normalized capacity distribution among users with equal power allocation. The same parameters as Fig. 8.6. The path loss g_k among users are based on the assumption of Fig. 8.5.

center users. In this testing, we reset rate ratios as $\eta_1 : \eta_2 : \ldots : \eta_8 = 1 : 1 : 2 : 2 : 3 : 3 : 6 : 6$ under the same power decay assumption. Fig. 8.9 shows again the provided algorithms and power allocation can almost match the predetermined requirement. However, only equal power allocation causes unbalanced results compared to the ideal ratios as shown in Fig. 8.10. Similar to Fig. 8.7, the users with less power decay g_k will get larger rate than expected values; users with heavy power decay merely get lower rate than expected values.

Note that we can find resource allocation with user-oriented assignment has better performance than that with subchannel-oriented assignment over all provided numerical results. It is because there exists user requested constraints in our problem now. User-oriented as-

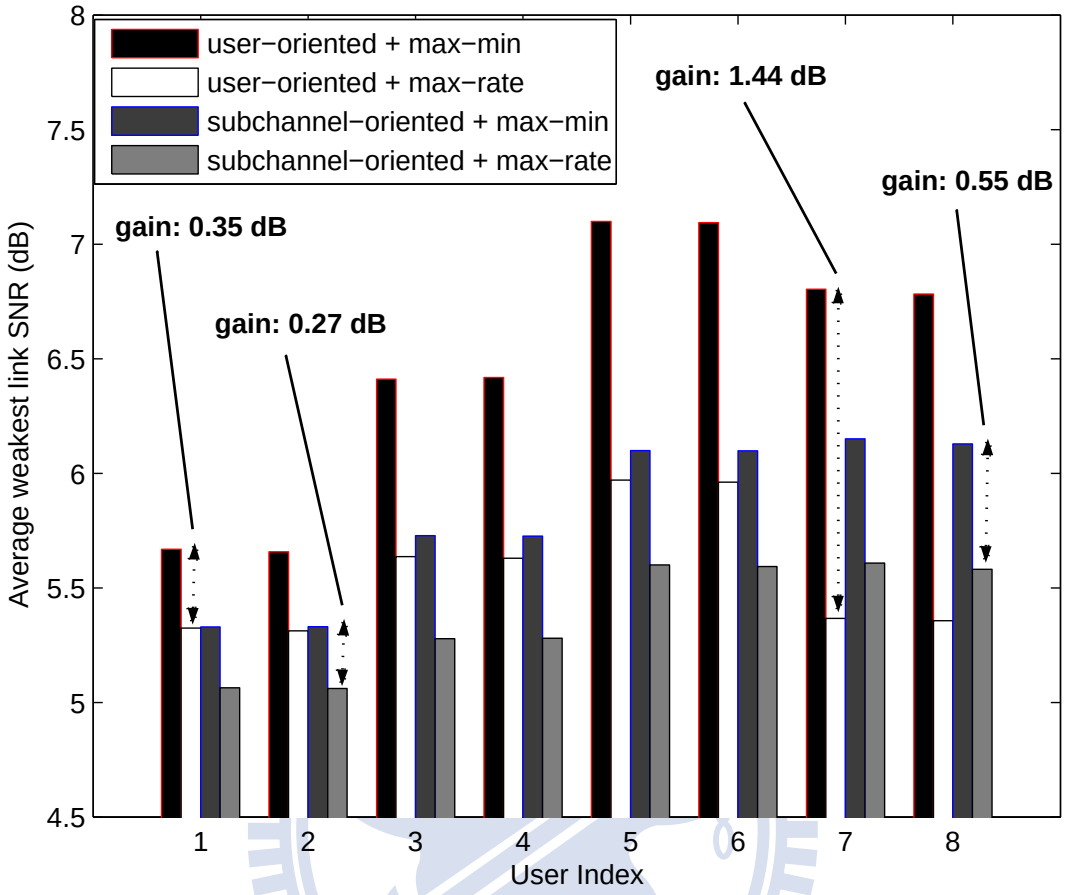

Figure 8.8: Average weakest link SNR per user (corresponding to the simulation assumptions and available capacity provided in Fig. 8.6).

signment can be more flexible than subchannel-oriented assignment to allocate resources according to instantly determined results.

Table 8.1: System capacity of multiuser MIMO-OFDM systems versus various allocation algorithms (nats/sec/Hz) under different power decay g_k among users.

Power allocation	user-oriented		subchannel-oriented		Satisfy rate constraints?
	max-min	max-rate	max-min	max-rate	
Provided method	11.852	12.168	11.606	11.900	Yes (shown in Fig. 8.6)
Equal power	13.435	13.732	13.362	13.613	No (shown in Fig. 8.7)

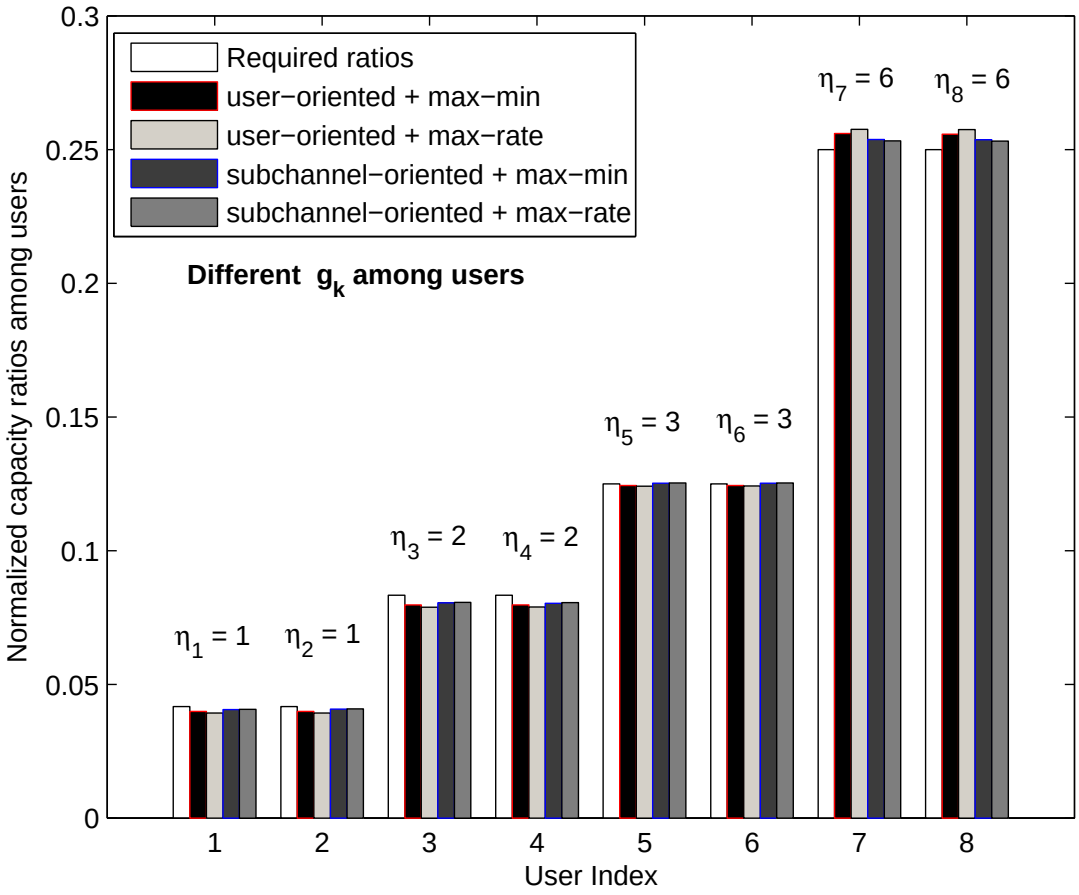

Figure 8.9: Normalized capacity distribution among users with proposed power allocation method. The rate constraints among users are extremely opposite to previous assumption $\eta_1 : \eta_2 : \ldots : \eta_8 = 1 : 1 : 2 : 2 : 3 : 3 : 6 : 6$. The path loss g_k among users are based on the assumption of Fig. 8.5.

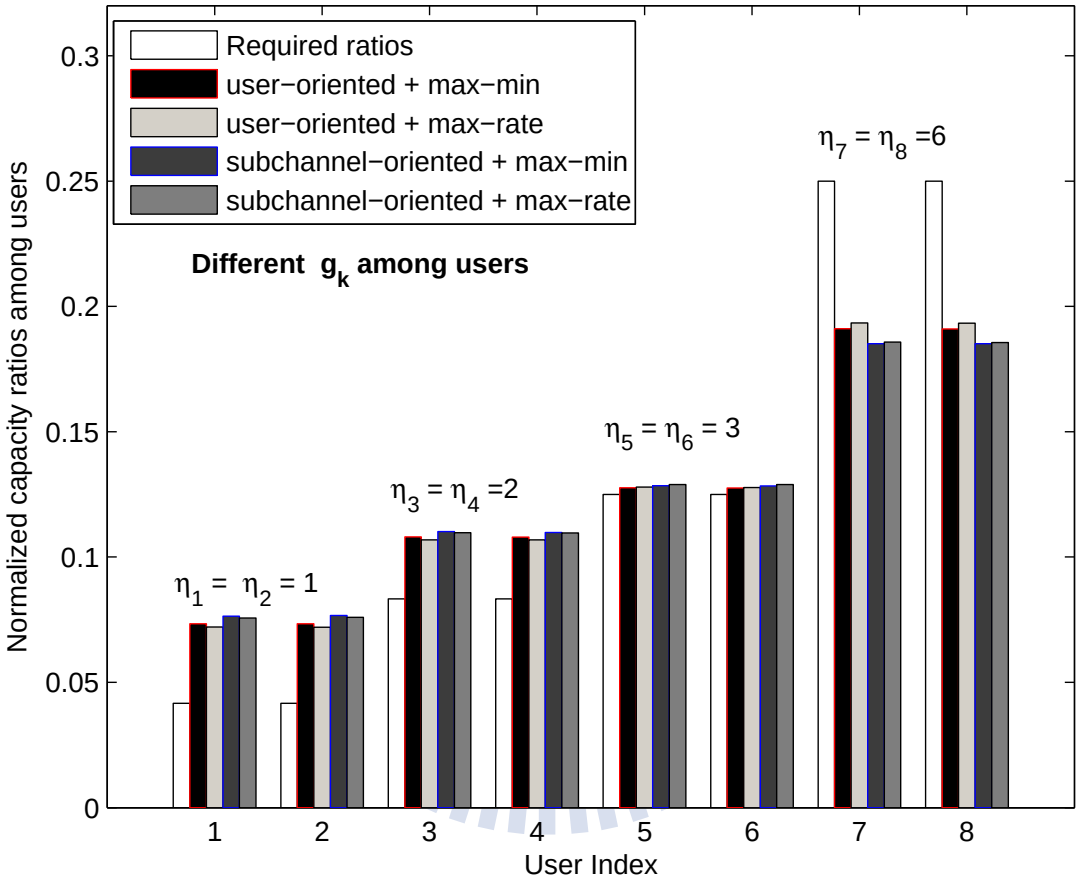

Figure 8.10: Normalized capacity distribution among users with equal power allocation. The rate constraints among users are extremely opposite to previous assumption $\eta_1 : \eta_2 : \ldots : \eta_8 = 6 : 6 : 3 : 3 : 2 : 2 : 1 : 1$. The path loss g_k among users are based on the assumption of Fig. 8.5.

Chapter 9

Conclusion

9.1 Dissertation Summary

In this dissertation, we have investigated different MIMO systems for realizing personalized parallel transmissions from two kinds of perspectives: narrowband system with personalized broadcast and broadband system with personalized scheduling. The former, the MIMO broadcast systems, utilizes spatial domain to simultaneously broadcast independently personalized data for multiple users. The related research topics were presented in Chapters 3, 4, and 5. The later, the MIMO-OFDM systems, utilizes frequency domain to simultaneously communicate with multiple users through subchannel assignment and scheduling. The corresponding research issues were listed in Chapters 7 and 8. The network MIMO systems is a special application of the MIMO broadcast systems from a single-cell scenario extended to a multi-cell environment. In Chapter 6, we combine network MIMO technique with frequency partitions to personalized transmit data among multiple cells. The details of research topics in this dissertation are listed as follows.

- Is transmit or receive beamforming more suitable for designing personalized multiuser MIMO broadcast systems?
- On the performance of transmit based MIMO broadcast systems in terms of link quality improvement and coverage extension by multiuser scheduling.
- Analysis of the effects caused by channel estimation errors in the receive ZF based MIMO broadcast systems.
- Performance enhanced 3-cell network MIMO architecture design under sectorized cells and FFR.
- Joint multiuser scheduling and subchannel assignment for multiuser MIMO-OFDM systems with coverage enhancement.

- Joint subchannel and power allocation for multiuser MIMO-OFDM systems with flexible proportional rates among users.

The contributions from these research works are listed as follows.

1. Provide quantitative comparison and tradeoff between the transmit and the receive ZF MIMO broadcast systems in terms of sum rate, feedback requirements, and sensitivity to feedback channel variations.

2. Present analytical expressions for the link outage probability, link diversity, and reliable coverage of the transmit ZF-DPC and ZF MIMO broadcast systems.

3. Provide analytical link performance and sum rate formulas for the receive ZF MIMO broadcast systems in the presence of channel estimation errors.

4. Design low-complexity 3-cell network MIMO architectures combined with FFR and tri-sector frequency partitions.

5. Analyze the achievable reliable coverage of the spatial multiplexing based MIMO-OFDM systems under random selection, multiuser scheduling, and jointly multiuser and frequency diversity scheduling scheme.

6. Design low-complexity subchannel assignment and power allocation method for the spatial multiplexing based MIMO-OFDM systems with proportional rate constraint among users.

The following summaries the results from the above contributions.

9.1.1 Beamforming Techniques for Multiuser MIMO Broadcast Systems

In Chapter 3, we compared the sum rate performance and feedback requirements when implementing the ZF technique at the transmitter end and receiver end for multiuser MIMO broadcast systems. We provide the performance tradeoff analysis between the transmit and receive ZF MIMO broadcast systems as shown in Table 3.1. Implementing more antennas at user handsets become more feasible thanks to the advanced antenna technologies.

For designing MIMO broadcast systems, the main superiority of the transmit ZF MIMO broadcast systems is the better sum-rate performance with simpler implementation at user terminals, but the transmit ZF MIMO broadcast systems is more sensitive to feedback channel variations. By contrast, the receive ZF MIMO broadcast systems is more robust to feedback channel variations with the cost of implementing ZF algorithm at user terminals. Hence, when feedback bandwidth is limited, it is more reasonable to adopt the receive ZF MIMO broadcast systems. When feedback bandwidth is sufficient, the transmit ZF MIMO broadcast systems can be used.

9.1.2 Analysis of Multiuser MIMO Broadcast Systems with Transmit Beamforming

In Chapter 4, we have analyzed the link outage, diversity order, and link coverage performance for the transmit based multiuser MIMO broadcast systems. We derive analytical closed-forms of the link outage probability, diversity order and reliable link coverage for both the transmit ZF-DPC and transmit ZF MIMO broadcast systems. We define the coverage extension ratio to demonstrate how multiuser scheduling can improve the reliable coverage of the MIMO broadcast system without increasing base station transmission power. From our analysis, the reliable coverage can be extended significantly as the number of users increases, but the performance gain due to multiuser scheduling is reduced as the antennas installed at the base station increases.

9.1.3 Analysis of Multiuser MIMO Broadcast Systems with Receive Beamforming

In Chapter 5, we have derived analytical closed forms including link outage, diversity order, reliable coverage, and sum rate performance for the receive ZF based MIMO broadcast systems with imperfect CSI-R caused by channel estimation errors. From the analytic and numerical results, we find that imperfect CSI-R will cause serious performance degradations on link quality in terms of zero diversity order and reliable coverage shrinkage. As for the impact of imperfect CSI-R on sum rate is that the sum-rate capacity will no longer linearly increase with SNR in decibel and be bounded by a value. This phenomenon is

entirely different from the effect caused by feedback error which only leads to slight sum-rate degradation but maintains the same performance slope. Although multiuser diversity can enhance both link quality performance and sum-rate performance, the effect caused by imperfect CSI-R can not be recovered by exploiting multiuser diversity, i.e. zero diversity order and bounded sum rate.

9.1.4 Architecture for Coordinated Multicell MIMO Systems

In Chapter 6, from the aspects of architecture and deployment, we have presented a FFR-based 3-cell network MIMO tri-sector base station architecture that can effectively overcome the inter-group interference and relieve the burden of executing the complex multi-base station joint processing for a huge number of cluster of cells. We further proposed a rearranged tri-sector frequency partition to exploit the interference mitigation capability of the network MIMO transmission. We demonstrated that using a 3-cell coordinated network MIMO with the proposed rearranged tri-sector frequency partition can outperform the seven-cell coordinated network MIMO with omni-directional cell. We also analyzed how to determine the interior region for the FFR-based systems and find that under 120^o sector antenna architecture. The proposed tri-sector frequency partition is more feasible for the FFR-based MIMO system than the regular tri-sector frequency partition. This kind of 3-cell coordinated network MIMO architectures are particularly useful because the IEEE 802.16m WiMAX standard body has specified that the default number of neighboring cells in the collaborative MIMO transmission is three.

9.1.5 Coverage Enhancement for Multiuser MIMO-OFDM Systems

In Chapter 7, we demonstrate that the reduced coverage of the spatial multiplexing based MIMO-OFDM systems due to split transmission power by equipping with multiple antennas can be improved significantly by taking advantage of utilizing joint multiuser diversity and frequency diversity. At first, we present analytical formulas to evaluate the link outage probability and reliable coverage for the spatial multiplexing based MIMO-OFDM systems without scheduling. For applying multiuser and frequency diversity, we consider three kinds

of multiuser scheduling and subchannel assignment algorithms. Firstly we present the COUS scheme to utilize multiuser diversity and provide the analytical closed form. When considering joint multiuser scheduling and frequency assignment, we propose a low-complexity COSA algorithm and a modified FOSA algorithm developed from the work in [71] for comparison. With respect to COSA, we provide the analytical approximations for link outage probability and reliable coverage by means of order statistics and *Glivenko-Cantelli Theorem*. Numerical results validate the accuracy of provided analytical formulas. We demonstrate that the proposed COSA can significantly enhance coverage performance for the spatial multiplexing based MIMO-OFDM systems, while achieving almost the same fairness performance as FOSA simultaneously. The key to efficiently enhance coverage for the spatial multiplexing based MIMO-OFDM systems is to jointly exploit multiuser and frequency diversity.

9.1.6 Capacity Enhancement for Multiuser MIMO-OFDM Systems

In Chapter 8, we investigate resource allocation frameworks in a spatial multiplexing based multiuser MIMO-OFDM system. Instead of maximal rate-achieving scenario, we consider a system with more robust and flexible transmission to achieve variable proportional rate constraints among served users. Our method including two stages: low-complexity suboptimal subchannel allocation algorithm at first and a computational efficient power allocation method later. The performance of the proposed algorithms are compared with maximal-rate achieving allocation methods. Simulation results shows that the capacity of proposed algorithm can approach to that of maximal-rate achieving algorithm but with more reliable transmission. Additionally, the predetermined proportional rate requirements can be met well. Importantly, our method have considered the effect of different power decay among users.

9.2 Suggestions for Future Research

Possible interesting research topics that can be extended from this dissertation are listed as follows:

- For the MIMO broadcast systems

  1. Utilize more general metrics to quantify the effects of feedback channel variations instead of the CV metric used in Chapter 3, e.g. quantization errors associated with the number of feedback bits; feedback delay caused by Doppler frequency and mobile velocity.
  2. Consider different kinds of receive beamforming for the MIMO broadcast systems, e.g. MMSE receiver [126] combined with multiuser scheduling.
  3. Compare performance tradeoff of various codebook-based multiuser MIMO broadcast systems subject to feedback channel variations.
  4. Performance analysis of the receive ZF based MIMO broadcast system with feedback channel error.
  5. Design powerful limited feedback scheme for the transmit based MIMO broadcast systems.

- For the network MIMO systems

  1. Design a low-complexity network MIMO transmission algorithm based on the proposed 3-cell network architecture in Chapter 6 since the ZF-DPC network MIMO algorithm is still quite complicated.
  2. Based on the proposed 3-cell network architecture, address the effects of multiple antennas installed in the mobile terminal.
  3. Design the protocols to determine when the network MIMO algorithm should be initiated for the outer region users in the FFR-based network MIMO.
  4. Design a flexible region for supporting 2-cell partial coordination and 3-cell full coordination among network MIMO group to eliminate the effect of transmission latency.
  5. Performance evaluation of a network MIMO system in a dynamic traffic environment.
  6. Consider how to involve network MIMO concept in the heterogeneous networks (HetNets) investigated in LTE-A standard.

- For the MIMO-OFDM systems

    1. Consider MIMO-OFDM system under realistic LTE-A and WiMAX standards in terms of performance evaluation and scheduling algorithm design.
    2. Extend single-cell design to multi-cell environment based on LTE-A and WiMAX standards.
    3. Integrate advanced network MIMO concept with the ongoing next generation MIMO-OFDM system in a realizable way.

Bibliography

[1] I. E. Telatar, "Capacity of multi-antenna Gaussian channels," *European Trans. Telecomm*, vol. 10, no. 6, pp. 585 – 595, Nov. 1999.

[2] G. J. Foschini and M. J. Gans, "On limits of wireless communications in a fading environment when using multiple antennas," *Wireless Pers. Commun.*, vol. 6, no. 3, pp. 311 – 335, Mar. 1998.

[3] M. Costa, "Writing on dirty paper," *IEEE Trans. on Information Theory*, vol. 29, no. 3, pp. 439 – 441, May 1983.

[4] G. Caire and S. Shamai, "On the achievable throughput of a multi-antenna Gaussian broadcast channel," *IEEE Trans. on Information Theory*, vol. 49, no. 7, pp. 1691 – 1706, Jul. 2003.

[5] M. Sharif and B. Hassibi, "Scaling laws of sum rate using time-sharing, DPC, and beamforming for MIMO broadcast channels," *Proc. of IEEE International Symposium on Information Theory*, p. 175, Jun. 2004.

[6] N. Jindal and A. Goldsmith, "Dirty-paper coding versus TDMA for MIMO broadcast channels," *IEEE Trans. on Information Theory*, vol. 51, no. 5, pp. 1783 – 1794, May 2005.

[7] M. Sharif and B. Hassibi, "A comparison of time-sharing, DPC, and beamforming for MIMO broadcast channels with many users," *IEEE Trans. on Commun.*, vol. 55, no. 1, pp. 11 – 15, Jan. 2007.

[8] S. Vishwanath, N. Jindal, and A. Goldsmith, "Duality, achievable rates, and sum-rate capacity of gaussian MIMO broadcast channels," *IEEE Trans. on Information Theory*, vol. 49, no. 10, pp. 2658 – 2668, Oct. 2003.

[9] P. Viswanath and D. Tse, "Sum capacity of the vector Gaussian broadcast channel and uplink-downlink duality," *IEEE Trans. on Information Theory*, vol. 49, no. 8, pp. 1912 – 1921, Aug. 2003.

[10] H. Weingarten, Y. Steinberg, and S. Shamai (Shitz), "The capacity region of the Gaussian multiple-input multiple-output broadcast channel," *IEEE Trans. on Information Theory*, vol. 52, no. 9, pp. 3936 – 3964, Sep. 2006.

[11] H. Viswanathan, S. Venkatesan, and H. Huang, "Downlink capacity evaluation of cellular networks with known-interference cancellation," *IEEE Trans. on Information Theory*, vol. 21, no. 5, pp. 802 – 811, Jun. 2003.

[12] S. B. Weinstein and P. M. Ebert, "Data transmission by frequency-division multiplexing using the discrete Fourier transform," *IEEE Trans. on Commun.*, vol. 19, no. 5, pp. 628 – 634, Oct. 1971.

[13] J. A. C. Bingham, "Multicarrier modulation for data transmission: an idea whose time has come," *IEEE Commun. Magazine*, vol. 28, no. 5, pp. 5 – 14, May 1990.

[14] G. Boudreau, J. Panicker, N. Guo, R. Chang, N. Wang, and S. Vrzic, "Interference coordination and cancellation for 4G networks," *IEEE Commun. Magazine*, vol. 47, no. 4, pp. 74 – 81, Apr. 2009.

[15] 3GPP TSG RAN 1 R1-101695. (2010, Feb.) "Text proposal for 3GPP TR36.814 on CoMP".

[16] *IEEE. Standard 802.16. Part 16: air interface for fixed and mobile broadband wireless access systems – DRAFT amendment to IEEE standard for local and metropolitan area networks - advanced air interface*, IEEE P802.16m/D4, Feb. 2010.

[17] M. K. Karakayali, G. J. Foschini, R. A. Valenzuela, and R. D. Yates, "On the maximum common rate achievable in a coordinated network," *IEEE International Conf. of Commun.*, vol. 9, pp. 4333 – 4338, Jun. 2006.

[18] M. K. Karakayali, G. J. Foschini, and R. A. Valenzuela, "Network coordination for spectrally efficient communications in cellular systems," *IEEE Trans. on Wireless Commun.*, vol. 13, no. 4, pp. 56 – 61, Aug. 2006.

[19] G. J. Foschini, M. K. Karakayali, and R. A. Valenzuela, "Coordinating multiple antenna cellular networks to achieve enormous spectral efficiency," *IEE Proc. Commun.*, vol. 153, no. 4, pp. 548 – 555, Aug. 2006.

[20] H. Zhang and H. Dai, "Cochannel interference mitigation and cooperative processing in downlink multicell multiuser MIMO networks," *EURASIP Journal on Wireless Commun. and Networking*, pp. 222 – 235, Feb. 2004.

[21] S. Shamai and B. M. Zaidel, "Enhancing the cellular downlink capacity via co-processing at the transmitting end," *IEEE Vehicular Technology Conf.*, vol. 3, pp. 1745 – 1749, May 2001.

[22] P. Viswanath, D. N. C. Tse, and R. Laroia, "Opportunistic beamforming using dumb antennas," *IEEE Trans. on Information Theory*, vol. 48, no. 6, pp. 1277 – 1294, Jun. 2002.

[23] N. Sharma and L. H. Ozarow, "A study of opportunism for multiple-antenna systems," *IEEE Trans. on Information Theory*, vol. 51, no. 5, pp. 1804 – 1814, May 2005.

[24] R. W. Heath, Jr., M. Airy, and A. J. Paulraj, "Multiuser diversity for MIMO wireless systems with linear receivers," *Proc. Asilomar Conf. Signals, Systems and Computers*, pp. 1194 – 1199, Nov. 2001.

[25] M. Airy, R. W. Heath, Jr., and S. Shakkottai, "Multi-user diversity for the multiple antenna broadcast channel with linear receivers: asymptotic analysis," *Proc. Asilomar Conf. Signals, Systems, and Computers*, pp. 886 – 890, Nov. 2004.

[26] C. J. Chen and L. C. Wang, "Performance analysis of scheduling in multiuser MIMO system with zero-forcing receivers," *IEEE Journal on Selected Areas in Commun.*, vol. 25, no. 7, pp. 1435 – 1445, Sep. 2007.

[27] Q. H. Spencer, A. L. Swindlehurst, and M. Haardt, "Zero-forcing methods for downlink spatial multiplexing in multi-user MIMO channels," *IEEE Trans. on Signal Processing*, vol. 52, no. 2, pp. 461 – 471, Feb. 2004.

[28] T. Yoo and A. Goldsmith, "On the optimality of multiantenna broadcast scheduling using zero-forcing beamforming," *IEEE Journal on Selected Areas in Commun.*, vol. 24, no. 3, pp. 528 – 541, Mar. 2006.

[29] L. Zheng and D. N. C. Tse, "Diversity and multiplexing: A fundamental tradeoff in multiple antenna channels," *IEEE Trans. on Information Theory*, vol. 49, no. 5, pp. 1079 – 1296, May 2003.

[30] C. J. Chen and L. C. Wang, "Enhancing coverage and capacity for multiuser MIMO systems by utilizing scheduling," *IEEE Trans. on Wireless Commun.*, vol. 5, no. 5, pp. 1148 – 1157, May 2006.

[31] L. C. Wang and C. J. Yeh, "Scheduling for multiuser MIMO broadcast systems: transmit or receive beamforming?" *to appear in IEEE Trans. on Wireless Commun. 2010.*

[32] A. Hedayat and A. Nosratinia, "Outage and diversity of linear receivers in flat-fading MIMO channels," *IEEE Trans. on Signal Processing*, vol. 55, no. 12, pp. 5868 – 5873, Dec. 2007.

[33] C. Wang, E. K. S. Au, R. D. Murch, W. H. Mow, R. S. Cheng, and V. Lau, "On the performance of the MIMO zero-forcing receiver in the presence of channel estimation rror," *IEEE Trans. on Wireless Commun.*, vol. 6, no. 3, pp. 805 – 810, Mar. 2007.

[34] IEEE C802.16m-09/0970. (2009, Apr.) "Collaborative zone to support multi-cell MIMO operation in IEEE 802.16m". [Online]. Available: http://www.ieee802.org/16/tgm/contrib/

[35] IEEE C802.16m-09/2280. (2009, Nov.) "Frequency planning for inter-cell interference reduction in 3-cell collaborative MIMO system". [Online]. Available: http://www.ieee802.org/16/tgm/contrib/

[36] L. C. Wang, K. C. Chawla, and L. J. Greenstein, "Performance studies of narrow beam trisector cellular systems," *International Journal of Wireless Information Networks*, vol. 5, no. 2, pp. 89 – 102, Jul. 1998.

[37] L. C. Wang, "A new cellular architecture based on an interleaved cluster concept," *IEEE Trans. on Vehicular Technology*, vol. 48, no. 6, pp. 1809 – 1818, Nov. 1999.

[38] H. Bolcskei, D. Gesbert, and A. J. Paulraj, "On the capacity of OFDM-based spatial multiplexing systems," *IEEE Trans. on Commun.*, vol. 50, no. 2, pp. 225 – 234, Feb. 2002.

[39] S. Catreux, L. J. Greenstein, and V. Erceg, "Some results and insights on the performance gains of MIMO systems," *IEEE Journal on Selected Areas in Commun.*, vol. 21, no. 5, pp. 839 – 847, Jun. 2003.

[40] S. Mudulodu and A. J. Paulraj, "A transmit diversity scheme for frequency selective fading channels," *IEEE Global Telecommun. Conf.*, vol. 2, pp. 1089 – 1093, Nov. 2000.

[41] H. Bolcskei and A. J. Paulraj, "Space-frequency coded broadnand OFDM systems," *IEEE Wireless Commun. and Networking Conf.*, vol. 1, pp. 1 – 6, Sep. 2000.

[42] B. Lu, X. Wang, and K. R. Narayanan, "LDPC-based space-time coded OFDM systems over correlated fading channels: Performance analysis and receiver design," *IEEE Trans. on Commun.*, vol. 50, no. 1, pp. 74 – 88, Jan. 2002.

[43] H. Bolcskei and M. Borgmann, "Noncoherent space-frequency coded MIMO OFDM," *IEEE Journal on Selected Areas in Commun.*, vol. 23, no. 9, pp. 1799 – 1810, Sep. 2005.

[44] H. Bolcskei, M. Borgmann, and A. J. Paulraj, "Impact of the propagation environment on the performance of space-frequency coded MIMO-OFDM," *IEEE Journal on Selected Areas in Commun.*, vol. 21, no. 3, pp. 427 – 439, Apr. 2003.

[45] Y. Peng, S. M. D. Armour, and J. P. McGeehan, "An investigation of dynamic subcarrier allocation in MIMO-OFDMA systems," *IEEE Trans. on Wireless Commun.*, vol. 56, no. 5, pp. 2990 – 3005, Sep. 2007.

[46] M. Sharif and B. Hassibi, "On the capacity of MIMO broadcast channels with partial side information," *IEEE Trans. on Information Theory*, vol. 51, no. 2, pp. 506 – 522, Feb. 2005.

[47] D. J. Love and R. W. Heath, Jr., "What is the value of limited feedback for MIMO channels?" *IEEE Commun. Magazine*, vol. 42, no. 10, pp. 54 – 59, Oct. 2004.

[48] N. Jindal, "MIMO broadcast channels with finite rate feedback," *IEEE Trans. on Information Theory*, vol. 52, no. 11, pp. 5045 – 5059, Nov. 2006.

[49] T. Yoo, N. Jindal, and A. Goldsmith, "Multi-antenna downlink channels with limited feedback and user selection," *IEEE Journal on Selected Areas in Commun.*, vol. 25, no. 7, pp. 1478 – 1491, Sep. 2007.

[50] C. Swannack, G. W. Wornell, and E. Uysal-Biyikoglu, "MIMO broadcast scheduling with quantized channel state information," *Proc. of IEEE International Symposium on Information Theory*, pp. 1788 – 1792, Jul. 2006.

[51] P. Ding, D. Love, and M. Zoltowski, "Multiple antenna broadcast channels with shape feedback and limited feedback," *IEEE Trans. on Signal Processing*, vol. 55, no. 7, pp. 3417 – 3428, Jul. 2007.

[52] K. Huang, J. G. Andrews, and R. W. Heath, Jr., "Performance of orthogonal beamforming with SDMA with limited feedback," *IEEE Trans. on Vehicular Technology*, vol. 58, no. 1, pp. 152 – 164, Jan. 2009.

[53] G. Caire, N. Jindal, M. Kobayashi, and N. Ravindran. "Multiuser MIMO achievable rates with downlink training and channel state feedback". [Online]. Available: http://arxiv.org/abs/0711.2642

[54] J. Zhang, R. W. Heath, Jr., M. Kountouris, and J. G. Andrews, "Mode switching for the multi-antenna broadcast channel based on delay and channel quantization," *EURASIP Journal on Advances in Signal Processing*, vol. 2009, article ID 802548.

[55] K. Huang, R. W. Heath, Jr., and J. G. Andrews, "Uplink SDMA with limited feedback: throughput scaling," *EURASIP Journal on Advances in Signal Processing*, vol. 2008, article ID 479357.

[56] M. Kountouris, D. Gesbert, and T. Sälzer, "Enhanced multiuser random beamforming dealing with the not so large number of users case," *IEEE Journal on Selected Areas in Commun.*, vol. 26, no. 8, pp. 1536 – 1545, Oct. 2008.

[57] M. Kountouris, R. de Francisco, D. Gesbert, D. T. Slock, and T. Sälzer, "Low complexity scheduling and beamforming for multiuser MIMO systems," *Proc. of IEEE Signal Processing Advances in Wireless Commun.*, pp. 1 – 5, Jul. 2006.

[58] R. de Francisco, M. Kountouris, D. T. Slock, and D. Gesbert, "Orthogonal linear beamforming in MIMO broadcast channels," *IEEE Wireless Commun. and Networking Conf.*, pp. 1210 – 1215, Mar. 2007.

[59] Z. Tu and R. S. Blum, "Multiuser diversity for a dirty paper approach," *IEEE Commun. Letter*, vol. 7, no. 8, pp. 370 – 372, Aug. 2003.

[60] G. Dimić and N. D. Sidiropoulos, "On downlink beamforming with greedy user selection: performance analysis and a simple new algorithm," *IEEE Trans. on Signal Processing*, vol. 53, no. 10, pp. 3857 – 3868, Oct. 2005.

[61] J. Kim, S. Park, J. H. Lee, J. Lee, and H. Jung, "A scheduling algorithm combined with zero-forcing beamforming for a multiuser MIMO wireless system," *IEEE Vehicular Technology Conf.*, vol. 1, pp. 211 – 215, Sep. 2005.

[62] A. Bayesteh and A. K. Khandani, "On the user selection for MIMO broadcast channels," *IEEE Trans. on Information Theory*, vol. 54, no. 3, pp. 1086 – 1107, Mar. 2008.

[63] WiMAX Forum. (2006, Aug.) "Mobile WiMAX - Part I: A technical overview and performance evaluation". [Online]. Available: www.wimaxforum.org

[64] F. Khan, *LTE for 4G Mobile Broadband: Air Interface Technologies and Performance*, 1st ed. Cambridge University Press, 2009.

[65] J. Ha, A. N. Mody, J. H. Sung, J. R. Barry, S. W. Maclaughlin, and G. L. Stüber, "LDPC coded OFDM with Alamouti/SVD diversity technique," *Wireless Pers. Commun.*, vol. 23, no. 1, pp. 183 – 194, Oct. 2002.

[66] S. Xiao, X. Xiao, B. Li, and Z. Hu, "Adaptive subcarrier allocation for multiuser MIMO OFDM systems in frequency selective fading channel," *Proc. of Wireless Commun., Networking and Mobile Computing*, vol. 1, pp. 61 – 64, Sep. 2005.

[67] Y. C. Liang, R. Zhang, and J. M. Cioffi, "Transmit optimization for MIMO-OFDM with delay-constrained and no-delay-constrined traffic," *IEEE Trans. on Signal Processing*, vol. 54, no. 8, pp. 3190 – 3199, Aug. 2006.

[68] F. S. Chu and K. C. Chen, "Radio resource allocation for mobile MIMO-OFDMA," *IEEE Vehicular Technology Conf.*, pp. 1876 – 1880, May 2008.

[69] G. Li and H. Liu, "On the optimality of downlink OFDMA MIMO systems," *Proc. Asilomar Conf. Signals, Systems, amd Computers*, pp. 324 – 328, Nov. 2004.

[70] M. Senel, V. Kapnadak, and D. J. Love, "Spatial multiplexing with opportunistic scheduling for multiuser MIMO-OFDM systems," *IEEE Global Telecommun. Conf.*, pp. 1 – 5, Nov. 2006.

[71] W. Rhee and J. M. Cioffi, "Increase in capacity of multiuser OFDM system using dynamic subchannel allocation," *IEEE Vehicular Technology Conf.*, pp. 1085 – 1089, May 2000.

[72] C. Mohanram and S. Bhashyam, "A suboptimal joint subcarrier and power allocation algorithm for multiuser OFDM," *IEEE Commun. Letter*, vol. 9, no. 8, pp. 685 – 687, Aug. 2005.

[73] Z. Shen, J. G. Andrews, and B. L. Evans, "Adaptive resource allocation in multiuser OFDM systems with proportional rate constraints," *IEEE Trans. on Wireless Commun.*, vol. 4, no. 6, pp. 2726 – 2737, Nov. 2005.

[74] I. C. Wong, Z. Shen, B. L. Evans, and J. G. Andrews, "A low complexity algorithm for proportional resource allocation in OFDMA systems," *IEEE Workshop on Signal Processing Systems*, pp. 1 – 6, Oct. 2004.

[75] C. Y. Wong, R. S. Cheng, K. B. Letaief, and R. D. Murch, "Multiuser OFDM with adaptive subcarrier, bit, and power allocation," *IEEE Journal on Selected Areas in Commun.*, vol. 17, no. 10, pp. 1747 – 1758, Oct. 1999.

[76] H. Yin and H. Liu, "An efficient multiuser loading algorithm for OFDM-based broadband wireless systems," *IEEE Global Telecommun. Conf.*, vol. 1, pp. 103 – 107, Nov. 2000.

[77] Y. J. Zhang and K. ben Letaief, "An efficient resource-allocation scheme for spatial multiuser access in MIMO/OFDM systems," *IEEE Trans. on Commun.*, vol. 53, no. 1, pp. 107 – 116, Jan. 2005.

[78] W. W. L. Ho and Y. C. Liang, "Optimal resource allocation for multiuser MIMO-OFDM systems with user rate constraints," *IEEE Trans. on Vehicular Technology*, vol. 58, no. 3, pp. 1190 – 1203, Mar. 2009.

[79] L. C. Wang and C. J. Yeh, "Comparison of transmit and receive zero-forcing schedulers for MIMO broadcast channels," *Proc. Wireless Personal Multimedia Commun.*, pp. 835 – 839, Sep. 2006.

[80] Z. Shen, R. Chen, J. G. Andrews, R. W. Heath, Jr., and B. L. Evans, "Sum capacity of multiuser MIMO broadcast channels with block diagonalization," *IEEE Trans. on Wireless Commun.*, vol. 6, no. 6, pp. 2040 – 2045, Jun. 2007.

[81] ——, "Low complexity user selection algorithms for multiuser MIMO systems with block diagonalization," *IEEE Trans. on Signal Processing*, vol. 54, no. 9, pp. 3658 – 3663, Sep. 2006.

[82] R. Chen, Z. Shen, J. G. Andrews, and R. W. Heath, Jr., "Multimode transmission for multiuser MIMO systems with block diagonalization," *IEEE Trans. on Signal Processing*, vol. 56, no. 7, pp. 3294 – 3302, Jul. 2008.

[83] M. Fuchs, G. D. Galdo, and M. Haardt, "Low complexity space-time-frequency scheduling for MIMO systems with SDMA," *IEEE Trans. on Vehicular Technology*, vol. 56, no. 5, pp. 2775 – 2784, Sep. 2007.

[84] S. Sigdel and W. A. Krzymień, "Simplified fair scheduling and antenna selection algorithms for multiuser MIMO orthogonal space-division multiplexing downlink," *IEEE Trans. on Vehicular Technology*, vol. 58, no. 3, pp. 1329 – 1344, Mar. 2009.

[85] O. Somekh, O. Simeone, Y. Bar-Ness, and A. M. Haimovich, "Distributed multi-cell zero-forcing beamforming in cellular downlink channels," *IEEE Global Telecommun. Conf.*, pp. 1 – 6, Nov. 2006.

[86] A. D. Wyner, "Shannon-theoretic approach to a Gaussian cellular multiple-access channel," *IEEE Trans. on Information Theory*, vol. 40, pp. 1713 – 1727, Nov. 1997.

[87] S. Jing, D. N. C. Tse, J. Hou, J. B. Spriag, J. E. Smee, and R. Padovani, "Multi-cell downlink capacity with coordinated processing," *Proc. Inform. Theory and Application Workshop*, Jan. 2007.

[88] Y. Liang, A. Goldsmith, G. Foschini, R. Valenzuela, and D. Chizhik, "Evolution of base stations in cellular networks: denser depolyment versus coordination," *IEEE International Conf. of Commun.*, pp. 4128 – 4132, Jan. 2008.

[89] J. Zhang, R. Chen, J. G. Andrews, A. Ghosh, and R. W. Heath, Jr., "Networked MIMO with clustered linear precoding," *IEEE Trans. on Wireless Commun.*, vol. 8, no. 4, pp. 1910 – 1921, Apr. 2009.

[90] F. Boccardi and H. Huang, "Limited downlink network coordination in cellular networks," *Proc. of IEEE International Symposium Personal, Indoor and Mobile Radio Commun.*, Sep. 2007.

[91] H. Huang, M. Trivellato, A. Hottinen, M. Shafi, P. J. Smith, and R. Valenzuela, "Increasing downlink cellular throughput with limited network MIMO coordination," *IEEE Trans. on Wireless Commun.*, vol. 8, no. 6, pp. 2983 – 2989, Jun. 2009.

[92] P. Marsch and G. Fettweis, "A framework for optimizing the uplink performance of distributed antenna systems under a constrained backhaul," *IEEE International Conf. of Commun.*, pp. 975 – 979, Jun. 2007.

[93] ——, "A framework for optimizing the downlink of distributed antenna systems under a constraint backhaul," *Proc. of the 13th European Wireless Conf.*, Apr. 2007.

[94] A. Papadogiannis, D. Gesbert, and E. Hardouin, "A dynamic clustering approach in wireless networks with multi-cell cooperative processing," *IEEE International Conf. of Commun.*, pp. 4033 – 4037, May 2008.

[95] S. Venkatesan, "Coordinating base stations for greater uplink spectral efficiency in a cellular network," *Proc. of IEEE International Symposium Personal, Indoor and Mobile Radio Commun.*, Sep. 2007.

[96] ——, "Coordinating base stations for greater uplink spectral efficiency: proportionally fair user rates," *Proc. of IEEE International Symposium Personal, Indoor and Mobile Radio Commun.*, Sep. 2007.

[97] H. Fujii and H. Yoshino, "Theoretical capacity and outage rate of OFDMA cellular system with fractional frequency reuse," *IEEE Vehicular Technology Conf.*, pp. 1676 – 1680, May 2008.

[98] M. Assaad, "Optimal fractional frequency reuse (FFR) in multicellular OFDMA system," *IEEE Vehicular Technology Conf.*, Sep. 2008.

[99] R. Y. Chang, Z. Tao, J. Zhang, and C. C. J. Kuo, "A graph approach to dynamic fractional frequency reuse (FFR) in multi-cell OFDMA networks," *IEEE International Conf. of Commun.*, Jun. 2009.

[100] H. Lei, L. Zhang, X. Zhang, and D. Yang, "A novel multi-cell OFDMA system structure using fractional frequency reuse," *Proc. of IEEE International Symposium Personal, Indoor and Mobile Radio Commun.*, pp. 1 – 5, Sep. 2007.

[101] C. S. Chiu and C. C. Huang, "Combined partial reuse and soft handover in OFDMA downlink transmission," *IEEE Vehicular Technology Conf.*, pp. 1707 – 1711, May 2008.

[102] Y. H. Pan and S. Aïssa, "Dynamic resource allocation with beamforming for MIMO OFDM systems: performance and effects of imperfect CSI," *IEEE Trans. on Wireless Commun.*, vol. 6, no. 12, pp. 4249 – 4255, Dec. 2007.

[103] Z. Luo, H. Gao, and Y. Liu, "Adaptive transmission with linear computational complexity in MIMO-OFDM systems," *IEEE Trans. on Commun.*, vol. 55, no. 10, pp. 1873 – 1877, Oct. 2007.

[104] M. K. Simon and M. S. Alouini, *Digital Communication over Fading Channels: A Unified Approach to Performance Analysis*, 1st ed. Wiley-Interscience, 2000.

[105] D. Tse and P. Viswanath, *Fundamentals of Wireless Communication.* Cambridge University Press, 2005.

[106] A. Paulraj, R. Nabar, and D. Gore, *Introduction to Space-Time Wireless Communications*, 1st ed. Cambridge University Press, 2003.

[107] D. A. Gore, R. W. Heath, Jr., and A. J. Paulraj, "Transmit selection in spatial multiplexing systems," *IEEE Commun. Letter*, vol. 6, no. 11, pp. 491 – 493, Nov. 2002.

[108] A. Vakili, A. Dana, M. Sharif, and B. Hassibi, "Differentiated rate scheduling for MIMO broadcast channels," *Proc. Allerton Conf. on Commun., Control, and Computation*, Sep. 2005.

[109] L. C. Wang and C. J. Yeh, "Comparison of scalar feedback mechanisms in MIMO scheduling systems," *Proc. Wireless Personal Multimedia Commun.*, pp. 1172 – 1176, Sep. 2005.

[110] M. Abramowitz and I. A. Stegun, *Handbook of Mathematical Functions with Formulas, Graphs, and Mathematical Tables*, 9th ed. Dover Publications, 1970.

[111] L. C. Wang and C. J. Yeh, "Multi-user MIMO broadcast systems with imperfect feedbacks," *International Wireless Commun. and Mobile Computing Conf.*, pp. 500 – 504, Jun. 2009.

[112] G. L. Stüber, *Principles of Mobile Communication*, 2nd ed. Kluwer Academic Pubishers, 2001.

[113] X. Zhang and B. Ottersten, "Performance analysis of V-BLAST structure with channel estimation errors," *4th IEEE Workshop on Signal Processing Advances in Wireless Commun.*, pp. 487 – 491, Jun. 2003.

[114] J. G. Proakis, *Digital Communications*, 4th ed. McGraw Hill, 2001.

[115] I. S. Gradshteyn and I. M. Ryzhik, *Table of Integrals, Series, and Products*, 7th ed. Academic Press, 2007.

[116] M. S. Alouini and A. J. Goldsmith, "Capacity of Rayleigh fading channels under different adaptive transmission and diversity-combining techniques," *IEEE Trans. on Vehicular Technology*, vol. 48, pp. 1165 – 1181, Oct. 1999.

[117] *IEEE. Standard 802.16-2004. Part 16: Air Interface for Fixed and Mobile Broadband Wireless Access Systems – Amendment for Physical and Medium Access Control Layers for Combined Fixed and Mobile Operation in Licensed Bands*, IEEE Std. 802.16-2005, Dec. 2005.

[118] H. Huang and R. A. Valenzuela, "Fundamental simulated performance of downlink fixed wireless cellular networks with multiple antennas," *Proc. of IEEE International Symposium Personal, Indoor and Mobile Radio Commun.*, vol. 1, pp. 161 – 165, Sep. 2005.

[119] A. T. James, "Distributions of matrix variates and latent roots derived from normal samples," *Ann. Math. Stat.*, vol. 35, no. 2, pp. 475 – 501, Jun. 1964.

[120] B. C. Arnold, N. Balakrishnan, and H. N. Nagaraja, *A First Course in Order Statistics*, 1st ed. Wiley-Interscience, 1992.

[121] A. W. van der Vaart and J. A. Wellner, *Weak Convergence and Empirical Processes: with Applications to Statistics*. Springer, 1996.

[122] F. W. J. Olver, D. W. Lozier, R. F. Boisvert, and C. W. Clark, *NIST Handbook of Mathematical Functions*. Cambridge University Press, 2010.

[123] R. K. Jain, D.-M. W. Chiu, and W. R. Hawe, "A quantitative measure of fairness and discrimination for resource allocation in shared computer system," *Tech. Rep. DEC-TR-301, Digital Euipment Corporation, USA*, 1984.

[124] L. C. Wang and C. J. Yeh, "Adaptive joint subchannel and power allocation for multi-user MIMO-OFDM systems," *Proc. of IEEE International Symposium Personal, Indoor and Mobile Radio Commun.*, Sep. 2008.

[125] E. K. P. Chong and S. H. Żak, *An Introduction to Optimization*, 2nd ed. John Wiley & Sons, Inc., 2001.

[126] H. Gao, P. J. Smith, and M. V. Clark, "Theoretical reliability of MMSE linear diversity combining in Rayleigh-fading additive interference channels," *IEEE Trans. on Commun.*, vol. 46, no. 5, pp. 666 – 672, May 1998.

Appendix

A Proof of Theorem 1

To ease analysis, we define a function $Z_i(s)$ as

$$Z_i(s) = \frac{\log\left(1 - \Gamma_{\mathrm{R}}(M_T - i + 1, M_T s\gamma_{th})\right)}{\log s} = \frac{\mathrm{Num}_i(s)}{\mathrm{Den}_i(s)} \ , \tag{A1}$$

where $s = \rho_i^{-1}$. When $\rho_i \to \infty$, $s \to 0$. Thus, we can have

$$\begin{aligned} D^i_{\mathrm{order}} &= -\lim_{\rho_i \to \infty} \frac{\log P^i_{\mathrm{out}}(\rho_i)}{\log \rho_i} \\ &= \lim_{s \to 0} Z_i(s) \ . \end{aligned} \tag{A2}$$

Note that $\lim_{s\to 0}\mathrm{Num}_i(s) = -\infty$ and $\lim_{s\to 0}\mathrm{Den}_i(s) = -\infty$ and according to the L'Hôpital's rule, we can obtain

$$\begin{aligned} D^i_{\mathrm{order}} &= \lim_{s \to 0} \frac{\mathrm{Num}'_i(s)}{\mathrm{Den}'_i(s)} \\ &= \lim_{s \to 0} \left[\frac{(M_T s\gamma_{th})^{M_T - i + 1}\, e^{-M_T s\gamma_{th}}}{\Upsilon(M_T - i + 1, M_T s\gamma_{th})} \right] \ , \end{aligned} \tag{A3}$$

where $\Upsilon(a, x) = \int_0^x t^{a-1} e^{-t} dt$ is the lower incomplete gamma function. With the property $\Upsilon(a, x)/x^a \to 1/a$ as $x \to 0$, we can obtain the diversity orider $D^i_{\mathrm{order}} = M_T - i + 1$ for an M_T-link ZF-DPC MIMO broadcast system without scheduling and ordering.

B Proof of Theorem 2

Similar to the proof of Theorem 1, we define $\tilde{Z}_1(s)$ as

$$\tilde{Z}_1(s) = \frac{\log\left([1 - \Gamma_{\mathrm{R}}(M_T, M_T s\gamma_{th})]^K\right)}{\log s} = \frac{\tilde{\mathrm{Num}}_1(s)}{\tilde{\mathrm{Den}}_1(s)} \ , \tag{B1}$$

where $s = \rho_1^{-1}$. Thus, the diversity order is

$$\begin{aligned}
\tilde{D}^1_{\text{order}} &= -\lim_{\rho_1 \to \infty} \frac{\log P^1_{\text{out}}(\rho_1)}{\log \rho_1} \\
&= \lim_{s \to 0} \tilde{Z}_1(s) \\
&\overset{(a)}{=} \lim_{s \to 0} \frac{\tilde{\text{Num}}_1'(s)}{\tilde{\text{Den}}_1'(s)} \\
&= \lim_{s \to 0} \left[\frac{K(M_T s\gamma_{th})^{M_T}\, e^{-M_T s\gamma_{th}}}{\Upsilon(M_T, M_T s\gamma_{th})} \right] \\
&\overset{(b)}{=} KM_T \ , \qquad \text{(B2)}
\end{aligned}$$

where (a) follows L'Hôpital's rule with $\lim_{s \to 0} \tilde{\text{Num}}_1(s) = -\infty$ and $\lim_{s \to 0} \tilde{\text{Den}}_1(s) = -\infty$ and (b) comes from the property $\Upsilon(a, x)/x^a \to 1/a$ as $x \to 0$.

C Proof of Theorem 3

With perfect CSI-R at receivers, say $\epsilon_e^2 = 0$, the link outage probability of (5.10) becomes

$$P_{\text{out}}(\rho) = \left(1 - \Gamma_{\text{R}}\left(M_R - M_T + 1, \frac{M_T \gamma_{th}}{\rho}\right)\right)^K \ , \qquad \text{(C1)}$$

where the variable is now ρ under certain determined parameters $\{M_T, M_R, K, \gamma_{th}\}$. To help analysis, we define the following function $Z(s)$ similar to the proof of Theorem A

$$Z(s) = \frac{K \log\left[1 - \Gamma_{\text{R}}\left(M_R - M_T + 1, M_T s\gamma_{th}\right)\right]}{\log s} = \frac{\text{Num}(s)}{\text{Den}(s)} \ , \qquad \text{(C2)}$$

where $s = \rho^{-1}$. Then, we have

$$\begin{aligned}
D^{\texttt{RZFB}}_{\text{order}} &= -\lim_{\rho \to \infty} \frac{\log P_{\text{out}}(\rho)}{\log \rho} \\
&= \lim_{s \to 0} Z(s) \ . \qquad \text{(C3)}
\end{aligned}$$

Since $\lim_{s \to 0} \text{Num}(s) = -\infty$ and $\lim_{s \to 0} \text{Den}(s) = -\infty$, we alternately derive (C3) based on L'Hôpital's rule as follows

$$\begin{aligned}
D^{\texttt{RZFB}}_{\text{order}} &= \lim_{s \to 0} \frac{\text{Num}'(s)}{\text{Den}'(s)} \\
&\overset{(a)}{=} \lim_{s \to 0} \left(\frac{K e^{-M_T s\gamma_{th}} (M_T s\gamma_{th})^{M_R - M_T + 1}}{\Upsilon(M_R - M_T + 1, M_T s\gamma_{th})} \right) \\
&\overset{(b)}{=} K(M_R - M_T + 1) \ , \qquad \text{(C4)}
\end{aligned}$$

where $f'(\cdot)$ be the differentiation of function $f(\cdot)$ and $\Upsilon(a,x) = \int_0^x t^{a-1}e^{-t}dt$ be lower incomplete gamma function. In (C4), the equality (a) is obtained by $\frac{\partial\Gamma(a,x)}{\partial x} = \frac{-x^{a-1}}{e^x}$, and the equality (b) comes from the property $\Upsilon(a,x)/x^a \to 1/a$ as $x \to 0$.

D Proof of Theorem 4

By definition of link diversity order, we have

$$\begin{aligned} D_{\text{order}}^{\texttt{RZFB}} &= -\lim_{\rho\to\infty}\frac{\log P_{\text{out}}(\rho)}{\log\rho} \\ &= \frac{-\left(1-\Gamma_{\text{R}}\left(M_R-M_T+1,\frac{M_T\gamma_{th}\epsilon_e^2}{(1+\epsilon_e^2)}\right)\right)^K}{\infty} \\ &= 0\ . \end{aligned} \tag{D1}$$

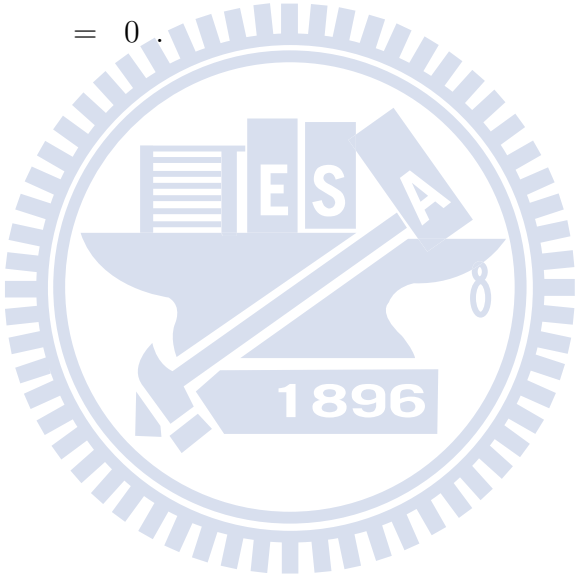

E Detailed Values of Beam Angles in Chapter 6.6

When mobile locates at the position **A**, the details of angles between the mobile and the main-beam direction of interfering base stations are

$$
\begin{aligned}
&I_1, I_2 : \hat{\theta}_i^A = \tan^{-1}\left(\frac{3R-2d}{\sqrt{3}R}\right) + \frac{\pi}{2}\,,\ \tilde{\theta}_i^A = \tan^{-1}\left(\frac{3R-2d}{\sqrt{3}R}\right) - \frac{\pi}{6}\,;\\
&I_3, I_6 : \hat{\theta}_i^A = \frac{\pi}{2} - \tan^{-1}\left(\frac{d}{\sqrt{3}R}\right)\,,\ \tilde{\theta}_i^A = \frac{2\pi}{3} + \tan^{-1}\left(\frac{d}{\sqrt{3}R}\right)\,;\\
&I_4, I_5 : \hat{\theta}_i^A = \frac{\pi}{2} - \tan^{-1}\left(\frac{3R+2d}{\sqrt{3}R}\right)\,,\ \tilde{\theta}_i^A = \frac{\pi}{6} + \tan^{-1}\left(\frac{3R+2d}{\sqrt{3}R}\right)\,;\\
&I_7, I_9 : \hat{\theta}_i^A = \pi - \tan^{-1}\left(\frac{\sqrt{3}R}{3R-d}\right)\,,\ \tilde{\theta}_i^A = \frac{\pi}{3} + \tan^{-1}\left(\frac{\sqrt{3}R}{3R-d}\right)\,;\\
&I_{10}, I_{18} : \hat{\theta}_i^A = \tilde{\theta}_i^A = \pi - \tan^{-1}\left(\frac{3\sqrt{3}R}{3R-2d}\right)\,;\\
&I_{11}, I_{17} : \hat{\theta}_i^A = \frac{\pi}{2} - \tan^{-1}\left(\frac{d}{2\sqrt{3}R}\right),\ \tilde{\theta}_i^A = \frac{\pi}{6} + \tan^{-1}\left(\frac{d}{2\sqrt{3}R}\right)\,;\\
&I_{12}, I_{16} : \hat{\theta}_i^A = \tilde{\theta}_i^A = \tan^{-1}\left(\frac{3\sqrt{3}R}{3R+2d}\right)\,;\\
&I_{13}, I_{15} : \hat{\theta}_i^A = \tan^{-1}\left(\frac{\sqrt{3}R}{3R+D}\right)\,,\ \tilde{\theta}_i^A = \frac{\pi}{3} + \tan^{-1}\left(\frac{\sqrt{3}R}{3R+D}\right)\,;\\
&I_8 : \hat{\theta}_i^A = \tilde{\theta}_i^A = \pi\,;\\
&I_{14} : \hat{\theta}_i^A = \tilde{\theta}_i^A = 0\ .
\end{aligned}
\tag{E1}
$$

When mobile locates on **B**, the angles related to the first-tier interfering base stations are

$$
\begin{aligned}
I_1 &: \hat{\theta}_i^B = \frac{\pi}{3} + \tan^{-1}\left(\frac{\sqrt{3}R}{d}\right),\ \tilde{\theta}_i^B = \frac{\pi}{6} - \tan^{-1}\left(\frac{d}{\sqrt{3}R}\right);\\
I_2 &: \hat{\theta}_i^B = \frac{2\pi}{3} + \tan^{-1}\left(\frac{\sqrt{3}R}{3R-2d}\right),\ \tilde{\theta}_i^B = \tan^{-1}\left(\frac{\sqrt{3}R}{3R-2d}\right);\\
I_3 &: \hat{\theta}_i^B = \frac{\pi}{6} + \tan^{-1}\left(\frac{3R-2d}{\sqrt{3}R}\right),\ \tilde{\theta}_i^B = \frac{2\pi}{3} + \tan^{-1}\left(\frac{\sqrt{3}R}{3R-2d}\right);\\
I_4 &: \hat{\theta}_i^B = \frac{\pi}{6} - \tan^{-1}\left(\frac{d}{\sqrt{3}R}\right),\ \tilde{\theta}_i^B = \frac{\pi}{2} + \tan^{-1}\left(\frac{d}{\sqrt{3}R}\right);\\
I_5 &: \hat{\theta}_i^B = \frac{\pi}{3} - \tan^{-1}\left(\frac{\sqrt{3}R}{3R+2d}\right),\ \tilde{\theta}_i^B = \frac{\pi}{3} + \tan^{-1}\left(\frac{\sqrt{3}R}{3R+2d}\right);\\
I_6 &: \hat{\theta}_i^B = \frac{\pi}{3} + \tan^{-1}\left(\frac{\sqrt{3}R}{3R+2d}\right),\ \tilde{\theta}_i^B = \frac{\pi}{2} + \tan^{-1}\left(\frac{3R+2d}{\sqrt{3}R}\right),
\end{aligned}
\tag{E2}
$$

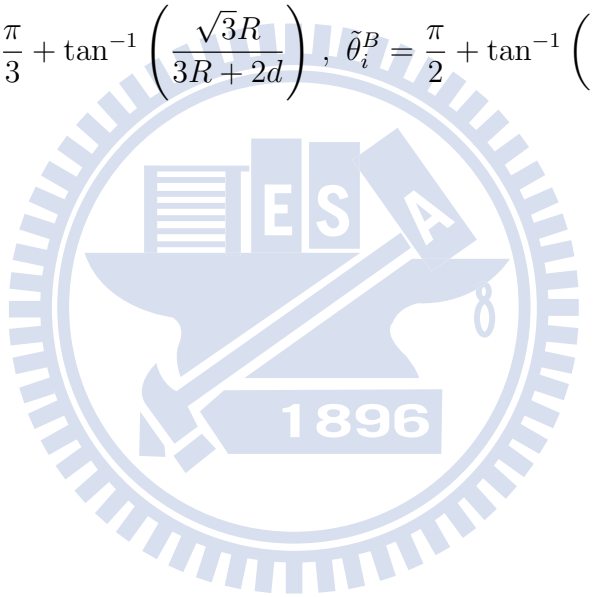

and the angles corresponding to the second-tier interfering base stations are

$$
\begin{aligned}
&I_7: \hat{\theta}_i^B = \frac{\pi}{3} + \tan^{-1}\left(\frac{2\sqrt{3}R}{d}\right),\ \tilde{\theta}_i^B = \frac{\pi}{2} + \tan^{-1}\left(\frac{d}{2\sqrt{3}R}\right);\\
&I_8: \hat{\theta}_i^B = \tilde{\theta}_i^B = \frac{5\pi}{6} + \tan^{-1}\left(\frac{3R-2d}{3\sqrt{3}R}\right);\\
&I_9: \hat{\theta}_i^B = \frac{2\pi}{3} + \tan^{-1}\left(\frac{\sqrt{3}R}{3R-d}\right),\ \tilde{\theta}_i^B = \frac{\pi}{6} + \tan^{-1}\left(\frac{3R-d}{\sqrt{3}R}\right);\\
&I_{10}: \hat{\theta}_i^B = \tilde{\theta}_i^B = \frac{2\pi}{3};\\
&I_{11}: \hat{\theta}_i^B = \frac{2\pi}{3} - \tan^{-1}\left(\frac{\sqrt{3}R}{3R-d}\right),\ \tilde{\theta}_i^B = \tan^{-1}\left(\frac{\sqrt{3}R}{3R-d}\right);\\
&I_{12}: \hat{\theta}_i^B = \tilde{\theta}_i^B = \frac{\pi}{6} + \tan^{-1}\left(\frac{3R-2d}{3\sqrt{3}R}\right);\\
&I_{13}: \hat{\theta}_i^B = \frac{\pi}{6} - \tan^{-1}\left(\frac{d}{2\sqrt{3}R}\right),\ \tilde{\theta}_i^B = \frac{\pi}{3} + \tan^{-1}\left(\frac{2\sqrt{3}R}{d}\right);\\
&I_{14}: \hat{\theta}_i^B = \tilde{\theta}_i^B = \frac{\pi}{3} - \tan^{-1}\left(\frac{3\sqrt{3}R}{3R+2d}\right);\\
&I_{15}: \hat{\theta}_i^B = \frac{\pi}{3} - \tan^{-1}\left(\frac{\sqrt{3}R}{3R+d}\right),\ \tilde{\theta}_i^B = \pi - \tan^{-1}\left(\frac{\sqrt{3}R}{3R+d}\right);\\
&I_{16}: \hat{\theta}_i^B = \tilde{\theta}_i^B = \frac{\pi}{3};\\
&I_{17}: \hat{\theta}_i^B = \frac{\pi}{3} + \tan^{-1}\left(\frac{\sqrt{3}R}{3R+d}\right),\ \tilde{\theta}_i^B = \frac{\pi}{3} - \tan^{-1}\left(\frac{\sqrt{3}R}{3R+d}\right);\\
&I_{18}: \hat{\theta}_i^B = \tilde{\theta}_i^B = \frac{\pi}{3} + \tan^{-1}\left(\frac{3\sqrt{3}R}{3R+2d}\right).
\end{aligned}
\tag{E3}
$$

Vita

Chu-Jung Yeh was born in Taipei, Taiwan, R.O.C., in March 1982. He received the B.S. degree in electrical engineering from National Dong Hwa University, Hualien, Taiwan, in 2004. He is currently working toward the Ph.D. degree with the Institute of Communications Engineering, National Chiao Tung University, Hsinchu, Taiwan. His current research interests are in the areas of MIMO systems with multiuser scheduling, network MIMO systems, resource management and performance analysis for cellular mobile broadband networks.

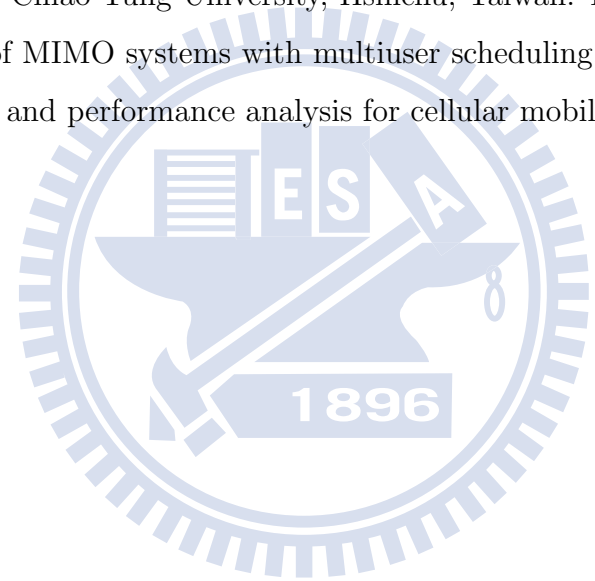

Publication List

Journal Paper

1. Li-Chun Wang and Chu-Jung Yeh, "Scheduling for multiuser MIMO broadcast systems: transmit or receive beamforming?" accepted by *IEEE Transactions on Wireless Communications*, Jul. 2010.

2. Li-Chun Wang and Chu-Jung Yeh, "Coverage analysis for multiuser MIMO broadcast systems," submitted to *IEEE Transactions on Wireless Communications*, Apr. 2010.

3. Li-Chun Wang and Chu-Jung Yeh, "3-Cell network MIMO architectures with sectorization and fractional frequency reuse," submitted to *IEEE Journal on Selected Areas in Communications*, special issue: Distributed Broadband Wireless Communications, Jun. 2010.

4. Li-Chun Wang and Chu-Jung Yeh, "Enhancing coverage for multiuser MIMO-OFDM systems by scheduling and subchannel assignment," to be submitted.

5. Chu-Jung Yeh, Li-Chun Wang, and Jwo-Yuh Wu, "Performance analysis for receive ZF based MIMO broadcast systems with channel estimation errors," to be submitted.

Book Chapter

1. Li-Chun Wang and Chu-Jung Yeh, "Antenna architectures for network MIMO," *Cooperative Cellular Wireless Networks*, (edited by Prof. Ekram Hossain, Prof. Dong In Kim and Prof. Vijay K. Bhargava, to be published by Cambridge University Press, ISBN-13: 9780521767125)

Patent

1. Chu-Jung Yeh, Li-Chun Wang and I-Kang Fu, "Method and apparatus for coordinated MIMO signal transmission among multiple cells in wireless OFDM systems," filed for the US patent with MediaTek. Inc., Application No. 61/172,331, Apr. 24, 2009.

2. Li-Chun Wang and Chu-Jung Yeh, "Resource allocation method for multi-users multiple input multiple output orthogonal frequency division multiplexing system and apparatus thereof," filed for the US patent with ITRI, Application No. 12/208319, Sep. 10, 2008 (Patent Application Publication US 2010/0061312 A1, Mar. 11, 2010).

Conference Paper

1. Li-Chun Wang and Chu-Jung Yeh, "A three-cell coordinated network MIMO with fractional frequency reuse and directional antennas," *IEEE International Conference on Communications (ICC)*, May 2010.

2. Li-Chun Wang and Chu-Jung Yeh, "Cell grouping and autonomous channel assignment for cooperative multi-cell MIMO systems," *IEEE International Symposium on Personal, Indoor and Mobile Radio Communications (PIMRC)*, Sep. 2009.

3. Li-Chun Wang and Chu-Jung Yeh, "Multi-user MIMO broadcast systems with imperfect feedbacks," *International Wireless Communications and Mobile Computing Conference (IWCMC)*, Jun. 2009.

4. Li-Chun Wang and Chu-Jung Yeh, "Adaptive joint subchannel and power allocation for multi-user MIMO-OFDM systems," *IEEE International Symposium on Personal, Indoor and Mobile Radio Communications (PIMRC)*, Sep. 2008.

5. Li-Chun Wang, Chu-Jung Yeh and Chi-Fang Li, "Coverage performance analysis of multiuser MIMO broadcast systems," *IEEE Vehicular Technology Conference (VTC) Spring*, May 2008.

6. Li-Chun Wang, Chu-Jung Yeh and Chi-Fang Li, "A closed-form approximation for

capacity of multiuser MIMO broadcast systems: A Virtual User Approach," *IEEE Wireless Communications and Networking Conference (WCNC)*, Mar. 2008.

7. Li-Chun Wang and Chu-Jung Yeh, "On the performance of zero-forcing beamforming for MIMO broadcast systems," *IEEE AP-S International Symposium on Antennas and Propagation*, Jun. 2007.

8. Li-Chun Wang, Cheng-Wei Chiu, Chu-Jung Yeh and Chi-Fang Li, "Coverage enhancement for OFDM-based spatial multiplexing systems by Scheduling," *IEEE Wireless Communications and Networking Conference (WCNC)*, Mar. 2007.

9. Li-Chun Wang, Cheng-Wei Chiu, Chu-Jung Yeh and Wern-Ho Sheen, "Coverage performance analysis of OFDM-based spatial multiplexing systems," *IEEE Vehicular Technology Conference (VTC) Spring*, Apr. 2007.

Technical Contribution

1. IEEE C802.16m-09/2280, "Frequency planning for inter-cell interference reduction in 3-Cell collaborative MIMO systems (15.5.2.3)." (Li-Chun Wang, Chu-Jung Yeh, and I-Kang Fu; 2009-11-05)

2. IEEE C802.16m-09/2024r3, "Self-organizing network in a FFR-based collaborative MIMO multi-cell wireless OFDMA systems (SON)." (Li-Chun Wang, Chu-Jung Yeh, I-Kang Fu, and Joey Chou; 2009-09-22)

3. IEEE C802.16m-09/0970, "Collaborative zone to support multi-cell MIMO operation in IEEE 802.16m." (Chu-Jung Yeh, Li-Chun Wang, I-Kang Fu, and Paul Cheng; 2009-04-28)